

International Perspectives on Environmental Nanotechnology

Applications and Implications

Conference Proceedings

Volume 1 - Applications

October 7-9, 2008

Chicago, Illinois

U.S. Environmental Protection Agency

Region 5

Superfund Division

EPA 905R09032

November 2009

Disclaimer

This report does not constitute U.S. Environmental Protection Agency policy. Mention of trade names or commercial products does not constitute endorsement or recommendation for use.

Acknowledgements

This conference and the production of these proceedings were made possible by the dedicated efforts of many individuals and the support of many organizations. Both in terms of providing finances and personnel, two offices within the United States Environmental Protection Agency (EPA) were the primary sponsors of this effort. These were the Office of Science Policy (OSP) within the Office of Research & Development (ORD) and the Superfund Division (SFD) of the Region 5 Offices.

The University of Illinois at Chicago (UIC), School of Public Health, was EPA's primary partner among many partner agencies and organizations. UIC staff contributed crucial registration services, catering arrangements, and logistical support. EPA contracted additional logistical and website support from Environmental Management Support, Inc.

Supplemental funding was provided by the National Science Foundation (NSF) through a grant to the Oregon Health & Science University (OHSU) to fund the conference-related travel expenses of keynote speakers; the National Institute of Environmental Health Sciences (NIEHS) of the National Institutes of Health to fund the conference-related travel of the luncheon speakers; and the United States Army Corps of Engineers.

The conference co-chairs are especially grateful to OSP and SFD management for unwavering, enthusiastic support regarding this grand endeavor. Specifically, we want to thank Mr. Jeff Morris, former acting Director of OSP and current ORD National Program Director for Nanotechnology and Mr. James Mayka, former Chief of Innovative Systems & Technology Branch and current Chief of Revitalization, Documents, & Agreements Branch, SFD.

Finally, we want to express our sincere gratitude to the many organizing and supporting committee members listed below, without whom this conference would have remained just a good idea.

Conference Organizing Committee



Conference Co-Chairs

Warren L. Layne
Region 5-SFD, EPA

Charles G. Maurice
ORD-OSP & R5-SFD, EPA

Air & Water Pollution Control Subcommittee

Diana Eignor
OW-OST, EPA

Brendlyn Faison
OW-OST, EPA

Fate & Transport Subcommittee

Michele Conlon
ORD-NERL, EPA

Barbara Karn
ORD-NCER, EPA

David LePoire
ANL, DOE

Madeleine Nawar
OAR-ORIA, EPA

Dennis Utterback
ORD-OSP, EPA

Eric Weber
ORD-NERL, EPA

Hazardous Waste Remediation Subcommittee

Deborah Elcock
ANL, DOE

Michael Gill
ORD-OSP & R9-SFD, EP

Jon Josephs
ORD-OSP & R2-SFD, EPA

Martha Otto
OSWER-OSRTI, EPA

Nancy Ruiz
Navy, DOD

Nano-Enabled Sensors & Monitoring Subcommittee

Heather Henry
NIEHS-SRP, NIH

Warren Layne
Region 5-SFD, EPA

Nora Savage
ORD-NCER, EPA

Toxicity & Risk Assessment Subcommittee

Beth Anderson
NIEHS-SRP, NI

Stephen Diamond
ORD-NHEERL, EPA

Mark Johnson
ATSDR

Igor Linkov
Army COE, DO

Charles Maurice
ORD-OSP & R5-SFD, EPA

Barbara Walton
ORD-NHEERL, EPA

Supporting Committees

Conference Registration Committee

Marilyn Bingham
Sch Publ Health, UIC

Joseph Zanoni
Sch Publ Health, UIC

Inter-Organizational Liaisons

Pankaj Parikh
Region 5-SFD, EPA

Paul Tratnyek
Dept Sci & Engin, OHSU

James Ursic
Region 5-SFD, EPA

Proceedings

Managing Editor

Stephen Ostrodka
Region 5-SFD, EPA

Publishing and Printing Staff

Pam Gallichio
Region 5-SFD, EPA

Mark Vendl
Region 5-SFD, EPA

Keynote Speakers

Marie-Isabelle Baraton, CNRS & Univ of Limoges, France
Air Pollution Control

Heechul Choi, Gwangju Instit of Sci & Technol, Republic of Korea
Hazardous Substances Remediation

Dermot Diamond, Dublin City Univ, Ireland
Nanotechnology-enabled Sensors & Monitoring

Anne Fairbrother, Parametrix, United States
Risk Assessment

Glen Fryxell, Dept of Energy, United States
Water Pollution Control

Jamie Lead, Univ of Birmingham, United Kingdom
Fate & Transport

Igor Linkov, Army Corps of Engineers, United States
Risk Assessment & Decision Analysis

Martin Philbert, Univ of Michigan, United States
Toxicology

Jo Anne Shatkin, CLF Ventures, Inc., United States
Toxicity & Risk Assessment

David Waite, Univ of New South Wales, Australia
Hazardous Substances Remediation

Preface

The International Environmental Nanotechnology Conference - Applications & Implications (IENC) was held on October 7-9, 2008, and was the 3rd in a series of environmental nanotechnology conferences led by the United States Environmental Protection Agency (EPA). The first two workshops focused on nanotechnology in the context of site remediation. During October 2005, the EPA in partnership with other federal agencies held the 2-day Workshop on Nanotechnology for Site Remediation¹ in Washington, DC. This was followed in September 2006 by the Nanotechnology for Site Remediation Workshop^{2,3} held jointly in Chicago by the Superfund Division of Region 5 and the Office of Science Policy (OSP) of the Office of Research and Development (ORD).

The IENC vision emerged during the 2006 workshop, stimulated by the recognition that broader coverage of environmental nanotechnology needed to be conducted. This broader context required greater spheres of knowledge, experiences, and perspectives which could be obtained both through expansion to the international stage with participants from around the world and through expansion of topics to include pollution control and nano-enabled monitoring. Such a broadening would exponentially increase the exchange of information and ideas, as well as synergistically advance the field.

Correspondingly, the IENC organizers designed a conference atmosphere conducive to interactive participation by organizing a mix of keynote, concurrent, poster, and panel discussion sessions. In this manner, cross-fertilization of information and insights would be enhanced both between and within disciplines, both in small and large group settings, and both in formal and less formal interactions.

The IENC was a monumental success, as the information exchanged and the synergistic energy created far exceeded the most optimistic expectations. Over the course of the 3-day conference, more than 80 presentations were conducted by scientists and engineers from 5 continents (Africa, Asia, Australia, Europe, and North America) and 12 countries (Australia, Canada, China, France, Ireland, Japan, Republic of Korea, South Africa, Spain, Taiwan, UK, and USA). Eight keynote and 2 luncheon plenary presentations provided nanotechnology-related introductions, insights, and overviews for various environmental contexts; the concurrent sessions provided deeper coverage of the various topics; and the poster session and panel discussions resulted in numerous insightful interactions.

These proceedings are intended to continue the international, cross-disciplinary exchanges regarding nanotechnology applications and implications for the environment.

Charles G. Maurice, Ph.D. & Warren L. Layne, Ph.D., Conference Co-Chairs
United States Environmental Protection Agency

1 proceedings available at http://www.epa.gov/ncer/publications/workshop/pdf/10_20_05_nanosummary.pdf

2 document number EPA 905K07001, December 2007

3 proceedings available at <http://www.epa.gov/osp/hstl/NanotechProceedings.pdf>

Table of Contents

<i>Acknowledgements</i>	3
<i>Keynote Speakers</i>	5
<i>Preface</i>	6
<i>Table of Contents</i>	7
<i>Opening Remarks</i>	11
Jon Josephs, Deborah Elcock, Michael Gill, Martha Otto, and Nancy Ruiz <i>Chapter 1 – Introduction, Using Nanomaterials for Remediation of Hazardous Substances</i>	17
T. David Waite, Quan Sun, and Steven E. Mylon <i>Oxidative Transformations Mediated by Nanoparticulate Zero Valent Iron</i>	19
Heechul Choi <i>Application of Nanomaterials for Environmental Remediation: Arsenic removal by Nano-scale Zero Valent Iron</i>	29
Barbara Karn, Todd Kuiken, Martha Otto, and Wei-Xian Zhang <i>In Situ Remediation: Nanotechnology’s Environmental Poster Child</i>	35
Gordon C. C. Yang <i>Removal and Degradation of Subsurface Pollutants by Nanoscale Bimetallic Pd/Fe Slurry Under an Electric Field</i>	41
Jingjing Zhan, Tonghua Zheng, Bhanukiran Sunkara, Gerhard Piringer, Yunfeng Lu, Gary McPherson, and Vijay John <i>Novel Zerovalent Iron/Silica Composites for Targeted Remediation of TCE Contaminated Water and Soil</i>	47
Wei-xian Zhang <i>Surface Chemistry of Nanoscale Zero-valent Iron (nZVI)</i>	53
Anna Ryu and Heechul Choi <i>Highly Efficient Nitrate Reduction by Bimetallic Nanoscale Zero-Valent Iron</i>	55
Souhail R. Al-Abed and Hyeok Choi <i>Implications of Fe/Pd Bimetallic Nanoparticles Immobilized on Adsorptive Activated Carbon for the Remediation of Groundwater and Sediment Contaminated with PCBs</i>	57
Marek H. Zaluski, Gary Wyss, Adam Logar, Nick Jaynes, Martin Foote, Gilbert M. Zemansky, Kenneth R. Manchester, Steve Antonioli, Mary Ann Harrington-Baker, David Reichhardt, Mark Ewanic, and Scott Petersen <i>Comprehensive Investigations on Nano-Size ZVI for Mending an Existing Permeable Reactive Barrier in the 100-D Area at the Hanford Site</i>	59

Paul G. Tratnyek, Vaishnavi Sarathy, Jae-Hun Kimyoon, Yoon-Seok Chang, and Bumhan Bae <i>Effects of Particle Size on the Kinetics of Degradation of Contaminants</i>	67
D. R. Baer, P. G. Tratnyek, J. E. Amonette, C. L. Chun, P. Nachimuthu, J. T. Nurmi, 8R. L. Penn, D. W. Matson, J.C. Linehan, Y. Qiang, and A. Sharma <i>Tuning the Properties of Iron Nanoparticles: Doping Effects on Reactivity and Aging</i>	73
Amid P. Khodadoust, Krishna R. Reddy, and Kenneth Darko-Kagya <i>Pentachlorophenol Reduction in Solid by Reactive Nanoscale Iron Particles</i>	79
Gautham Jegadeesan, Souhail R. Al-Abed, Hyeok Choi, and Kirk G. Scheckel <i>Arsenic Adsorption and As (III) Oxidation on TiO₂ Nanoparticles: Macroscopic and Spectroscopic Investigations</i>	83
Daniel W. Elliott, and Wei-xian Zhang <i>Differential Reactivity of nZVI Towards Lindane and Implications for QA/QC and Field-Scale Use</i>	91
Robert J. Ellis, Harry S. Brenton, David S. Liles, Chase McLaughlin, and Nick Wood <i>Nanoscale Zero Valent Iron Phase II Injection Field Pilot Study, Phoenix-Goodyear Airport North Superfund Site, Goodyear, Arizona</i>	99
Chunming Su, Robert Puls, Susan O’Hara, Thomas Krug, Mark Watling, Jacqueline Quinn, and Nancy Ruiz <i>Pilot Field Test of the Treatment of Source Zone Chlorinated Solvents Using Emulsified Zero- Valent Iron</i>	101
Weile Yan, Xiao-qin Li, and Wei-xian Zhang <i>Nanoscale Zero-Valent Iron (nZVI): the Core-Shell Structure and Sequestration of Heavy Metals</i>	107
D. Bhattacharyya, J. Xu, D. Meyer, Y. Tee, and L. Bachas <i>Nanotechnology-Based Membrane Systems for Detoxification of Chlorinated Organics from Water</i>	113
Shas Mattigod, Dawn Wellman, Henry Pate, Kent Parker, Emily Richards, Glen Fryxell, and Richard Skaggs <i>A Field Demonstration of a Novel Functionalized Mesoporous Sorbent Based Battelle ISIS Tech- nology for Mercury Removal</i>	117
Shirish Agarwal, Souhail R. Al-Abed, and Dionysios D. Dionysiou <i>Dechlorination of Polychlorinated Biphenyls by Pd/Mg Bimetallic Corrosion Nano-Cells</i>	123
Gilbert M. Zemansky, Adam Logar, Kenneth R. Manchester, Marek H. Zaluski, Michael Hogan, Nick Jaynes, and Scott Petersen <i>Sand-Tank Test on Injectability of Nano-Size ZVI into Saturated Sand for Mending an Existing Permeable Reactive Barrier in the 100-D Area at the Hanford Site</i>	129

Gary Wyss, Adam Logar, Martin Foote, Nick Jaynes, Marek H. Zaluski, Michael Hogan, and Scott Petersen <i>Geochemical Laboratory Testing of Nano-Size ZVI for Mending an Existing Permeable Reactive Barrier in the 100-D Area at the Hanford Site</i>	135
Nick Jaynes, Adam Logar, Martin Foote, Gary F. Wyss, Marek H. Zaluski, Michael Hogan, and Scott Petersen <i>Screening of Available ZVI Products for Mending an Existing Permeable Reactive Barrier in the 100-D Area at the Hanford Site</i>	141
Charles G. Maurice <i>Chapter 2 – Introduction, Using Nanomaterials in Air & Water Pollution Control</i>	147
Glen E. Fryxell, Richard Skaggs, Shas V. Mattigod, Dawn Wellman, Kent Parker, Wassana Yantasee, R. Shane Addleman, Xiaohong S. Li, and Yongsoon Shin <i>Water Pollution Control Using Functional Nanomaterials</i>	149
Marie-Isabelle Baraton <i>Nanoparticle-based Gas Sensors for an Intelligent Air Quality Monitoring Network</i>	151
Love Sarin, Natalie Johnson, Indrek Kulaots, Brian Lee, Steven Hamburg, and Robert Hurt <i>Nanotechnology for Suppressing Mercury Release from Fluorescent Lamps</i>	157
V. Tiwari, V. Sethi, and P. Biswas <i>One Step Flame Synthesis of TiO₂/CeO₂ Nanocomposite with Controlled Properties for VOC Photooxidation</i>	165
Shebere Adam, Melissa Torres, Karna Barquist, and Sarah C. Larsen <i>Environmental Applications of Nanocrystalline Zeolites</i>	173
M. Hlophe and T. Hillie <i>The Testing of a Nonmembrane Filtration Unit for the Production of Potable Water fom a Brackish Groundwater Source</i>	179
Gordon C.C. Yang and Chia-Heng Yen <i>Treatment of Hi-tech Industrial Wastewaters Using Iron Nanoparticles</i>	185
You Qiang , Andrzej Paszczynski, Amit Sharma, Agnes Che, and Ryan Souza <i>Conjugates of Enzyme-Magnetic Nanoparticles for Water Remediation</i>	193
David J. LePoire <i>Exploring a Framework of Nanotechnology Research and Applications in Addressing Global Climate Change Issues</i>	201
B. Neppolian, Evrim Celik, and H. Choi <i>Photocatalytic degradation of 4-chlorophenol using new visible light responsive ZrTiO₄/Bi₂O₃ nano-size photocatalysts</i>	205

Heather Henry	
<i>Chapter 3 – Introduction, Nanotechnology-Enabled Sensors & Monitoring</i>	209
Dermot Diamond	
<i>Current, Emerging and Future Technologies for Sensing the Environment</i>	211
Li Han, Kim Guzan, Anthony Andradý, and David Ensor	
<i>Nanofiber Sensor Platform for Environmental Pollutant Monitoring and Detection</i>,.....	223
Ryan S. Westafer, Michael H. Bergin, Dennis W. Hess, William D. Hunt, Galit Levitin, and Desmond D. Stubbs	
<i>Ozone Sensors for Real-time Passive Wireless Application</i>	231
Am Jang, Kang K. Lee, Se H. Lee, Chong H. Ahn, and Paul L. Bishop	
<i>Development of Disposable Microfabricated Chip Sensor Using Nano Bead Packing Method to Measure ORP</i>	239
Ian M. Kennedy	
<i>Metal Oxide Nanoparticles: Applications for Biosensors and Toxicity Studies</i>	245
Hatice Şengül and Thomas L. Theis	
<i>Environmental Aspects of Applications of Quantum Dot-Based Nanosensors</i>	253
<i>Panel Discussion: Nanosensors – Where Are We Going?</i>	261
Warren L. Layne	
<i>Chapter 4 – Introduction, Analysis & Characterization of Nanomaterials</i>	265
Emily K. Leshner, Sungyun Lee, and James F. Ranville	
<i>Detection and Characterization of Inorganic Nanoparticles Using Inductively Coupled Plasma- Mass Spectrometry in Hyphenated and Real Time Single Particle Modes</i>	267
Mark. A. Chappell, Aaron J. George, Katerina M. Dontsova, Beth E. Porter, Cynthia L. Price, Pingheng Zhou, Eizi Morikawa, J. Bennett Johnston Sr., Alan J. Kennedy, and Jeffery A. Steevens	
<i>Surfactive Stabilization of Multi-Walled Carbon Nanotube Dispersions with Dissolved Humic Substances</i>	273
Maria Casado and Jamie R. Lead	
<i>Interactions Between Engineered Iron Oxide Nanoparticles and Microorganisms</i>	281
Emilia Cieslak and Jamie R. Lead	
<i>Ultracentrifugation onto Supporting Grids as a TEM Specimen Preparation Method for Carbonaceous Nanoparticles</i>	285
<i>Chapter 5 –Report Backs and Panel Discussion: Applications</i>	289

Opening Remarks

The Importance of Nanotechnology to U.S. EPA Region 5



*Bharat Mathur, Deputy Regional Administrator
U.S. Environmental Protection Agency - Region 5, Chicago, Illinois*

The United States Environmental Protection Agency (EPA) Region 5 has had some experience with the application of nanotechnology in the Midwest. The region is conducting a pilot study on the use of palladium-activated nanoscale zero-valent iron in the ongoing cleanup of chlorinated hydrocarbon contamination at the Nease Chemical Superfund site near Salem, Ohio. This is one of only 34 sites in the world where nanotechnology methods currently are being tested for site remediation. Region 5 staff members also have taken part in six previous nanotechnology conferences, and they helped write the Agency's landmark nanotechnology white paper. This work discussed the state of the art and suggested future directions for EPA's nanotechnology efforts. The report called for extensive intramural and extramural research into the potential risks that engineered nanomaterials may pose to human health and the environment.

More than 700 products on the market are made from or with nanotechnology or engineered nanomaterials. Worldwide, about \$9 billion is spent annually by governments and the private sector on nanotechnology research. More than \$32 billion in nanotechnology products were sold globally last year. Researchers project that, by 2014, nanotechnology will be a \$2.6 trillion business.

Nanomaterials present a wealth of new opportunities. Among those are opportunities for detection and removal of toxic chemicals and for pollution control. Good luck in your efforts to achieve new and better environmental protection methods without new risks to the environment and human health.

Nanotechnology Perspective and Activity in the U.S. EPA Office of Research and Development



*George Gray, Assistant Administrator for Research and Development
U.S. Environmental Protection Agency, Washington, DC*

This truly is an important time in the development of nanotechnology. The use of these technologies and materials is going to increase in the consumer and industrial sectors in the future. Right now, nanomaterials are used in a variety of consumer products, such as sunscreens and tennis rackets. It is very clear that nanotechnology also has significant potential for helping EPA and everyone who cares about protecting the environment. This conference will be looking closely at some of the applications that nanotechnology will have for helping us clean up the environment. While nanotechnology clearly offers us many potential benefits, EPA recognizes the need to be careful and to make sure that these materials are managed appropriately, in order to minimize any risks that might come when these materials are released into the environment.

EPA's charge is to work with other federal partners to address potential environmental and public health concerns that might arise as nanomaterials are developed, manufactured, used, and disposed. To help meet this challenge, the President's 2009 budget for EPA increases the federal government's nanotechnology environmental health and safety budget to \$76 million, double what it was just three years ago. There is recognition that the development of this important technology means that resources must be provided to make sure that any potential risks are understood and managed. EPA's own research and development budget is proposed to increase by about \$4.5 million in 2009 to a total of almost \$15 million, which is double the size of our program in 2007.

EPA is developing its program in consultation and concert with other federal agencies. In working with other federal agencies and with the international community, the Agency gives special attention to understanding which nanomaterials are most likely to enter the environment, and what will happen to them when they do. It is important to understand how they behave as they travel through different environmental media.

An exciting new development is the announcement of two joint National Science Foundation and EPA research centers for looking at the environmental implications of nanotechnology. These centers are located in North Carolina at Duke University and at the University of California in Los Angeles. These centers are designed to bring multidisciplinary teams together to study how nanomaterials might interact with humans and with the environment, helping EPA develop assessment and management strategies to address potential risks. These centers also will network with research organizations, industry, and government agencies to emphasize the interdisciplinary nature of the work that is necessary to move forward our understanding of nanotechnology effects.

EPA is tapping into the intelligence, experience, and passion of EPA researchers and also working with external university researchers, through various grant programs, to bring the different disciplines needed together to do the best research. A great example of this is work by Dr. Bellina Veronesi in EPA's Health and Environmental Sciences Research Laboratory. She was looking at some titanium dioxide in connection with in vitro work. One of the important things she did was tap into one of our external grantees, a group at Carnegie Mellon University that was working on characterizing materials. They worked to characterize the state of a manufactured nanomaterial in the various media in which it was used. They also examined the relationship between the concentration in the material, its size, and the response seen in the cells. The study allowed tremendous insight into how these nanotechnologies may behave in natural media.

I encourage the participants of this conference to consider the ideas of characterization and collaboration as this meeting moves forward. Characterization of manufactured nanomaterials is becoming a bigger issue. Appropriate characterization of these materials is essential in understanding their applications and their potential implications. Collaboration is important in making nanotechnology research more powerful, important, and useful than it might be if researchers limit themselves to their own narrow areas.

U.S. Federal Interagency and International Perspectives on Nanotechnology



*Jeff Morris, National Program Director for Nanotechnology
Office of Research & Development, U.S. Environmental Protection Agency, Washington, DC*

These are clearly exciting times for the development and use of nanotechnology products, including the use of nanotechnology to achieve environmental benefits. However, while the unique properties of nanomaterials offer many potential benefits, we also recognize that we need to determine whether there could be unintended adverse impacts when they are released into the environment. Our challenge is to address potential environmental and public health issues as nanomaterials are developed, brought to the market place, and eventually disposed of or recycled. If we can do so, we will help maximize the net societal benefit of these new materials and products.

Looking at the potential environmental benefits and impacts of nanomaterials, it is important to consider decision-support contexts: how our scientific information informs decision making, whether those decisions are applying clean-up approaches or regulating a nanoparticle as a new chemical. We can consider this context in terms of four simple, but not so easy, questions. While these questions are focused on implications, they also apply to applications in the sense that – as we look to nanotechnology for pollution prevention and mitigation solutions – we must take care to consider the implications of those applications. These questions are:

1. What nanomaterials, in what forms – now and in the future – are most likely to result in environmental exposure?
2. What nanomaterial properties or characteristics affect toxicity?
3. Are nanomaterials with these properties likely to enter environmental media or biological systems at concentrations of concern, and what does this mean for risk?
4. If the answer to number 3 is “yes,” can we change properties or mitigate exposure to make them safer?

These questions are the focus of research at the interagency level, as reflected in the *Strategy for Nanotechnology-Related Environmental, Health, and Safety Research*¹ published in February 2008 by the Subcommittee on Nanoscale Science, Engineering, and Technology (NSET) for the National Nanotechnology Initiative (NNI).

There is also much activity in the international arena. Two particularly active organizations are the International Standards Organization (ISO) and the Organization for Economic Cooperation and Development (OECD). Through its Technical Committee 229, the ISO has formed working groups to look at terminology and nomenclature; measurement and characterization; and health, safety, and environmental standards. Through its Working Party on Manufactured Nanomaterials, the OECD has in its two years of existence embarked on a number of activities, including building a database of nanotechnology research, comparing research strategies, and reviewing OECD chemical test guidelines for their applicability to nanomaterials. The most ambitious OECD activity is its new program to test 14 nanomaterials across dozens of health and environmental endpoints.

Looking at the benefits and potential impacts of nanotechnology is indeed an exciting and interesting endeavor, but it is more than that: it is about solving problems and answering questions so that maximum societal benefit, which means minimizing adverse impact, can be obtained from nanotechnology. This conference provides an excellent venue for discussing these issues. We have a lot to learn from one another: much good work has been done, as the presentation abstracts for this conference demonstrate. Yet there remains much more to if we are to better understand how to maximize the benefits of, and minimize any potential risks from, manufactured nanomaterials.

¹ Accessible at http://www.nano.gov/NNI_EHS_Research_Strategy.pdf

Save

Chapter 1 – Introduction

Using Nanomaterials for Remediation of Hazardous Substances

Jon Josephs, United States Environmental Protection Agency

Deborah Elcock, United States Department of Energy

Michael Gill, United States Environmental Protection Agency

Martha Otto, United States Environmental Protection Agency

Nancy Ruiz, United States Department of the Navy

The following chapter on remediation of soils, sediments and groundwater contains 22 papers and one abstract for platform and poster presentations. As reported in the overview paper by Barbara Karn and her co-authors entitled “In Situ Remediation: Nanotechnology’s Environmental Poster Child,” research in this area has been especially fruitful, leading to commercialization of nanotechnologies for site remediation. This paper noted that one EPA survey identified 34 sites in the United States and other countries where tests (and, in some cases, full-scale remediation) of nanotechnologies for site remediation, have been performed. Reflecting the importance of both research and practice in this area, the papers presented at this conference dealt with basic research studies, applied research and practical applications.

The chapter includes papers for two keynote addresses. Professor T. David Waite of the University of New South Wales in Australia spoke about his basic research on “Oxidative Transformations Mediated by Nanoparticulate Zero Valent Iron” (nZVI) during the first keynote address. Although nZVI has been used chiefly as a reducing agent, Dr. Waite has been a pioneer in investigating oxidative transformations mediated by nZVI. In his conference paper, he reported about studies using nZVI with and without stabilizers (starch, alginate and carboxymethylcellulose) to treat a model contaminant (formic acid). The results provided new insights and raised new questions for advancing the use of nZVI for promoting the oxidation of contaminants.

Professor Heechul Choi of the Gwangju Institute of Science and Technology in the Republic of Korea gave a keynote address entitled “Application of Nanomaterials for Environmental Remediation: Arsenic Removal by Nanoscale Zero-Valent Iron.” Dr. Choi described laboratory studies using sand columns containing nZVI to treat arsenic-contaminated water, including groundwater collected in Bangladesh and Nepal. The purpose of this research was to determine the feasibility of nZVI for treating water contaminated by arsenic in its trivalent and pentavalent forms. Reaction rates were rapid and insights were gained regarding the capacity of nZVI to bind arsenic and the mineral transformations involved.

Like the investigations described in the keynote addresses, nearly all of the papers in this chapter deal chiefly with nZVI. Basic research, applied research and commercial applications were

described. Many nZVI materials, several treatment approaches and many different contaminants were involved in the work that is described.

nZVI materials described in the papers include: silica/nZVI composites, palladized nZVI immobilized on activated carbon, nZVI stabilized with various substances to decrease aggregation and nZVI containing various doping agents (e.g., copper, nickel, palladium). In addition, commercially produced nZVI products from a number of manufacturers were used in some of the work described.

Treatment approaches include: nZVI mobilized by an electric field, nZVI contained in a semi-permeable membrane for water filtration and nZVI delivered to subsurface contamination in a vegetable oil emulsion.

Contaminants treated include: chlorinated solvents, nitrate, polychlorinated biphenyls (PCBs), hexavalent chromium, pentachlorophenol, arsenic and lindane.

Actual and planned site-specific applications of nZVI are described in a number of the papers. One paper describes a pilot-scale field test of nZVI injection to treat trichloroethene at a Superfund site in Goodyear, Arizona. Another describes a field test of emulsified nZVI to treat chlorinated solvents at the Marine Corps Recruit Depot site, Parris Island, South Carolina. There are four papers related to the feasibility of using nZVI for mending an existing permeable reactive barrier at the Department of Energy's Hanford, Washington, site.

Three of the papers did not focus on nZVI. One is about a field demonstration at a silver mining site where functionalized mesoporous sorbent was used for mercury removal. There are also papers about nanoscale titanium dioxide for treating arsenic and about dechlorination of PCBs by palladium/magnesium corrosion nano-cells. These two papers describe basic research studies.

After most of the platform presentations, there were question and answer (Q&A) discussions. This chapter also contains summaries of the Q&A discussions which were prepared by EPA contractor staff. These summaries have not been reviewed by the speakers or by the session chairpersons. In summarizing sometimes long and complicated questions, comments and answers, the summaries often have lost accuracy and detail. Nonetheless, the Q&A summaries do provide useful information about the audience reactions to the presentations.

Oxidative Transformations Mediated by Nanoparticulate Zero Valent Iron

T. David Waite and Quan Sun, School of Civil & Environmental Engineering,
University of New South Wales, Sydney, Australia

*Steven E. Mylon, Lafayette College, Department of Chemistry,
Lafayette College, Easton, Pennsylvania, U.S.A.*

Abstract

While there has been extensive investigation of the ability of zero valent iron (ZVI) to induce reductive transformations of contaminants, there has been much less study of oxidative transformations induced by nanosized ZVI (nZVI). In this presentation, current understanding of the mechanism by which nZVI-mediated oxidative transformations occur will be presented as will information on the chemical and biological impacts of these oxidative processes. Current state of knowledge concerning the factors controlling the rate and extent of nZVI-mediated oxidation will be described and recent studies of approaches to enhancing the oxidative ability of nZVI will be reviewed.

Introduction

Early studies of contaminant remediation using nZVI focused on the anoxic pathway for the reduction of potential contaminants such as chlorinated hydrocarbons [1, 2]. Recently however, there is evidence that nZVI may, under appropriate solution conditions, initiate the oxidative degradation of contaminants [3-6]. This pathway is particularly useful for the destruction of compounds such as organophosphates and organo-sulfides. Under oxic conditions, the oxidation of Fe^0 to Fe^{2+} is accompanied by the production of H_2O_2 from the reduction of O_2 . The resulting combination of H_2O_2 and Fe^{2+} (otherwise known as “Fenton’s reagent”) possesses strong oxidizing capability toward a variety of organic compounds that results from the production of hydroxyl radicals upon the oxidation of ferrous iron by H_2O_2 .

Development of a kinetic model that adequately describes the key steps in the overall reaction mechanism is important in both validating our conceptual understanding of the process and in optimization of the process. To this end, we chose to employ Fe^0 in the oxidation of very dilute solutions of the simple model compound, formic acid. Formic acid was chosen because of its very simple oxidative degradation pathway [7], the previous success in modeling this degradation via the Fenton process, and the ease of examination of its degradation at submicromolar concentrations through use of radiolabelled formic acid [8].

As a first attempt at optimizing the oxidizing capacity of Fe^0 , we chose to functionalize the nZVI with the high molecular weight (HMW) organic polymers, starch, carboxy methyl cellulose (CMC), and alginate. Functionalization by any of these HMW compounds is expected to produce a steric/electrosteric barrier to aggregation of the nZVI [9-11], and thus increase the effective reactive surface area though the impact of this process on nZVI reactivity is unclear. In ad-

dition to elucidating the impact on reactivity of surface functionalization, clarifying key reaction steps involved in oxidative degradation of solution species constituted an important goal of this investigation. Other approaches to increasing the oxidizing capacity of nZVI will be overviewed in the presentation.

Methods

Nanoparticle Synthesis

Nano-sized zero valent iron particles were synthesized through the reduction of ferrous iron ($\text{FeCl}_2 \cdot 4\text{H}_2\text{O}$, 99%, Sigma) in the presence of sodium dithionate ($\text{Na}_2\text{S}_2\text{O}_4$, 85% purity, Sigma) [12]. This process requires a high solution pH which was accomplished through the addition of NaOH (Ajax Finechem). Alginate as alginic acid (Sigma-Aldrich), starch (Sigma-Aldrich) and carboxymethylcellulose (CMC, Sigma-Aldrich) were employed as stabilizers to the nZVI. In each case, the appropriate amount of stabilizer (0.3% w/w for starch, 0.1% w/w for CMC and 0.1 %w/w for alginate) was added to the ferrous iron solution prior to reduction with sodium dithionate. After synthesis, the particles were centrifuged, the supernatant disposed of, and the particles were washed in a dilute solution of HCl (pH = 4). This washing cycle was performed three times in all cases. All experiments were conducted within 24 hours of nanoparticle synthesis in order to avoid the effects of oxidation of primary stock solutions.

Experimental Setup and Analytical Methods

All experiments were carried out at controlled temperature ($25 \pm 0.5^\circ\text{C}$) in a 250 mL water jacketed beaker that was covered in aluminum foil. During the reactions, the samples were continuously sparged with O_2 gas in order to maintain a constant O_2 (aq) concentration in solution. The pH of the reaction solution was maintained at 3.0 ± 0.1 through the drop-wise addition of dilute solutions of HCl (aq) or NaOH (aq). At the start of each reaction, the appropriate amount of nZVI was added to the reaction vessel containing 200 nM of 14-C labeled formic acid (Sigma Aldrich). An nZVI concentration of 0.5 g/L was used in all investigations reported here. A sample was taken immediately after the addition of nZVI which corresponded to the time-point T_0 and at regular intervals after this for 90 minutes. At each time-point, 5.0 mL of sample were drawn from the beaker. To suppress the Fenton reaction in each sample, 1.0 mL of a phosphate buffered (pH 6.3) EDTA solution (0.5 M EDTA) (Sigma-Aldrich) was added to the sample. The sample was centrifuged (Clements 2000) for a minimum of 2 minutes at 3500 rpm. After the centrifugation, 1.0 mL of the solution was withdrawn for analysis in a scintillation counter (14-C analysis) and an appropriate amount of sample was added to a phosphate buffered solution for H_2O_2 analysis. Replicates of all experiments were performed.

Scintillation Analysis for 14-C Quantification

A 1.0 mL aliquot of the centrifuged reaction sample was added to a scintillation vial (Whatman) followed by two drops of concentrated HCl to decrease the solution pH. The resulting solution was sparged with air for a minimum of 30 sec in order to drive off the dissolved $^{14}\text{C}\text{-CO}_2$. After sparging, 10.0 mL of scintillation fluid was added to the vial and the concentration of 14-C remaining was quantified by scintillation counting.

Hydrogen Peroxide Quantification

Hydrogen peroxide produced from the two electron reduction of oxygen was measured by a fluorescence technique using amplex red (AR) and horseradish peroxidase (HRP) as reagents. H_2O_2 in the presence of HRP reacts with amplex red with 1:1 stoichiometry to produce fluorescent resorufin which has absorption and fluorescence emission maxima at 563 and 587 nm respectively [13]. Excitation/emission spectra were acquired on a Cary spectrofluorimeter. Emission intensities at 587 nm were compared against linear calibration curves generated from H_2O_2 standards.

Fe(II) quantification

Fe^{2+} concentrations were measured with the ferrozine reagent. Samples (50 μl) were taken from the reaction vessel and added to test tubes containing 5.95 ml of phosphate buffer (pH 6.3) containing 200 μM of the ferrozine reagent. The concentration of Fe^{2+} -Ferrozine complex were determined from absorbance readings at 562 nm (Cary 50).

Kinetic Modeling

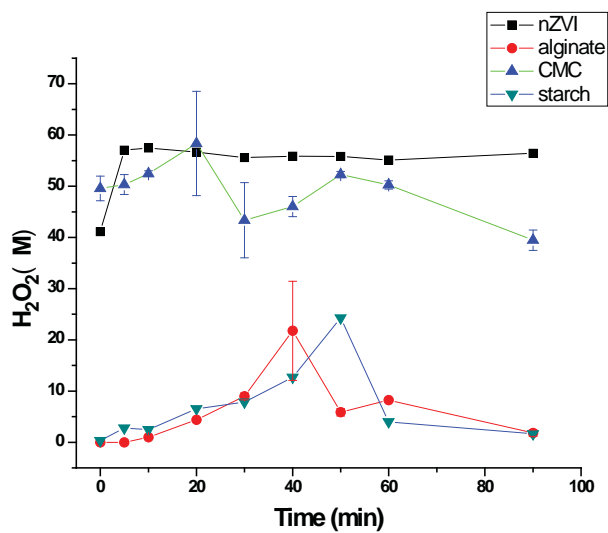
Model simulations were undertaken using the kinetic modeling software Kintecus [14]. Table 1 describes the reaction set used as input for the program. This reaction scheme (Table 1) has been shown to effectively simulate the homogeneous oxidation of formic acid in the presence of Fe^{2+} and H_2O_2 . [15, 16]. Sensitivity analysis used to simplify the conceptual model for the heterogeneous oxidation of formic acid employed the software Atropos [17].

Table 1. Kinetic Model for Formic Acid Oxidation using Fenton's Reagent at pH =3.

Reaction	Rate Constant ($\text{M}^{-1}\text{s}^{-1}$)
$\text{Fe}^{2+}(\text{aq}) + \text{H}_2\text{O}_2(\text{aq}) \longrightarrow \text{Fe}^{3+}(\text{aq}) + \text{OH}^{\cdot}(\text{aq}) + \text{OH}^{-}(\text{aq})$	55
$\text{Fe}^{3+}(\text{aq}) + \text{H}_2\text{O}_2(\text{aq}) \longrightarrow \text{Fe}^{2+}(\text{aq}) + \text{HO}_2^{\cdot}(\text{aq}) + \text{H}^{+}(\text{aq})$	2.00×10^{-3}
$\text{Fe}^{2+}(\text{aq}) + \text{OH}^{\cdot}(\text{aq}) \longrightarrow \text{Fe}^{3+}(\text{aq}) + \text{OH}^{-}(\text{aq})$	3.2×10^8
$\text{Fe}^{3+}(\text{aq}) + \text{HO}_2^{\cdot}(\text{aq}) \longrightarrow \text{Fe}^{2+}(\text{aq}) + \text{O}_2(\text{aq}) + \text{H}^{+}$	7.82×10^5
$\text{Fe}^{2+}(\text{aq}) + \text{HO}_2^{\cdot}(\text{aq}) \longrightarrow \text{Fe}^{3+}(\text{aq}) + \text{H}_2\text{O}_2(\text{aq})$	1.34×10^6
$\text{HO}_2^{\cdot}(\text{aq}) + \text{HO}_2^{\cdot}(\text{aq}) \longrightarrow \text{H}_2\text{O}_2(\text{aq}) + \text{O}_2(\text{aq})$	2.33×10^6
$\text{H}_2\text{O}_2(\text{aq}) + \text{OH}^{\cdot}(\text{aq}) \longrightarrow \text{HO}_2^{\cdot}(\text{aq}) + \text{H}_2\text{O}(\text{l})$	3.3×10^7
$\text{HO}^{\cdot}(\text{aq}) + \text{HO}_2^{\cdot}(\text{aq}) \longrightarrow \text{H}_2\text{O}(\text{aq}) + \text{O}_2(\text{aq})$	7.15×10^9
$\text{HO}^{\cdot}(\text{aq}) + \text{HO}^{\cdot}(\text{aq}) \longrightarrow \text{H}_2\text{O}_2(\text{aq})$	5.2×10^9
$\text{HO}^{\cdot}(\text{aq}) + \text{HCOOH} / \text{HCOO}^{-}(\text{aq}) \longrightarrow \text{CO}_2(\text{aq}) + \text{HO}_2^{\cdot}(\text{aq})$	6.5×10^8

Results

A)



B

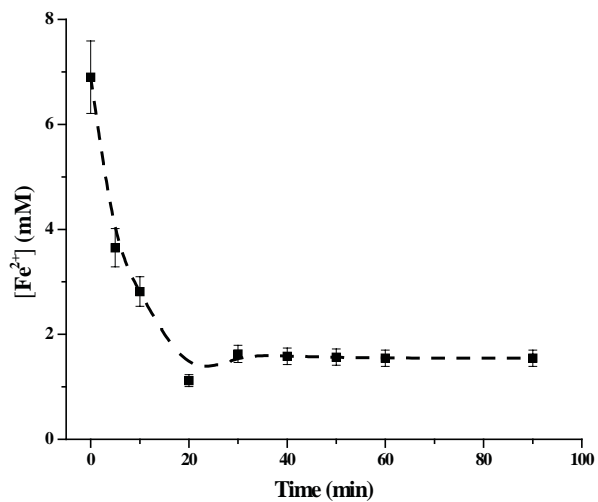


Figure 1. A) Hydrogen peroxide concentrations as a function of time for experiments run with bare nZVI (squares), alginate functionalized nZVI (circles), CMC functionalized nZVI (triangles) and starch functionalized nZVI (reverse triangles). B) Typical Fe^{2+} profile for the reaction of nZVI with O_2 . The dashed line is drawn only as a guide.

The production of both Fe^{2+} and H_2O_2 after the addition of nZVI to acidic oxygen saturated aqueous solutions occurs on time scales too fast to resolve using the sampling techniques described above. For this reason, concentrations of both Fe^{2+} and H_2O_2 at T_0 are always greater than zero despite not having added either to the reaction vessel (Figure 1A and B).

For the bare (unfunctionalized) nanoparticles, the H_2O_2 concentrations rapidly attained a near constant value of around 60 μM which was maintained over the course of each 90 minute experiment.

The concentrations of H_2O_2 produced by the three types of organic functionalized nZVI particles are compared in Figure 1 with that produced for the bare particles. While the maximum nitration of peroxide produced by the CMC functionalized particles is similar to that produced by the bare particles (and around 60 mM), the amounts produced by the starch and alginate coated nZVI particles are substantially less at around 25 mM. Interestingly, the production of H_2O_2 by the functionalized nZVI particles is a more gradual process than is the case for bare nZVI. In the case of starch and alginate coated nZVI, peak H_2O_2 concentrations were not reached until *ca.* 40 minutes after the reaction commenced. As described in the Methods section, 14-C labeled formic acid (200 nM) was used as a probe for oxidation in this study both because of the simplicity of the oxidation process and the existence of a workable model of the process. For the case of bare nZVI, after 90 minutes, we observed a loss of *ca.* 12% of the formic acid with most occurring within the first 20 minutes of the reaction (figure 2). For starch, CMC and alginate functionalized nanoparticles, *ca.* 12%, *ca.* 10% and *ca.* 12% of the 14-C labeled formic acid was lost due to oxidation (figure 3). In the starch and alginate functionalized systems, the greatest rate of formic acid oxidation appeared to coincide with peak H_2O_2 concentrations.

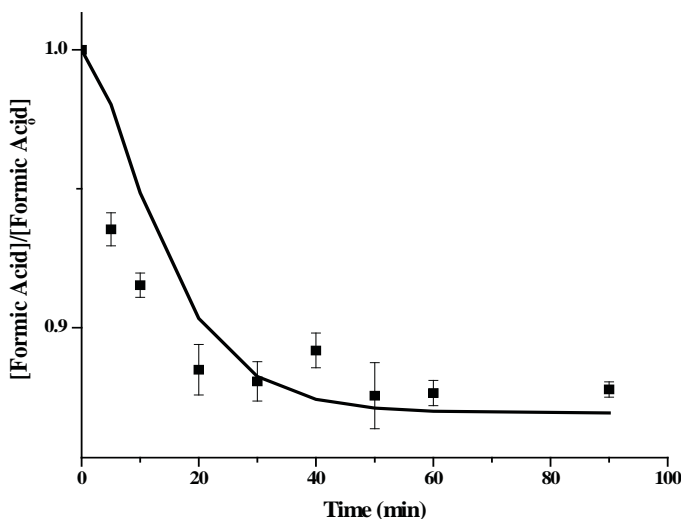
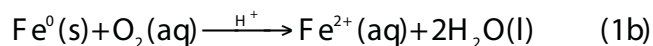
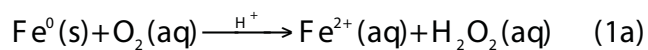


Figure 2. Experimental (squares) results demonstrating the oxidation of formic acid (initial concentration 200 nM) in the presence of nZVI (0.5 g/L) at pH = 3.0. The solid line is the best fit to a model that conceptualizes the heterogeneous reactions that result in the oxidation of Fe^0 by dissolved oxygen and the heterogeneous loss of OH^\cdot and H_2O_2 .

Discussion

Reactive Oxygen Species Generation by nZVI in Oxygen Saturated Solutions

The heterogeneous oxidation of Fe^0 that occurs upon its addition to acidic oxygen saturated aqueous solutions results in the formation of the aquated Fe^{2+} cation and either hydrogen peroxide or water or according to either equation 1a or 1b respectively.



The products of reaction 1a (Fenton's reagent) can further react according to equation 2 to form hydroxyl radicals.

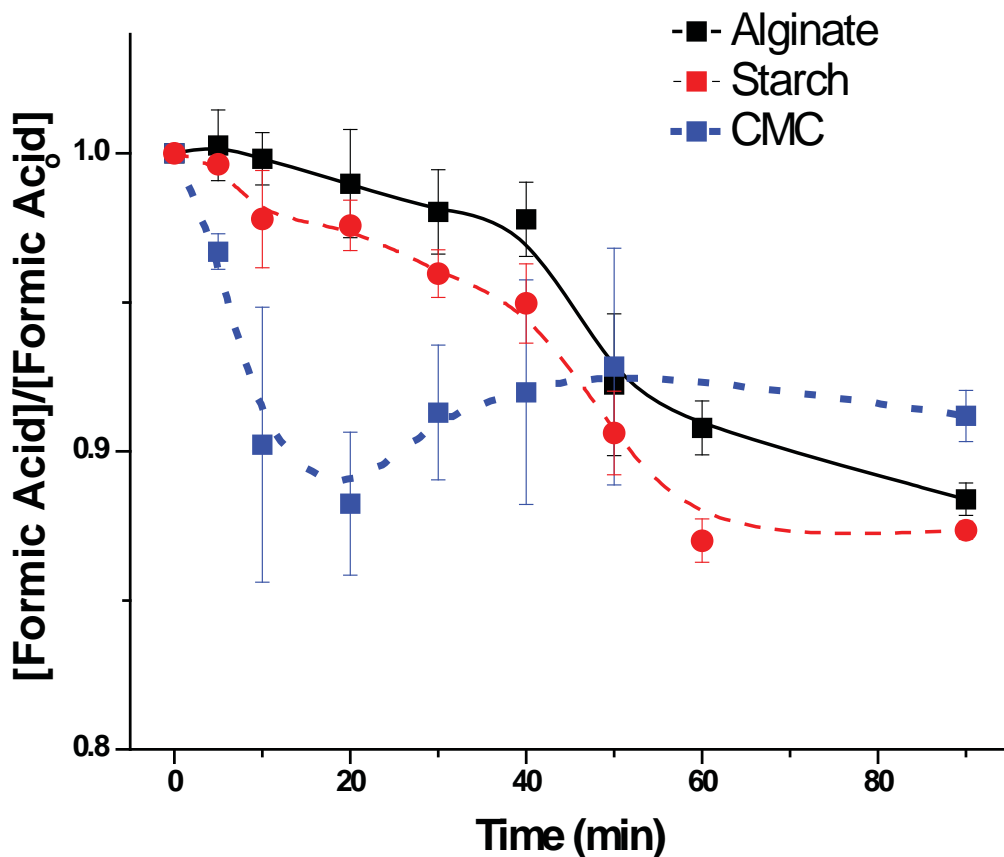
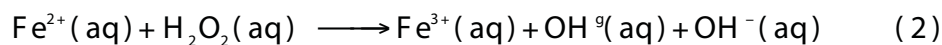


Figure 3. Loss of $^{14}\text{COOH}$ after the application of functionalized nZVI. When functionalized with either starch or alginate, the rate of $^{14}\text{COOH}$ appears to coincide with the peak H_2O_2 concentrations seen in figure 1.

At pH 3, our working model describing the Fenton mechanism in the presence of the target compound (14-C labeled formic acid) is detailed in Table 1 with the appropriate rate constants included [7].

Only the homogeneous reactions in a system in which Fe(II), H₂O₂ and HCOOH are the initial reactants are given in Table 1. Despite the initial pulse of both Fe(II) and H₂O₂ generated upon the addition of nZVI to the reaction mixture, our attempts to apply the complete kinetic model shown in Table 1 to the oxidation of formic acid by nZVI demonstrates were not successful. The homogeneous model for the Fenton process drastically overestimates the extent of formic acid oxidation beginning with the T0 concentrations for both Fe²⁺ and H₂O₂.

While no definitive explanation is evident, we could conclude that: 1) the heterogeneous degradation of H₂O₂ by Fe⁰ has been omitted and/or 2) the heterogeneous reaction between Fe⁰ and OH[•] has been omitted. Given the efficiency of the Fenton process in the homogeneous reaction, it appears quite likely that these heterogeneous reactions result in the loss of H₂O₂ or OH[•] and thus out-compete the Fenton reaction and the oxidation of formic acid by OH[•]. One possible reason for this is that reaction 2 occurs at or in the vicinity of the Fe(0) surface followed by the fast surface mediated loss of OH[•].

To substantiate this hypothesis, we constructed a conceptual kinetic model that attempts to account for the heterogeneous processes that are missing in the homogeneous Fenton model. Specifically, this model includes the two electron oxidation of Fe⁰ by O₂ that yields Fe²⁺ and H₂O₂ (*reaction 1a*) and the heterogeneous loss of both OH[•] and H₂O₂ on the nZVI surface:

We accounted for the diffusion of both Fe²⁺ and H₂O₂ to the bulk solution where they can react according to the homogeneous Fenton model. A key assumption required to model this process is concentration of reactive Fe⁰. From transmission electron microscopy (TEM) images (not shown), a reasonable estimate of the diameter of the quasi spherical nZVI particles is 40 nm. Based on this, the initial particle concentration in our reactions was *ca.* 2x10¹⁵/ liter. After calculating particle surface area for nZVI and the area of one face of an average iron unit cell, we deduced that a reasonable estimation of the initial concentration of Fe⁰ sites in the solution, was on the order of 800 μM.

Using our estimated value for the initial reactive site concentration for Fe⁰ Figure 2 shows that our conceptual model for the oxidation of formic acid fits the data quite well while only requiring the optimization of three rate different constants for new reactions in the model. The three reactions included with the Fenton model are: 1) the heterogeneous two electron oxidation of Fe⁰ by O₂ yielding Fe²⁺ and H₂O₂, 2) the diffusion of Fe²⁺ to the bulk solution, and 3) the diffusion of H₂O₂ to the bulk solution. Our model presupposes that only OH[•] formed in the bulk is available to oxidize HCOOH. The fact that the concentration profile for formic acid oxidation using nZVI in our batch reactor is modeled quite well (Figure 3) validates, to a first approximation, our conceptual model describing the factors that limit the complete oxidation of formic acid in our system.

Effects of High Molecular Weight Organic Molecules as Capping Agents for nZVI

Because of the absence of repulsive surface charge, the iron nanoparticles formed during the synthesis of nZVI are known to aggregate. Laser light diffraction measurements on suspended nZVI

solutions demonstrated a nearly normal distribution about a mean particle diameter of ca 7.7 μm (data not shown). Transmission Electron Microscopy confirmed the existence of large aggregate made up of nanoparticles (primary particles) on the order of 20 nm in diameter

The functionalization of nZVI with starch, CMC or alginate had nearly the same effect on the oxidation of formic acid model system. For starch, CMC and alginate functionalized nanoparticles, *ca.* 12%, *ca.* 10% and *ca.* 12% of the 14-C labeled formic acid was lost due to oxidation (Figure 3). Thus there was no significant enhancement of the oxidative capacity of nZVI when using any of these functionalization schemes. While functionalized nZVI have demonstrated enhanced reductive capacity compared to the bare nZVI, Joo and Zhao [6] showed that functionalization of nZVI with CMC inhibits the oxidation of lindane and atrazine. They attributed this to the additional pathway for OH^\bullet consumption because hydroxyl radicals are known to react with C-C bonds within the organic polymers. All three systems appeared to show similar loss of formic acid over the 90 minutes that the reaction was monitored. However, the kinetics of formic acid oxidation in each case differed from the system where bare nZVI alone were employed. Figure 3 illustrates the time profile for the oxidation of formic acid when functionalized nZVI were employed. When alginate and starch were used to functionalize the nZVI, there was a lag in the loss of formic acid which is probably due to the difficulty of dissolved oxygen in accessing the nZVI surface. As one might expect, this lag corresponds to a lag in H_2O_2 production in both cases. The concentration of H_2O_2 reached a maximum almost immediately in the system where bare nZVI was used, and this was clearly not the case for the alginate and starch systems.

The CMC system appears to be more similar to the bare nZVI system than either the alginate or starch systems which is most likely due to differences in surface coverage rather than specific differences in the chemistry or reactivity of the capping agent in the presence of H_2O_2 or hydroxyl radicals. The average molecular weight (M_w) for CMC is *ca.* 90,000 Da while that of alginate is 35,000 Da. It seems apparent that at the concentrations of each organic stabilizer (0.3% w/w for starch, 0.1% w/w for CMC and 0.1 %w/w for alginate) access to the surface by O_2 is not inhibited compared to the case of unfunctionalized nZVI. Despite the differences in the kinetics of formic acid oxidation, the net loss of formic acid in the three systems is nearly the same. Whether this lag in peak H_2O_2 production and concomitant formic acid oxidation can be exploited to increase the net oxidative capacity of nZVI through changes in the degree of functionalization or by altering solution remains a question for future study.

References

1. Tratnyek, P.G. (1996) Putting corrosion to use: Remediation of contaminated groundwater with zero-valent metals. *Chemistry & Industry* 13, 499-503.
2. Tratnyek, P.G., et al. (2001) Effects of natural organic matter, anthropogenic surfactants, and model quinones on the reduction of contaminants by zero-valent iron. *Water Research* **35**(18), 4435-4443.
3. Feitz, A.J., et al. (2005) Oxidative transformation of contaminants using colloidal zero-valent iron. *Colloids and Surfaces a-Physicochemical and Engineering Aspects* **265**(1-3), 88-94.
4. Joo, S.H., et al., Quantification of the oxidizing capacity of nanoparticulate zero-valent iron. *Environmental Science & Technology*, 2005. **39**(5): p. 1263-1268.

5. Joo, S.H., A.J. Feitz, and T.D. Waite (2004) Oxidative degradation of the carbothioate herbicide, molinate, using nanoscale zero-valent iron. *Environmental Science & Technology* **38**(7), 2242-2247.
6. Joo, S.H. and D. Zhao (2008) Destruction of lindane and atrazine using stabilized iron nanoparticles under aerobic and anaerobic conditions: Effects of catalyst and stabilizer. *Chemosphere* **70**(3), 418-425.
7. Duesterberg, C.K., W.J. Cooper, and T.D. Waite (2005) Fenton-mediated oxidation in the presence and absence of oxygen. *Environmental Science & Technology* **39**(13), 5052-5058.
8. Kwan, W.P. and B.M. Voelker (2004) Influence of Electrostatics on the Oxidation Rates of Organic Compounds in Heterogeneous Fenton Systems. *Environ. Sci. Technol.* **38**(12), 3425-3431.
9. He, F. and D. Zhao (2007) Manipulating the Size and Dispersibility of Zerovalent Iron Nanoparticles by Use of Carboxymethyl Cellulose Stabilizers. *Environ. Sci. Technol.* **41**(17), 6216-6221.
10. He, F. and D.Y. Zhao (2005) Preparation and characterization of a new class of starch-stabilized bimetallic nanoparticles for degradation of chlorinated hydrocarbons in water. *Environmental Science & Technology* **39**(9), 3314-3320.
11. Chen, K.L., S.E. Mylon, and M. Elimelech (2006) Aggregation kinetics of alginate-coated hematite nanoparticles in monovalent and divalent electrolytes. *Environmental Science & Technology* **40**(5), 1516-1523.
12. Sun, Q., et al. (2008) Comparison of the reactivity of nanosized zero valent iron (nZVI) particles produced by borohydride and dithionite reduction of iron salts. *NANO* (in press).
13. Garg, S., A.L. Rose, and T.D. Waite (2007) Production of reactive oxygen species on photolysis of dilute aqueous quinone solutions. *Photochemistry and Photobiology* **83**(4), 904-913.
14. Ianni, J.C., (2005) Kintecus.
15. Duesterberg, C.K., W.J. Cooper, and T.D. Waite, (2005) Fenton-Mediated Oxidation in the Presence and Absence of Oxygen. *Environmental Science and Technology* **39**(13), 5052-5058.
16. Kwan, W.P. and B.M. Voelker (2002) Decomposition of Hydrogen Peroxide and Organic Compounds in the Presence of Dissolved Iron and Ferrihydrite. *Environmental Science and Technology* **36**(7), 1467-1476.
17. Ianni, J.C. (2003) Atropos.

Save

Application of Nanomaterials for Environmental Remediation: Arsenic removal by Nano-scale Zero Valent Iron

*Heechul Choi, Department of Environmental Science and Engineering,
Gwangju Institute of Science and Technology, Republic of Korea*

Abstract

Nanoscale zero-valent iron (NZVI) was synthesized and tested for the removal of As(III) and As(V), which are highly toxic, mobile, and predominant arsenic species in anoxic groundwater. SEM-EDX, AFM, and XRD were used to characterize particle size, surface morphology, and corrosion layers formed on pristine NZVI and As-treated NZVI. XRD and SEM results revealed that NZVI gradually converted to magnetite/maghemite corrosion products mixed with lepidocrocite. The HR-TEM study of pristine NZVI showed a core-shell-like structure, where more than 90% of nano particles were under 30 nm in diameter. Mossbauer spectroscopy further confirmed its structure in which 19% were in zero-valent state with outer cluster of 81% iron oxides. As(III) adsorption kinetics were rapid and occurred on a scale of minutes following a pseudo-first-order rate expression. The observed reaction rate constants are about 1000 times higher than literature values for As(III) adsorption on micron ZVI. Batch experiments were performed to determine the feasibility of NZVI as an adsorbent for As treatment in groundwater. Freundlich adsorption isotherm was applied to fit the sorption data. The effects of competing anions revealed that HCO_3^- , H_4SiO_4^0 , and $\text{H}_2\text{PO}_4^{2-}$ are potential interferences in the As adsorption. Our results suggest that NZVI is a suitable candidate for both in-situ and ex-situ groundwater treatment due to its high reactivity.

Introduction

Arsenic (As) is well known as one of strongest carcinogenic compounds and one of biggest environmental issues for water treatment and groundwater remediation. It is naturally present in water in different oxidation states and acid-base species depending on redox and pH conditions [Ferguson and Gavis (1972)]. Arsenic has been introduced into the environment through a combination of natural processes (weathering reactions, biological activities, and volcanic emissions) as well as anthropogenic activities [Smedley and Kinniburgh (2002)]. The natural occurrence of As in groundwater is of great concern due to the toxicity of As and the potential for chronic exposure [Anderson and Bruland (1991), Sanjeev and Malay (1999)]. To limit and control the effect of As in natural water system, EPA has set the arsenic standard for drinking water at 0.01 parts per million (10 parts per billion) to protect consumers served by public water systems from the effects of long-term, chronic exposure to arsenic.

In groundwater, As exists as inorganic arsenite, As(III) (H_3AsO_3 , H_2AsO_3^- , HAsO_3^{2-}), and arsenate, As(V) (H_3AsO_4 , H_2AsO_4^- , HAsO_4^{2-}) [Ferguson and Gavis (1972), Manning et al. (2002)]. The As(III) species remains protonated as HAsO_3^0 at pH below 9.2 [Smith et al. (1992), Tseng et al. (1968)], whereas the As(V) species exists as oxyanions (H_2AsO_4^- , HAsO_4^{2-}) at neutral pH. More-

over, the formation of As(III) species is favored in soil and groundwater with low redox potential whereas As(V) exists at a redox potential above 100 mV and in an oxidizing environment [Smith et al. (1992)].

Many methods are currently in use for removing As from drinking water supplies including anion exchange, reverse osmosis, lime softening, microbial transformation, chemical precipitation, and adsorption [Ferguson and Gavis (1972), Monique Bissen (2003)]. Recently, the versatility of nanoscale zero-valent iron (NZVI) material has been demonstrated for potential use in environmental engineering [Wang and Zhang (1997)]. Additionally, the attention has been focused on As(III) and As(V) removal using NZVI in the subsurface environment [Kanel et al. (2006), Kanel et al. (2005)]. The As(III) removal mechanism is mainly due to spontaneous adsorption and co-precipitation of As(III) with iron(II) and iron(III) oxides/hydroxides, which form in-situ during ZVI oxidation (corrosion) [Manning et al. (2002), Farrell et al. (2001), Ponder et al. (2000), Su and Puls (2001a, b)]. Due to the extremely small particle size, large surface area, and high in-situ reactivity, these materials have great potential in a wide array of environmental applications such as soil, sediment, and groundwater remediation [Ponder et al. (2000), Hsing-Lung and Wei-xian (1999)]. In addition, due to small size and capacity to remain in suspension, NZVI can be transported effectively by groundwater [Zhang (2003)] and can be injected as sub-colloidal metal particles into contaminated soils, sediments, and aquifers [Hsing-Lung and Wei-xian (1999), Cantrell and Kaplan (1997)].

Methods

The chemical reagents used in the study (NaAsO_2 , HCl, NaOH, NaH_2PO_4 , KI, and NaBH_4) were reagent grade obtained from Aldrich Chemical Co. In some experiments, groundwater from Bangladesh and Nepal were used (pH = 6.5–7.0) with total alkalinity, dissolved organic carbon (DOC), iron (Fe^{2+}), sulfate (SO_4^{2-}), and phosphate ($\text{H}_2\text{PO}_4^{2-}$), respectively [Mukherjee and Bhattacharya (2001)]. The groundwater samples were collected in 50 mL polypropylene flasks and acidified with 1 mL of concentrated HNO_3 for cation analyses on site. Replicate samples used for anion analyses were filtered with a 0.45- μm membrane and not acidified following the method reported by Berg et al. [Berg et al. (2001)]. All the experiments were performed in 0.01 M NaCl background solution of As(III). The NZVI material was synthesized by dropwise addition of 1.6 M NaBH_4 aqueous solution to a Ne gas-purged 1 M $\text{FeCl}_3 \cdot 6\text{H}_2\text{O}$ aqueous solution at around 23°C with magnetic stirring as described by Wang and Zhang.

Results and Discussion

Solid samples collected from pristine NZVI and 100 mg/L As(III)-treated NZVI after 7, 30, and 60 days and imaged by SEM are shown in Figure 1a-d. Synthetic NZVI particles were in the size range of 10-100 nm as measured by SEM. Adsorption of As causes increases in particle aggregation due to iron (III) oxide/hydroxide precipitation as time elapsed for over 2 months period. SEM images clearly reveals a growth of a fine needle-like crystallite, which transform to an apparent amorphous phase. The thin crystallites (about 100 nm long by 20 nm wide) are energetically unstable and disappear to be replaced by more stable phases according to the Gay-Lussac-Oswald ripening rule.

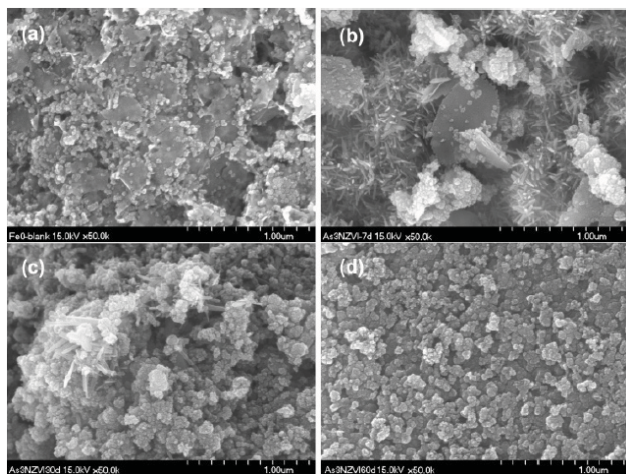


Figure 1. SEM image of pristine NZVI (a) and As(III) sorbed on NZVI for 7 (b) , 30 (c), and 60 d (d), respectively. Reaction conditions: 100 mg/L As(III) adsorbed on 50 g/L NZVI in 0.01 M NaCl at pH 7, 25 °C.

The XRD analysis of NZVI, commercial ZVI (Kanto Chemical Co.) and As(III)-treated NZVI samples are compared after reaction during 1, 7, 30, and 60 days (Figure 2). The zero valence state and crystalline structure of NZVI were confirmed when comparing with Kanto Chemical Co. ZVI material. X-ray diffractograms demonstrate that the NZVI corrosion products are a mixture of amorphous iron(III) oxide/hydroxide, magnetite (Fe_3O_4), and/or maghemite ($\gamma\text{-Fe}_2\text{O}_3$), and lepidocrocite ($\gamma\text{-FeOOH}$). These Fe(II)/(III) and Fe(III) corrosion products indicate that Fe (II) formation is an intermediate step in the NZVI corrosion process. In the 24-h reaction product, an amorphous domain is seen among magnetite, lepidocrocite peaks, and a predominant ZVI (Fe^0) peak. Amorphous products were replaced by magnetite and lepidocrocite over a 2-month period. After 60 days, the As(III)-NZVI corrosion product had predominantly magnetite and lepidocrocite crystalline composition. Similar results were reported by Manning et al. in corrosion products from ZVI powder.

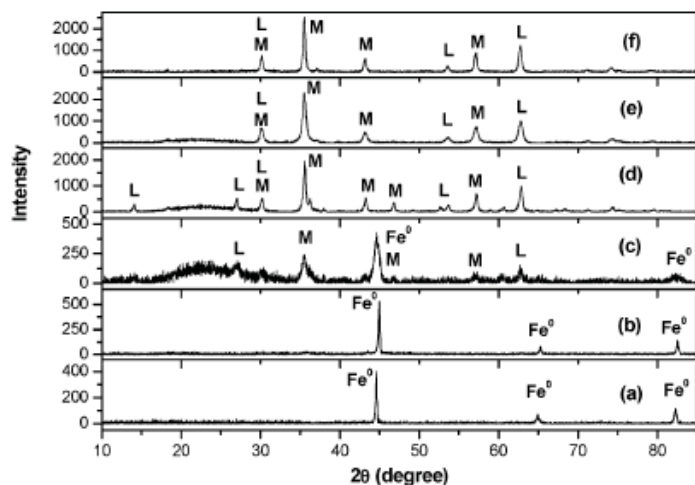


Figure 2. X-ray diffraction analysis of NZVI, commercial ZVI (Kanto Chemical Co.) (a), pris-

tine NZVI (b), and 100 mg/L As(III) sorbed on 50 g/L NZVI in 0.01 M NaCl for 1(c), 7 (d), 30 (e), and 60 d (f), respectively. Peaks are due to magnetite/maghemite (M) ($\text{Fe}_3\text{O}_4/\gamma\text{-Fe}_2\text{O}_3$), lepidocrocite ($\gamma\text{-FeOOH}$) (L), and NZVI (Fe^0), respectively.

As(III) adsorption kinetics were rapid and occurred on a scale of minutes following a pseudo-first-order rate expression. The observed reaction rate constants are about 1000 times higher than literature values for As(III) adsorption on micron ZVI.

Conclusion

NZVI has applicability in ex-situ as well as in-situ remediation of pollutants including arsenic. NZVI can be used to remediate pollutants already present in soil and groundwater. In addition, NZVI promotes anaerobic microbial growth in the subsurface by increasing pH, decreasing redox potential, producing hydrogen gas, and releasing ferrous iron. We have presented evidence that As(III) can be removed by adsorption on NZVI on a minute time scale. As(III) strongly sorbs on NZVI in a wide range of pH, and various As(III) and As(V) coprecipitates on iron(III) oxide/hydroxide corrosion products are involved. Engineering studies to develop this NZVI technology are currently going on in our laboratory. The results of this study show that NZVI is an efficient material for the treatment of As(III) and may be used in a permeable reactive barrier as well as for ex-situ groundwater treatment.

References

- Ferguson, J.F. and Gavis, J. (1972) "A review of the arsenic cycle in natural waters." *Water Res.* 6(11), 1259-1274.
- Smedley, P.L. and Kinniburgh, D.G. (2002) "A review of the source, behaviour and distribution of arsenic in natural waters." *Applied Geochemistry* 17(5), 517-568.
- Anderson, L.C.D. and Bruland, K.W. (1991) "Biogeochemistry of arsenic in natural waters: the importance of methylated species." *Environ. Sci. Technol.* 25(3), 420-427.
- Sanjeev, B. and Malay, C. (1999) "Removal of Arsenic from Ground Water by Manganese Dioxide--Coated Sand." *J. Environ. Eng.* 125(8), 782-784.
- Manning, B.A., Hunt, M.L., Amrhein, C. and Yarmoff, J.A. (2002) "Arsenic(III) and Arsenic(V) Reactions with Zerovalent Iron Corrosion Products." *Environ. Sci. Technol.* 36(24), 5455-5461.
- Smith, A.H., Hopenhayn-Rich, C., Bates, M.N., Goeden, H.M., Hertz-Picciotto, I., Duggan, H.M., Wood, R., Kosnett, M.J. and Smith, M.T. (1992) "Cancer risks from arsenic in drinking water." *Environ. Health Perspect.* 97, 259-267.
- Tseng, W.P., Chu, H.M., How, S.W., Fong, J.M., Lin, C.S. and Yeh, S.J. (1968) "Prevalence of skin cancer in an endemic area of chronic arsenism in Taiwan." *J. Natl. Cancer Inst.* 40, 453-463.
- Monique Bissen, F.H.F. (2003) "Arsenic—a Review. Part II: Oxidation of Arsenic and its Removal in Water Treatment." *Acta Hydrochim. Hydrobiol.* 31(2), 97-107.
- Wang, C.B. and Zhang, W.X. (1997) "Synthesizing nanoscale iron particles for rapid and complete dechlorination of TCE and PCBs." *Environ. Sci. Technol.* 31(7), 2154-2156.

- Kanel, S.R., Greneche, J.M. and Choi, H. (2006) "Arsenic(V) Removal from Groundwater Using Nano Scale Zero-Valent Iron as a Colloidal Reactive Barrier Material." *Environ. Sci. Technol.* 40(6), 2045-2050.
- Kanel, S.R., Manning, B., Charlet, L. and Choi, H. (2005) "Removal of Arsenic(III) from Groundwater by Nanoscale Zero-Valent Iron." *Environ. Sci. Technol.* 39(5), 1291-1298.
- Farrell, J., Wang, J., O'Day, P. and Conklin, M. (2001) "Electrochemical and Spectroscopic Study of Arsenate Removal from Water Using Zero-Valent Iron Media." *Environ. Sci. Technol.* 35(10), 2026-2032.
- Ponder, S.M., Darab, J.G. and Mallouk, T.E. (2000) "Remediation of Cr(VI) and Pb(II) Aqueous Solutions Using Supported, Nanoscale Zero-valent Iron." *Environ. Sci. Technol.* 34(12), 2564-2569.
- Su, C. and Puls, R.W. (2001a) "Arsenate and Arsenite Removal by Zerovalent Iron: Effects of Phosphate, Silicate, Carbonate, Borate, Sulfate, Chromate, Molybdate, and Nitrate, Relative to Chloride." *Environ. Sci. Technol.* 35(22), 4562-4568.
- Su, C. and Puls, R.W. (2001b) "Arsenate and Arsenite Removal by Zerovalent Iron: Kinetics, Redox Transformation, and Implications for in Situ Groundwater Remediation." *Environ. Sci. Technol.* 35(7), 1487-1492.
- Hsing-Lung, L. and Wei-xian, Z. (1999) "Transformation of Chlorinated Methanes by Nanoscale Iron Particles." *J. Environ. Eng.* 125(11), 1042-1047.
- Zhang, W.-x. (2003) "Nanoscale Iron Particles for Environmental Remediation: An Overview." *J. Nanopart. Res.* 5(3), 323-332.
- Cantrell, K.J. and Kaplan, D.I. (1997) "Zero-Valent Iron Colloid Emplacement in Sand Columns." *J. Environ. Eng.* 123(5), 499-505.
- Mukherjee, A.B. and Bhattacharya, P. (2001) "Arsenic in groundwater in the Bengal Delta Plain: Slow poisoning in Bangladesh." *Environ. Rev.* 9, 189-220.
- Berg, M., Tran, H.C., Nguyen, T.C., Pham, H.V., Schertenleib, R. and Giger, W. (2001) "Arsenic Contamination of Groundwater and Drinking Water in Vietnam: A Human Health Threat." *Environ. Sci. Technol.* 35(13), 2621-2626.

Conference Questions and Answers

Question:

At what flow rate did you successfully remove iron arsenate from the stream in your column experiment?

Answer:

The flow rate was low in the experiment-approximately 1.4 milliliters per minute (mL/min). It is an engineering process that we can design properly before applying the technology in a real situation.

Question:

At what rate did you refresh the column material so that it remained effective?

Answer:

We prepared a glass column packed with sand then injected it with nZVI particles. Two to three pore volumes were flushed through the column before injecting an arsenic-spiked influent. The column was effective for a maximum of 80 days, but the experiment was a preliminary task to test the feasibility of nZVI as a technology for arsenic removal. The experiment was not properly designed for implementation.

Question:

How was the column material regenerated?

Answer:

Arsenic becomes fixed on the nZVI surface, so the used nZVI was disposed and the columns refilled with fresh nZVI. We did experiments to see if arsenic desorbed from the iron back into solution, and a small amount was found to desorb. In the modified membrane experiments, we also looked at minimizing biofouling, because that is a common problem when using membrane technologies. There is good potential for using the modified membrane for arsenic removal. Current membrane technologies for arsenic removal are expensive and have fluctuating removal efficiencies depending on the arsenic species.

Question:

Did the size of the iron nanoparticles affect removal efficiency?

Answer:

We were able to synthesize nZVI in a range of sizes from 2–5 nm to 50–70 nm. One would expect that the higher surface area of the 2–5 nm particle size would have higher removal efficiencies. However, we found that the 20–30 nm range had the best removal efficiency. The very small particles were readily oxidized when exposed to an air or water interface, which decreased their removal efficiency.

Question:

Why do you describe the system as “dynamic?”

Answer:

Various processes occur.

In Situ Remediation: Nanotechnology's Environmental Poster Child

Barbara Karn, U.S. Environmental Protection Agency

Todd Kuiken, Woodrow Wilson Center, Project on Emerging Nanotechnologies

Martha Otto, U.S. Environmental Protection Agency

Wei-Xian Zhang, Lehigh University

According to the National Nanotechnology Initiative, an interagency consortium of U.S. Federal agencies, nanotechnology is the understanding and control of matter at dimensions of roughly 1 to 100 nanometers, where unique phenomena enable novel applications. Encompassing nanoscale science, engineering and technology, nanotechnology involves imaging, measuring, modeling, and manipulating matter at this length scale. While industrial sectors involving semiconductors, memory and storage technologies, display, optical and photonic technologies, energy, bio and health sectors produce the most nanomaterial-containing products, there are efforts to use nanotechnology as an environmental technology to improve the environment through pollution prevention and cleanup of legacy problems such as hazardous waste sites. Although the technology seems to be a beneficial replacement of current practices of site remediation, there may be some risks and possibly unintended consequences. This paper presents a background and overview of the current practice, research results, and issues surrounding the use of nanotechnology for environmental remediation.

More than 80% of documented Superfund hazardous waste sites have contaminated groundwater. Most early treatment remedies for groundwater contamination were primarily pump and treat operations. These systems involve pumping out contaminated water, removing the pollutants above ground (e.g., using air stripping, chemical treatment, etc.), and returning the treated water to the aquifer. The average pump and treat operation can cost \$10 million or more.

The Superfund program which includes the National Priorities List is just one of many cleanup programs. Site cleanups may be conducted by several different organizations, e.g., EPA, the U.S. Department of Defense (DOD), the U.S. Department of Energy (DOE), and other civilian federal agencies, State environmental agencies, corporations, and private parties. In addition to Superfund, these organizations conduct site remediation under a variety of other programs: the Brownfields program (under the Small Business Liability Relief and Brownfields Revitalization Act of 2002), corrective action programs under Subtitle C of the Resource, Conservation, and Recovery Act (RCRA), and the Underground Storage Tank program, under Subtitle I of RCRA. A 2004 EPA report estimated that it will take 30 to 35 years and cost up to \$250 billion to clean up the nation's hazardous waste sites. Developing cost-effective, in situ groundwater treatment technologies could save billions of dollars in cleanup costs.

Nanoremediation refers to the use of nanoscaled materials in the clean-up of hazardous waste sites. It has the potential not only to reduce the overall costs of cleaning up large scale contami-

nated sites, but it also reduces cleanup time, eliminates the need for treatment and disposal of contaminated dredged soil, reduces some contaminant concentrations to near zero, and can be done in situ. For environmental applications, nanotechnology offers the potential to use novel functional materials, processes, and devices that display unique activity toward recalcitrant contaminants, exhibiting enhanced mobility in environmental media, and desired application flexibility (Sun et al., 2006).

In addition to groundwater remediation, nanotechnology holds promise in reducing the presence of dense non-aqueous phase liquid (DNAPL). Because of their minute size, nanoparticles may be able to pervade very small spaces in the subsurface and remain suspended in groundwater, allowing the particles to travel farther than larger, macro-sized particles and achieve wider distribution. However, in practice, field tests indicate that the particles do not move far from the injection point (Tratnyek & Johnson, 2006). Nanoparticles can be highly reactive due to their large surface area to volume ratio and the presence of a greater number of reactive sites than their larger counterparts. This allows for increased contact with contaminants, resulting in rapid degradation.

Nanoscale iron particles (nZVI) represent one of the first generation nanoscale environmental technologies (Wang and Zhang, 1997). Other methods of remediation using nanotechnology have also been explored including use of materials such as nanoscale zeolites, carbon nanotubes and fibers, enzymes, various noble metals (mainly as bimetallic nanoparticles-BNP), and titanium dioxide (Table 1).

In laboratory and field-scale studies, nZVI particles have been shown to rapidly degrade trichloroethene (TCE), a common contaminant at Superfund sites. nZVI can serve as a source of hydroxide radicals at acidic pH values in ex situ treatment systems (Keenan and Sedlak, 2008). nZVI may also be used for the remediation of pesticides using FeO electrodes as the source of nZVI (Zhang and Lemley, 2006).

Nanoparticles such as nZVI, bi-metallic nanoscale particle (BNPs), and emulsified zero-valent iron (EZVI) may effectively reduce the following contaminants: perchloroethylene (PCE), TCE, cis-1, 2-dichloroethylene (c-DCE), vinyl chloride (VC), and 1-1-1-tetrachloroethane (TCA), along with polychlorinated biphenyls (PCBs), halogenated aromatics, nitroaromatics and heavy metals such as chromium (Table 1).

Thirty four sites have been identified where nanoremediation methods were tested for site remediation. These sites are in six countries (including the U.S.), and ten states in the U.S. Various types of nanoparticles were used including: nZVI, BNPs, and EZVI. The available data suggest that use of nanoscaled materials for site remediation is more efficient and economical than using microscaled materials of the same composition. As the technology is applied at an increasing number of sites with varying geologies, more data will become available on performance and cost, providing site managers and other stakeholders additional information to determine whether the technology might be applicable to specific sites.

In order to be effective, nZVI needs to form stable dispersions in water so that it can be delivered to water-saturated porous material in the contaminated area. However, limited mobility has been reported since, once released into the environment, engineered nanoparticles may aggregate to some degree. The fate and mobility of the nanoparticles are dependent on the characteristics of

Table 1. List of manufactured nanoparticles and the pollutants potentially remediated*

<u>Nanocrystalline zeolites</u> Toluene, nitrogen dioxide	<u>Activated carbon fibers</u> Benzene, toluene, xylene, ethylbenzene, heavy metal ions	<u>CeO₂-carbon nanotubes (CNTs)</u> Arsenate
<u>CNTs functionalized with polymers or Fe</u> <i>p</i> -nitrophenol Benzene, toluene, dimethylbenzene, heavy metal ions, TCE	<u>Single-walled CNTs</u> Trihalomethanes (THMs)	<u>Multi-walled CNTs</u> Heavy metal ions, THMs, Chlorophenols, Herbicides, Microcystin toxins
<u>Self-assembled monolayer on mesoporous supports (SAMMS)</u> Inorganic ions, Heavy metal ions, Actinides, Lanthanides	<u>TiO₂ photocatalysts</u> Heavy metal ions, Azo dyes, Phenol, Aromatic pollutants, toluene	<u>Zero-valent iron nanoparticles</u> Polychlorinated biphenyls (PCBs), Inorganic ions, Chlorinated organic compounds, Heavy metal ions
<u>Bimetallic nanoparticles Pd/Fe nanoparticles</u> PCBs, Chlorinated ethene, Chlorinated methanes	<u>Ni/Fe nanoparticles Pd/Au nanoparticles</u> TCE, PCBs, Dichlorophenol, Trichlorobenzene, Chlorinated ethene, Brominated organic compounds	

*Adapted from Theron et al. 2008.

the particle and the characteristics of the environmental system and will determine the effectiveness of the nanoparticle in treating the contaminant. More research is needed to determine whether the nanoparticles could migrate from the treatment zone, associate with suspended solids or sediment, bioaccumulate, or enter drinking water sources.

A range of ecotoxicological effects of various types of nanomaterials have been reported, including effects on microbes, plants, invertebrates and fish (Boxall et al., 2007). Although available data indicate that current risks of engineered nanoparticles in the environment to environmental and human health are probably low, knowledge of the potential impacts of engineered nanoparticles in the environment on human health is still limited (Boxall et al., 2007).

Most societal issues are based on the unknown risks of using nanoscale materials for site remediation. At one end of the spectrum, some nongovernmental groups invoked the precautionary principle in an attempt to halt all use of the technology until proven safe. EPA's Nanotechnology White Paper (EPA 2007) points out the positive aspects of using nanomaterials in environmental remediation, but also calls for research on the possible negative effects.

Future studies need to evaluate the potential impacts these nanoparticles could have on ecosystems outside the remediation zone. In addition, instrumentation and measurement techniques need to be developed in order to evaluate and monitor how far these nanoparticles can travel, their effects on flora and fauna and any bioaccumulation potential they may present. The potential is great for this technology to decrease the cost of remediation, reduce the time it takes to clean up a site, and improve the overall reduction/elimination of contaminants. The net effect would be to reduce the amount and time of exposure for those living in and around the contaminated site. In order to prevent any potential adverse environmental impacts, proper evaluation of these nanoparticles needs to be addressed before this technique is utilized on a mass scale.

References

- Boxall, A.B.A., Tiede, K. and Chaudhry, Q. 2007. Engineered nanomaterials in soils and water: how do they behave and could they pose a risk to human health? *Nanomedicine*. 2(6), 919-927.
- EPA. 2007. Nanotechnology White Paper. U.S. Environmental Protection Agency Report EPA 100/B-07/001, Washington, DC.
- EPA, 2004. Cleaning up the Nation's waste sites: Markets and technology trends. U.S. Environmental Protection Agency Report 542-R-04-015, Washington, DC.
- Keenan, C.R. and Sedlak, D.L. 2008. Factors Affecting the Yield of Oxidants from the Reaction of Nanoparticulate Zero-Valent Iron and Oxygen. *Environmental Science and Technology*. 42(4), 1262-1267.
- Sun, Y.P., Li, X., Cao, J., Zhang, W., Wang, H.P. 2006. Characterization of zero-valent iron particles. *Advances in Colloid and Interface Science*. 120, 47-56.
- Theron, J., Walker, J.A., Cloete, T.E. 2008. Nanotechnology and water treatment: Applications and emerging opportunities. *Critical Reviews in Microbiology*. 34, 43-69.
- Tratnyek, P.G. and Johnson, R.L. 2006. Nanotechnologies for environmental cleanup. *NanoToday*. 1(2), 44-48.
- Wang, C. and Zhang, W.-X. 1997, Synthesizing nanoscale iron particles for rapid and complete dechlorination of TCE and PCBs. *Environmental Science and Technology*, 31, 2154-2156.
- Zhang, H.C. and Lemley, A.T. 2006. Reaction mechanism and kinetic modeling of DEET degradation by flow-through anodic Fenton treatment (FAFT). *Environmental Science and Technology*. 40, 4488-4494.

Conference Questions and Answers

Question:

What constitutes a successful cleanup using nanotechnology? In other words, how long must monitoring be conducted, and what concentration levels must be reached?

Answer (Michael Gill, EPA):

The answer is the same for all cleanup technologies. It depends on the goals set in the Record of Decision. How long the remediation takes to reach cleanup goals depends on how thorough the site characterization was and on how well the remedial technology was implemented.

Save

Removal and Degradation of Subsurface Pollutants by Nanoscale Bimetallic Pd/Fe Slurry Under an Electric Field

*Gordon C. C. Yang, Institute of Environmental Engineering,
National Sun Yat-Sen University, Kaohsiung, Taiwan*

Abstract

In this work a novel, hybrid technology combining the injection of nanoscale bimetallic Pd/Fe slurry (hereinafter referred to as the “Slurry”) and electrokinetic (EK) remediation process was employed for the removal and degradation of trichloroethylene (TCE) and nitrate in the subsurface. Laboratory-prepared palladized nanoiron was stabilized using 1 vol% polyacrylic acid to form the Slurry, which was used later for the injection to the subsurface. To evaluate the treatment efficiency of combined technologies of the injection of the Slurry and EK process in treating subsurface pollutants, a bench-scale electrokinetic system with a horizontal soil column was employed. To mimic the horizontal flow of groundwater, both electrode compartments were filled with a simulated groundwater and the horizontal soil compartment was packed with loamy sand soil polluted by a selected target contaminant (e.g., TCE or nitrate). Test conditions used were: (1) electric potential gradient: 1 V/cm; (2) daily addition of 20 mL of the Slurry (2.5 g/L and 4.0 g/L for the cases of TCE and nitrate, respectively) to the electrode reservoir(s); and (3) reaction time: 6 days. The addition of the Slurry to the anode reservoir yielded the lowest residual TCE or nitrate concentration in the entire reaction system. However, the predominant reaction mechanisms for removal and degradation of TCE and nitrate are found to be different.

Introduction

Zero-valent iron (ZVI) is a material has been proven to be capable of reductively degrading various chlorinated solvents and a variety of other contaminants in aqueous phase (Gilham and O’Hannessin, 1994; Matheson and Tratnyek, 1994). Among others, Wang and Zhang (1997) reported the employment of nanoscale zero-valent iron for environmental remediation. Zhang et al. (1998) further showed nanoscale bimetallic Pd/Fe particles outperformed microscale ZVI in the aspects of a higher dechlorination rate and a lesser amount of intermediate products.

Electrokinetic remediation (EK) is capable of using electric currents to extract heavy metals, certain organic compounds, or mixed inorganic and organic species from soils (even with low hydraulic conductivity) and slurries (Eykholt, 1992; Acar and Alshawabkeh, 1993; Probst and Hicks, 1993). Remediation of contaminated soil and groundwater by EK coupled with other technologies are commonly studied and practiced. However, here only the integration of nanoscale ZVI injection and EK process will be of interest (Yang et al., 2007; Yang et al., 2008). Very recently, an U.S. patent for a novel process using EK to assist the transport of a nanoparticle-containing slurry through a polluted porous medium has been granted to the author of this work (Yang, 2008).

The objective of this work was to utilize electrokinetics as the driving force for transporting the “Slurry” (i.e., nanoscale palladized iron slurry) in the soil matrix and to investigate the effects of the injection position of the Slurry in a simulated subsurface environment on removal and degradation of TCE and nitrate.

Materials and Methods

In this work all chemicals used are reagent grade. The author used a solution chemistry method for the preparation of nanoiron (i.e., iron nanoparticles) (Glavee et al., 1995). 1 vol% of poly acrylic acid (PAA) with a molecular weight of ca. 2,000 g/mol was used as a dispersant in this work for stabilizing Pd/Fe nanoparticles to form the Slurry. The preparation methods of the concerned Slurry and artificially contaminated loamy sand soils (with trichloroethylene and nitrate, respectively) can be found elsewhere (Yang et al., 2007; Yang et al., 2008). In various tests the initial TCE masses in the soil matrices ranged from 109.49 mg to 126.25 mg (i.e., 160 to 181 mg/kg), whereas the initial nitrate content in the whole system was kept constant at 6218.80 mg.

The specimen of contaminated loamy sand soil was fed into a horizontal column, which was further subjected to an electric field to evaluate the performance of the integrated technology. The schematic diagram and detailed description of the experimental set-up of the EK remediation system has been reported elsewhere (Yang et al., 2008). The electrode compartments were filled with a simulated groundwater (Yang et al., 2007; Yang et al., 2008). In all tests, the following experimental conditions were employed: (1) a constant electric potential gradient of 1 V/cm; (2) daily injection of 20 mL of PAA-modified nanosized Pd/Fe slurry (@ 2.5 g/L and 4.0 g/L, respectively for TCE and nitrate) at different positions; and (3) a treatment time of 6 days.

Results and Discussion

In this work an attempt was made to transport the injected PAA-modified Slurry in the subsurface for the removal and degradation of contaminant(s). Here the nanosized Pd/Fe slurry was considered as a “mobile reactive nanoiron” (as compared with a stagnant iron wall in the sense of conventional permeable reactive barriers). Ideally, the “mobile reactive nanoiron” would be transported to the hot spot by the electroosmotic (EO) flow induced by EK. After the contact of nanosized Pd/Fe and contaminated soil, the target pollutants would be degraded as a result of chemical reduction (or possibly oxidation in some other cases) by nanosized Pd/Fe.

Remediation of trichloroethylene (TCE) contamination

When the hybrid technology was employed TCE was substantially removed and degraded as a result of a combined effect of reductive dechlorination by nanoscale Pd/Fe bimetal and enhanced transport of such nanoparticles through the soil body (from the anode compartment to the cathode compartment) by the EO flow. It was found that the anode reservoir is the best injection position for the Slurry in terms of TCE remediation as compared with other injection positions. Figure 1 illustrates the results of various tests in this regard. Here Tests 1 and 2 referred to the cases for which the concerned Slurry was injected into the anode compartment and cathode compartment, respectively. When EK was coupled with the injection of the Slurry into the anode compartment, the residual TCE mass in soil was determined to be about 7.56%. In a similar test with the Slurry injection into the cathode compartment, the residual TCE content was found to be much higher, namely 29.04%. According to Figure 1, the practice of injecting the Slurry into

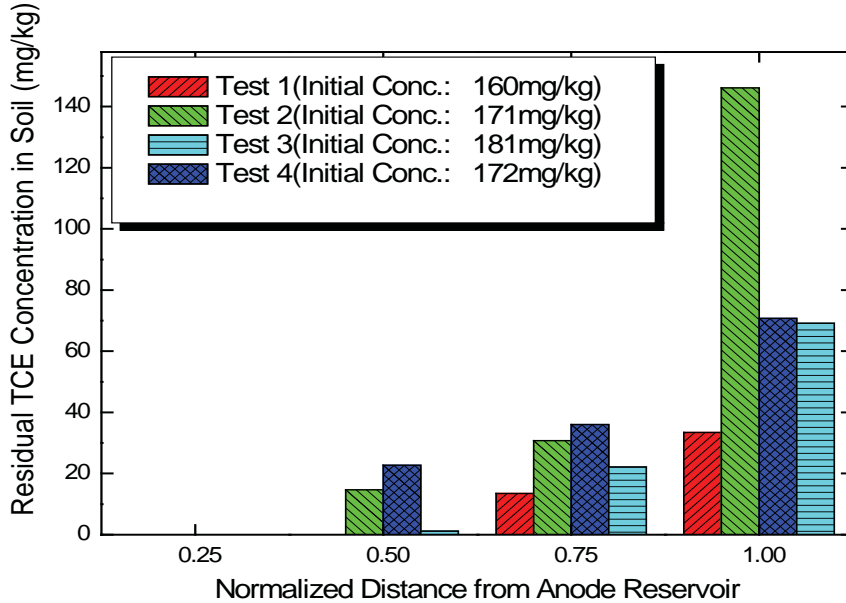


Figure 1. Patterns of residual TCE distribution in soil columns for various test runs (Notes: A test period of 6 days was kept constant in all tests. Test 1: daily injection of 20 mL nanosized Pd/Fe slurry into the anode reservoir; Test 2: daily injection of 20 mL nanosized Pd/Fe slurry into the cathode reservoir; Test 3: daily injection of 10 mL nanosized Pd/Fe slurry into each electrode reservoir; Test 4: EK process alone without injection of the Slurry to any electrode compartment; and Test 5: a blank test without application of the electric field and injection of the Slurry to the remediation system)

the cathode compartment should also play a significant role in dechlorination of TCE. This is because that TCE removed from the soil body to the cathode reservoir would be hydrodechlorinated by the nanoscale bimetallic Pd/Fe particles therein.

Remediation of nitrate contamination

Table 1 shows the test results for subsurface decontamination of nitrate using the integrated technology of the injection of the Slurry and EK process. When the Slurry was injected into the anode reservoir (i.e., Test 6), it was found to be the super most in terms of nitrate removal from the soil body. The relevant nitrate removal efficiencies for the soil body and whole system (including the soil body and electrode reservoirs) were determined to be 99.5% and 99.2%, respectively. This is ascribed to the fact that migration of nitrate ions toward the anode had enhanced their reaction with the nanosized Pd/Fe bimetal in the anode reservoir and/or an encounter of nitrate ions with Pd/Fe nanoparticles transported by the EO flow toward the cathode. Of course, as time elapsed, a pH of about 3 in the anode reservoir or the acid front would also play a role of acid washing of the nanosized Pd/Fe bimetal preventing the formation of passive layer of iron oxides on the surface. On the other hand, a rather alkaline environment in the cathode reservoir would enhance the formation of iron oxides on the surface of nanosized Pd/Fe bimetal resulting

Table 1. The distribution of residual nitrate in different fractions of the soil column and electrode reservoirs

Test No.	Residual nitrate content (mg)					
	Anode reservoir	Soil fraction 0-5 cm from the anode reservoir	Soil fraction 5-10 cm from the anode reservoir	Soil fraction 10-15 cm from the anode reservoir	Soil fraction 15-20 cm from the anode reservoir	Cathode reservoir
5	203.23	779.17	28.05	19.65	9.05	0
6	15.15	8.30	3.64	16.41	2.78	0.12
7	2000.15	2423.52	122.96	85.39	1348.59	32.66
8	594.78	0	0	55.56	0	0
9	242.96	213.49	0	0	0	0

Notes: (1) The initial nitrate content in the whole system was kept constant at 6218.80 mg in all tests and also a test period of 6 days. (2) Test 5: no nanosized Pd/Fe slurry was injected to the system; Test 6: daily injection of 20 mL nanosized Pd/Fe slurry into the anode reservoir; Test 7: daily injection of 20 mL nanosized Pd/Fe slurry into the cathode reservoir; Test 8: daily injection of 10 mL nanosized Pd/Fe slurry respectively to the positions 5 cm and 10 cm from the anode reservoir; and Test 9: daily injection of 10 mL nanosized Pd/Fe slurry respectively to the positions 5 cm and 10 cm from the cathode reservoir.

in a much lower surface reactivity as in the case of the Slurry injection into the cathode reservoir. This would explain why Test 7 yielded very poor efficiencies of nitrate removal, 36.0% for the soil body and 3.3% for the whole system.

Conclusions

A hybrid technology of injecting the nanoscale bimetallic Pd/Fe slurry coupled with the application of an electric field is an effective remediation method for subsurface contamination. The research findings are summarized as follows:

The injection position of the nanosized Pd/Fe slurry was found to be critical to the overall treatment performance, with the injection into the anode reservoir being the best. This is ascribed to the greatest extent of transport of the Slurry toward the cathode by the largest quantity of the EO flow in this case.

The best TCE removal and degradation was obtained for the test having the nanoscale bimetallic Pd/Fe slurry merely injected into the anode reservoir. In this case, only 7.56% of the initial TCE mass remained in soil after a treatment time of 6 days.

By injecting PAA-modified nanoscale Pd/Fe slurry into the anode reservoir of the EK system, an efficiency of over 99% nitrate removal and degradation for the entire system was achieved. Presumably, the driving force of moving nitrate ions by electromigration and negatively charged

PAA-modified nanoparticles toward the anode by electrophoresis must be the predominant migration mechanisms in this case. Chemical reduction of nitrate would occur mostly in the anode reservoir where nanosized Pd/Fe bimetal existed. The cathode reservoir was found to be the worst injection spot. Besides, injecting nanoscale Pd/Fe bimetal to a position in between the electrode reservoirs turned out to be not a good practice either.

Acknowledgments

This work was sponsored by Taiwan National Science Council (Project Nos. NSC 93-2211-E-110-006 & NSC 94-2211-E-110-014).

References

- Acar, Y.B., and A.N. Alshwabkeh. (1993). "Principles of electrokinetic remediation." *Environ. Sci. Technol.* 27, 2638-2647.
- Gilham, R.W., and S.F. O'Hanessian. (1994). "Enhanced degradation of halogenated aliphatics by zero-valent iron." *Ground Water.* 32, 958-967.
- Eykholt, G.R. (1992). "Driving and complicating features of the electrokinetic treatment of contaminated soils." Ph.D. thesis, Dept. Civ. Eng., Univ. Texas at Austin, TX, U.S.A.
- Glavee, G.N., K.J. Klabunde, C.M. Sorensen, G.C. Hadlipanayis. (1995). "Chemistry of borohydride reduction of iron (II) and iron (III) ions in aqueous and nonaqueous media formation of nanoscale Fe⁰, FeB, and Fe₂B powders." *Inorg. Chem.* 34, 28-35.
- Matheson, L.J., and P.G. Tratnyek. (1994). "Reductive dehalogenation of chlorinated methanes by iron metal." *Environ. Sci. Technol.* 28, 2045-2053.
- Probstein, R.F., and R.E. Hicks. (1993). "Removal of contaminants from soils by electric fields." *Sci.* 260 (5107), 498-503.
- Wang, C.B., and W.X. Zhang. (1997). "Synthesizing nanoscale iron particles for rapid and complete dechlorination of TCE and PCBs." *Environ. Sci. Technol.* 31, 2154-2156.
- Yang G.C.C. (2008). "Method for treating a body of a polluted porous medium." U.S. Patent 7,334,965.
- Yang, G.C.C., C.H. Hung, and H.C. Tu. (2008). "Electrokinetically enhanced removal and degradation of nitrate in the subsurface using nanosized Pd/Fe slurry." *J. Environ. Sci. Health A.* 43, 945-951.
- Yang, G.C.C., H.C. Tu, and C.H. Hung. (2007). "Stability of nanoiron slurries and their transport in the subsurface environment." *Sepa. Purif. Technol.* 58, 166-172.
- Zhang, W.X., C.B. Wang, and H.L. Lien. (1998). "Treatment of chlorinated organic contaminants with nanoscale bimetallic particles." *Catal. Today*, 40, 387-395.

Conference Questions and Answers

Question:

Is the electrokinetic remediation process needed if the natural ground-water flow is carrying the nanoparticles to where you want them to go?

Answer:

Electrokinetics help to increase the speed of ground-water flow to the target.

Question:

The results of your research seem positive. Do you have any plans to step up implementation?

Answer:

Yes, I would like to transfer this technology to whoever would like to use it.

Novel Zerovalent Iron/Silica Composites for Targeted Remediation of TCE Contaminated Water and Soil

Jingjing Zhan, Tonghua Zheng, Bhanukiran Sunkara, Gerhard Piringer, Yunfeng Lu, Gary McPherson, and Vijay John, Department of Chemical and Biomolecular Engineering, Tulane University, New Orleans, Louisiana, U.S.A.

Abstract

Nanoscale zero-valent iron (ZVI) particles are a preferred option for the reductive dehalogenation of trichloroethylene (TCE). However, it is difficult to transport these particles to the source of contamination due to aggregation. This study describes a novel approach to the preparation of ZVI nanoparticles that are efficiently and effectively transported to contaminant sites. The technology developed involves the encapsulation of ZVI nanoparticles in porous sub-micron silica spheres which are easily functionalized with alkyl groups. These composite particles have the following characteristics (1) They are in the optimal size range for transport through sediments (2) dissolved TCE adsorbs to the organic groups thereby significantly increasing contaminant concentration near the ZVI sites (3) they are reactive as access to the ZVI particles is possible (4) when they reach bulk TCE sites, the alkyl groups extend out to stabilize the particles in the TCE bulk phase or at the water-TCE interface (5) the materials are environmentally benign. These concepts are examined through reactivity studies, and transport studies using column transport, capillary and microcapillary transport studies. These iron/silica aerosol particles with controlled surface properties also have the potential to be efficiently applied for in situ remediation and permeable reactive barriers construction.

In extensions of the work, we have shown that these particles function effectively as reactive adsorbents for TCE. Our work will describe the synthesis of such composite nanoscale materials through an aerosol-assisted method and through solution methods, to illustrate the versatility and ease of materials synthesis, scale up and application.

Introduction

The widespread occurrence of dense non-aqueous phase liquids (DNAPLs) such as trichloroethylene (TCE) in groundwater and soil is of serious environmental concern. Remediation of these contaminants is of utmost importance for the cleanup of contaminated sites [1, 2]. Prior studies have shown that nanoscale zero-valent iron (ZVI) particles are a preferred option for reductive dehalogenation of TCE due to their environmentally benign nature, high efficiency and low cost [3, 4]. However, bare nanoiron particles have a strong tendency to agglomerate due to their intrinsic magnetic interactions and high surface energies, forming aggregates that plug and inhibit their flow through porous media [5-7]. For successful in-situ remediation, it is necessary for injected reactive decontamination agents to migrate through the saturated zone to reach the contaminant.

Our research is directed towards the development of novel supported iron/silica composites that are effective for groundwater remediation and have good mobility through soils. Spherical silica particles containing nanoscale zero valent iron were synthesized through an aerosol-assisted process. Incorporation of iron into porous submicron silica particles protects ferromagnetic iron nanoparticles from aggregation and increases their subsurface mobility. Aerosolized silica particles with functional alkyl moieties such as ethyl groups on the surface, clearly adsorb solubilized trichloroethylene (TCE) in water, increasing the local concentration of TCE in the vicinity of iron nanoparticles. The particle size is in the optimal range for transport through soils and sediments. Additionally, the particles can partition significantly to the interface of bulk water-TCE further facilitating mobility and access to bulk TCE.

Brief Results and Discussion

To achieve these objective we use an aerosol-assisted technology as a simple, scalable and efficient method to obtain colloidal spherical particles [8, 9]. The set-up and the process are shown in Figure 1 [10]. As aerosol droplet passes through the heated zone of the furnace, hydrolysis and condensation of silicates leads to the formation of spherical silica particles containing FeCl_3 . Figure 2 shows the fairly homogeneous distribution of Fe throughout Fe/ethyl-silica particles the particles [11].

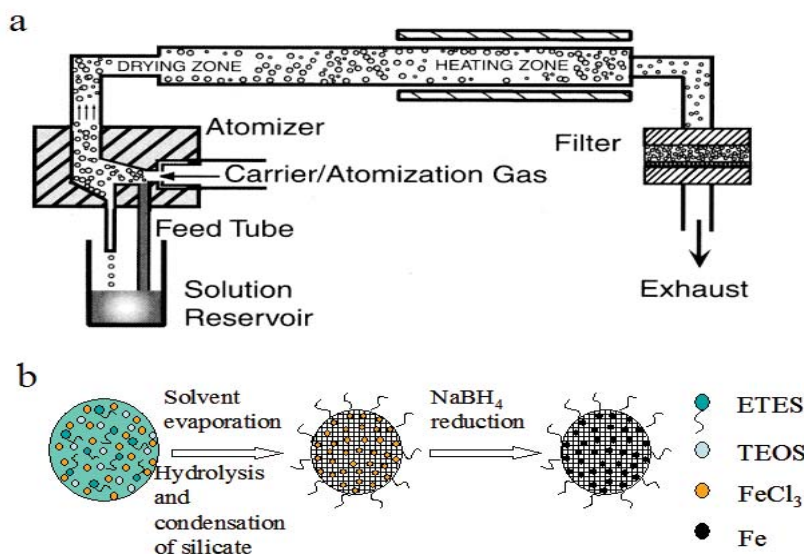


Fig 1: Schematic of (a) the aerosol reactor for particle synthesis; (b) the process for the preparation of Fe/ethyl-silica composite porous particles. The reactions occur in a solvent aerosol droplet.

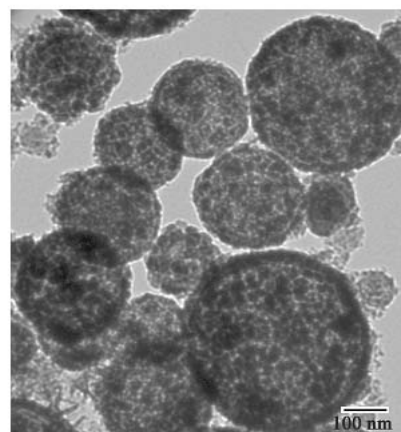


Fig 2: Transmission electron micrograph of Fe/ethyl-silica composite porous particles.

Reaction characteristics of two composite particles are shown in Figure 3 [10]. The remarkable aspect of reaction in the composite particles is the characteristics of the Fe/ethyl-silica system which shows an immediate sharp reduction of the TCE peak to ~45% of its original value followed by a slower reaction rate (Fig 3a). The control sample of Fe/silica does not show this dramatic reduction in solution TCE concentration. We explain the apparent enhancement of TCE removal by Fe/ethyl-silica particles as a consequence of TCE partitioning to the hydrophobic ethyl groups of the functionalized silica. This is the first instance where adsorption of TCE to the particles is exploited in enhancing local concentrations in the vicinity of the zero-valent iron.

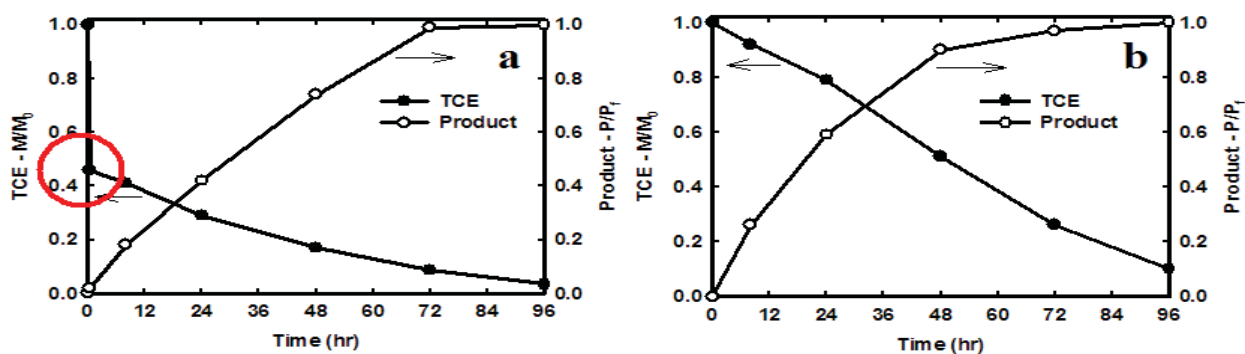


Fig. 3: TCE removal from solution and product gas evolution rates for (a) Fe/silica and (b) Fe/ethyl-silica. M/M_0 is the fraction of the original TCE remaining, and P/P_f is the ratio of the gas product peak to the gas product peak at the end of 96 hours.

The size range of particles synthesized through the aerosol process is in the range 100- 800 nm. This is the optimal size range for particles to transport through the sediment as predicted by the Tufenkji-Elimelech model. Particles that are too large do not pass through sediment pores while particles that are too small become intercepted by sediment grains while undergoing Brownian motion. Particles of the optimal size range follow flow streamlines accurately and transport efficiently through sediments. Accordingly, we have tested the transport characteristics of the aerosol based particles using model sediments, using column transport experiments. Figure 4 illustrates the set-up and the elution results [11]. The results indicate that most of the RNIP-10DS was trapped within the first few centimeters of the column, and visible penetration does not exceed the middle of the column. In contrast, the aerosol based apticles elute efficiently. Capillary and microcapillary experiments to demonstrate efficient transport, also indicate that the particles

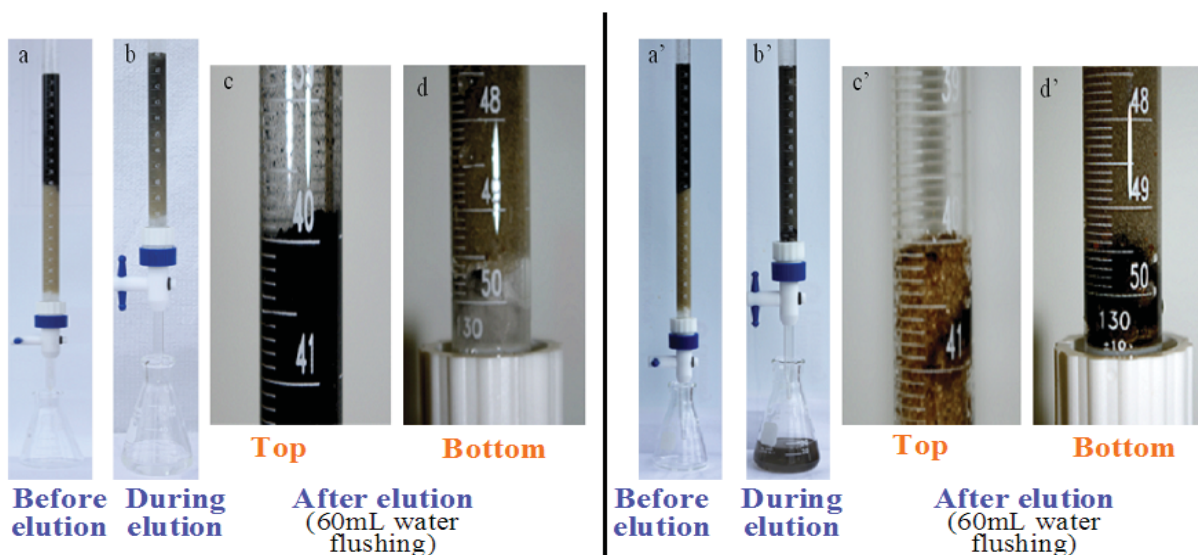


Fig. 4: Elution characteristics of RNIP-10DS particles (left) and Fe/ethyl-silica (right) in vertical columns with flow rate: 18 mL/min.

move efficiently in capillaries. Finally, we observe in microcapillary experiments that the particles upon encountering droplets of TCE partition to the TCE-water interface.

Summary

In summary, we demonstrate some novel concepts in the design of reactive-adsorptive particles with optimal mobilities in TCE remediation. The concept is summarized in the schematic below (Figure 5). The particles are synthesized through an aerosol process which can be scaled up because it is an inherently continuous process. In transport through an aqueous phase, the alkyl groups of the silica do not extend out into the aqueous phase but stay confined to the silica surface. At the same time, they serve as adsorbents for dissolved TCE and concentrate TCE onto the particles serving as sponges for dissolved TCE. Additionally, there is reaction with the TCE comes into contact with the entrapped ZVI nanoparticles in the silica matrix. When in contact with a bulk phase of TCE, it is envisioned that the alkyl groups can extend out into the solvent thereby increasing the hydrodynamic diameter and decreasing the effective density of the colloidal particle. Our hypothesis is therefore that the extension of alkyl groups into the solvent might help stabilize the particles in the organic phase.

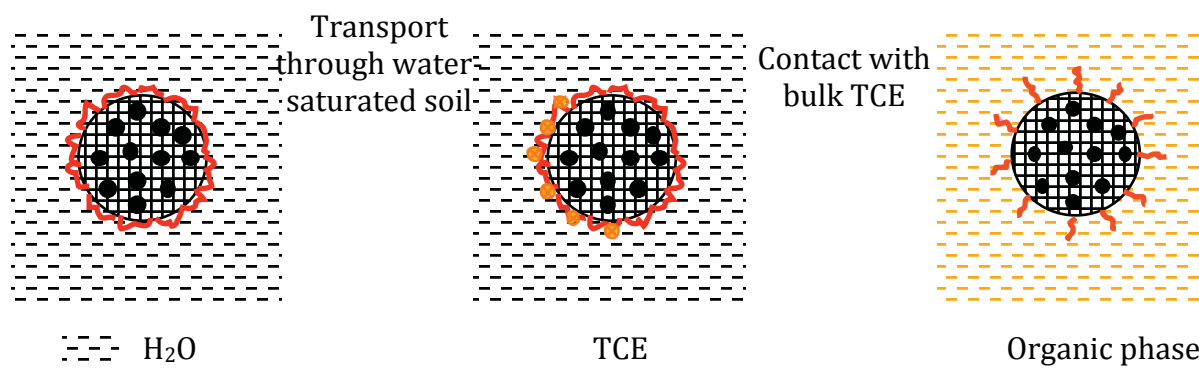


Figure 5: Schematic illustrating characteristics of the alkyl functionality of Fe/Ethyl-Silica particles.

We thus demonstrate new technology in the environmental remediation of chlorinated hydrocarbons through the development of composite supported nanoparticles prepared through an aerosol-assisted route. Further development and optimization of these systems to enhance adsorption, reaction and transport characteristics are in progress.

Acknowledgements

We are grateful to the Environmental Protection Agency for funding this work through Grant EPA – GR832374

References

1. Orth, W. S.; Gillham, R. W., Dechlorination of Trichloroethene in Aqueous Solution Using Fe⁰. *Environ. Sci. Technol.* **1996**, *30*, (1), 66-71.
2. Roberts, A. L.; Totten, L. A.; Arnold, W. A.; Burris, D. R.; Campbell, T. J., Reductive Elimination of Chlorinated Ethylenes by Zero-Valent Metals. *Environ. Sci. Technol.* **1996**, *30*, (8), 2654-2659.
3. Wang, C. B.; Zhang, W. X., Synthesizing Nanoscale Iron Particles for Rapid and Complete Dechlorination of TCE and PCBs. *Environ. Sci. Technol.* **1997**, *31*, (7), 2154-2156.
4. Liu, Y.; Majetich, S. A.; Tilton, R. D.; Sholl, D. S.; Lowry, G. V., TCE Dechlorination Rates, Pathways, and Efficiency of Nanoscale Iron Particles with Different Properties. *Environ. Sci. Technol.* **2005**, *39*, (5), 1338-1345.
5. Schrick, B.; Hydutsky, B. W.; Blough, J. L.; Mallouk, T. E., Delivery Vehicles for Zerovalent Metal Nanoparticles in Soil and Groundwater. *Chem. Mater.* **2004**, *16*, (11), 2187-2193.
6. He, F.; Zhao, D., Preparation and Characterization of a New Class of Starch-Stabilized Bi-metallic Nanoparticles for Degradation of Chlorinated Hydrocarbons in Water. *Environ. Sci. Technol.* **2005**, *39*, (9), 3314-3320.
7. Saleh, N.; Sirk, K.; Liu, Y.; Phenrat, T.; Dufour, B.; Matyjaszewski, K.; Tilton, R. D.; Lowry, G. V., Surface modifications enhance nanoiron transport and NAPL targeting in saturated porous media. *Environ. Eng. Sci.* **2007**, *24*, (1), 45-57.
8. Lu, Y.; Fan, H.; Stump, A.; Ward, T. L.; Rieker, T.; Brinker, C. J., Aerosol-assisted self-assembly of mesostructured spherical nanoparticles. *Nature* **1999**, 398.
9. Zheng, T.; Pang, J.; Tan, G.; He, J.; McPherson, G. L.; Lu, Y.; John, V. T.; Zhan, J., Surfactant templating effects on the encapsulation of iron oxide nanoparticles within silica microspheres. *Langmuir* **2007**, *23*, (9), 5143-7.
10. Zheng, T.; Zhan, J.; He, J.; Day, C.; Lu, Y.; McPherson, G. L.; Piringer, G.; John, V. T., Reactivity Characteristics of Nanoscale Zerovalent Iron-Silica Composites for Trichloroethylene Remediation. *Environ. Sci. Technol.* **2008**, *42*, (12), 4494-4499.
11. Zhan, J.; Zheng, T.; Piringer, G.; Day, C.; McPherson, G. L.; Lu, Y.; Papadopoulos, K. D.; John, V. T., Transport and partitioning characteristics of nanoscale functional zero-valent iron/silica composites for in-situ remediation of trichloroethylene. *Environ. Sci. Technol.* **2008**, *42*, (23), 8871-8876.

Conference Questions and Answers

No questions.

Save

Surface Chemistry of Nanoscale Zero-valent Iron (nZVI)

*Wei-xian Zhang, Department of Civil and Environmental Engineering,
Lehigh University, Bethlehem, Pennsylvania, U.S.A.*

Abstract

Zero-valent iron nanoparticle technology is becoming an increasingly popular choice for treatment of hazardous and toxic wastes, and for remediation of contaminated sites. In the U.S. alone, more than 30 projects have been documented since 2001. More are planned or ongoing in North America, Europe and Asia. The diminutive size of the iron nanoparticles helps to foster effective subsurface dispersion while their large specific surface area corresponds to enhanced reactivity for rapid contaminant transformation. Recent innovations in nanoparticle synthesis and production have resulted in substantial cost reductions and increased availability of nanoscale zero-valent iron for large scale applications. In this presentation, methods of nZVI synthesis and characterization will be reviewed. Applications of nZVI for treatment of both organic and inorganic contaminants will be discussed. Key issues related to field applications such as fate/transport, toxicity and potential environmental impact are also explored.

Conference Questions and Answers

Question:

If it is so difficult to quantify the amount of nZVI in a material, how can you stoichiometrically quantify the amount of nZVI needed for a remedial alternative?

Answer:

High-strength X-rays can measure the nZVI, but not all laboratories have this equipment. Measuring the total reducing power may be the solution.

Save

Highly Efficient Nitrate Reduction by Bimetallic Nanoscale Zero-Valent Iron

Anna Ryu and Heechul Choi, Department of Environmental Science and Engineering, Gwangju Institute of Science and Technology, Buk-gu, Gwangju, Republic of Korea

Abstract

Nitrate is extensive contaminant in groundwater and wastewater which can cause blue baby syndrome or eutrophication. Bimetallic nanoscale zero-valent iron (NZVI) was synthesized in this study and tested for the nitrate reduction. Ni or Pd was used for bimetal synthesis. Particle size of bimetallic NZVI was mostly 10-50 nm and connected each other like chain. XRD result confirmed that the iron synthesized is zero-valent state in amorphous phase showing major peak at 45°. For batch test 3, 5, or 10 g/L of iron dose was used for reduction of 1000 mg/L NO_3^- without pH control. For the higher concentration of nitrate, 2000 and 4000 mg/L, 10 g/L of iron dose was used. The result of batch test showed that reduction of nitrate by bimetallic NZVI is very fast and efficient. Nitrate in several thousand mg/L level could be reduced within only few minutes by bimetallic NZVI. Also, the results showed that Ni-NZVI has better efficiency than Pd-NZVI on nitrate reduction.

Introduction

Nitrate is one of the major contaminant in groundwater and wastewater. It appears in tens of ppm level in groundwater and in tens to thousands of ppm level in wastewater. If nitrate is exposed to human body it can cause bluebaby or if it is exposed to ecosystem it can cause eutrophication. Until now many researches have been done to remove nitrate such as biological treatment, ion exchange, etc. However, there are many limitations for these methods (Pintar et al., 2001). In biological method it takes long time to remove nitrate while it can remove high concentration of nitrate. Ion exchange method can be applied in the place which high concentration can be treated. Many catalysts were tested to reduce nitrate, however, only tens of ppm level nitrate removal were tested (Sá et al., 2005, Rodríguez et al., 2005). Therefore, there is a need for the development of efficient removal method of highly concentrated nitrate within short time. NZVI is getting attention due to its efficient reduction capacity. However, until now very few studies has been done on reduction of nitrate by NZVI (Choe et al, 2000., Sohn et al, 2006, Wang et al., 2006). In this study nitrate reduction by bimetallic NZVI was tested for high concentration of nitrate solution.

Method

NZVI was synthesized adding NaBH_4 solution into $\text{FeSO}_4 \cdot 6\text{H}_2\text{O}$ solution with 30 % of alcohol. Then NZVI was washed with alcohol and DI water. For bimetallic NZVI synthesis NiCl_2 or PdCl_2 was added to NZVI containing DI water and shaken at 150 rpm for 30 min. Bimetallic NZVI was washed with DI water again and used for the batch test.

Batch test has been done using 10mL serum vial. Nitrate solution was prepared using KNO_3 and

initial concentrations were 1000, 2000 and 4000 mg/L. pH was not controlled during the experiment and samples were reacted at 60 rpm on the rotator. Nitrate, nitrite and ammonium ion was analyzed using ion chromatography (DX-120, DIONEX).

Results and Discussions

NZVI was synthesized with the particle size mostly in 10 – 50 nm with 3-4 nm of oxide layer on the surface. X-ray diffraction result confirmed NZVI is amorphous phase of zero valent iron (data not shown). The nitrate reduction result showed that bimetallic NZVI could efficiently reduce nitrate. Ni coated NZVI (Ni-NZVI) could reduce 99.9 % of 1000 mg/L nitrate within 1 min with 10 g/L iron dose. When iron dose was 5 g/L, 98 % of initial nitrate was reduced within 1 min and with 3 g/L of iron dose 86 % and 97 % was reduced within 1min and 20 min, respectively. In case of Pd coated NZVI (Pd-NZVI), 10 g/L of Pd-NZVI could reduce nitrate completely within 1 min. But with 5 g/L and 3 g/L iron dose could reduce 91% and 71 % within 1 min and 95 % and 80 % of nitrate within 20 min, respectively. From this result, nitrate reduction by bimetallic NZVI showed extremely fast reaction compared to the previous studies for the nitrate reduction.

Conclusions

NZVI showed efficient reduction capacity of nitrate. It could reduce thousands of ppm level nitrate within minutes. Ni-NZVI showed better reduction capability than Pd-NZVI. This can be one of good alternative method of existing nitrate removal technologies which have many limitations, especially for the highly concentrated nitrate solution treatment.

References

- Pintar, A., Batista, J., Levec, J. (2001) "Catalytic denitrification: Direct and indirect removal of nitrates from potable water." *Catalysis Today*, 66, (2-4), 503-510.
- Sá, J., Gross, S., Vinek, H. (2005) "Effect of the reducing step on the properties of Pd-Cu bimetallic catalysts used for denitration." *Applied Catalysis A: General*, 294, (2), 226-234.
- Rodríguez, R., Pfaff, C., Melo, L., Betancourt, P. (2005) "Characterization and catalytic performance of a bimetallic Pt-Sn/HZSM-5 catalyst used in denitration of drinking water." *Catalysis Today*, 107-108, 100-105.
- Choe, S.; Chang, Y.-Y.; Hwang, K.-Y.; Khim, J., (2000) "Kinetics of reductive denitrification by nanoscale zero-valent iron." *Chemosphere* 41, (8), 1307-1311.
- Sohn, K.; Kang, S. W.; Ahn, S.; Woo, M.; Yang, S. K., (2006) "Fe(0) nanoparticles for nitrate reduction: Stability, reactivity, and transformation." *Environmental Science and Technology* 40, (17), 5514-5519.
- Wang, W.; Jin, Z. h.; Li, T. l.; Zhang, H.; Gao, S., (2006) "Preparation of spherical iron nanoclusters in ethanol-water solution for nitrate removal." *Chemosphere* 65, (8), 1396-1404.

Conference Questions and Answers

No questions.

Implications of Fe/Pd Bimetallic Nanoparticles Immobilized on Adsorptive Activated Carbon for the Remediation of Groundwater and Sediment Contaminated with PCBs

*Souhail R. Al-Abed and Hyeok Choi, National Risk Management Research Laboratory,
U.S. Environmental Protection Agency, Cincinnati, OH, U.S.A.*

Abstract

In order to respond the current limitations and challenges in remediating groundwater and sediment contaminated with polychlorinated biphenyls (PCBs), we have recently developed a new strategy, integration of the physical adsorption of PCBs with their electrochemical dechlorination by introducing activated carbon (AC) impregnated with iron/palladium (Fe/Pd) bimetallic nanoparticles (reactive AC or RAC). Since the synthesis and environmental application of the RAC system are now in its infant period, detailed research studies have been followed before its scale up and ultimately field application. In this study, we address various aspects of the RAC system treating aqueous phase PCBs and PCBs-contaminated sediment.

Introduction

Clean up of soil and sediment contaminated with PCBs has been a challenging task due to the high stability and low aqueous solubility of PCBs and their high affinity for organic substances in the environment (1). The US Environmental Protection Agency reported in 1998 that approximately 10% of the sediment in the United States poses potential environmental risk to fish, wildlife, and eventually human (2). Heavily used dredging and disposal method is expensive and the method is just clean up of a site, meaning physical transfer of the PCBs from one site to another secure site. Alternatively in situ capping, employing a physical barrier of AC-amended sand layer, has been proposed to isolate the contaminated sites from the surrounding environment (3). The AC capping approaches do not degrade PCBs but only physically sequester them. Meanwhile, complete electrochemical dechlorination of PCBs to biphenyl (BP) on reactive metallic particles such as Fe, Fe/Pd and Mg/Pd has been reported (4). Due to its high reactivity, nanoscale bimetallic system as an applied environmental nanotechnology seems promising in the treatment of aqueous phase PCBs. However, its effectiveness to treat PCBs strongly adsorbed to sediment matrix is doubtful since the availability of hydrophobic PCBs for the dechlorination on metal surface is extremely limited. In order to address this concern, we have recently synthesized RAC composite for adsorption and simultaneous dechlorination of PCBs.

Method

The detailed description for the synthesis procedures of RAC was reported in our previous paper (5). Briefly, for its high reactivity and desired properties, the physicochemical properties of RAC were tailor-designed at nanoscale through i) introduction of mesoporous AC for Fe placement, ii) in situ incorporation of Fe in the AC pores and its thermal treatment for strong iron/carbon metal-support interaction, iii) sodium borohydride reduction of iron oxide to elemental iron, and iv) modification of Fe surface with a discontinuous layer of noble metal Pd. The RAC treated

aqueous phase PCBs and eventually PCB-spiked sediment (Cesar Creek, Cincinnati, Ohio) and PCB-contaminated sediment (Waukegan Harbor, Illinois).

Results and Discussion

The restriction of Fe crystal growth in the mesopores of AC during its thermal treatment induced 6–12 nm Fe nanoparticles on which 2–3 nm Pd particles were deposited and the resulting RAC had high surface area of 358 m²/g and pore volume of 0.352 cm³/g for PCBs adsorption, and 14.4 % Fe and 0.68% Pd contents for PCBs dechlorination (5). The electrochemical dechlorination of PCBs and the physical adsorption of PCBs and their reaction intermediates could be simultaneously achieved with the RAC. In this study, we elucidate its mechanistic aspects through sacrificial batch experiments treating aqueous phase 2-chlorobiphenyl (2-CIBP), including adsorption of 2-CIBP from liquid phase to RAC solid phase, transformation of the adsorbed 2-CIBP to BP by Fe/Pd, and partitioning of the formed BP between liquid and AC phases. Optimization of the RAC system is also discussed to investigate how the RAC properties influence its performance on PCBs adsorption and dechlorination, including Fe content and role of Pd. Some other critical aspects such as adsorption and dechlorination capacity, ageing and oxidation, and Fe/Pd leaching of RAC, and structure specific resistance of some selected PCB congeners to dechlorination are addressed. Finally, we demonstrate the treatability of RAC to PCB-contaminated sediment.

Conclusions

Due to its simultaneous action for adsorption and dechlorination, RAC composite is interesting and promising for the remediation of environmentally contaminated sites with PCBs or other chlorinated hydrophobic compounds. In addition, the RAC composite introduced here are practical and plausible for large-scale field applications over other approaches using colloidal Fe/Pd nanoparticles and passive AC capping material. A new strategy and concept of “reactive” capping barrier composed of the RAC is also proposed as a new environmental risk management option for PCBs-contaminated sites.

References

- Agarwal, S., S. R. Al-Abed, and D. D. Dionysiou. (2007) “In Situ Technologies for Reclamation of PCB-Contaminated Sediments: Current Challenges and Research Thrust Areas.” *J. Environ. Eng.* 133 (12), 1075-1078.
- EPA’s Contaminated Sediment Management Strategy; U.S. Environmental Protection Agency, Office of Water: Washington, DC, 1998; EPA-823-R-98-001.
- McDonough, K. M., P. Murphy, J. Olsta, Y. Zhu, D. D. Reible, and G. V. Lowry. (2007) “Development and Placement of a Sorbent-Amended Thin Layer Sediment Cap in the Anacostia River.” *Soil Sediment Contam.* 16 (3), 313-322.
- Fang, Y., and S. R. Al-Abed. (2007) “Partitioning, Desorption, and Dechlorination of a PCB Congener in Sediment Slurry Supernatants.” *Environ. Sci. Technol.* 41 (17), 6253-6258.
- Choi, H., S. R. Al-Abed, S. Agarwal, and D. D. Dionysiou, “Synthesis of Reactive Nano Fe/Pd Bimetallic System-Impregnated Activated Carbon for the Simultaneous Adsorption and Dechlorination of PCBs.” *Chem. Mater.* 20 (11), 3649-3655.

Comprehensive Investigations on Nano-Size ZVI for Mending an Existing Permeable Reactive Barrier in the 100-D Area at the Hanford Site

Marek H. Zaluski, Gary Wyss, Adam Logar, Nick Jaynes, Martin Foote, Gilbert M. Zemansky, Kenneth R. Manchester, Steve Antonioli, Mary Ann Harrington-Baker, MSE Technology Applications, Butte, Montana, U.S.A.

David Reichhardt, Montana Tech, Butte, Montana, U.S.A.

Mark Ewanic, Montana Department of Environmental Quality

Scott Petersen, Fluor Hanford, Washington, U.S.A.

Abstract

MSE Technology Applications, Inc. has conducted investigations associated with the injection of nano-size zero-valent iron (nZVI) into the subsurface at the 100-D Area at the U.S. Department of Energy (DOE) Hanford Site in Washington State. The purpose of this work was to demonstrate the feasibility of using nZVI to repair portions of the In Situ Redox Manipulation (ISRM) barrier located in the 100-D Area of the Hanford Site that was installed to intercept hexavalent chromium (Cr^{6+}) plume moving towards the Columbia River. We conducted a comprehensive investigation on available ZVI materials that included screening of these materials, geochemical and injectability laboratory studies and computer modeling. The investigation identified RNIP-M2 (RNIP), product by Toda Kogyo Corporation, as most suitable for mending the ISRM barrier. This work was conducted through the support of Fluor Hanford, a subcontractor to the DOE, under Contract Number 30994.

Introduction

We have conducted investigations associated with the injection of nano-size zero-valent iron (nZVI) into the subsurface at the 100-D Area at the U.S. Department of Energy (DOE) Hanford Site in Washington State. The purpose of this work was to demonstrate the feasibility of using nZVI as a source of electrons to repair portions of the ISRM barrier. The ISRM barrier was installed at that site to intercept a Cr^{6+} plume moving towards the Columbia River. The ISRM barrier was installed from 1999 to 2002 (DOE, 2006) by injecting sodium dithionite to the Ringold Formation aquifer and creating persistent reducing conditions by converting native Fe^{3+} to Fe^{2+} . Although laboratory and field tests indicated that the barrier would effectively treat Cr^{6+} for nearly 20 years, a few of the barrier wells exhibited signs of breakthrough after less than two years. The work reported here was performed to support testing an alternative technology to mend the ISRM barrier, by injecting nZVI into the Ringold aquifer through existing wells.

Comprehensive Investigations

We conducted a comprehensive investigation of available ZVI materials. It included assembly of a database, laboratory screening of the most promising nZVI materials, geochemical and injectability laboratory studies, and computer modeling. This investigation, described further in this paper, resulted in the selection of RNIP-M2, manufactured by Toda Kogyo Corporation, as the

most suitable nZVI material for mending the ISRM barrier.

Screening of Available ZVI Materials

We developed (Jaynes et al. 2008) a database that contained 30 ZVI candidate materials (Table 1). We also developed a scoring system based on a number of selection criteria, which we felt best described the material's injectability and Cr⁶⁺ reduction capacity. Based on this scoring system, the top six ranked materials (EZVI, Polyflon Particles, NanoFe I, NanoFe II, Zloy, and RNIP-M2) were selected for initial laboratory screening tests.

Table 1. ZVI Materials and Manufacturers

ZVI Material Name	Manufacturer
Cellulose stabilized NZVI	Auburn University
CIP-EQ	BASF
CIP-EW	BASF
CIP-HQ	BASF
CIP-HS	BASF
Connelly CC-1200	Connelly GPM Inc.
EZVI	Toxicological and Environmental Associates Inc.
EHC-M™	Adventus Americas Inc.
H-200	Hepure Technologies Inc.
HC-5	Hepure Technologies Inc.
HC-15	Hepure Technologies Inc.
H2OMet-56™	Quebec Metal Powders Ltd.
H2OMet-414™	Quebec Metal Powders Ltd.
H2OMet-XT™	Quebec Metal Powders Ltd.
Iron Metal	CERAC
LD-80	North American Hoganas Inc.
Metamateria A	Metamateria Partners
Metamateria B	Metamateria Partners
Metamateria C	Metamateria Partners
Micropowder S-3700™	International Specialty Products
NanoFe™	Lehigh Nanotech – dist. By PARS Environmental
NanoFe™ Slurry I	Lehigh Nanotech
NanoFe™ Slurry II	Lehigh Nanotech
NF-325	North American Hoganas Inc.
Peerless™ Iron Powder	Peerless Metal Powders and Abrasives
Polyflon Particles	Crane Polymetallix – dist. by Nanitech LLC
R-12	North American Hoganas Inc.
RNIP-10DS	Toda Corporation
RNIP-M2	Toda Corporation
Zloy™	OnMaterials LLC.

Laboratory Preliminary Screening

Batch screening tests were performed on the selected six materials (Jaynes et al. 2008). The experiments consisted of a 4-hour batch test performed on a mixture of the ZVI material, clean silica sand and surrogate groundwater to evaluate the materials' ability to create a reducing environment and reduce Cr^{6+} . All six materials were successful at reducing the dissolved chromium and were advanced for further testing.

Injection screening tests were performed to evaluate the ability of the six ZVI compounds to permeate and deposit throughout the entire cross section of horizontally placed flow cells, and their effect on hydraulic conductivity (K) (Jaynes et al. 2008). Each material was injected through two flow cells packed with a blend of silica sand. Samples of solid cores and flow cell effluent were analyzed for iron to evaluate the depositional characteristics of each nZVI material. Two of the nZVI compounds were advanced to the geochemical column screening tests.

Geochemical column screening tests were conducted on Polymetallix and RNIP-M2 (Jaynes et al. 2008). Micropowder™ S-3700 material (MP) was also tested for comparison purposes due to its previous history with the investigations (Fluor Hanford, 2004, DOE, 2006, and Oostrom, et al., 2005). Surrogate groundwater containing 572 ppb Cr^{6+} was injected through vertical columns for approximately 20 pore volumes. The columns were filled with sand containing 1.5% (high) and 0.075% (low) nZVI. The materials were evaluated on their ability to reduce Cr^{6+} without

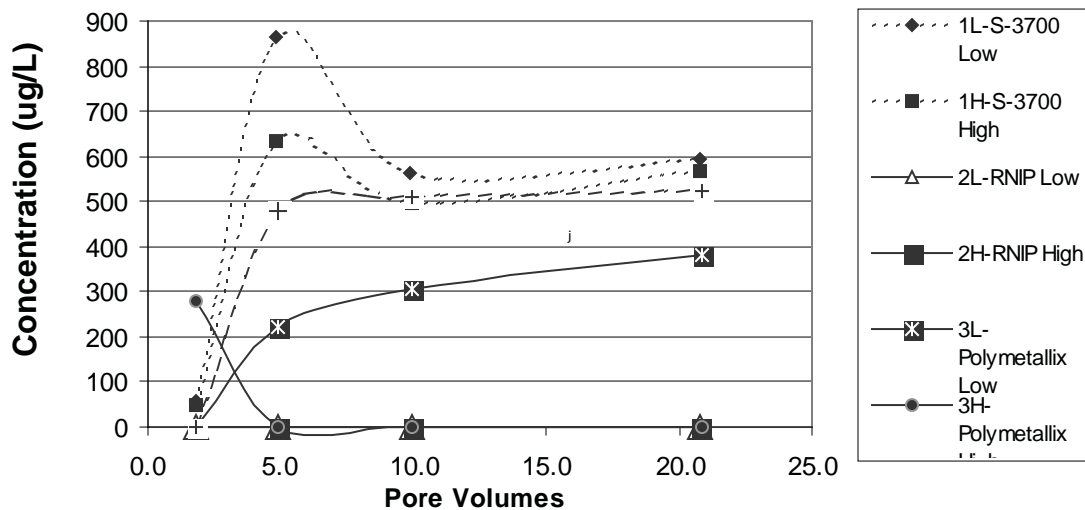


Figure 1. Geochemical Screening test - Chromium Reduction (some data for RNIP not visible as it reduced Cr^{6+} to zero)

producing any unwanted by-products such as ammonia. The Cr⁶⁺ results (Figure 1) show RNIP and high concentration of Polymetallix reducing Cr⁶⁺ concentration to zero; thus they were advanced to the rigorous geochemical laboratory tests. MP was ineffective at significantly reducing Cr⁶⁺ concentrations and was dropped from further consideration.

Geochemical Laboratory Testing

The experiments used vertical columns that were packed with nZVI material and Ringold Formation sediment (Wyss et al. 2008). A column flow rate of 1 ml/min was used to replicate the regional groundwater flow rate in the high permeable zones of the 100-D Area. Three concentrations [1.5% (high), 0.15% (medium), and 0.015% (low)] of each nZVI material were used in the columns; three columns of each were prepared and run under identical conditions. The surrogate groundwater chemical composition mimicked the composition of the groundwater. Approximately 40 (37 to 48) pore volumes of surrogate groundwater were passed through each column, and effluent samples were taken at six different times during the experiments.

The primary objective of the geochemical testing was to determine which of the nZVI materials could sustain reduction of Cr⁶⁺ for the longest time period. At the high nZVI concentration both materials were able to remove the Cr⁶⁺ to levels below detection. At the medium concentration (Figure 2) the RNIP material removed the Cr⁶⁺ nearly completely throughout the entire duration of the test, while the Polymetallix material was removing only 20% to 25% of the Cr⁶⁺ by the end of the test. The low concentration RNIP material removed approximately 75% of the Cr⁶⁺ during the initial stages of the test, and only approximately 15% at its end. The low concentration Polymetallix ZVI columns were not able to remove any appreciable amount of Cr⁶⁺. Thus, only RNIP-M2 was advanced to the injectability testing.

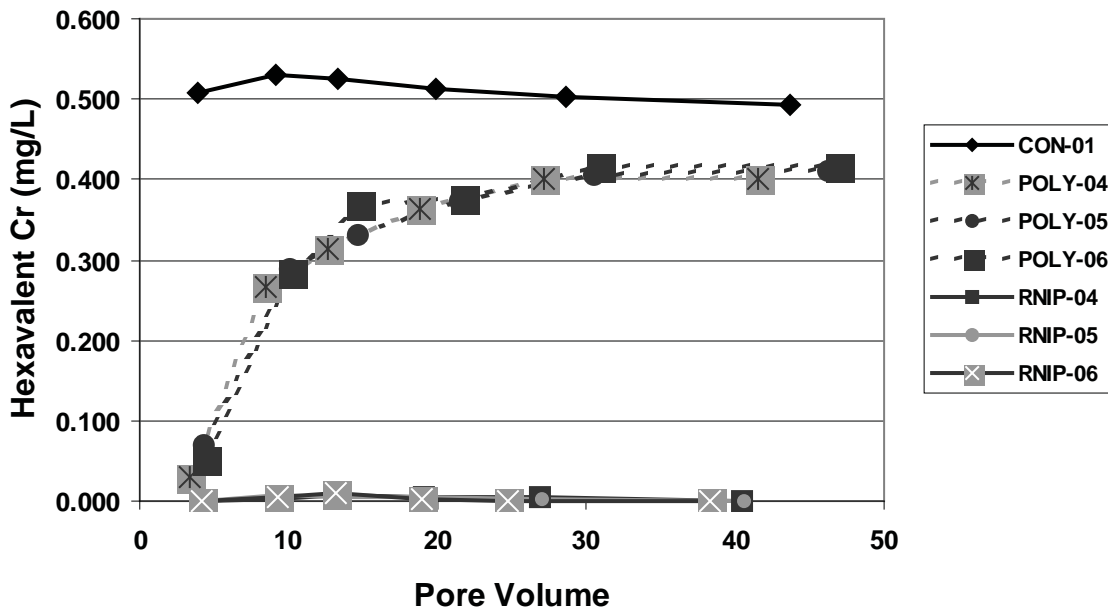


Figure 2. Geochemical Test - Chromium Reduction by 0.15 Concentration of nZVI

Injectability Testing

Injectability testing of RNIP included laboratory experiments with 3-m long horizontal flow cells, and a short injectability test using a large sand tank.

Flow cell injectability test was conducted in duplicates using 3-m long horizontal flow cells into which nZVI fluid, containing 1% RNIP, was injected at four different flow velocities. Though, this experiment was conducted to evaluate the effect of long term RNIP injection on the K of the medium, its primary purpose was to develop a mathematical expression for deposited nZVI as a function of injection time, distance from the injection point, and nZVI-fluid velocity (Zaluski et al. 2008). This function was then used in a computer model to predict a post-injection distribution of deposited ZVI in the Ringold aquifer (Zaluski et al. 2008). In addition, the flow cell tests demonstrated an important phenomenon of amassing of nZVI particles, defined as an increase in concentration of the nZVI suspended particles above that in the influent.

Sand tank injectability test was conducted to simulate an actual field injection in a Hanford well. It used a 5-foot diameter, 5-foot tall cylindrical tank with a 6-inch diameter injection well installed in its center (Zemansky et al. 2008). A solution containing 1% RNIP was injected at a flow rate of 3 gpm for 100 minutes into a synthetic aquifer composed of medium and very coarse sand arranged in three layers. Measurements of fluid variables and fluid samples were taken during the injection. After the injection, sand from the tank was excavated and sampled. It was found that iron deposition occurred predominantly in the very coarse sand layer. The zone of highest deposition formed a ring around the injection well at a radial distance of about 1.5 ft from the center of the tank (Figure 3). This test confirmed that RNIP could be injected into the Ringold-like aquifer without excessive increase of the K.

Computer Modeling

For the computer modeling we used the PORFLOW™ model and focused on prediction of spatial distribution of nZVI emplaced in the Ringold aquifer by injecting RNIP fluid (Zaluski et al. 2008). By using a previously defined deposition function for RNIP and simulating different injection rates of nZVI fluid we defined the optimal injection rate of 0.00089 m³/s (14 gpm) that was related to nearly maximum concentration of nZVI in the highest-K strata of the Ringold aquifer at the distance of 7 m (Figure 4). The 7 m distance equals half of the ISRM barrier width and was considered a target for deposition of at least 0.001 Kg of nZVI per Kg of soil or 1 g/Kg. The model predicted that the concentration of nZVI at that location would be 4.7 g/Kg.

Conclusions

The comprehensive investigation that included assembly of a database of available ZVI materials, their laboratory screening, geochemical and injectability laboratory studies, and computer modeling appeared to be well set for the selection of the most applicable nZVI material for field testing. The RNIP-M2 nZVI manufactured by Toda Kogyo Corporation was determined to be the most suitable for mending the ISRM barrier. The investigations conclude that it is possible to deposit 4.8 g/Kg of nZVI in soil at 7 m from the injection well.



Figure 3. Sand Tank Study - Iron Deposition Near Bottom of Very Coarse Sand Layer.

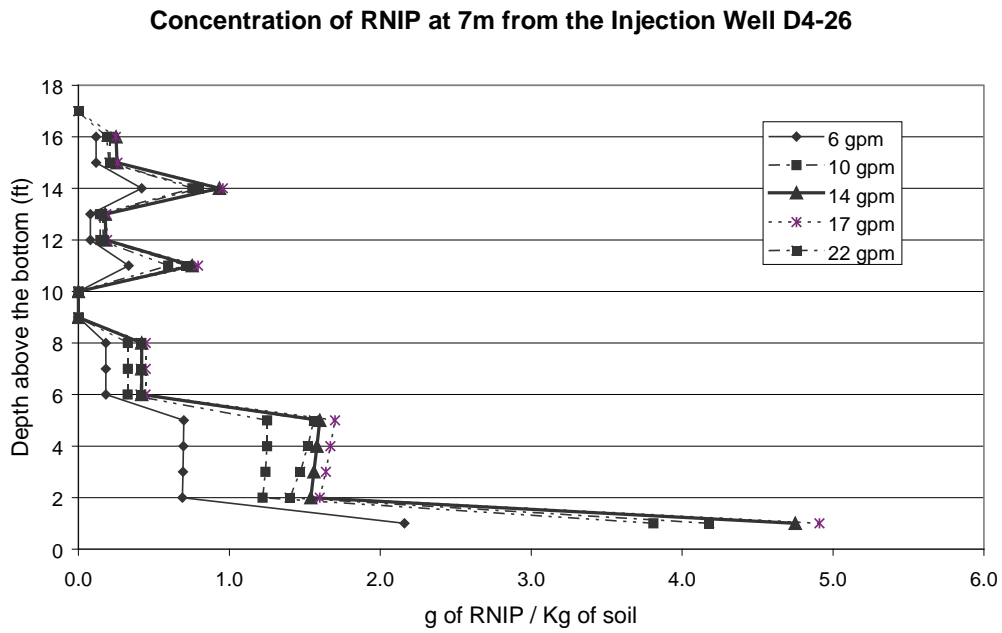


Figure 4. Concentration of RNIP at 7 m from the Injection Well D4-26

Acknowledgements

The authors appreciate the insight of and helpful discussions with Drs. P. Tratnyek, G. Lowry, C. Palmer, and A. Jazdanian during execution of the investigations.

References

- DOE (2006). "The Second CERCLA Five-Year Review Report for the Hanford Site." DOE/RL-2006-20, Revision 1.
- Fluor Hanford (2004). Evaluation of Amendments for Mending the ISRM Barrier. WMP-28124, Rev. 0, Fluor Hanford, Richland, Washington.
- Jaynes N., A. Logar, M. Foote, G. F. Wyss, M. H. Zaluski, M. Hogan, and S. Petersen. (2008). "Screening of Available ZVI Products for Mending an Existing Permeable Reactive Barrier in the 100-D Area at the Hanford Site". Proceedings of International Environmental Nanotechnology Conference, EPA, Chicago, Illinois.
- Jazdanian A. of Toda America (2008). Personal communication.
- Oostrom, M., T.W. Wietsma, M. A. Covert and V.R. Vermeul. (2005). "Experimental study of micron-size zero-valent iron emplacement in permeable porous media using polymer enhanced fluids. Report PNNL-15573, Pacific Northwest National Laboratory, Richland, WA.
- Wyss G., A. Logar, M. Foote, N. Jaynes, M. H. Zaluski, M. Hogan, and S. Peterson. (2008). "Geochemical Laboratory Testing of Nano-Size ZVI for Mending an Existing Permeable Reactive Barrier in the 100-D Area at the Hanford Site". Proceedings of International Environmental Nanotechnology Conference, EPA, Chicago, Illinois.
- Zaluski, M. H., G. M. Zemansky, A. Logar, K. R. Manchester, A. K Runchal, D. Reichhardt, and S. Petersen. (2008). "Predictive Numerical Model of Post-Injection Distribution of Nano-Size ZVI in the Ringold Aquifer for Mending an Existing Permeable Reactive Barrier in the 100-D Area at the Hanford Site". Proceedings of International Environmental Nanotechnology Conference, EPA, Chicago, Illinois.
- Zemansky, G. M., A. Logar, K. R. Manchester, M H. Zaluski, M. Hogan, N. Jaynes, and S. Petersen. (2008). "Sand-Tank Test on Injectability of Nano-Size ZVI into Saturated Sand For Mending an Existing Permeable Reactive Barrier in the 100-D Area at the Hanford Site". Proceedings of International Environmental Nanotechnology Conference, EPA, Chicago, Illinois.

Conference Questions and Answers

Question:

What polymers were used with the two ZVI compounds, RNIP-M2 and Polymetallix?

Answer:

The polymer olefin-maleic was used with RNIP-M2. The polymer used with Polymetallix will be listed on our poster at the poster session.

Save

Effects of Particle Size on the Kinetics of Degradation of Contaminants

*Paul G. Tratnyek and Vaishnavi Sarathy, Division of Environmental and Biomolecular Systems
Oregon Health and Science University, Portland, Oregon, U.S.A.*

*Jae-Hun Kimyoon and Yoon-Seok Chang, School of Environmental Science and Engineering
POSTECH, Pohang, South Korea*

*Bumhan Bae, Department of Civil and Environmental Engineering
Kyungwon University, SungNam, South Korea*

Abstract

The putative “nano-size effect” on reaction of Fe^0 with contaminants is examined using a graphical representation that allows simultaneous comparison of mass-normalized (k_M) and surface-area normalized (k_{SA}) rate constants. Generic $\log k_{SA}$ vs. $\log k_M$ plots show the precise relationship between these parameters that is necessary to constitute evidence for a nano-size effect on the intrinsic reactivity of the particles. Data for carbon tetrachloride and other contaminants show that this intrinsic nano-size is not always observed.

Introduction

There are many reports suggesting that nano-sized particles exhibit greater reactivity than micro-sized particles of the same material. Where nano-sized particles of Fe^0 are to be used for degradation of contaminants, the putative nano-size effect on the desired reaction is frequently invoked as an advantage over conventional approaches that involve micron- or millimeter sized Fe^0 (Li et al. 2006; Lien et al. 2006). However, most reports of increased rates of contaminant degradation by nano- Fe^0 are preliminary in that they leave a host of potentially significant (and often challenging) material or process variables either uncontrolled or unresolved. In particular, many studies do not clearly distinguish between mass-normalized and surface-area-normalized rate constants, or do not use robust methods for calculating the latter from the former.

To improve on this situation, some recent studies have attempted to isolate particle size as a variable by performing series of experiments with nanoparticles that vary in size but are effectively identical in composition and structure (Vikesland et al. 2007). In practice, however, these conditions are never completely achieved and it is difficult to determine the degree to which uncontrolled or unknown factors are confounded with particle size effects. Therefore, alternative approaches are needed that can provide a more complete assessment of the factors that influence the rates of reactions involving nanoparticles using the full range of data types that are commonly available.

Methods

The approach that we have found to be most useful is representation of the kinetic data for contaminant degradation on a log-log plot of surface area normalized rate constants (k_{SA} , $\text{L m}^{-2} \text{hr}^{-1}$) versus the corresponding mass normalized rate constants (k_M , $\text{L g}^{-1} \text{hr}^{-1}$), where the two types of

rate constants are related by the specific surface area of the particles (a_s , m^2g^{-1}) according to the equation:

$$\log k_{\text{SA}} = \log k_{\text{M}} - \log a_s \quad (1)$$

Equation 1 is simply the log transform of the basic kinetic model for pseudo-first-order contaminant transformation by Fe^0 (Johnson et al. 1996; Tratnyek et al. 2003). Most studies use this kinetic model, so we have been able to compile data on k_{SA} and k_{M} for a variety of contaminants over a range of conditions. In addition, we have adopted a practice of summarizing almost all new kinetic data measured in our laboratories in k_{SA} vs. k_{M} plots; most recently, these include data for chlorinated propanes, explosives, and dioxins. Once assembled, k_{SA} vs. k_{M} plots can be used to test specific hypotheses about relative reaction rates or to search for patterns that might be indicative of useful relationships. Some of these applications are exemplified below.

Results and Discussion

Equation 1 defines the disposition of data on $\log k_{\text{SA}}$ vs. $\log k_{\text{M}}$ plots and determines some of their general features.

First, note the diagonal contours labeled 0.05 to 300 m^2g^{-1} . Each of these lines represents a single value of a_s (with slope = 1 and intercept = $-\log a_s$). Data from a set of experiments on a particular material where all subsamples of the material are assumed to have the same a_s will plot directly on the corresponding diagonal line.

For a measured value of k_{M} , uncertainty in a_s will not alter the distribution of data on the abscissa but will alter its position on the ordinate (i.e., the points will move vertically on the plot). Conversely, particles of varying size (and therefore, a_s) but consistent composition (and therefore k_{SA}) will give a horizontal line (e.g., 2 in Figure 1).

Any determinate or indeterminate variability in k_{obs} will cause the data to be distributed along (not around) the diagonal contours. Indeterminate variability would be experimental error in the measurement of k_{obs} , and determinate variability in k_{obs} could be the effect of pH, contaminant type, contaminant concentration, etc. Another scenario that would produce data that plot along a single contour (e.g., the line labeled 3 in Figure 1) would be for a contaminant reacting with a range of different materials all having the same a_s .

We can now use Figure 1 to clarify the nature of the putative “nano-size effect” on reactivity of Fe^0 with contaminants. Relative to the point labeled 1, decreasing particle size with no change in the intrinsic reactivity of the particle surface (at this level of approximation represented by k_{SA}) increases k_{M} along the line labeled 2. Increasing the intrinsic reactivity of the particle surface without changing the specific surface area (a_s) increases both k_{SA} and k_{M} proportionately along the line labeled 3. Only the area enclosed by these lines (and shaded in gray) represents an increase in k_{SA} that exceeds that expected effect of increased a_s due to decreased particle size. Thus, only data that fall in the gray area would support the idea that nanoparticles of Fe^0 have a greater intrinsic reactivity than larger particles.

We first utilized $\log k_{\text{SA}}$ vs. $\log k_{\text{M}}$ plots to test for nano-size effects on reduction of two contaminants (carbon tetrachloride and benzoquinone) in Nurmi et al. (Nurmi et al. 2005). A major conclusion that we drew from that analysis was that nanoparticles have larger k_{M} 's than micro-sized

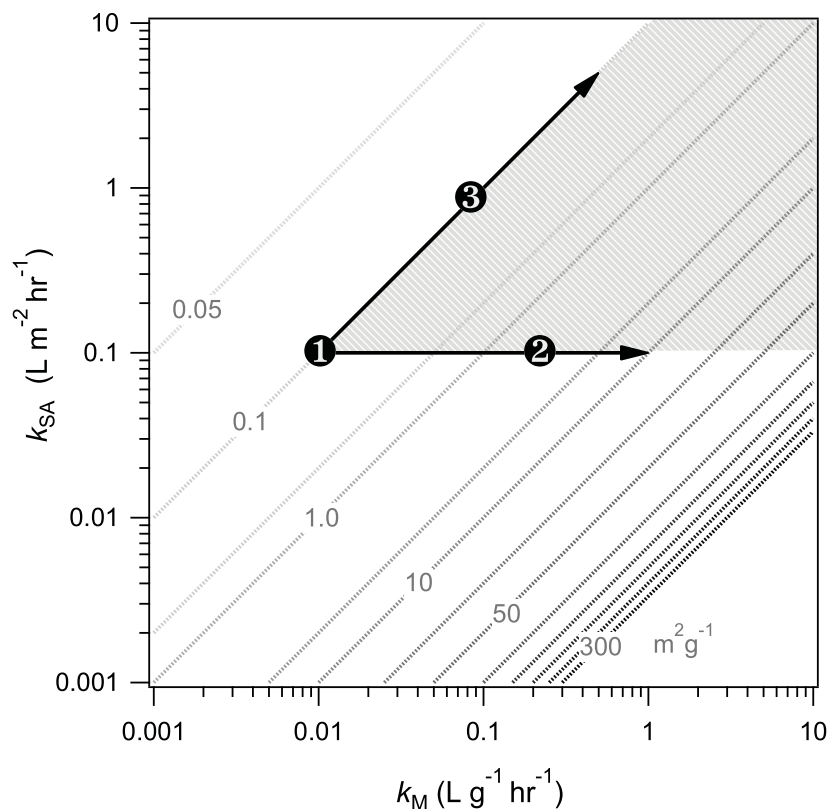


Figure 1. Generic k_{SA} vs. k_M plot showing general features and the primary effects of particle size on rate constants. Relative to the point labeled 1 (which is typical of carbon tetrachloride reduction by micron-sized Fe^0), data supporting an intrinsic nano-size effect must plot in the area shaded gray.

iron, but the k_{SA} 's are similar (i.e., there is no intrinsic nano-size effect for this system). This conclusion was based on only three types of Fe^0 : micro-sized electrolytic Fe^0 from Fisher (Fe^{EL}), nano-sized Fe^0 made by precipitation from solution with borohydride and obtained from Wei-Xian Zhang (Fe^{BH}), and nano-sized Fe^0 made by reduction of Fe_2O_3 with H_2 and obtained from Toda Kogyo Corp. (Fe^{H2}). For each type of iron, however, a range of experimental conditions (pH, buffer, etc.) was represented, as was the effect of uncertainty in a_s . Thus, we anticipated that the conclusions drawn from the analysis would be fairly general for CCl_4 .

Since then, we have extended our analysis to include more of our own data for CCl_4 , many more types of Fe^0 , and most of the previously published data for CCl_4 vs. Fe^0 (Tratnyek et al. 2005). A cartoon version of the result was published in (Tratnyek and Johnson 2006), and Figure 2 shows the actual data. For reduction of CCl_4 by Fe^0 , the analysis confirms that k_M is greater for nano Fe^0 (asterisks) than micro Fe^0 (circles) but that there is no nano-size effect on k_{SA} .

Another conclusion that can be drawn from Figure 2 is that k_M and k_{SA} are both smaller for low-purity iron (solid circles) than high purity iron (nano or micro). Taken together, these results suggest that purity is more important than (nano) size in determining the “intrinsic” reactivity of Fe^0 with CCl_4 .

These conclusions, drawn from Figure 2, are based only on data for reduction of CCl_4 , so we

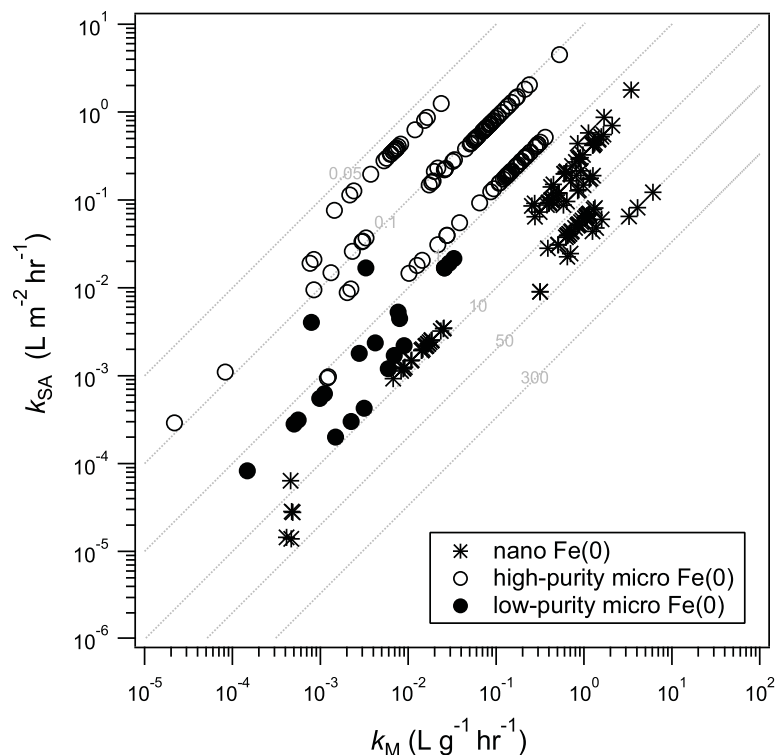


Figure 2. Comparison of rate constants for reduction by nano Fe⁰ and two types of micro-sized Fe⁰ (high-purity laboratory-grade, included Fisher electrolytic; and low-purity construction-grade, including Connelly and Peerless).

have begun to extend this analysis to other types of contaminants including chlorinated aliphatic contaminants (ethanes, ethanes, and propanes); chlorinated aromatics (PCBs, PCDDs, etc.); and explosives (TNT, RDX, HMX). The results are preliminary, but in general they suggest that less reactive contaminants tend to be more sensitive to nano-size effects, and, even for the least reactive contaminants, the nano-size effect on reaction rates is comparable in magnitude to other effects, like those of additives like bimetals and organic coatings.

Conclusions

In most cases, k_M for reactions with nano-sized particles will be greater than k_M for the same reaction with larger particles. However, this difference is often due entirely to the greater surface specific surface area of smaller particles, which provides more total surface area for a given mass of reactant. Cases where there appears to be a nano-size effect on the intrinsic reactivity (i.e., k_{SA}) of Fe⁰ particles with contaminants are more likely to be found with less reactive contaminants.

Acknowledgements

This work was supported by grants from the Nanoscale Science, Engineering, and Technology Program (DE-AC05-76RLO 1830) and the Environmental Management Sciences Program (DE-FG07-02ER63485) of the U.S. Department of Energy (DOE), Office of Science. It has not been subject to review by DOE and therefore does not necessarily reflect the views of the DOE, and no official endorsement should be inferred.

References

- Johnson, T. L., M. M. Scherer, and P. G. Tratnyek (1996). "Kinetics of halogenated organic compound degradation by iron metal." *Environ. Sci. Technol.* 30(8): 2634-2640.
- Li, L., M. Fan, R. Brown, J. Van Leeuwen, J. Wang, Y. Song, and P. Zhang (2006). "Synthesis, properties, and environmental applications of nanoscale iron-based materials: A review." *Crit. Rev. Environ. Sci. Technol.* 36(5): 405-431.
- Lien, H.-L., D. W. Elliott, Y. -P. Sun, and W. -X. Zhang (2006). "Recent progress in zero-valent iron nanoparticles for groundwater remediation." *J. Environ. Eng. Manag.* 16(6): 371-380.
- Nurmi, J. T., P. G. Tratnyek, V. Sarathy, D. R. Baer, J. E. Amonette, K. Pecher, C. Wang, J. C. Lineham, D. W. Matson, R. L. Penn, and M. D. Driessen (2005). "Characterization and properties of metallic iron nanoparticles: Spectroscopy, electrochemistry, and kinetics." *Environ. Sci. Technol.* 39(5): 1221-1230.
- Tratnyek, P. G. and R. L. Johnson (2006). "Nanotechnologies for environmental cleanup." *Nano-Today* 1(2): 44-48.
- Tratnyek, P. G., V. Sarathy, and B. Bae (2005). Nanosize effects on the kinetics of contaminant reduction by iron oxides, Preprints of Extended Abstracts. 230th ACS National Meeting. Washington, DC, American Chemical Society, Division of Environmental Chemistry. 45: 673-677.
- Tratnyek, P. G., M. M. Scherer, T. J. Johnson, and L. J. Matheson (2003). Permeable reactive barriers of iron and other zero-valent metals. *Chemical Degradation Methods for Wastes and Pollutants: Environmental and Industrial Applications*. M. A. Tarr. (Ed.) New York, Marcel Dekker: 371-421.
- Vikesland, P. J., A. M. Heathcock, R. L. Rebodos, and K. E. Makus (2007). "Particle size and aggregation effects on magnetite reactivity toward carbon tetrachloride." *Environ. Sci. Technol.* 41(15): 5277-5283.

Conference Questions and Answers

Question:

Did the data for PCB (polychlorinated biphenyl) congeners (e.g. orthho-substituted congeners that tend to be resistant to reactive dechlorination) on surface area-normalized reaction rate constants data show evidence of the nanoscale effect?

Answer:

A lot of work needs to be done to answer this, including collecting more data on the reaction kinetics. Our earlier work showed that various ZVI products degraded carbon tetrachloride fast enough, but some yielded more favorable products than the others. Therefore, we can hypothesize that nano-size surface sites can produce different branching among reaction patterns.

Comment:

By definition, nanoparticles fall within the size range of 1 to 100 nm. Your work seems to show

that some of the nanoscale iron particles actually fall in the microscale range.

Response:

Yes. That is why a large nano-size effect with respect to the surface-area normalized first-order rate constant was not observed.

Comment:

If you make nanoparticles small enough, surface effects do play a role, especially for PCBs and the types of byproducts that form. Therefore, your generalized conclusion that nanoparticles do not behave differently, is not true in all cases.

Response:

This is true. I would counter that, however, by saying that the approach is useful for interrogating questions like yours, because the rigor by which you define the specific surface area term can be refined. Therefore, if you think hard about how you define reactive surface area, you can play games with this kind of plot and actually test the hypothesis you advocate.

Question:

Do you believe that micron-sized particles with a surface area of around 1 square meter BET (Brunauer, Emmett, and Teller) would have the same reactivity as particles with a primary particle size of 70–80 nm and a secondary particle size of 1–2 microns? We go to great lengths to manufacture nZVI with a primary particle size of 70–80 nm, yet end up with a secondary particle size of 1-2 microns. There is no point to this effort if there is no impact of surface area on reactivity.

Answer:

I would use the plot of $\log k_M$ (mass normalized first-order rate constant) versus $\log k_{SA}$ (surface-area normalized first-order rate constant) and consider how to define the reactive surface area. The plot may show that you are not using the right specific surface area. As a result, only a fraction of the surface area is actually available, and the intrinsic reactivity would be much higher.

Tuning the Properties of Iron Nanoparticles: Doping Effects on Reactivity and Aging

D. R. Baer, Pacific Northwest National Laboratory

P. G. Tratnyek, Oregon Health and Sciences University

J. E. Amonette, Pacific Northwest National Laboratory

C. L. Chun, University of Minnesota

P. Nachimuthu, Pacific Northwest National Laboratory

J. T. Nurmi, Oregon Health and Sciences University

R. L. Penn, University of Minnesota

D. W. Matson, and J.C. Linehan, Pacific Northwest National Laboratory

Y. Qiang, and, A. Sharma, University of Idaho

Abstract

Predicting and controlling the behaviors of nanoparticles in the environment requires understanding the impact of trace elements and impurities (including dopants) on properties, including reactivity and lifetime. The significant impact of many trace elements on the redox activity of iron metal and iron oxide nanoparticles in natural and engineering systems is well established. However, the fundamental mechanisms responsible for specific behaviors and the relationship of the mechanisms to the structural characteristics of the particles and dopants are not as well understood. In addition, the role of trace elements on particle aging and the overall reaction lifetime has not yet received much attention. Here we report the impact of three different processing methods on the reactivity of iron metal-core oxide-shell nanoparticles with carbon tetrachloride.

Introduction

Iron and iron bimetallic nanoparticles (NPs) have been shown to have favorable reaction kinetics towards a variety of environmentally important solute species, including chlorinated hydrocarbons, oxyanions, and metal cations. They have also been observed to produce different, and sometimes more benign, reaction products than microscale iron particles. In recently completed work, we have found that nanoparticulate iron is highly dynamic and that NP aging in solution can have significant impacts on reaction processes⁽¹⁾. Although such changes complicate full understanding of the behavior and lifecycle of NPs, to the degree that these aging processes can be understood and influenced by NP coatings, size, and composition, they also provide an opportunity to predict and control NP behavior.

The general objective of our research is to understand how the environmental fate and chemical

behavior of iron/iron oxide NPs (including transformations of NPs by aging and transformations by NPs of solutes such as chlorinated hydrocarbons or other environmental contaminants) are controlled by reactions within the NPs (i.e., between the core, shell, and coatings), and interactions between the NPs and the geochemical milieu consisting of water, major solutes (inorganic anions), and minor solutes (contaminants). A particular focus is on understanding the factors that influence contaminant reaction pathways with the secondary objective of using the understanding to “design” NPs for desired lifetime behavior (lifecycle) by altering aspects of the NP including size and composition (dopants and coatings).

In earlier work examining the interactions of iron metal-core oxide-shell nanoparticles with carbon tetrachloride (CT) in aqueous solution, we have found that many nanoparticles show the similar reaction rates but some particles have a more environmentally friendly reaction pathway.⁽²⁾ Follow up work demonstrated that both the reaction rate and the reaction pathways vary as function of time in solution⁽¹⁾. Understanding and controlling the reaction properties of NPs requires knowledge of how particles evolve in time, how that evolution alters particle reactivity, and the role of impurities, coatings and trace elements on that time evolution.

The impact of metal doping of NPs has received increased research attention. Although iron metal-core oxide-shell NPs have been observed to enhance both reactivity and modify reaction pathways^(3,4), other workers note that the process is really not well understood and that some of the observed enhancements are readily observed in deionized water but not simulated groundwater⁽⁵⁾. To understand how iron metal-core oxide-shell NPs that are doped with catalyst metals actually function, it is important to have knowledge both of reaction behaviors (as a function of time if possible) and the structure and distribution of the doping material.

Materials and Tests

We have examined the impact of Cu, Ni, and Pd on the reactivity and aging behaviors of iron metal-core oxide-shell NPs with the objectives of understanding their reaction pathways and engineering/designing particles with desired reaction pathways and lifetimes. Metal dopants were added to Fe metal-core oxide-shell particles in three slightly different ways. Solution deposition was conducted by adding a metal sulfate salt solution to nano-sized core-shell particles (RNIP-10DS) obtained from Toda Kyoto Corporation (Schaumburg, IL). These metal core particles were made by reducing goethite or hematite and in hydrogen⁽⁶⁾. We have also synthesized similar particles by a hydrogen reduction process starting with ferrihydrite, but adding the metal dopants as the ferrihydrite was forming in solution or to the formed particles before hydrogen reduction⁽⁷⁾. In addition, high purity iron metal-core oxide-shell nanoparticles were prepared by a sputter aggregation process⁽⁸⁾.

The materials were characterized by a variety of methods, including inductively coupled plasma mass spectrometry (ICP-MS)[for trace elemental analysis], transmission electron microscopy (TEM) and energy dispersive X-ray spectroscopy (EDS) [with a particular focus on locating the trace elements], X-ray diffraction (XRD) [to determine the phases and amounts of phases present], and X-ray photoelectron spectroscopy (XPS)[to determine surface compositions and chemical states]⁽⁹⁾. Reaction studies were conducted to quantify reactivity and branching ratio of products for the reductive degradation of CT^(1,2,7).

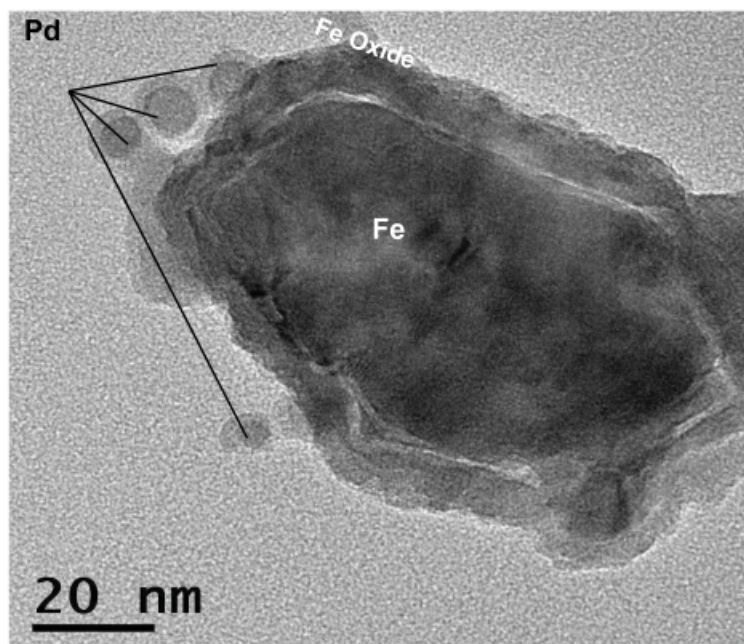


Figure 1. TEM image of iron metal-core oxide-shell NP doped with Pd before the hydrogen reduction process. Individual Pd nanoparticles are readily observed mostly on the outside of the iron NP shell.

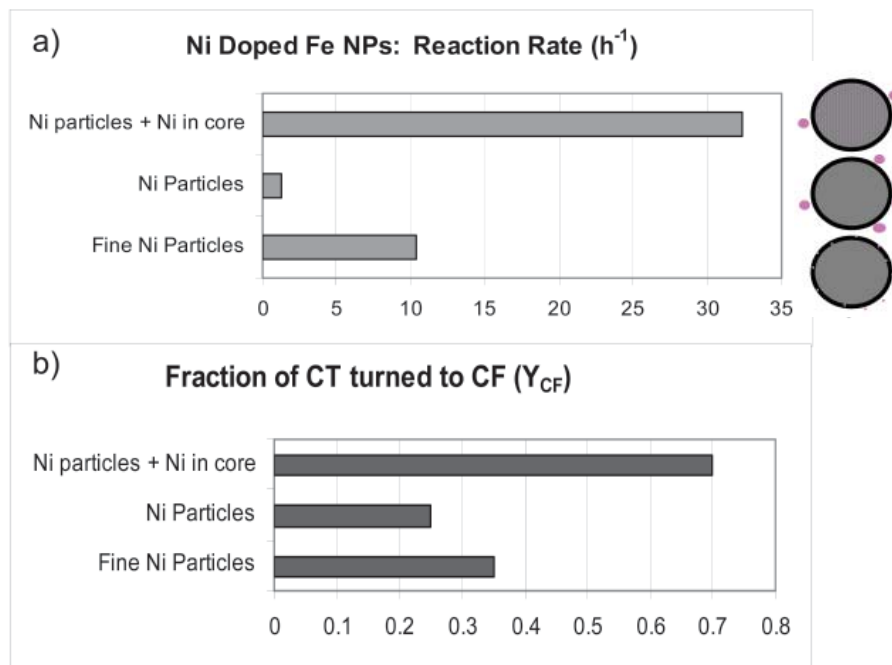


Figure 2. The reactivity of Fe metal-core oxide shell nanoparticles doped with ~1 mole% Ni through the three processes producing different distributions of Ni. a) Particle reaction rates with CT; b) Fraction of CT transformed to CF (Y_{CF}). Schematic representations of the particles demonstrate the different Ni distributions in the particles.

Results and Discussion

The combined results of XRD, TEM with EDS, XPS and ICP-MS indicate that the three different metal doping processes produce particles with different distributions of the metal. The solution deposition process produces very small metal dopants distributed within and on the iron oxide shell. These particles are not easily directly observed. Particles produced by the hydrogen reduction process produce larger nanoparticles (2-3 nm) of the catalytic metal on the surface of the oxide (as shown in Fig 1). If the oxide was co-precipitated with the formation of the ferrihydrite, dopant metal is contained within the iron metal core as well as occurring in the identifiable particles. An example of the types of metal NPs formed during the hydrogen reduction process for Pd doping is shown in Fig 1. The effects of different types of doping are shown schematically along with reactivity data for one particle type in Fig. 2.

As one example of the results, we compare the impact of approximately 1 mole % Ni added to the nanoparticles on the reactivity with CT. Even though the amount of Ni added to these particles is nearly identical, the rates of CT loss are significantly different indicating that the distribution of the metal can have significant impact on the particle reactivity. In Figure 2a, the reaction rates for the reduction of CT are shown. The rate differs by about an order of magnitude. In figure 2b, the chloroform (CF) yield (Y_{CF}) is shown for each of the particle types. Y_{CF} is unity for complete conversion of CT to CF and zero for complete conversion of CT to the more benign products of reduction. In this context a lower value is better and significant differences among the three types of doped particles are observed. In particular, the material containing Ni within the iron core and distributed as nanoparticles on the oxide surface is the most reactive but also has the poorest Y_{CF} . In contrast, the material containing Ni only as nanoparticles on the surface of the oxide shell is the least reactive but has the best (lowest) Y_{CF} .

The above comparisons are the result of experiments performed at a single time point, for freshly synthesized or doped materials. However, reactivity can vary with time; thus it is important to quantify changes as particles age in solution. Measurements of reaction rates every twenty four hours for several days show that the reaction rates for Ni doped materials increase with time a four day period, ultimately having a low Y_{CF} and relatively high reaction rates⁽⁷⁾.

We have found the in some circumstances the reactivity of NPs with CT mirrors general corrosion behavior⁽¹⁾. Measurements of the corrosion behavior of the commercial RNIP particles and ultra pure nanoparticles shows that the corrosion rates of the pure particles may be more than four times slower than the commercially available material⁽¹⁰⁾. Our work and the work of others⁽¹¹⁾ have demonstrated that the reactivity of some NPs nanoparticles can vary significantly on examining fresh wet or dried particles. It is therefore clear that particle processing and handling, the presence of coatings or contaminants, as well as the distribution of dopants can significantly alter particle reaction behavior.

Acknowledgements

This work has been supported by the U.S. Department of Energy (DOE) Office of Science, Offices of Basic Energy Science and Biological and Environmental Research. A portion of this research was performed using EMSL, a national scientific user facility sponsored by the U.S. Department of Energy's Office of Biological and Environmental Research located at Pacific Northwest National Laboratory.

References

1. V. Sarathy, P. G. Tratnyek, J. T. Nurmi, D. R. Baer, J. E. Amonette, C. Wang, C.L. Chun, N. Lee Penn, G. Lai, and E. J. Reardon. (2008). "Aging of Iron Nanoparticles in Aqueous Solution: Effects on Structure and Reactivity." *J. Phys. Chem. C* 112, 2286-2293.
2. J. T. Nurmi, P. G. Tratnyek, V. Sarathy, D. R. Baer, J. E. Amonette, K. Pecher, C. Wang, J. C. Linehan, D.W. Matson, R. L. Penn, and M. D. Driessen. (2005). "Characterization and Properties of Metallic Iron and Iron-Oxide Nanoparticles: Spectroscopy, Electrochemistry, and Kinetics." *Environmental Science and Technology* 39 (5), 1221-1230.
3. H. L. Lien and W. X. Zhang. (2007). "Nanoscale Pd/Fe Bimetallic Particles: Catalytic Effects of Palladium on Hydrodechlorination." *Applied Catalysis B-Environmental* 77(1-2), 110-116.
4. W. Z. Zhang. (2003). "Nanoscale Iron Particles for Environmental Remediation: An overview." *J. Nanoparticle Research* 5(3-4), 323-332.
5. C. E. Schaefer, C. Topoleski, M. E. Fuller. (2007). "Effectiveness of Zerovalent Iron and Nickel Catalysts for Degrading Chlorinated Solvents and n-Nitrosodimethylamine in Natural Groundwater." *Water Environment Research* 79 (1), 57-62(6).
6. M. Uegami, J. Kawano, T. Okita, Y. Fujii, K. Okinaka, K. Kakuya, and S. Yatagi . "Iron particles for purifying contaminated soil or ground water" United States Patent 7022256 Toda Kogyo Corporation, Hiroshima-shi, Japan, Issued April 2006.
7. C. L. Chun, D. R. Baer, D. Matson, J. E. Amonette, and R. Lee Penn. "Characterizations and Reactivity of Metal-Doped Iron and Magnetite Nanoparticles." in Preprints of Extended Abstracts, Division of Environmental Chemistry, 233rd ACS National Meeting, American Chemical Society: Chicago, IL, 2007, Vol. 47, No. 1 408-412.
8. J. Antony, Y. Qiang, D. R. Baer, and C. Wang. (2006). "Synthesis and Characterization of Stable Iron-Iron Oxide Core-Shell Nanoclusters for Environmental Applications." *J. Nanoscience and Nanotechnology* 6 (2), 568-572.
9. D. R. Baer, P. G. Tratnyek, Y. Qiang, J. E. Amonette, J. C. Linehan, V. Sarathy, J. T. Nurmi, C. M. Wang, and J. Antony. (2007). "Synthesis, Characterization and Properties of Zero Valent Iron Nanoparticles." in *Environmental Applications of Nanomaterials: Synthesis, Sorbents, and Sensors*, G. Fryxell, G. Cao, London, United Kingdom: Imperial College Press. Pages: 49-86.
10. D. R. Baer, J. E. Amonette, M. H. Engelhard, D. J. Gaspar, A.S.Karakoti, S. Kuchibhatla, P. Nachimuthu, J. T. Nurmi, V. Sarathy, S. Seal, P. G. Tratnyek, and C.M. Wang. (2008). "Characterization Challenges for Nanomaterials." *Surface and Interface Analysis* 40, 529-537.
11. J. E. Erbs, B. Gilbert, and R. L. Penn. (2008). "Influence of Size on Reductive Dissolution of Six-Line Ferrihydrite." *J. Phys. Chem. C* 112, 12127-12133.

Conference Questions and Answers

Question:

Doesn't the reduction of nickel and cadmium used in doping of nanoscale iron particles impact the results you observed?

Answer:

Probably, but we do not fully understand how yet. We do know that doping changes not only the particles' reactivity with carbon tetrachloride, but also the overall reactivity and nature of the shell on the nanoparticles. Therefore, a lot of possible effects must be considered.

Question:

How much effect does the oxide shell around the iron core have on electron tunneling, the rates of processes, etc?

Answer:

We are starting some experiments to measure the effects of the shell. We have conducted AC-XDS to look at charging and line shifts, which show differences in the conducting properties of shells. We saw differences in the properties of aged and fresh shells. We are now doing experiments to see if we can change the property and answer questions such as: Should we dope the particles? If sulfur is present, does it change the property? How much does aging change the property?

Question:

Would the degree of aggregation versus crystallinity also be important?

Answer:

Yes. When we start with a highly crystalline material and the outside changes, it looks aggregated, somewhat porous, and not at all crystalline. If we start with a really active material, it repassivates, and the repassivated state has different properties.

Pentachlorophenol Reduction in Solid by Reactive Nanoscale Iron Particles

Amid P. Khodadoust, Krishna R. Reddy, and Kenneth Darko-Kagya, University of Illinois at Chicago, Department of Civil and Materials Engineering, Chicago, Illinois, U.S.A.

Abstract

Reactive nanoscale iron particles (RNIP) have been recently investigated for the effective treatment of various aquifer systems. The objective of this study was to investigate the efficiency of RNIP to promote the reductive degradation of pentachlorophenol (PCP) in subsurface soils with low permeability and high permeability using clayey and sandy soils, respectively. Typically, RNIP cannot be applied in the subsurface effectively without surface modification; therefore, the effect of surface modification of RNIP on degradation of PCP in soils was evaluated using RNIP slurries with and without aluminum lactate. A series of batch experiments was conducted using kaolin and natural sand soils spiked with PCP at 100 mg/kg and RNIP at two concentrations of 1 and 4 g/L. RNIP was modified with 10% aluminum lactate (w/w). For both soils, the degradation (reduction) of PCP in soil increased with reaction time for all systems, while degradation of PCP in soil was greater for systems without lactate and for systems with the higher concentration of RNIP (4 g/L). Higher RNIP concentrations resulted in greater degradation of PCP in soil, while longer reaction periods led to greater degradation of PCP in soil (1 and 4 g/L RNIP, with or without lactate). The results show that the greatest degradation after 7 days occurred for the systems with 4 g/L of bare RNIP in both soils. PCP degradation of 35 and 41 percent in natural sand was obtained for RNIP with and without lactate, respectively. PCP degradation of 34 and 64 percent in kaolin was obtained for RNIP with and without lactate, respectively. PCP degradation was greater for kaolin than for natural sand using 4 g/L bare RNIP, while PCP degradation in both soils was comparable using 4 g/L modified RNIP.

Introduction

Pentachlorophenol (PCP) has been used extensively as a general biocide for a variety of purposes such as agriculture and timber preservation. Worldwide use of PCP has led to severe contamination problems particularly around former timber treatment plant sites. PCP was widely used as a wood preservative in the U.S. for several decades, and there are currently Superfund sites (surface and subsurface soils) contaminated with PCP which is considered a priority pollutant by the U.S. EPA (Keith and Telliard, 1979). Various methods employed to remediate PCP from contaminated soils include soil washing, chemical oxidation, and bioremediation; however, these methods are either ineffective or expensive in subsurface soils. Kim and Carraway (2000) found zerovalent iron to be more efficient than other modified zerovalent iron used in their study for dechlorination of PCP, where nearly 50% of the PCP was removed in a few hours. Morales et al. (2002) showed the affinity of zerovalent iron for the dehalogenation of chlorinated phenols. Under either aerobic or anaerobic conditions, the reduction of reducible halogenated organics such as PCP is possible through the surface reactions on the surface of zerovalent iron in the presence of hydrogen ion where iron (Fe^0) is oxidized to ferrous iron (Fe^{2+}):



where R-Cl and R-H are the halogenated and reduced organic compounds, respectively.

RNIP can be used to increase the reactivity of iron towards halogenated organics due to the increased surface area of nanoscale iron particles. The objective of this study was to investigate the efficiency of RNIP to promote the reductive degradation of PCP in subsurface soils with low permeability and high permeability using clayey and sandy soils, respectively. Typically, RNIP cannot be applied for transport in the subsurface effectively without surface modification (Schrick et al., 2004). Therefore, this study was aimed at investigating the efficiency of bare and lactate-modified RNIP to promote the reductive degradation of PCP in the soils. Aluminum lactate used for surface modification of RNIP is an environmentally benign species for subsurface applications of RNIP.

Methods

Soils. The soils used in these experiments were kaolin soil and natural sand soil as low permeability and high permeability soils, respectively. The natural sand was a sandy field soil from the Chicago area taken from the C-horizon (the unconsolidated material underlying the solum or true soil) with known in-situ bulk densities and saturated hydraulic conductivities (Soil Conservation Service, USDA). The C-horizon was chosen because contaminants are generally located within this horizon. The soil had hydraulic conductivity of 0.007 cm/s, pH of 7.9, porosity of 39.6 percent and organic content of 0.98 percent, while containing 99.1 percent sand. The kaolin had hydraulic conductivity of 10^{-8} cm/s, pH of 4.9 and no organic content.

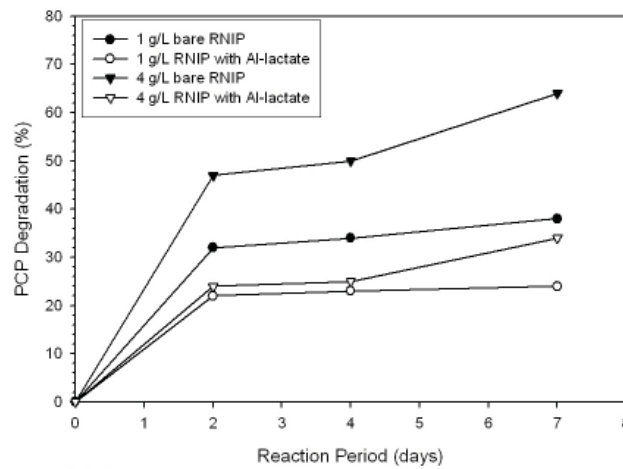
RNIP slurry. A buffered electrolyte solution was used as simulated groundwater and used to prepare RNIP slurry. The electrolyte contained 0.006 M of sodium bicarbonate, 0.002 M of calcium chloride and 0.002 M of magnesium chloride. The pH, total dissolved solids (TDS) and electrical conductivity of the electrolyte solution were 7.76, 500 mg/L and 1020 $\mu\text{S}/\text{cm}$, respectively. The RNIP was obtained from Toda Kogyo (Japan). The RNIP had average particle diameter of 70 nm (50-300 nm), pH of 10.7, and BET surface area of 37.1 m^2/g .

Reactivity experiments. To prepare PCP-spiked soils, a soil-hexane-PCP mixture was stirred to mix the soil and the PCP; the soil-hexane slurry was then allowed to dry in the hood over a period of one week. The dried PCP-spiked soil was thereafter used for reactivity studies. The kaolin and natural sand soils were each spiked with PCP to obtain a target concentration of 100 mg/kg PCP. To determine the reactivity of PCP in soil with RNIP, the spiked soils were mixed with electrolyte solution containing RNIP modified with 10% aluminum lactate using a soil:solution mixing ratio of 1:5 (g:mL) on a rotating shaker. After the reaction period of 2, 4 and 7 days, the soil slurry was centrifuged at 7000 rpm to separate the soil and the RNIP solution. The residual soil and solution were analyzed for unreacted PCP. The soils were extracted with a 75% (v/v) solution of ethanol and water using a 1:5 (g:mL) extraction ratio for 24 hours to extract the PCP from soils (Khodadoust et al., 1999). The PCP in the extract was analyzed using gas chromatography.

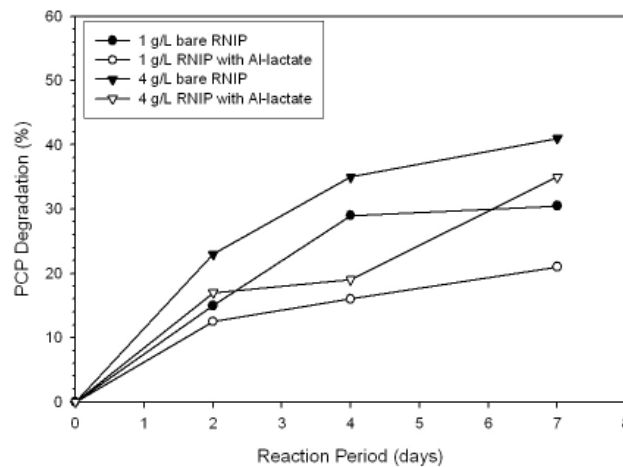
Results and Discussion

The results from the reactivity experiments are shown in Figures 1a and 1b for degradation of

PCP in kaolin and natural sand, respectively. The data presented in Figure 1 show the degradation of PCP in soil with time as function of RNIP concentration and modification with aluminum lactate. The results show that the degradation (reduction) of PCP in soil increased with reaction time for all systems, while degradation of PCP in soil was greater for systems without lactate and for systems with higher concentration of RNIP (4 g/L). In this preliminary study, RNIP concentrations greater than 4 g/L were not used. Higher RNIP concentrations would likely result in greater degradation of PCP in soil based on the trends for degradation of PCP shown in Figure 1, while greater degradation of PCP in soil would occur at longer reaction times for all systems (1 and 4 g/L RNIP, with or without lactate). The results for kaolin show that the greatest degradation after 7 days occurred for the system with 4 g/L of RNIP without lactate (64 percent) while the next highest degradation occurred for the system with 1 g/L RNIP without lactate (38 percent). The results for natural sand show that the greatest degradation after 7 days occurred for the systems with 4 g/L of RNIP (35 and 41 percent for RNIP with and without lactate, respective-



(a) Kaolin



(b) Natural Sand

Figure 1. Degradation of PCP in Soils using Bare and Modified RNIP

ly). For both the kaolin and natural sand soils, the lowest degradation occurred for the system with 1 g/L RNIP with lactate. Lower pH values occurred in systems with aluminum lactate with the lowest pH for the system with 4 g/L RNIP modified with aluminum lactate ; pH values of 6.4 and 7.0 were obtained at initial time and seven-day reaction period, respectively. The solubility of PCP increased at higher solution pH due to the ionization of PCP at pH values greater than 4.7 (the pKa value of 4.7 for PCP). Greater desorption of PCP may have occurred at the higher pH values for systems without lactate, while lesser desorption of PCP occurred for natural sand which had organic matter. Overall for the 7-day reaction period, the preliminary results indicate that the degradation of PCP in the kaolin and natural sand soils increased with reaction time and with increasing RNIP concentration (with and without lactate). The results also indicate that the modification of RNIP with lactate resulted in lower degradation of PCP in both soils (for kaolin : 47 percent lower for 4 g/L RNIP and 37 percent lower for 1 g/L RNIP ; for natural sand : 15 percent lower for 4 g/L RNIP and 31 percent lower for 1 g/L RNIP).

Conclusions

The reactivity of lactate-modified RNIP for degradation of PCP in both the kaolin and natural sand soils was found to be less than the reactivity of bare RNIP, while the degradation of PCP for kaolin was higher than for natural sand.

Acknowledgements

This project is funded by the National Science Foundation Grant No. 0727569 and is gratefully acknowledged.

References

- Keith, L.H., and W. A. Telliard (1979). "Priority Pollutants: I- A Perspective View." *Environ Sci Technol.* 13, 416-423.
- Khodadoust, A.P., M.T. Suidan, C.M. Acheson, and R.C. Brenner (1999). "Solvent Extraction of Pentachlorophenol from Contaminated Sols using Water-Ethanol Mixtures." *Chemosphere* 38, 2681-2693.
- Kim, Y. H., and E. R. Carraway (2000). "Dechlorination of Pentachlorophenol by Zerovalent Iron and Modified Zerovalent Irons." *Environ. Sci. Technol.*, 34, 2014-2017.
- Morales, J., R. Hutcheson, and I. F. Cheng (2002). "Dechlorination of Chlorinated Phenols by Catalyzed and Uncatalyzed Fe(0) and Mg(0) Particles." *J. Haz. Mater.* B90, 97-108.
- Schrick, B., B. Hydutsky, J. Blough, and T. Mallouk (2004). "Delivery Vehicles for Zerovalent Metal Nanoparticles in Soil and Groundwater." *Chemistry of Materials* 16, 2187-2193.

Conference Questions and Answers

No questions.

Arsenic Adsorption and As (III) Oxidation on TiO₂ Nanoparticles: Macroscopic and Spectroscopic Investigations

Gautham Jegadeesan

Pegasus Technical Services, Inc, Cincinnati, Ohio, U.S.A,

Souhail R. Al-Abed, Hyeok Choi, and Kirk G. Scheckel

*National Risk Management Research Laboratory, U.S. Environmental Protection Agency
Cincinnati, Ohio, U.S.A.*

Abstract

Engineered nanoparticles (NPs) (particle sizes ranging from 1-100 nm) have unique physical and chemical properties that differ fundamentally from their macro-sized counterparts. In addition to their smaller particle size, nanoparticles possess unique characteristics such as large surface to volume ratio and higher chemical reactivity, which are conducive for their application in environmental remediation, especially adsorption of target contaminants. In this study, we examined the sorption of arsenite (As (III)) and arsenate (As (V)) on amorphous and crystalline TiO₂ nanoparticles. Macroscopic investigations on arsenic sorption indicated that maximum As (V) coverage on both crystalline and amorphous TiO₂ occurred in the pH range of 3.8-6.5. The effect of pH on As (III) sorption onto amorphous TiO₂ was less pronounced, in comparison to crystalline TiO₂. XAS analysis provided evidence of partial As (III) oxidation on amorphous TiO₂ and not on the crystalline TiO₂, likely due to the surface chemistry of the particles and the presence/ absence of surface hydroxyl groups. Electrophoretic mobility measurements and XAS analysis indicated that As (III) and As (V) form binuclear bidentate inner-sphere complexes with amorphous TiO₂. As (III) and As (V) sorption isotherms indicated that sorption capacities of the different TiO₂ polymorphs were dependent on the sorption site density, surface area (particle size) and crystalline structure. When surface coverages were normalized to specific surface areas, crystalline TiO₂ appeared to exhibit higher capacities. However, a reverse trend was observed when arsenic sorption was expressed on a per unit mass basis.

Introduction

Inorganic forms of arsenic (As), arsenate (As (V)) and arsenite (As (III)), in drinking water are a prevalent problem globally. Due to their carcinogenic effects at elevated concentrations, the acceptable limit for As in drinking water has been lowered to 10 μ g L⁻¹ [1]. Past efforts have focused on sorption and/or co-precipitation of arsenic using oxides of Fe, Al, Mn and Ti as sorbents [2-7]. Among TiO₂ sorbents, crystalline TiO₂ is preferred over its amorphous polymorphs for TiO₂-assisted photocatalytic processes, as the former is more photoactive [4-7]. Thus, most studies have focused on the use of crystalline TiO₂ for arsenic sorption and As (III) oxidation and no studies have been reported, to our knowledge, using amorphous TiO₂. However, crystalline TiO₂ particles were observed to exhibit low sorption capacity for As (III) on a unit mass basis [4-7]. Macroscopic investigations have indicated that amorphous metal oxides of Fe, Al and Mn have large sorption capacities (per unit mass basis) compared to their crystalline polymorphs

due to significant increase in sorption sites and surface areas [8]. Further, the surface structure of the minerals, amorphous or crystalline, can affect their chemistry and reactivity with metal contaminants [8]. In comparison to most crystalline TiO₂ particles, amorphous TiO₂ particles are expected to have small coherent particle size, disordered surface states and high specific surface area. Even though amorphous TiO₂ may not be efficient in the photo-catalytic oxidation of As (III), they may be more effective in As (III) removal in non photo-catalytic processes.

Therefore, in this study, we evaluate the sorption of As (III) and As (V) on amorphous TiO₂ particles. Arsenic sorption behavior and the effect of crystalline composition is evaluated by comparing the sorption capacities of different crystalline TiO₂ and (for the first time) amorphous TiO₂ particles. Further, we evaluate the structure of the two arsenic species on both TiO₂ surfaces using x-ray absorption spectroscopy (XAS) techniques. The results show that the different polymorphs of TiO₂ exhibit different arsenic sorption capacities, largely due to varying site density, surface structure and mineralogy.

Experimental Methods

Amorphous TiO₂ nanoparticles were prepared via a sol-gel method at room temperature (25 °C), similar to the procedure described by Choi et al [9]. The amorphous particles (designated as S-TiO₂) were calcined at 250, 400, 500 and 600 °C to induce transformations to different crystalline compositions and particles obtained were designated as A-TiO₂, B-TiO₂, C-TiO₂ and D-TiO₂, respectively. Additionally, commercially available crystalline TiO₂ particles (designated H-TiO₂, Hydroglobe Inc., NJ) were also used in the experiments. The crystalline composition and size, specific surface area and zeta potential of the TiO₂ particles were determined. Stock solutions (1000 mg L⁻¹) of As (III) (NaAsO₂, 100 %, Sigma Aldrich, MO) and As (V) (Na₂HAsO₄·7H₂O, 100 %, Sigma Aldrich, MO) were prepared in a background electrolyte of 0.001N NaCl. As (III) stock solutions were prepared in an anaerobic glove box and maintained at neutral pH (~7.0) to minimize its oxidation to As (V). All batch sorption experiments were conducted in triplicate. Arsenic adsorption edge was determined using 1 mg L⁻¹ As (III) and As (V) solutions. Initially, the pH of the arsenic solution was adjusted to values ranging between 3 and 11 using either 0.01N HCl or 0.01N NaOH. Subsequently, 0.2 g L⁻¹ S and H-TiO₂ was added to centrifuge tubes containing 50 mL of the solution and the suspension was tumbled in rotary shakers at 30±2 rpm. The final pH of the suspension was recorded after 72 hours. For XAS analysis, wet paste residues of S and H-TiO₂ (As sorbed on TiO₂) from the batch sorption experiments described above and corresponding to arsenic coverage of 0.05-0.26 mg m⁻², were collected and transferred to sealed vials in an anaerobic glove box. Arsenic K-edge (11 867 eV) spectra were collected at the MR-CAT (Sector 10-ID) and XOR-PNC (Sector 20-BM) beamlines at the Advanced Photon Source (APS) at Argonne National Laboratory (ANL, Argonne, IL), equipped with a Si (111) double-crystal monochromator. XAS data analysis was done in a standard manner including data averaging and background subtraction with the linear function through the pre-edge region using Athena version 0.8.050, FEFF 7.0 and ARTEMIS.

Results and Discussion

As can be seen in Table 1, S-TiO₂ was amorphous, while H-TiO₂ was 100 % anatase (crystalline). Calcination of the S-TiO₂ particles at 250 and 400°C resulted in the formation of semi-crystalline particles (A and B-TiO₂), with complete crystallization observed above 500°C. BET

N₂ isotherms indicated that amorphous S-TiO₂ had the highest surface area (408.5 m² g⁻¹). The specific surface area decreased with increasing crystallinity of in-house prepared TiO₂ from 367.8 m² g⁻¹ (A-TiO₂) to 38.8 m² g⁻¹ (D-TiO₂). The pH_{pzc} (pH at point of zero charge) of amorphous S-TiO₂ and A-TiO₂ were almost 4.5, respectively, while that of semi-crystalline B-TiO₂ and crystalline C and D-TiO₂ were higher (6.0-6.1).

Table 1. Properties of TiO₂ nanoparticles

TiO ₂ type	Calcined Temperature (°C)	Crystal phase	Crystal Size	Surface Area (m ² g ⁻¹)	Zeta Potential (pH _{PZC})		
					Before As sorption	As (III) Sorption	As (V) Sorption
S-TiO ₂	25	Amorphous	-	408.5	4.5	4.6	4.2
A-TiO ₂	250	Amorphous /Anatase	5	367.8	4.6	-	-
B-TiO ₂	400	Amorphous /Anatase	10	129.8	6.1	-	-
C-TiO ₂	500	Anatase	15	74.8	6.1	-	-
D-TiO ₂	600	Anatase	20	38.8	6.0	-	-
H-TiO ₂	NA*	Anatase	NA*	98.3	4.8	4.6	3.6

*N.A: Data not available

Arsenic Adsorption Envelopes

Arsenic sorption on amorphous S-TiO₂ and crystalline H-TiO₂ particles as a function of equilibrium (final) pH is provided in Figure 1. At equilibrium, As (V) sorption on both S and H-TiO₂ was the highest (> 90 % removal) between pH 3.5 and 6.9, corresponding to surface coverages (Γ , mg m⁻²) of 0.012 mg m⁻² and 0.05 mg m⁻², respectively (Figure 1). The surface coverage of As (V) on H-TiO₂ was higher than that on S-TiO₂ for all pH values, even though sorption capacities per unit mass basis (mg g⁻¹) were similar. In the alkaline pH range (beyond pH 10), As (V) sorption on both particles decreased precipitously, with the decrease observed to be higher for S-TiO₂ (Γ =0.002 mg m⁻²). Compared to arsenate, the effect of pH on As (III) sorption on S-TiO₂ was less pronounced. Approximately 95 % of As (III) (Γ = 0.011 mg m⁻²) was removed using S-TiO₂ in the equilibrium pH range of 3.7-8.9 (Figure 1A and 1B), with a marginal decrease observed beyond pH~8.9. On the other hand, As (III) sorption on H-TiO₂ was observed to increase from Γ of 0.024 mg m⁻² to Γ of 0.046 mg m⁻² with increasing pH from 3.8-9.0, and then decreased beyond pH 9.8. However, the difference in As (III) sorption profiles between S and H-TiO₂ particles can be attributed to significantly higher sorption site density for amorphous S-TiO₂, resulting in complete arsenic removal at conditions of less than maximum surface coverage. EM measurements indicated that the pH_{pzc} for both S-TiO₂ (from 4.5 to 4.2) and H-TiO₂ (from 4.8 to 3.6) decreased upon As (V) sorption (Table 1). The formation of inner-sphere complexes is known to shift the pH_{pzc} to lower values [10]. Our observations here suggested that As (V) sorption on both S and H-TiO₂ occurred via the formation of inner-sphere complexes. Negligible shift in pH_{pzc} values for both TiO₂ particles upon As (III) sorption indicated the possibility of As (III) sorption via the formation of either outer-sphere or neutrally charged inner-sphere complexes [3-4].

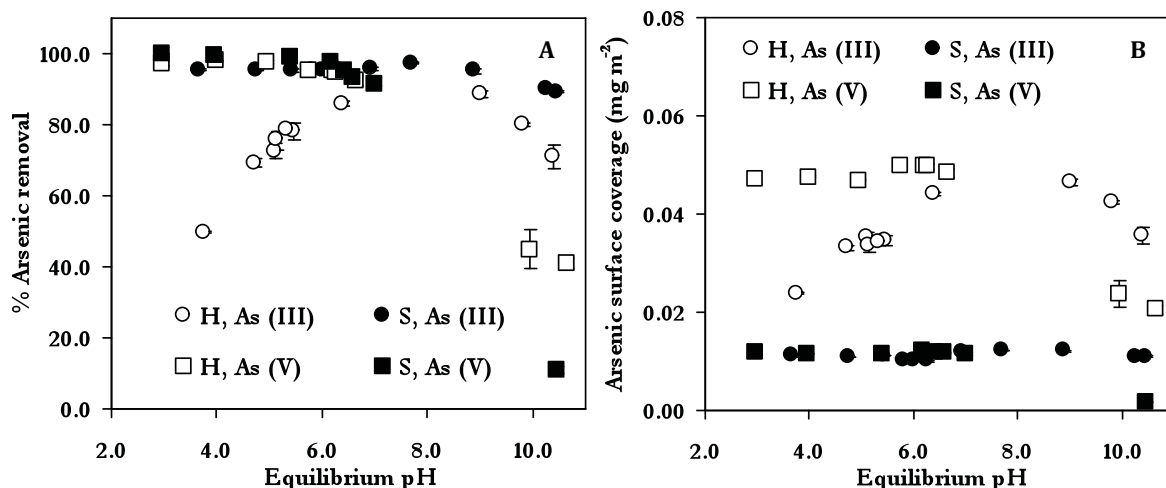


Figure 1. Arsenic sorption on amorphous (S, closed symbols) and crystalline (H, open symbols) TiO₂ in terms of (A) % As removal and; (B) As surface coverage. Experimental conditions: 1 mg L⁻¹ As (III) and As (V); 0.2 g L⁻¹ TiO₂.

Arsenic Association with TiO₂

The significant feature in the XANES spectra on As (III) sorbed S-TiO₂ was the presence of two distinct edges, occurring close to 11 870 and 11 874 eV (Figure 2). A shift in the binding energy of 0.5 eV was observed for the first peak when compared to the As (III) reference standard. The second absorption maxima were characteristic of As (V), indicating the possibility of As (III) oxidation. In comparison, As (III) treated H-TiO₂ showed only a single peak at 11 870 eV, suggesting no As (III) oxidation. XANES spectra on As (V) sorption on both TiO₂ particles corresponded well with the absorption maxima at 11874 eV for As (V) reference standards. Figure 3 illustrates the raw EXAFS spectra ($k^3\chi(k)$) and the corresponding radial structure function (RSF) in R-space (Å) for As (III) treated TiO₂ samples (solid lines). The fits of the theoretical expressions (dotted lines) are also shown and the structural parameters are listed in Table 2. For As (III) sorbed H-TiO₂ (Figures 3), about 2.4 oxygen atoms formed a coordinated complex with the central As atom at a distance of 1.76 Å, confirming the presence of As (III), which was in

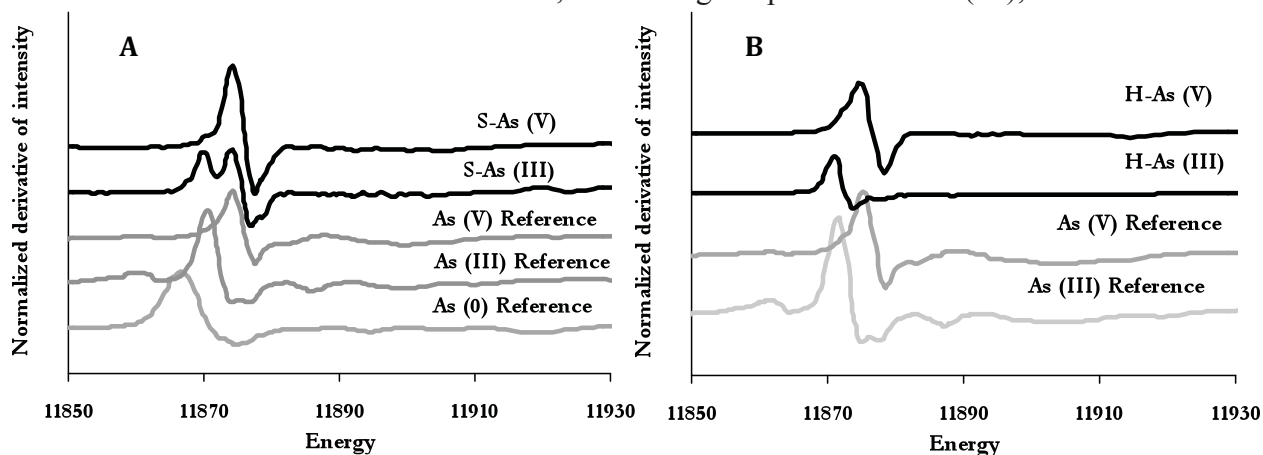


Figure 2. XANES first derivative plots of As (III) and As (V) sorbed (a) S-TiO₂ and (b) H-TiO₂. XANES spectra of As (0), As (III) and As (V) reference standards are also provided.

Table 2. EXAFS Fit Parameter Results for As (III) and As (V) sorption on S-TiO₂ and H-TiO₂

TiO ₂ type	Initial As species	Interatomic shell	χ^{2a}	ΔE_0 (eV)	CN	R (Å)	σ^2 (Å ²)
H-TiO ₂	As (III)	As-O	117	5.9±2.7	2.4±0.3	1.76±0.02	0.003
		As-Ti			1.8±1.0	3.33±0.02	0.009
S-TiO ₂	As (III)	As-O	144	2.9±1.6	3.3±0.4	1.69±0.02	0.001
		As-Ti			1.8±0.9	3.27±0.02	0.004
H-TiO ₂	As (V)	As-O	124	5.8±2.1	3.9±0.4	1.69±0.01	0.003
		As-Ti			2.2±1.2	3.34±0.02	0.006
S-TiO ₂	As (V)	As-O	257	6.7±2.4	4.3±0.6	1.69±0.01	0.002
		As-Ti			1.6±1.0	3.30±0.01	0.0003

The amplitude reduction factor (S_0^2) = 0.9 for all fits; ΔE_0 = energy offset; CN = coordination number; R = interatomic distance; σ^2 = Debye-Waller parameter. The estimated standard deviations for the parameters are reported.

^a The normalized fit error, $\chi^2 = [(\chi_{obs} - \chi_{cal}) / \chi_{obs}]^2$. χ^2 range reported in literature = 66-448 [2, 24]

agreement with previous publications [2-5]. However, the first-shell backscatter peak for As (III) sorbed S-TiO₂ was observed at R = 1.69 Å (Figures 3). This As-O interatomic distance corresponded well with that for As (V) species, definitively indicative of As (III) oxidation on S-TiO₂. The second peak in the FT was attributed to As-Ti interactions at 3.33 Å composed of 1.8 atoms for H-TiO₂ and at 3.27 Å composed of 1.8 atoms for S-TiO₂ (Table 1), indicating the formation of bidentate binuclear complex, consistent with previous studies.

Fitting the As-O first shell contributions to the EXAFS spectra (Figure 3) on As (V) treated H-TiO₂ and S-TiO₂ particles yielded 4.3 oxygen atoms for S-TiO₂ and 3.9 oxygen atoms for H-TiO₂ at a distance of 1.69 Å (Table 1). The distance and the CN (4.0 ± 0.5) were diagnostic of As (V). The contributions of the second-shell peaks were weaker than that of the first-shell peaks. The second shell peaks in the FT plots is due to the As-Ti correlations of 1.6 Ti atoms at 3.30 Å for As (V) treated S-TiO₂, 2.2 Ti atoms at 3.34 Å for As (V) treated H-TiO₂ (Table 1). Previous studies on As (V) adsorption on metal oxides of Fe, Al and Ti had shown that As-metal interactions corresponded to three different types of complexes: monodentate mononuclear complex (As-Fe = 3.60 Å), bidentate binuclear complex (As-Fe = 3.24-3.26 Å, As-Ti = 3.30 Å, As-Al = 3.11 Å) and a bidentate mononuclear complex (As-Fe = 2.83-2.85 Å) [2-5]. Based on theoretical EXAFS fits, it is believed that As (V) adsorption on both S-TiO₂ and H-TiO₂ was characteristic of a bidentate binuclear complex.

Conclusion

Even though, the capacities of the TiO₂ particles prepared in the study (S, A, B, C and D) for arsenic sorption were almost comparable to one another, they were significantly lower than the commercially available H-TiO₂, which can only be attributed to the particle characteristics and preparation procedures. Sorption behavior on metal oxides is largely dependent on the surface structure, crystallinity, particle size and surface energy, all of which are dependent on the particle preparation techniques. However, due to their large surface area, disordered structure and pos-

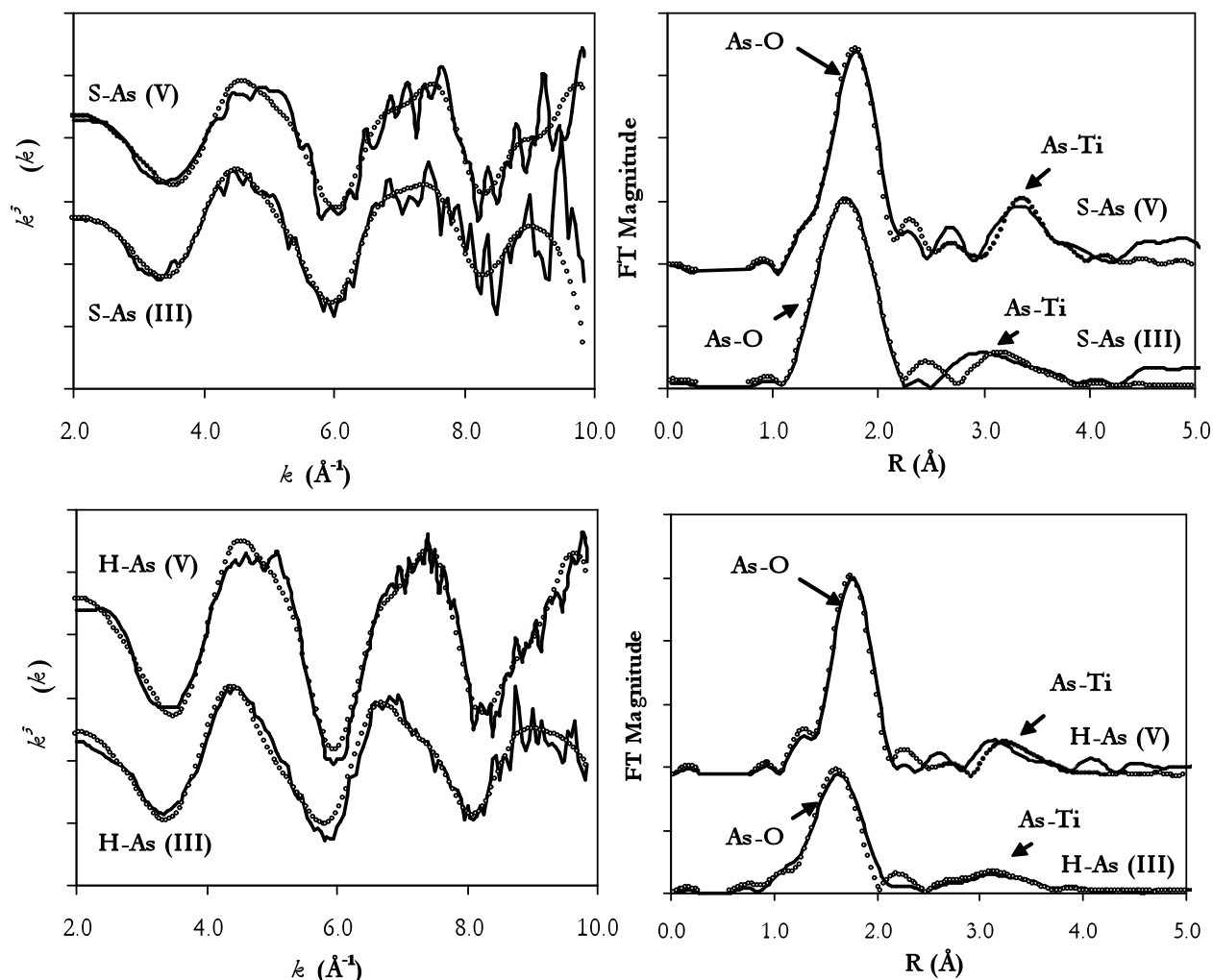


Figure 3. k^3 weighted χ functions and corresponding radial structure functions (RSF) (solid lines) and fits derived from the theoretical EXAFS function (dotted lines). (a) $k^3 \chi(k)$ for As (III) and As (V) sorption on S-TiO₂; (b) Fourier transform of $\chi(k)$ for As (III) and As (V) sorption on S-TiO₂; (c) $k^3 \chi(k)$ for As (III) and As (V) sorption on H-TiO₂ and; (d) Fourier transform of $\chi(k)$ for As (III) and As (V) sorption on H-TiO₂.

sible altered chemical and physical properties compared to crystalline TiO₂, amorphous TiO₂ can be useful in enhancing arsenic sorption (per unit mass basis). Further, the possibility of As (III) oxidation on the surface enhances the possibility of higher effectiveness of As (III) treatment process.

References

1. U.S. Environmental Protection Agency, Implementation guidance for the arsenic rule. In Office of Water, Ed. U.S. Environmental Protection Agency, Washington, DC: 2002; Vol. EPA-816-K-02-018.
2. Manning, B. A.; Fendorf, S. E.; Goldberg, S. (1998). "Surface structures and stability of arsenic (III) on goethite: Spectroscopic evidence for inner-sphere complexes." *Environ. Sci. Technol.* 32, 2383-2388.

3. Arai, Y.; Elzinga, E. J.; Sparks, D. L. (2001). "X-ray absorption spectroscopic investigation of arsenite and arsenate adsorption at the aluminum oxide-water interface." *J. Colloid Interface Sci.* 235, 80-88.
4. Pena, M.; Meng, X. G.; Korfiatis, G. P. (2006). Jing, C. Y., Adsorption mechanism of arsenic on nanocrystalline titanium dioxide. *Environ. Sci. Technol.* 40, 1257-1262.
5. Ferguson, M. A.; Hoffmann, M. R.; Hering, J. G. (2005). "TiO₂-photocatalyzed As (III) oxidation in aqueous suspensions: Reaction kinetics and effects of adsorption." *Environ. Sci. Technol.* 39, 1880-1886.
6. Lee, H.; Choi, W. (2002). "Photocatalytic oxidation of arsenite in TiO₂ suspension: Kinetics and mechanisms." *Environ. Sci. Technol.* 36, 3872-3878.
7. Dutta, P. K.; Ray, A. K.; Sharma, V. K.; Millero, F. J. (2004). "Adsorption of arsenate and arsenite on titanium dioxide suspensions." *J. Colloid Interface Sci.* 278, 270-275.
8. Dixit, S.; Hering, J. G. (2003). "Comparison of Arsenic (V) and Arsenic (III) Sorption onto Iron Oxide Minerals: Implications for Arsenic Mobility." *Environ. Sci. Technol.* 37, 4182-4189.
9. Yoo, K. S.; Choi, H.; Dionysiou, D. D. (2005). "Synthesis of anatase nanostructured TiO₂ particles at low temperature using ionic liquid for photocatalysis." *Catalysis Comm.* 6, 259-262.
10. Stumm, W. (1999) *Chemistry of the solid-water interface.* Wiley-Interscience: New York.

Conference Questions and Answers

No questions.

Save

Differential Reactivity of nZVI Towards Lindane and Implications for QA/QC and Field-Scale Use

Daniel W. Elliott, Geosyntec Consultants, Lawrenceville, New Jersey, U.S.A.

*Wei-xian Zhang, Dept. of Civil and Environmental Engineering,
Lehigh University, Bethlehem, PA, USA*

Abstract

Since the initial field demonstration of nZVI as a potential groundwater remediation tool in 2000, the emerging technology has received considerable attention among academic researchers, regulators, and the regulated community alike. However, evidence from field studies suggests a very wide range of nZVI performance which can be at least partly attributed to the intrinsic properties of the iron itself. Because nZVI is reactive, its fundamental properties can change over time. A key challenge is to objectively develop tools to characterize nZVI efficacy given the relative lack of QA/QC data from manufacturers. Herein, data from the nZVI-mediated degradation of lindane in 95% ethanol was used to illustrate the implications of varying iron reactivity and to underscore the need for standardized QA/QC protocols for nanoscale iron products. Lindane, a well studied pesticide in ubiquitous use around the world from the 1940s into the 1990s, represented an excellent reference contaminant because of its ability to degrade by multiple pathways including dehydrohalogenation and dihaloelimination. Specific QA/QC parameters recommended include pH/ORP profile, particle size distribution, specific surface area, zeta potential/isoelectric point, and batch contaminant degradation test. These data should enable the consulting, regulated, and regulator communities to better predict nZVI reactivity prior to use in the field.

Introduction

Since the initial “proof of concept” field study conducted in 2000, the emerging nanoscale zero-valent iron (nZVI) technology has received considerable interest among researchers, regulators, consultants, and the regulated community. In addition to expanding the list of amenable reductates, key research advancements over the past 8 years have included the development of novel surface-modified nZVI systems to improve colloidal stability (Lowry et al., 2005), characterization of the nZVI aggregation (Lowry et al., 2007), improved assessment of transport capabilities (Mallouck et al, 2007; Clement et al., 2008), and determination of the effects of particle age and solution pH on reactivity (Liu and Lowry, 2006), among others. Progress has also been realized regarding the commercial production of nZVI material. Although the reduction of aqueous ferrous or ferric salts by sodium borohydride is the most widely used method to produce nZVI for research purposes, most commercial and/or industrial approaches involve either physical (e.g. high energy milling or ultrasound shot peening) or chemical syntheses (e.g. vapor deposition of iron pentacarbonyl, $\text{Fe}(\text{CO})_5$ under helium or gas-phase reduction of goethite or hematite by hydrogen at high temperature (Li et al., 2006).

According to recent peer-reviewed field studies, the effectiveness of the injected nZVI has varied considerably with some investigators reporting excellent contaminant degradation while others described mixed results (Elliott and Zhang, 2001; Glazier, et al., 2003; Gavaskar et al., 2005; Henn and Waddill, 2006). This variability partly reflects the intrinsic reactivity of the nZVI and propensity for its properties to change over time. The paucity of quality assurance and quality control (QA/QC) data from manufacturers, coupled with the lack of field performance data, may be hindering more widespread acceptance of the nZVI technology.

Lindane, the gamma isomer of hexachlorocyclohexane (γ -HCH) with molecular formula $C_6H_6Cl_6$, is a well studied pesticide which was in ubiquitous use around the world from the 1940s until the 1990s. The structure of lindane, depicted in Figure 1, features three of its chlorine substituents occupying more stable (i.e. less reactive) equatorial positions and three occupying less stable (i.e. more reactive) axial positions (March, 1985). Lindane is capable of undergoing degradation via both base-catalyzed dehydrohalogenation to form a pentachloro alkene or dihaloelimination to form a tetrachloro alkene (Cristol, 1947; Cristol et al., 1951). Herein, the nZVI-mediated degradation of lindane in 95% ethanol was used to illustrate the potentially dramatic

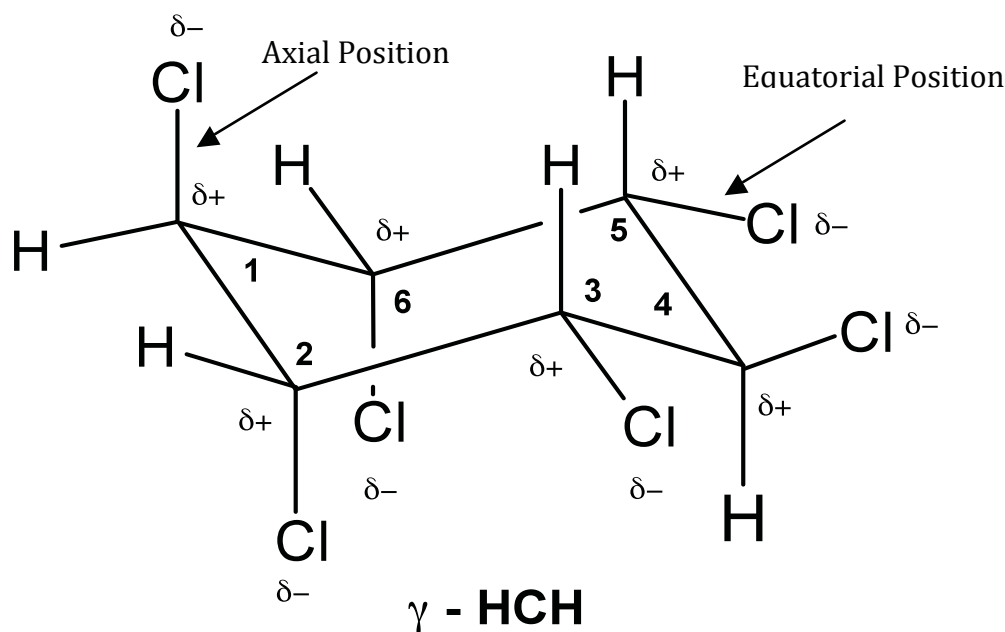


Figure 1. The structure of γ -hexachlorocyclohexane (lindane).

effects of varying iron reactivity and to highlight the need for basic QA/QC data to be available from nZVI manufacturers.

Methods

High concentrations (e.g. 1-2 mM) of lindane in 95% ethanol (EtOH) were treated by 9.4 – 26.5 grams per liter, g/L of two different nZVI materials in 120 milliliter (mL) glass amber reactors. Types II and II iron were produced by the borohydride reduction of aqueous ferrous sulfate and had average size ranges of 60 – 70 nanometers (nm) and less than 50 nm, respectively. Quantification of lindane and its degradation products was accomplished using a Shimadzu

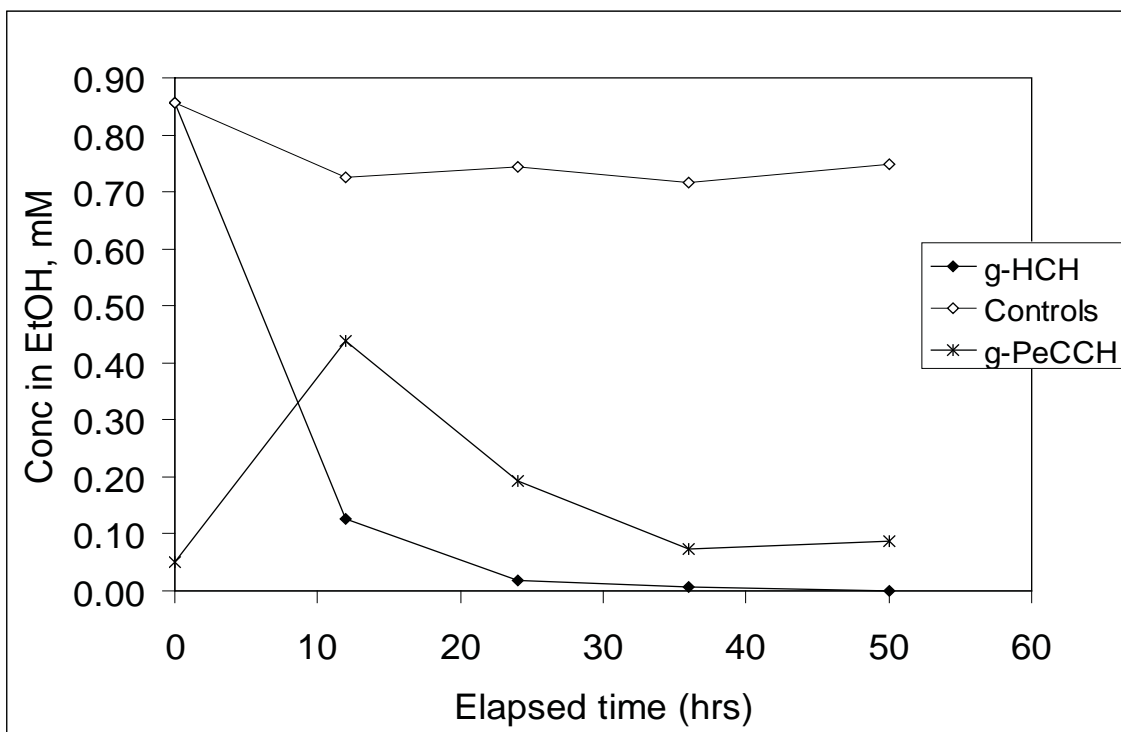
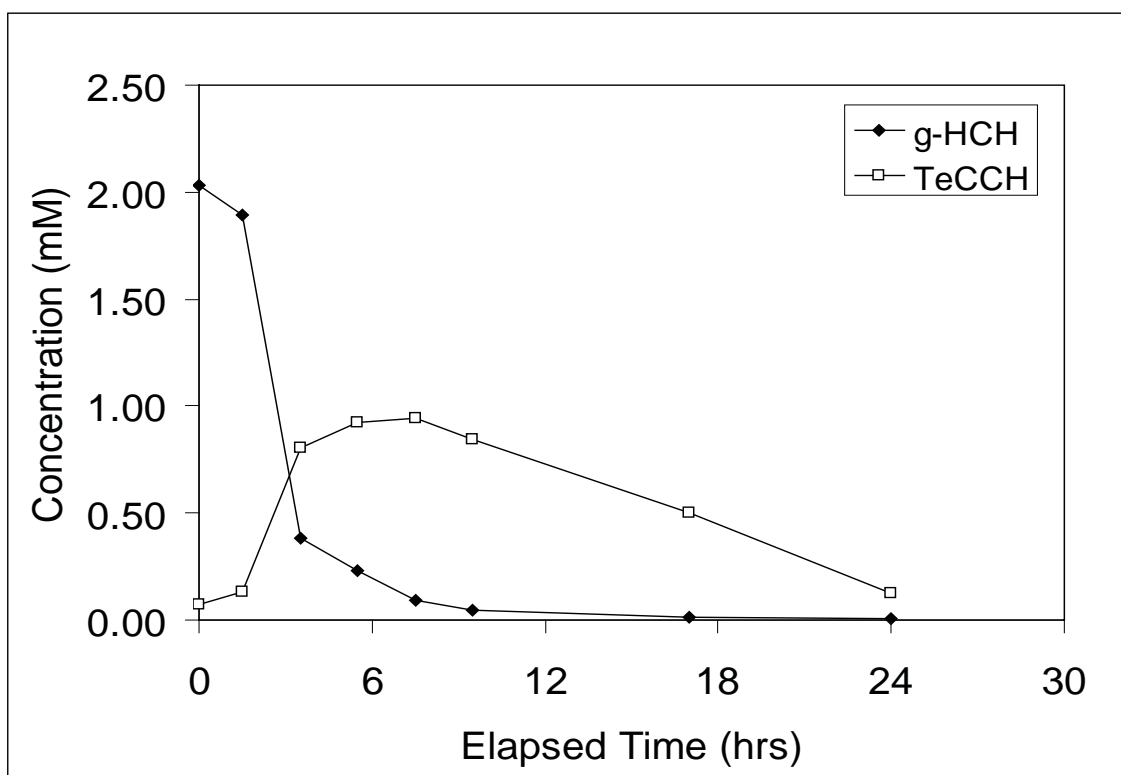


Figure 2. Reactions of Types II (top) and III (bottom) nZVI with lindane in 95% EtOH. GC/MS identified the sole intermediate with Type II nZVI as γ -TeCCH, a product of the reductive dihaloelimination (loss of 2Cl) of lindane. The sole intermediate with Type III iron was

17A gas chromatograph (GC) with an Alltech Econocap EC-5 capillary column (30 m length by 0.25 mm internal diameter and 0.25 micrometer, μm film thickness) and a Shimadzu QP-5000 mass spectrometer (MS). Following settling using a lab magnet, 10 μL aliquots were injected using a gas tight 25 μL Hamilton syringe into the GC/MS. Injector and detector temperatures were 200°C and 300°C, respectively, and a two-stage temperature ramp was used as follows: 110°C for 2 min, 110°C to 200°C at 15°C/min, and 200°C to 240°C at 5°C/min.

Results and Discussion

As shown in Figure 2, the type II iron degraded more than 95% of the lindane within 24 hours yielding γ -tetrachlorocyclohexene (TeCCH) as the principal degradation product. Identified by GC/MS, TeCCH was generated by the reductive dihaloelimination of vicinal axial chlorines and no other carbon-based degradation products were observed. By comparison, type III iron also degraded the majority of the lindane within 24 hours but this time via a different intermediate, γ -pentachlorocyclohexene (PeCCH), as shown in Figure 2. PeCCH represents the expected product of the dehydrohalogenation of lindane. Based on its smaller average particle size, the type III iron would be expected to be the more reactive of the two nZVIs evaluated. Consistent with the behavior of nZVI as a strong electron donor with a variety of contaminants, one would expect to observe some degree of reduction. However, nZVI also has the capability to reduce water yielding hydrogen and hydroxide (Matheson and Tratnyek, 1994). Therefore, in this work,

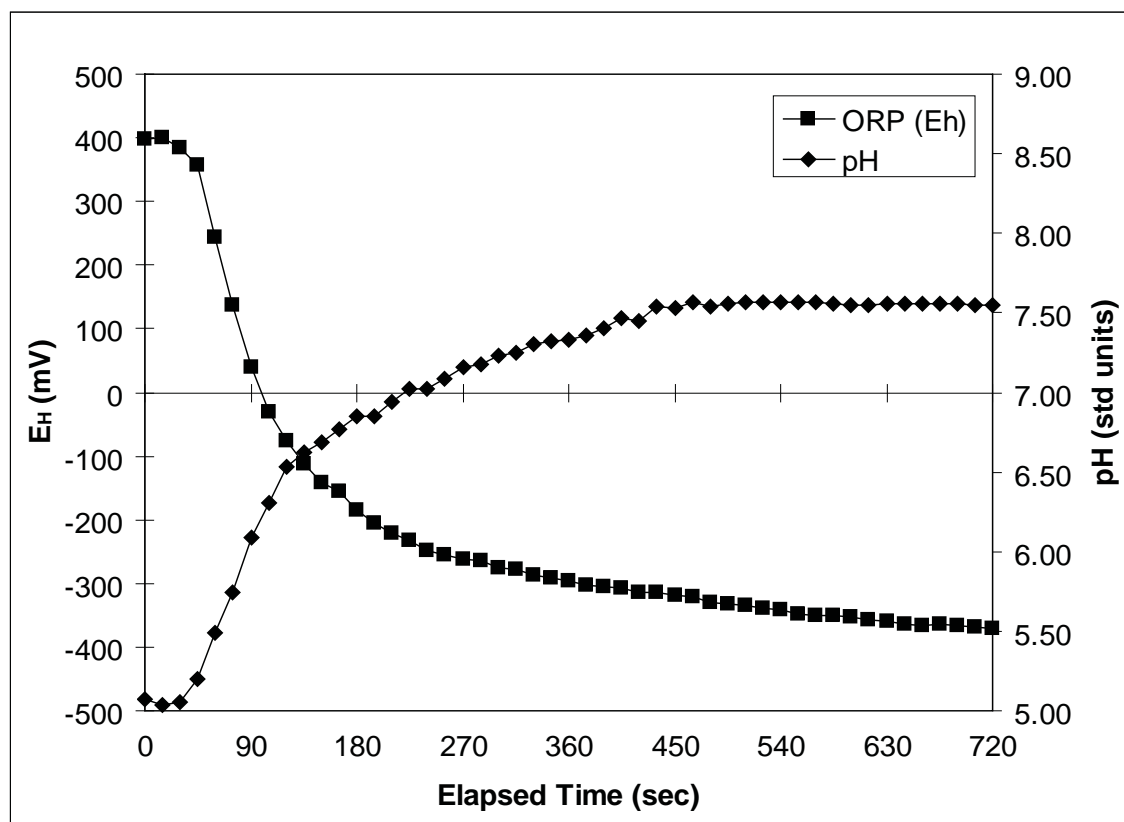


Figure 3. pH/ORP signature from 0.10 g/L nZVI in DI water at 25°C under well-mixed conditions. For this data presentation, electrode ORP values were converted to Eh.

we hypothesize that the more reactive type III iron rapidly reduced enough water to elevate the solution pH and enable dehydrohalogenation to dominate over reduction.

In previous work, we relied upon parameters including pH/oxidation reduction potential (ORP) profile, particle size distribution (PSD), specific surface area (SSA), zeta (ζ) potential/isoelectric point (IEP), and batch contaminant degradation as nZVI characterization tools (Elliott and Zhang, 2006; Zhang et al., 2006). These parameters were measured as close to the time of usage as possible to provide the most representative values. The pH/ORP profile, as depicted in Figure 3, provides an estimation of the nZVI reducing power. The larger the pH increase and ORP decrease, the more reactive the nZVI. Measured ORP values of the nZVI injectate should be about -400 millivolts (mV) or lower to ensure sufficient reactivity. Transmission Electron Microscopy (TEM) can be used to show that the average nZVI size range is on the order of $50\text{--}200$ nm. SSA, which represents the amount of iron (or iron oxide) surface per unit weight, is important because degradation-related rate constants have been linked to the availability of reactive surface (Johnson et al., 1996). Using an SSA analyzer, Lehigh nZVI materials typically range from $30\text{--}35$ m²/g (Zhang et al., 2006). Type III nZVI has been determined to have a ζ potential, or approximate surface potential, of -27.55 mV in water at pH 8.77 (Elliott and Zhang, 2006). According to the Colloid Science Laboratory, Inc. (Westhampton, NJ), particles with ζ potential greater than $+30$ mV or more negative than -30 mV are considered stable with maximum instability (i.e. aggregation) at ζ potential values close to 0. Similarly, IEP refers to the solution pH at which the total surface charge is equal to 0. The surface charge is a function of the degree of ionization of surficial hydroxide groups within the oxidized “shell” that surrounds the Fe(0) core. As shown in Figure 4, the overall surface charge of nZVI tends to be negative at solution pH values greater than about 8.1 standard units. This is important because the more negative the surface charge, the lower the interparticle aggregation potential and greater the repulsion from natural aquifer media. Batch tests using a readily degradable reference contaminant like trichloroethene (TCE) solutions can also provide a good indicator of reactivity. Depending upon the TCE concentration (e.g. 1 mg/L) and nZVI dose (e.g. 1–10 g/L), half-lives are generally hours to days.

Conclusions

The iron-mediated transformation of lindane in 95% ethanol by two different pathways highlighted the intrinsic variability in nZVI materials. The pH/ORP profile, PSD, SSA, ζ potential/IEP, and batch TCE reduction test represent reasonable first-generation QA/QC parameters for nZVI materials. This data should better enable nZVI users to assess reactivity prior to utilization in the field, provide a higher degree of confidence, and help to facilitate more widespread acceptance of the technology.

References

- Clement, T.P, Goswami, R.R., Barnett, M.O., and D. Zhao. (2008) “Two-Dimensional Transport Characteristics of Surface-Stabilized Zero-Valent Iron Nanoparticles in Porous Media.” *Environ. Sci. Technol.* 42 (3), 896-900.
- Cristol, S.J. (1947) “Alkaline Treatment of the HCHs.” *J. Chem. Soc.* 69, 338-342.
- Cristol, S.J., Hause, N.L., and J.S. Meek. (1951) “Mechanisms of Elimination Reactions: III. The

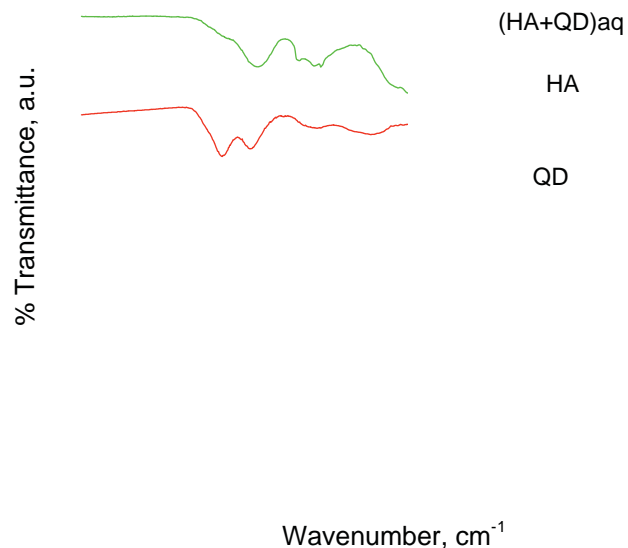


Figure 4. IR spectra for TOPO-capped CdSe QD, Suwannee River HA and the phase-transfer showing the 2200-400 cm^{-1} region which emphasizes the C=O and P=O band stretches.

Kinetics of Alkaline Dehydrochlorination of the Benzene Hexachloride Isomers.” *J. Am. Chem. Soc.* 73, 674-679.

Elliott, D.W. and W.X. Zhang. (2001) “Field Assessment of Nanoscale Bimetallic Particles for Groundwater Treatment.” *Environ. Sci. Technol.* 35 (24), 4922-4926.

Elliott D.W. and W.X. Zhang. (2006) “Applications of Iron Nanoparticles for Groundwater Remediation.” *Remediation* 16 (7), 7-21.

Gavaskar, A., Tatar, L, and W. Condit. (2005) “Cost and Performance Report: Nanoscale Zero-Valent Iron Technologies for Source Remediation.” Contract Report CR-05-007-ENV. Naval Facilities Engineering Command: Port Hueneme, CA. 44 pp.

Glazier, R., Venkatakrishnan, R., Nash, R., Gheorghiu, F., Walata, L., and W.X. Zhang. (2003) “Nanotechnology Takes Root.” *J. Civil Eng.* 73, 64-69.

Henn, K.W. and D.W. Waddill. (2006) “Utilization of Nanoscale Zero-Valent Iron for Source Remediation – A Case Study.” *Remediation* 16, 57-77.

Johnson, T.L, Scherer, M.M., and P.G. Tratnyek. (1996) “Kinetics of Halogenated Organic Compound Degradation by Iron Metal.” *Environ. Sci. Technol.* 30 (8), 2634-2640.

Li, L., Fan, M., Brown, R.C., Van Leeuwen, J., Wang, J., Wang, W., Song, Y., and P. Zhang. (2006) “Synthesis, Properties, and Environmental Applications of Nanoscale Iron-Based Materi-

als: A Review.” Crit. Rev. Environ. Sci. Tech. 36, 405-431.

Liu, Y. and G.V. Lowry. (2006) “Effect of Particle Age (Fe^0 Content) and Solution pH on nZVI Reactivity: H_2 Evolution and TCE Dechlorination.” Environ. Sci. Technol. 40 (19), 6085-6090.

Lowry, G.V., Saleh, N., Phenrat, T., Sirk, K., DuFour, B., Ok, J., Sarbu, T., Matyjaszewski, K., and R.D. Tilton. (2005) “Adsorbed Triblock Copolymers Deliver Reactive Iron Nanoparticles to the Oil/Water Interface.” Nano Letters. 5 (12), 2489-2494.

Lowry, G.V., Saleh, N., Sirk, K., and R.D. Tilton. (2007) “Aggregation and Sedimentation of Aqueous Nanoscale Zerovalent Iron Dispersions.” Environ. Sci. Technol. 41 (1), 284-290.

Mallouck, T.E., Hydutsky, B.W., Mack, E.J., Beckerman, B.B., and J.M. Skluzacek. (2007) “Optimization of Nano- and Microiron Transport through Sand Columns Using Polyelectrolyte Mixtures.” Environ. Sci. Technol. 41 (18), 6418-6424.

March, J. (1985). Advanced Organic Chemistry: Reactions, Mechanisms, and Structure (3rd edition, 1346 pp.) Wiley-Interscience, New York, NY.

Matheson, L.J. and P.G. Tratnyek. (1994) “Reductive Dehalogenation of Chlorinated Methanes by Iron Metal.” Environ. Sci. Technol. 28 (12), 2045-2053.

Zhang, W.X., Elliott, D.W., and X.Q. Li. (2006) “Zero-Valent Iron Nanoparticles for Abatement of Environmental Pollutants: Materials and Engineering Aspects.” Crit. Reviews Solid State Mat. Sci. 31, 111-122.

Conference Questions and Answers

No questions.

Save

Nanoscale Zero Valent Iron Phase II Injection Field Pilot Study, Phoenix-Goodyear Airport North Superfund Site, Goodyear, Arizona

*Robert J. Ellis, Harry S. Brenton, David S. Liles, Chase McLaughlin,
and Nick Wood, ARCADIS-US, Inc., U.S.A.*

Abstract

Bench scale kinetics testing and a Phase II field injection test were completed to evaluate using Polyflon Company PolyMetallix™ nanoscale zero valent iron (nZVI) to treat trichloroethene (TCE) at the Phoenix-Goodyear Airport North Superfund Site in Goodyear, Arizona. Pre-injection dissolved-phase TCE concentrations in source g/L) in aquifer groundwater ranged from approximately 3,000 micrograms per liter (g/L) in monitoring well IRZ-IW-03. Based on injection well IRZ-IW-05, to 7,000 recent characterization efforts, TCE concentrations are present from 110 to 120 feet below ground surface (bgs), approximately 25 to 35 feet below the top of the water table.

During bench-scale testing conducted in 2007, technical and quality protocols for nZVI production were defined. Results of the bench scale testing indicated:

nZVI, with and without the dispersing agent sodium hexametaphosphate (SHMP), remains very reactive up to 30 days after production, indicating good product shelf-life;

nZVI remains very reactive in the presence of site groundwater, despite elevated ionic strength;

Degradation rate constants for destruction of TCE in the presence of the nZVI with and without SHMP are similar and significantly higher than degradation rate constants under natural attenuation conditions;

Post-production nZVI processing via high-speed shearing forces produced by colloid milling minimizes agglomeration, with minimal impact on reactivity.

During Phase II Field testing conducted in June 2008, 10,400 liters (2,750 gallons) of a 2.1 grams per liter (g/l) nZVI suspension with SHMP totaling 22 kilograms (49 pounds) of nZVI were injected into the aquifer through injection well IRZ-IW-05 over a three day period utilizing an onsite colloid mill. Significant changes in groundwater chemistry were observed during the injection at monitoring well IRZ-IW-01, located 1.5 meters (m) (5 feet) from the injection well, including a 400 millivolt (mV) decrease in oxidation reduction potential (ORP) and decrease in dissolved oxygen to below detection. The average injection rate was 6.3 liters per minute (l/m) (1.6 gallons per minute [gpm]). A decrease in injection rate over the duration test was observed, indicating an apparent decrease in permeability within the aquifer. The apparent loss of permeability may be temporary due to geochemical reactions, such as hydrogen gas production and amorphous mineral precipitation, or semi-permanent, due to emplacement of nZVI particles within the aquifer. Post-injection hydraulic testing will evaluate the nature and duration of the

permeability loss. Available laboratory results from the post-injection hydraulic testing and two months of periodic groundwater monitoring at three monitoring wells will be discussed.

Conference Questions and Answers

Question:

Is there not a disconnect between the decrease in the effective injection rate and the expected decrease in the hydraulic conductivity of the aquifer?

Answer:

I agree that there is a disconnect, but it can be explained by reactions in the aquifer (in addition to physical clogging) that affect hydraulic conductivity. For example, corrosion of the iron affects surface properties, the size of particles, and agglomeration of particles.

Comment:

I do not think that the injection of iron and the resulting decrease in effective injection rate was unexpected and, thus, should be considered a failure.

Response:

I agree the decrease was not unexpected. However, it is just an indication that injection via installed wells may not be the best approach, because it will be a challenge to inject more iron into the wells, if necessary. We have tried rehabilitating the wells by redeveloping them with only limited success. A better approach might be injection with Geoprobe® or hydrofracking.

Question:

You indicated that nZVI remains a viable remedial option for source area treatment at the site. Did you perform EPA's nine-criteria evaluation for choosing a remedy to come to this conclusion?

Answer:

To clarify, the technology may be retained for the evaluation against other remedial options, and may not be the final solution for the source area.

Question:

What do you mean by the effervescence "locking up" the formation?

Answer:

The formation of hydrogen gas bubbles occupies space in porous media inhibiting the migration of the injection fluid.

Pilot Field Test of the Treatment of Source Zone Chlorinated Solvents Using Emulsified Zero-Valent Iron

Chunming Su and Robert Puls, USEPA National Risk Management Research Laboratory, Ada, Oklahoma, U.S.A.

Susan O'Hara, Thomas Krug, and Mark Watling, Geosyntec Consultants, Guelph, Ontario, Canada

Jacqueline Quinn, NASA, Kennedy Space Center, Florida, U.S.A.

Nancy Ruiz, Naval Facilities Engineering Service Center, Port Hueneme, California, U.S.A.

Abstract

A pilot field test is being conducted to evaluate the effectiveness of emulsified zero-valent iron (EZVI) injection for treating source zone chlorinated solvents (tetrachloroethene or PCE and daughter products) in Parris Island, SC. Both Direct Injection and Pneumatic Injection are able to effectively deliver EZVI within the subsurface. Groundwater analysis, compound-specific $\delta^{13}\text{C}$ isotope values, and lump-sum $\delta^{37}\text{Cl}$ isotope results show that degradation of PCE and its daughter products (trichloroethene or TCE, cis-DCE) are occurring. Following injection, significant increases in dissolved ferrous iron, volatile fatty acids, and total organic carbon were observed. EZVI technology is simple to implement at the field scale; however, repeated EZVI injection seems to be needed to achieve complete contaminant destruction at this site.

Introduction

Many studies have demonstrated that on an equal mass basis zero-valent iron nanoparticles show faster reductive dechlorination rates for chlorinated hydrocarbons than does granular iron, giving hope that sooner site cleanup may be achievable at some sites having source zones (Liu et al., 2005; Li et al., 2006). Previous laboratory batch and column tests (Geiger et al., 2003, O'Hara et al., 2006) and field test (Quinn et al., 2005, O'Hara et al., 2006) show that the emulsified zero-valent iron (EZVI) technology, developed at the University of Central Florida and the National Aeronautics and Space Administration (NASA), is a promising approach to treat dense non-aqueous phase liquids (DNAPL) at source zones. The essence of the technology is creation of surfactant-stabilized, biodegradable emulsion droplets composed of oil-liquid membrane surrounding nanoscale zero-valent iron (nZVI) particles in water. The corn oil in the membrane combines with the DNAPL so as to enhance contact between the ZVI and the DNAPL. The ZVI provides rapid abiotic degradation of the DNAPL and the corn oil also serves as a long-term electron donor source to enhance microbial degradation.

In this study, we further tested this technology at a pilot scale at Parris Island Marine Corps Recruit Depot (MCRD), Parris Island, SC. The DNAPL source area at a former dry cleaning facility is the site of the field demonstration at Parris Island MCRD. The objectives of the field

test are to (1) examine two injection technologies for EZVI delivery, i.e, Direct Injection using a direct push rig or Pneumatic Injection using nitrogen gas to create fracture in the subsurface in two side-by-side treatment areas; (2) evaluate the performance of nanoscale EZVI to remediate a shallow (<20 ft) tetrachloroethene (PCE) DNAPL source area; and (3) investigate the fate and transport of nanoscale EZVI.

Materials and Methods

Soil and groundwater samples were collected from the site in June 2005 and 2006 to assess contaminant distribution within the treatment areas, and a network of performance monitoring wells was installed at the site in June 2006 (Fig. 1). In the Direct Injection Plot, we installed one 13.5-ft deep and 2-inch diameter monitoring well (PMW-1) screened from 3.5 ft to 13.5 ft below ground surface (bgs). In the Pneumatic Injection Plot, we installed five 19-ft deep and 2-inch diameter monitoring wells (PMW-2, PMW-3, PMW-4, PMW-5, and PMW-6) screened from 4.0 ft to 19 ft bgs. In addition, we installed seven multilevel monitoring wells (0.5-inch diameter) screened at seven levels (mid-screen at 4.0, 6.5, 9.0, 11.5, 14.0, 16.5, and 19 ft for ML3, ML4, ML5, and ML6; mid-screen at 3.5, 6.0, 8.5, 11.0, 13.5, 16.0, and 18.5 ft for ML2 and ML7). Groundwater and soil core samples were collected prior to EZVI injection to establish baseline conditions for the demonstration. We made EZVI on-site by mixing nano-scale iron (RNIP-10-DS from Toda), corn oil, surfactant (Sorbitan Trioleate Span®85, and tap water in a ratio of 10%:38%:1%:51% by weight in drums using top mounted industrial mixer. Before injection, EZVI was pumped from mixing drums into injection tanks. EZVI was injected into the treatment areas in October 2006 (Fig. 1) and performance monitoring is ongoing and expected to be completed by October 2008. In the direct injection plot, 150 gallons of EZVI were injected into four locations between 6 and 12 ft bgs. In the Pneumatic Injection Plot, 575 gallons of EZVI were

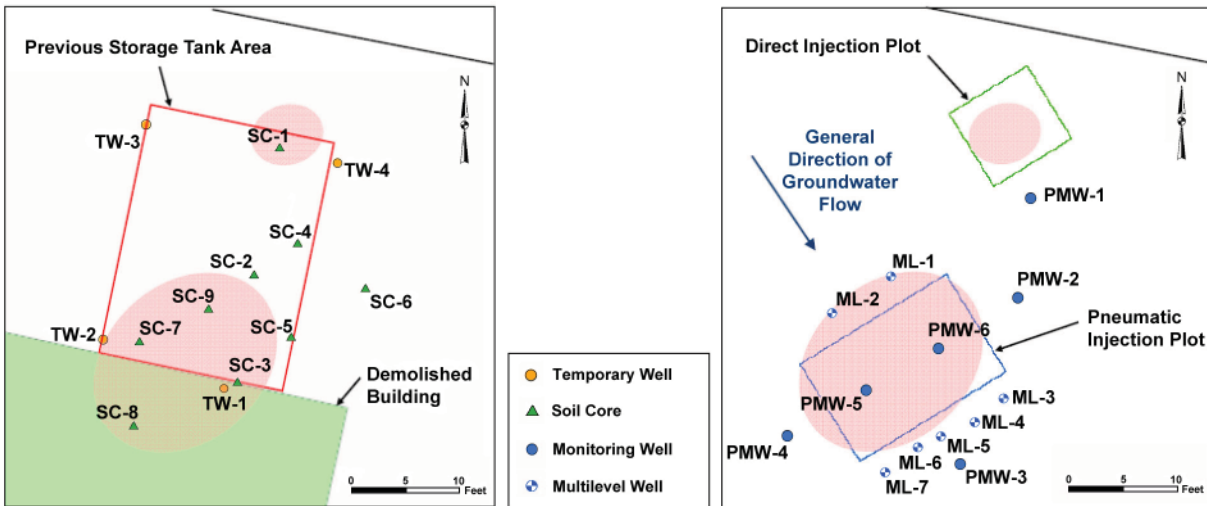


Figure 1. Demonstration site: soil cores and groundwater samples were collected in June 2005 and June 2006 to further evaluate contaminant distribution; wells were installed in July 2006 to target the source areas identified through cores.

injected into eight locations between 7 and 19 ft bgs (two locations using Direct Injection). EZVI daylighted in both Direct Injection and Pneumatic Injection test plots as a result of incomplete plugging of holes left by previous soil core collection for site characterization. EZVI also daylighted around monitoring well ML3.

Groundwater parameters were measured in a flow-through cell using a variety of probes for temperature, conductivity, turbidity, pH, redox potential, and dissolved oxygen. Alkalinity, total dissolved ferrous iron, and total dissolved sulfide were measured at the field site using freshly collected groundwater samples. Groundwater samples were collected for laboratory analysis for volatile organic carbons (VOCs), dissolved hydrocarbon gases (DHG's), volatile fatty acids (VFA's), total organic carbon (TOC), total inorganic carbon (TIC), total dissolved metals, and anions. Selected groundwater samples were also analyzed for carbon-13 compound specific isotope ratios and chlorine-37 isotope ratios in extracted VOC's. Solids collected from well purge water were analyzed by X-ray diffraction.

Results and Discussion

Groundwater flow rate at the site ranged from 0.15 to 0.18 ft/day. Pre-injection site characterization (methanol extraction of soil cores and base-line groundwater analysis) revealed that DNAPL was present in several locations in the Pneumatic Injection plot and in ML2-5 (13.5 ft bgs). DNAPL was present in well water in ML2-7 (18.5 ft bgs), PMW-4, and PWM-5 during post-injection sampling events. This indicates that DNAPL was mobilized in the subsurface after EZVI injection.

Visual examination for the presence of EZVI in soil cores collected following EZVI injection showed that both Direct Push and Pneumatic Injection technologies were able to effectively deliver EZVI within the subsurface, and Pneumatic Injection achieved a greater distance of delivery.

Groundwater monitoring results show a decrease in PCE and trichloroethene (TCE) concentra-

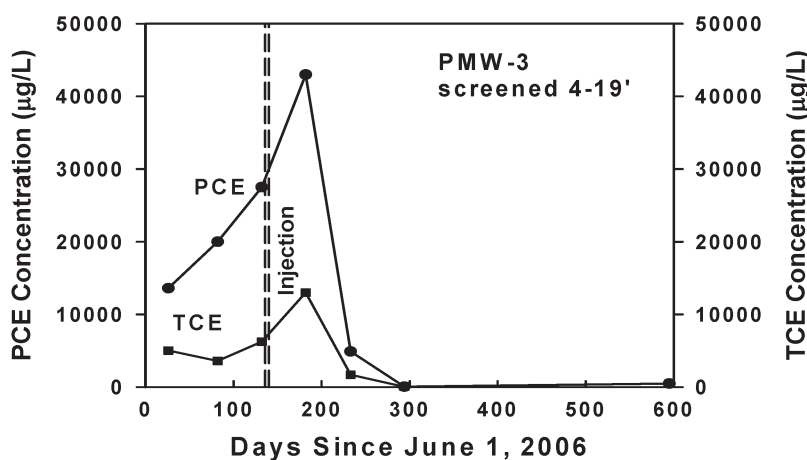


Figure 2. Concentrations of PCE and DCE in monitoring well PMW-3.

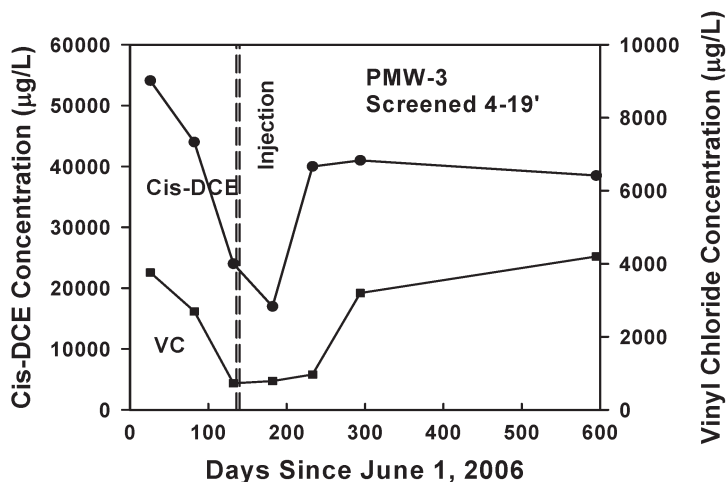


Figure 3. Concentrations of Cis-DCE and VC in monitoring well PMW-3.

tions in PMW-3 downgradient of the treatment areas following EZVI injection (Fig. 2), with an increase in degradation products including cis-DCE, VC, and ethene. Compound-specific carbon-13 isotope results suggest that degradation of PCE and its daughter products are occurring because most of the $\delta^{13}\text{C}$ isotope values increased (less negative) over time after EZVI injection (Tables 1-2). The $\delta^{37}\text{Cl}$ isotope values for the whole extracted chlorinated solvents from groundwater measured in March 2007 are also greater than those measured before injection, further support the notion that chlorinated hydrocarbons are degrading. Both abiotic and biotic mechanisms may be operative at the site. Other notable changes are significant increases in VFAs (primarily acetic and propionic acids) and TOC. Also observed are small decreases in pH, and increases in dissolved ferrous iron. X-ray diffraction results of suspended solids collected from monitoring wells during well purging show transformation of elemental iron to magnetite (Fe_3O_4) and lepidocrocite ($\gamma\text{-FeOOH}$) in ML3-1 and ML3-2 (Fig. 4).

Conclusions

In general, downgradient wells show decreases in PCE/TCE with increases in degradation products including significant increases in ethane. Upgradient wells, PWM-4, and PMW-5 show continued presence of DNAPL although significant production of ethene in PMW-4 and PMW-5 indicates that degradation is ongoing in the area. Monitoring of performance will be continued with soil cores collected for examination of transformation of nanoscale iron.

Acknowledgements

The demonstration work is collaboration among the United States Environmental Protection Agency (EPA), Geosyntec, NASA, and the Naval Facilities Engineering Service Center. Funding was provided by the Department of Defense's Environmental Security Technology Certification Program and the EPA. This paper does not reflect EPA, U.S. Navy, and NASA's policy. The $\delta^{13}\text{C}$ isotope analysis was performed by University of Oklahoma and $\delta^{37}\text{Cl}$ isotope analysis by University of Illinois at Chicago.

Table 1. Compound specific $\delta^{13}\text{C}$ isotope values (mean \pm standard deviation, n = 2, per mil) for the October 2006 groundwater samples (nd: non-detect; coel: coelution)

Well	PCE	TCE	cis-DCE	trans-DCE	1,1-DCE	VC	ethene	ethane
ML2-3	-26.1	-27.3 \pm 0.2	-29.3	nd	-35.2	-31.2 \pm 0.2	-29.7 \pm 0.3	-29.4
ML2-5	-27.6	-32.3	-32.0	nd	-40.5	-27.9	nd	nd
ML5-3	-18.8	-18.3	-28.4	nd	coel	-37.8 \pm 0.5	-29.6 \pm 0.1	-37.1
ML5-5	-25.8	-26.7	-29.0	nd	-37.1	-37.0 \pm 0.2	-28.8 \pm 0.2	nd
PMW-5	-27.0 \pm 0.2	-30.9 \pm 0.1	-28.2 \pm 0.3	nd	coel	-27.6	-30.8 \pm 0.3	-37.0
PMW-3	-27.2	-31.3	-27.6 \pm 0.2	nd	coel	-39.1	-29.1	-36.0
PMW-3 Dup	-27.1	-31.0	-27.5	nd	coel	-39.1 \pm 0.1	-29.3	-34.5

Table 2. Compound specific $\delta^{13}\text{C}$ isotope values (mean \pm standard deviation, n = 2, per mil) for the March 2007 groundwater samples

Well	PCE	TCE	cis-DCE	trans-DCE	1,1-DCE	VC	ethene	ethane
ML2-3	-26.4 \pm 0.3	-24.6	-26.5	-40.7	coel	-36.8 \pm 0.4	-37.1 \pm 0.1	-43.3 \pm 0.1
ML2-5	-29.0	-33.1 \pm 0.1	-30.5 \pm 0.0	-41.5 \pm 0.8	-41.9	-34.9	-42.1 \pm 0.1	-52.6
ML5-3	-18.3 \pm 0.3	-23.6 \pm 0.0	-26.0 \pm 0.1	-36.7 \pm 0.4	-34.4 \pm 0.5	-29.0 \pm 0.1	-34.8 \pm 0.3	nd
ML5-5	-14.0	-23.7 \pm 0.4	-28.1	-40.1	-39.8	-32.5 \pm 0.4	-38.2 \pm 0.4	-46.5 \pm 0.5
PMW-5	-27.9	-26.8	-29.7	-38.8	-39.1	-36.0 \pm 0.2	-41.6 \pm 0.3	-47.9 \pm 0.7
PMW-5 Dup	-28.1 \pm 0.0	-26.9 \pm 0.2	-29.5 \pm 0.0	-39.7 \pm 0.5	-39.1	-35.9	-42.1 \pm 0.1	-48.0 \pm 0.1
PMW-3	-24.5	-25.3	-28.3	-39.4	-39.2 \pm 0.1	-36.7 \pm 0.1	-41.8 \pm 0.4	-48.0 \pm 0.1

Table 3. $\delta^{37}\text{Cl}$ isotope values (per mil) for the whole extracted chlorinated solvents from groundwater before and after EZVI injection

Well	October 2006 before injection	March 2007 after injection
ML2-3	3.99	5.43
ML2-5	2.57	3.30
ML5-3	4.43	5.11
ML5-5	4.29	4.85
PMW-5	3.46	4.55
PMW-5 Dup		4.38
PMW-3	3.29	4.71
PMW-3 Dup	4.32	

References

- Geiger, C.L., C.A. Clausen, K. Brooks, C. Clausen, C. Huntley, L. Filipek, D.D. Reinhart, J. Quinn, T. Krug, S. O'Hara, and D. Major. (2003). "Nanoscale and Microscale Iron Emulsions for Treating DNAPL." Amer. Chem. Soc. Symp. Ser. 837, 132-140.
- Li, X.Q., D.W. Elliott, and W.X. Zhang. (2006). "Zero-Valent Iron Nanoparticles for Abatement of Environmental Pollutants: Materials and Engineering Aspects." Crit. Rev. Solid State Mater. Sci. 31, 111-122.
- Liu, Y., H. Choi, D. Dionysiou, and G.V. Lowry. (2005). "Trichloroethene Hydrodechlorination in Water by Highly Disordered Monometallic Nanoiron." Chem. Mater. 17, 5315-5322.

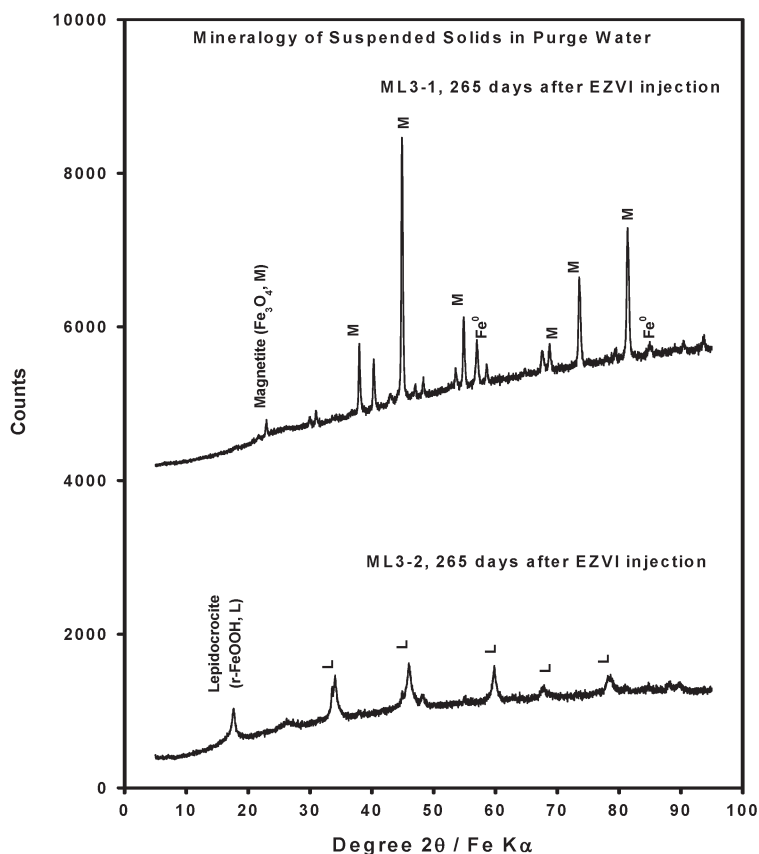


Figure 4. (a) X-ray diffractogram of solids.

Quinn, J., Geiger, C.L., C. Clausen, K. Brooks, Coon, C., S. O'Hara, T. Krug, D. Major, Yoon, W.S., Gavaskar, A, and T. Holdsworth. (2005). "Field Demonstration of DNAPL Dehalogenation Using Emulsified Zero-Valent Iron." *Environ. Sci. Technol.* 39, 1309-1318.

O'Hara, S., T. Krug, J. Quinn, C. Clausen, and C. Geiger. (2006) "Field and Laboratory Evaluation of the Treatment of DNAPL Source Zones Using Emulsified Zero-Valent Iron." *Remediation.* 16, 35-56.

Conference Questions and Answers

Question:

How did you decide to use pneumatic fracturing for the injection rather than other methods?

Answer:

A number of injection methods were tried at the NASA site. The conclusion was that the two most promising injection methods were direct injection using Geoprobe® and pneumatic fracturing using nitrogen gas.

Nanoscale Zero-Valent Iron (nZVI): the Core-Shell Structure and Sequestration of Heavy Metals

Weile Yan, Xiao-qin Li, and Wei-xian Zhang, Department of Civil and Environmental Engineering, Lehigh University, Bethlehem, Pennsylvania, U.S.A.

Research on environmental applications of zero-valent iron (nZVI) in the past decade has been focused primarily on the remediation of halogenated hydrocarbons. In these applications, nZVI acts as a highly efficient electron donor, converting the contaminants into benign or less toxic forms via reductive transformation¹⁻².

Recent spectroscopic and microscopic characterizations (X-ray Photoelectron Spectrometry (XPS) and Transmission Electron Microscopy (TEM)) of nZVI suggest that the nanoparticles comprise of a metallic core surrounded by a thin shell of amorphous iron oxyhydroxide (FeOOH)³. A more direct way to visualize the core-shell structure is afforded by the STEM-XEDS (scanning transmission electron microscope - X-ray Energy Dispersive Spectrometry) technique. Figure 1 shows an annular dark-field (ADF) image and the corresponding STEM-XEDS elemental maps. The Fe L_{α} map exhibits strong intensity in the bulk of the agglomerate, but depicts a clear decrease in intensity at the edge region corresponding to the amorphous shell. By comparison, the O K_{α} map (Figure 1(c)) has a fairly flat contrast level across the centre of the agglomerate but is much brighter at the edge in the amorphous region, suggesting that it is an iron oxide or iron oxyhydroxide shell. Overlay of the elemental maps, as shown in Figure 1(d) where red and green represent O and Fe respectively, clearly illustrates the presence of the amorphous FeOOH phase both at the agglomerate surface and between the individual particles. The two nano-constituents in the core-shell structure impart combinational properties for pollutant removal, in which the metal iron acts as the electron source and gives rise to a reducing character, while the oxide shell facilitates sorption of contaminants via electrostatic interactions and surface complex formation.

The core-shell structure of nZVI is expected to lead to new applications in contaminant separation and remediation, among which sequestration of heavy metals has shown promising potential in recent studies. Batch experiments show rapid and efficient sequestration of Zn(II), Cd(II), Pb(II), Ni(II), Cu(II), and Ag(I) with nZVI. Detailed characterization of reacted nZVI materials with high-resolution X-ray Photoelectron Spectrometry (HR-XPS) shows that metals such as Zn(II) and Cd(II) with standard potential E^0 close to or more negative than that of iron are immobilized as Zn(II) and Cd(II) with no change in their oxidation states. Their removal mechanisms likely involve surface sorption by the iron oxyhydroxide shell. For metals with E^0 substantially higher than that of iron, such as Cu(II), Ag(I) and Hg(II), they are essentially removed via reduction to their elemental states. Metals with E^0 comparable to that of iron, e.g. Ni(II), are immobilized as Ni(0) and Ni(II) species on the nZVI surface, indicating Ni(II) uptake invokes both reduction and sorption⁴⁻⁵. In the case of hexavalent chromium (Cr(VI)), XPS analysis reveals that Cr(VI) is reduced to Cr(III) and subsequently incorporated into the iron oxyhydroxide layer of nZVI to form co-precipitation product with stoichiometric formula approximating

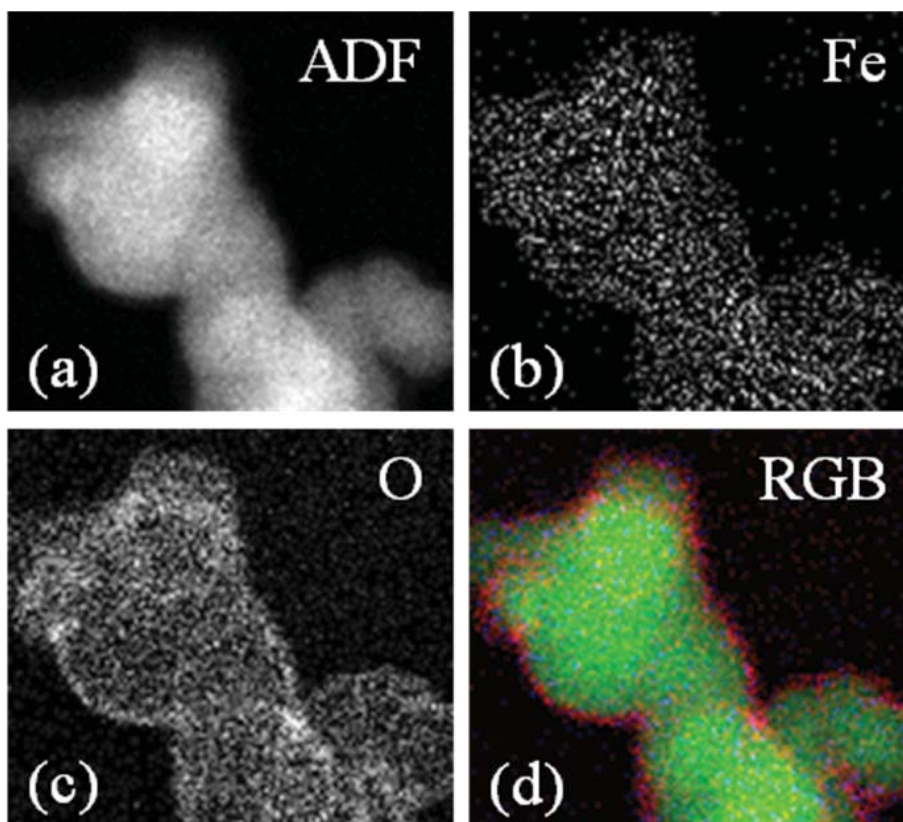


Figure 1. (a) ADF image and the corresponding (b) Fe L_{α} , and (c) O K_{α} STEM-XEDS elemental maps of an nZVI agglomerate. The color image in (d) is an overlay of the elemental maps (red-O; green-Fe), which emphasizes the presence of the amorphous oxide layer at the agglomerate surface and between the individual particles.

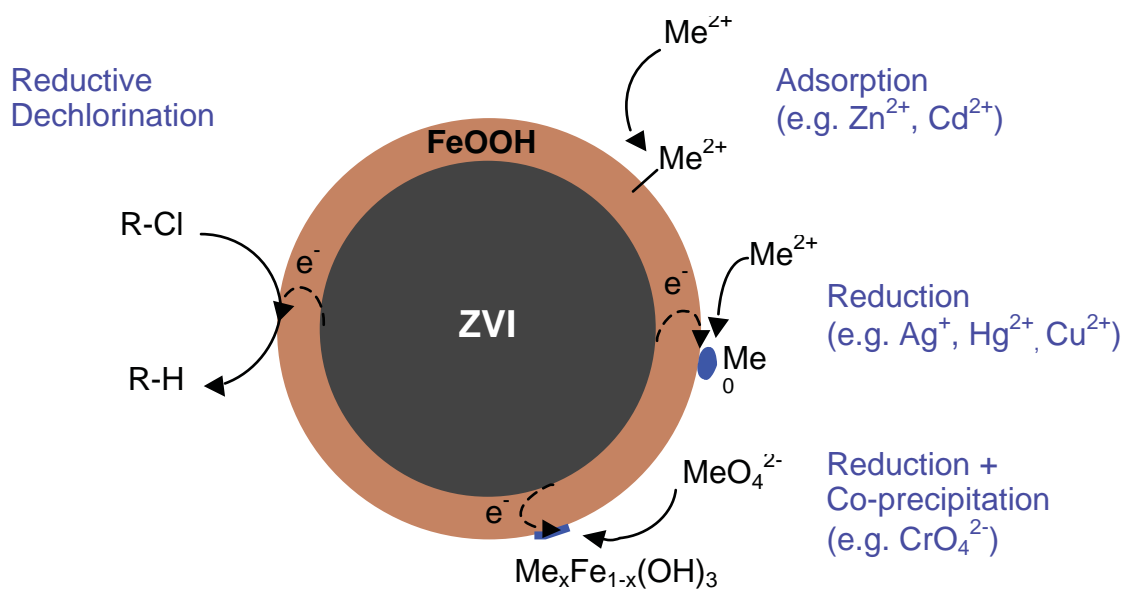


Figure 2. Conceptual model of ZVI core-shell structure and various reaction pathways for environmental contaminants. RCl represents chlorinated hydrocarbons. Me represents metals. The oxidation states of the depicted metals are for examples only and are not definitive.

$\text{Cr}_{0.67}\text{Fe}_{0.33}\text{OOH}^6$. Figure 2 illustrates conceptually the core-shell structure and the various reactive pathways exhibited by nZVI for contaminant removal.

The dual mechanisms and the large surface area afforded by the minute size of the nanoparticles provide significant advantages compared to the conventional treatment options. For example, the apparent reaction rate constant (K_{obs}) of nZVI is estimated to be more than 200 times higher than a commercial grade microscale ZVI powder for Cu(II) sequestration. On the other hand, the surface-area normalized rate constants (K_{SA}) of the two materials are comparable (5.1 vs. 5.8 L/m²min), confirming that the enhanced kinetics of nZVI is primarily attributable to its large reactive surface. Since this surface-area effect is not specific to individual contaminants, it is expected that nZVI may possess significant kinetic advantages for the treatment of other metal species as well. Preliminary kinetic assessment shows that virtually all Hg(II) ions ($C_0=40\text{mg/L}$) were removed from the solution phase in less than 2 minutes with 2g/L nZVI while uptake of Hg(II) by an mZVI material at the same mass loading was considerably slower (Figure 3).

Capacity of metal sequestration was evaluated through batch experiments at a fixed dosage of nZVI particles and varying initial metal concentrations. Figure 4 shows the results of Cu(II) sequestration with nZVI. The Y-axis represents Cu(II) removal per gram of nZVI while X-axis is the initial mass ratio of Cu to Fe. The slope from the origin to individual data point gives the percentage Cu(II) removal. The dashed line with a slope of unity represents the hypothetical scenario in which Cu(II) ions are completely sequestered. It is evident in this figure that with excess doses of nZVI, which corresponds to initial Cu/Fe mass ratio < 0.81, the experiment data

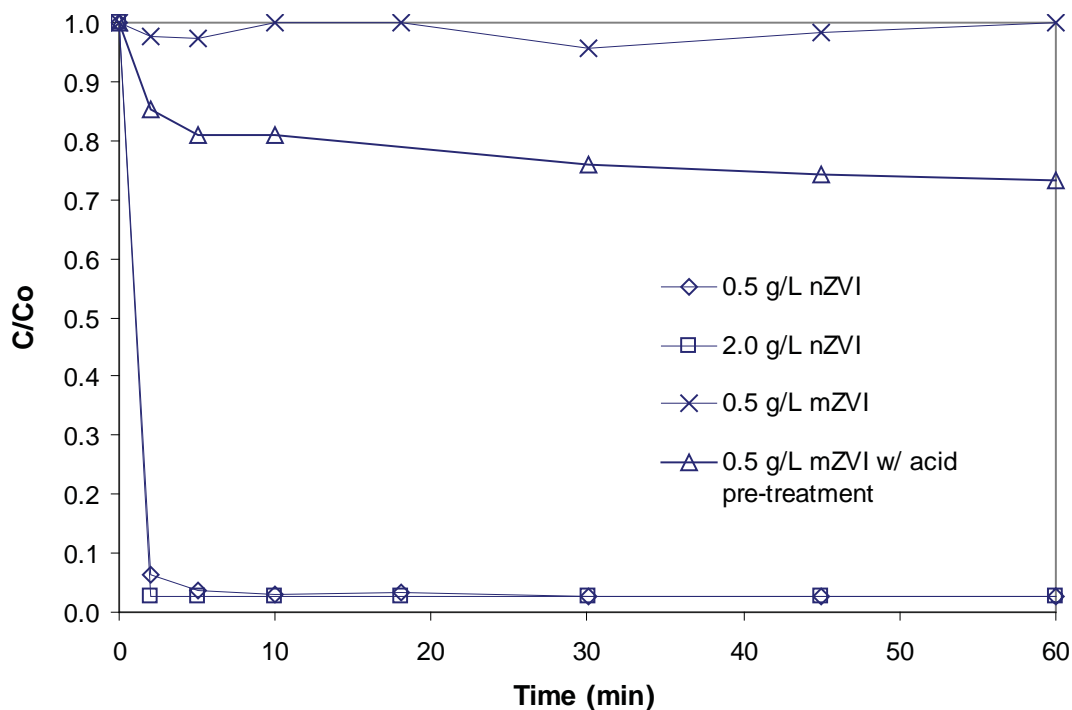


Figure 3. Uptake of Hg(II) ions by various doses of nZVI and commercial grade microscale iron powder (mZVI). The initial concentrations of Hg(II) were 40mg/L.

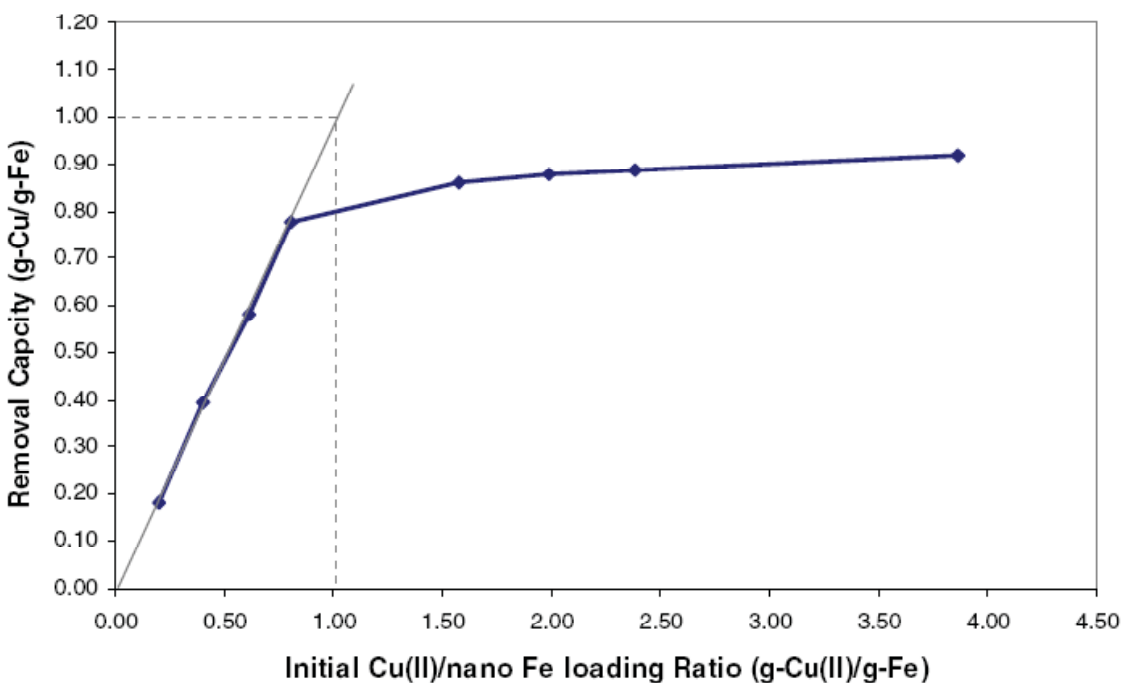


Figure 4. Cu(II) removal capacity of nZVI. The initial concentrations of Cu(II) varied from 50 to 1000 mg/L, while the concentrations of nZVI were fixed at 0.25g/L. The auxiliary line (dashed) represents the hypothetical case in which Cu(II) was completely removed by iron.

matched well with the dashed line, indicating all Cu(II) ions in the aqueous phase were sequestered. At higher Cu/Fe mass ratios, iron becomes the limiting species. The slope of the experimental curve decreases sharply and approached asymptotically a horizontal line. The maximum capacity of Cu(II) removal, as deduced from the Y-axis of the experimental curve at the highest Cu/Fe ratio, is ca. 0.922g-Cu/g-nZVI. Further analysis using XPS and X-ray diffraction (XRD) confirm that the immobilized copper species exists entirely as elemental copper. CuO or Cu₂O was not detected by these analyses, providing convincing evidence that Cu(II) sequestration involve purely the reduction process.

The measured capacity has several important technical implications. The maximum Cu uptake capacity translates to 29meq-Cu/g-nZVI. In comparison, the exchange densities of synthetic ion-exchanger resins are typically in the range of 1-10 meq/g⁷. Widely-applied iron oxide-based sorbents such as goethite (α-FeOOH) and amorphous iron oxide offer total adsorption capacity of no greater than 0.5 meq/g. nZVI material therefore exhibits higher capacity for Cu(II) sequestration than conventional sorption-based technologies. Since Cu(II) is immobilized via reduction by nZVI and the stoichiometry of the reaction being 1: 1 on the molar basis, the experimental capacity indicates the metallic iron (Fe(0)) in nZVI particles is approximately 81wt%. Through geometric correlation, it can be deduced that the average oxide shell thickness in the particle is ca. 3nm, which is in good agreement with the thickness estimated using TEM and XPS techniques³. Hence, the Cu(II)-nZVI reaction can serve as a fast and reliable method to probe the reductive capacity of nZVI and to predict the oxide-layer thickness.

Effect of pH on metal sequestration was studied within a broad environmentally-relevant pH range. Consistent Cu(II) sequestration performance (>95%) was observed with nZVI over a pH range of 3.0 to 8.5. A slight dip in Cu(II) removal at pH < 4 was noted, which could be attributed to the increase in metallic iron loss due to corrosion by water. In contrast to nZVI, conventional iron-oxide sorbents are highly sensitive to pH and have been shown to be ineffective at pH < 4 for Cu(II)⁸. The relative independence on pH implies nZVI retains a high reductive reactivity across a wide pH range, another advantage of nZVI relative to traditional metal sequestration methods.

The results presented here demonstrate that nZVI has promising applications in the treatment and remediation of heavy metal species. Kinetically, it delivers remarkable rate enhancement compared to microscale iron materials due to its diminutive size and the large reactive surface area. With reference to the traditional metal remediation technologies which rely on the principles of sorption or ion exchange, nZVI possesses significantly higher reactive capacities and removal efficiency as a result of its dual capabilities of reduction and sorption afforded by the unique core-shell structure.

References

- Wang, C. B.; Zhang, W. X., Synthesizing nanoscale iron particles for rapid and complete dechlorination of TCE and PCBs. *Environmental Science & Technology* 1997, 31, (7), 2154-2156.
- Matheson, L. J.; Tratnyek, P. G., Reductive Dehalogenation of Chlorinated Methanes by Iron Metal. *Environmental Science & Technology* 1994, 28, (12), 2045-2053.
- Martin, J. E.; Herzing, A. A.; Yan, W.; Li, X.; Koel, B. E.; Kiely, C. J.; Zhang, WX. Determination of the Oxide Layer Thickness in Core-Shell Zerovalent Iron Nanoparticles. *Langmuir* 2008, 24(8), 4329-4334.
- Li, X. Q.; Zhang, W. X., Iron nanoparticles: the core-shell structure and unique properties for Ni(II) sequestration. *Langmuir* 2006, 22, (10), 4638-4642.
- Li, X. Q.; Zhang, W. X., Sequestration of metal cations with zerovalent iron nanoparticles - A study with high resolution X-ray photoelectron spectroscopy (HR-XPS). *Journal of Physical Chemistry C* 2007, 111, (19), 6939-6946.
- Cao, H. S.; Zhang, W. X., Stabilization of chromium ore processing residue with 452 nanoscale iron particles. *Journal of Hazardous Materials* 2006, 132, (2-3), 213-453 219.
- Crittenden, J. C.; Trussell, R. R.; Hand, D. W.; Howe, K. J.; Tchobanoglous, G. *Water Treatment: Principles and Design*, 2nd ed., John Wiley & Sons: New York, 2005.
- Morel, F. M. M.; Hering, J. G. *Principles and Applications of aquatic chemistry*. Wiley: New York, 1993.

Conference Questions and Answers

Question:

As the metal is adsorbed to the nZVI, it is reduced to the zero-valent state and there is a corresponding oxidation of the nZVI to iron (II) and iron (III). Do you see a later adsorption phase of

the metals to the iron oxides?

Answer:

We haven't examined this yet as we have been looking at the initial adsorption stage. But understanding the long-term stability and long-term properties of the oxidized nZVI and the effect on metals concentrations in the aqueous phase would be helpful.

Question:

Would you expand on the process for getting the sample from solution into the X-ray photoelectron spectroscope?

Answer:

The samples were filtered rapidly, and we collected the solid phase dry in oxygen. From that point onward, the sample work was conducted using a nitrogen-filled atmosphere to avoid impact to the oxidation state of the metal.

Nanotechnology-Based Membrane Systems for Detoxification of Chlorinated Organics from Water

D. Bhattacharyya, J. Xu, D. Meyer, Y. Tee and L. Bachas, Dept. of Chemical and Materials Engineering, University of Kentucky, Lexington, Kentucky, U.S.A.

Introduction

The development of nanosized materials has brought important and promising techniques into the field of environmental remediation of chlorinated organics. Nanostructured metals have become an important class of materials in the field of catalysis, optical, electronic, magnetic and biological devices due to the unique physical and chemical properties (1-7). This research deals with the synthesis of structured bimetallic nanoparticles (Fe/Pd, Fe/Ni) for the dechlorination of toxic organics (3-5). Nanoparticle synthesis in aqueous phase for dechlorination studies has been reported. However, in the absence of polymers or surfactants particle can easily aggregate into large particles with wide size distribution. In this study, we report a novel in-situ synthesis method of bimetallic nanoparticles embedded in polyacrylic acid (PAA) functionalized microfiltration membranes by chemical reduction of metal ions bound to the carboxylic acid groups. Membrane-based nanoparticle synthesis offers many advantages: reduction of particles loss, prevention of particles agglomeration, application of convective flow, and recapture of dissolved metal ions.

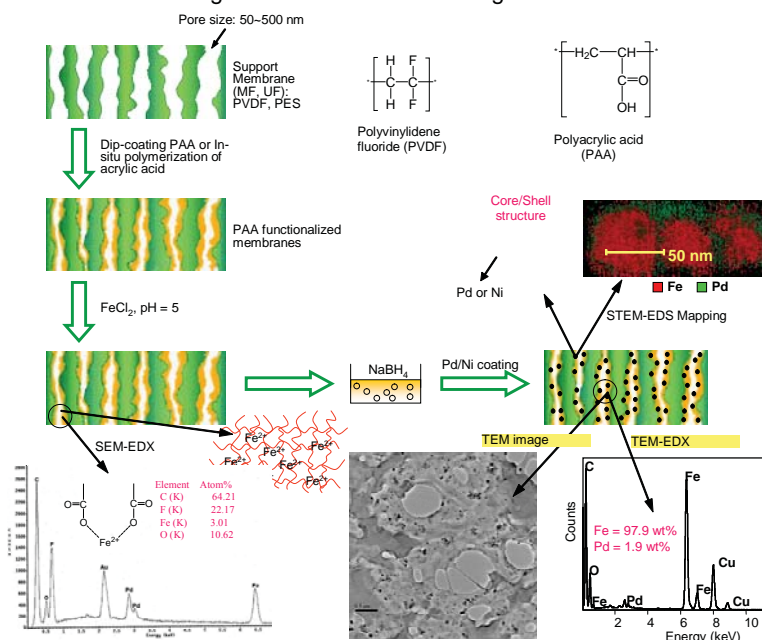
Research Objectives and Experimental Protocols

The objective of this research is to synthesize and characterize nanostructured bimetallic particles in membranes, understand and quantify the catalytic hydrodechlorination mechanism, and develop a membrane reactor model to predict and simulate reactions under various conditions. In this study (3), the PAA functionalization (Figure 1) was achieved by filling the porous PVDF membranes with acrylic acid and subsequent in-situ free radical polymerization. Target metal cations (iron in this case) were then introduced into the membranes by ion exchange process. Subsequent reduction resulted in the formation of metal nanoparticles (around 30 nm). Polymer immobilization eliminates worker exposure issues relating to nanoparticles.

Results and Discussions

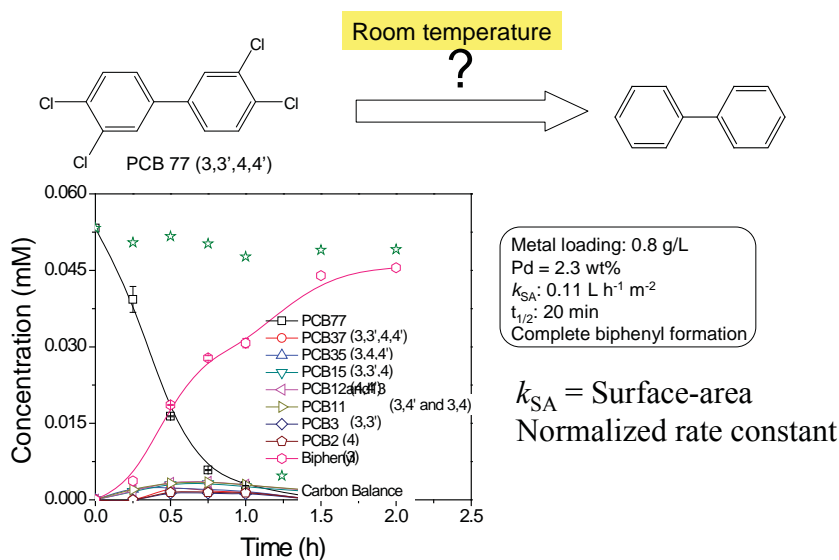
Bimetallic (core/shell) nanoparticles can be formed by post deposition of secondary appropriate metal such as Pd ($\text{Pd}^{2+} + \text{Fe}^0 \rightarrow \text{Fe}^{2+} + \text{Pd}^0$) or Ni. The membranes and bimetallic nanoparticles were characterized by: SEM, TEM, TGA, and FTIR. A specimen-drift-free X-ray energy dispersive spectroscopy (EDS) mapping system was performed to determine the two-dimensional element distribution inside the membrane matrix at nano scale. This high resolution mapping allows for the correlation and understanding the nanoparticle structure, second metal composition in terms of nanoparticle reactivity. Chlorinated aliphatics such as trichloroethylene (TCE) and conjugated aromatics such as polychlorinated biphenyls (PCBs) were chosen as the model compounds to investigate the catalytic properties of bimetallic nanoparticles and the reaction mechanism and kinetics. We demonstrated complete (with product and intermediates

Figure 1. Synthesis of Nanostructured Metals in Functionalized Membranes for Degradation of Chlorinated Organics



analysis) dechlorination of trichloroethylene (TCE) and selected PCBs by nanosized metals. The 2nd dopant metal (such as, Ni, Pd) plays a very important role in terms of catalytic property (hydrodechlorination) and the significant minimization of intermediates formation. In addition to the rapid degradation (by Fe/Ni) of TCE (trichloroethylene) to ethane, we were also able to achieve complete dechlorination of selected chloro-biphenyls (PCBs) using milligram quantities immobilized Fe/Pd nanoparticles in membrane domain. Figure 2 shows that complete conversion

Figure 2. PCB 77 (3,3',4,4') dechlorination by membrane based Fe/Pd (Pd=2.3 wt%) nanoparticles at room temperature



of PCB's to biphenyl can be obtained. Effects of second metal coating, particle size and structure and temperature were studied on the performance of bimetallic systems.

In order to predict reaction at different conditions, a two-dimensional steady state model (8) was developed to correlate and simulate mass transfer and reaction in the membrane pores under convective flow mode. The 2-D equations were solved by COMSOL (Femlab). The influence of changing parameters such as reactor geometry (i.e. membrane pore size) and Pd coating composition were evaluated by the model and compared well with the experimental data. The role of hydrogen generation by the Fe corrosion reaction and the surface reactivity is important for the detoxification reactions. The intrinsic rate constant (k_{in}) has been determined by fitting the model with the experimental data. K_m is the only parameter that was taken as fitting parameters for model validation and simulation. All other parameters were determined by independent calculations or experiments.

Acknowledgements

This research work is supported by the NIEHS-SBRP program and by US DOE-KRCEE.

References

- Lowry, G. V.; Johnson, K. M. Congener-specific dechlorination of dissolved PCBs by microscale and nanoscale zerovalent iron in a water/methanol solution. *Environ. Sci. Technol.* 2004, 38, 5208-5216.
- Meyer, D. E.; Bhattacharyya, D., Impact of Membrane Immobilization on Particle Formation and Trichloroethylene Dechlorination for Bimetallic Fe/Ni Nanoparticles in Cellulose Acetate Membranes, *J. Phys. Chem. B.*, 2007, 111, 7142-7154.
- Xu, J., and Bhattacharyya, D., Fe/Pd Nanoparticle Immobilization in Microfiltration Membrane Pores: Synthesis, Characterization, and Application in the Dechlorination of Polychlorinated Biphenyls, *Ind. Eng. Chem. Res.*, 2007, 46, 2348-2359.
- Xu, J. and Bhattacharyya, D., Membrane-based Bimetallic Nanoparticles for Environmental Remediation: Synthesis and Reactive Properties, *Environ. Prog.*, 2005, 24, 358-366.
- Xu, J., Dozier A. and Bhattacharyya, D., Synthesis of nanoscale bimetallic particles in polyelectrolyte membrane matrix for reductive transformation of halogenated organic compounds, *J. Nanoparticle Res.*, 2005, 7, 449-467.
- Dotzauer, D. M.; Dai, J.; Sun, L.; Bruening M. L., Catalytic Membranes Prepared Using Layer-by-Layer Adsorption of Polyelectrolyte/Metal Nanoparticle Films in Porous Supports, *Nano Letters*, 2006, 6, 2268-2272.
- Tee, Yit-Hong, Grulke, E., Bhattacharyya, D., "Role of Ni/Fe Nanoparticle Composition on the Degradation of Trichloroethylene from Water", *Industrial Engineering & Chemistry Research*, 44, 7062-7072 (2005).
- Xu, J., and Bhattacharyya, D., "Modeling of Fe/Pd Nanoparticle-Based Functionalized Membrane Reactor for PCB Dechlorination at Room Temperature", *J. Physical Chemistry C*, 112, 9133-9144 (2008).

Conference Questions and Answers

Question:

Did you experience any problems with the accumulation of hydrogen gas in the polymer?

Answer:

No. We measured hydrogen gas, but it did not accumulate in the polymer.

A Field Demonstration of a Novel Functionalized Mesoporous Sorbent Based Battelle ISIS Technology for Mercury Removal

*Shas Mattigod, and Dawn Wellman, Battelle, Pacific Northwest Division,
Richland, Washington, U.S.A.*

Henry Pate, Battelle, Battelle Florida Materials Research Facilities, Ponce Inlet, Florida, U.S.A.

*Kent Parker, Emily Richards, Glen Fryxell, and Richard Skaggs, Pacific Northwest Division,
Richland, Washington, U.S.A.*

Abstract

At Battelle, we have developed a novel sorbent technology based on Self-Assembled Monolayers on Mesoporous Support (SAMMS™) that can specifically adsorb mercury and other heavy metals. Bench-scale tests demonstrated that this material can effectively remove mercury from a barren effluent from a mine site. As a follow up, a field test was conducted at a mine site that deployed SAMMS™ material integrated into a floating treatment platform – InStream™. This Battelle treatment platform (InStream-SAMMS Integrated System ISIS) consisting of rotating sorbent cassettes was designed as a low-cost method to scavenge contaminants from abandoned effluent impoundments. The mine effluent consisting of spent cyanide leach solution contained $\sim 1100 \pm 30$ ppb of mercury. Using sorbent cassettes containing ~ 600 g of SAMMS™ material, the mercury concentrations in approximately 4300 gallons of effluent was reduced to ~ 170 ppb in less than 73 hours. This Battelle ISIS technology demonstrated a potential for a low-cost alternative treatment system for abandoned mine effluent impoundments.

Introduction

At Battelle, we have developed a novel sorbent technology SAMMS™ that can specifically adsorb mercury and other heavy metals, oxyanions and radionuclides from aqueous and non-aqueous, waste streams (1 – 10). The adsorption characteristics (capacity and kinetics) of these SAMMS™ materials have been well established by extensive bench-scale tests. (5, 7-9, 11, 12)

We have successfully demonstrated the mercury removal efficiencies of the SAMMS™ material on a wide range of contaminated waste streams ranging from produced water to various laboratory wastes. We have licensed the thiol-SAMMS™ technology to Steward Environmental Solutions for industrial scale manufacture and sale. We recognized that an important potential field-of-use of this novel sorbent is in treating enormous number of industrial heavy metal contaminated water impoundments (e.g., sludge ponds, evaporation ponds, pit lakes, contaminated lakes, etc.) throughout the U.S. The key to cost-effective treatment of these impoundments involves the use of advanced sorbents offering rapid kinetics, heavy loading capacity, and high selectivity for heavy metals of concern deployed through a relatively passive system having low capital and operating costs. To this end, we decided to develop a novel technology platform (Battelle ISIS) that combined the thiol-SAMMS™ technology with another Battelle's patented technology, Instream™ to remove in-situ, mercury and other heavy metal contaminants from

impoundments resulting from mining, power generation, cement manufacturing and other industrial activities.

The InStream™ technology was originally invented as a revolutionary floating platform aerator for lagooned wastes. Our goal for this project was to demonstrate in the field, the effectiveness of the Battelle ISIS technology for removing mercury from mine waste effluents.

Methods

A barren effluent sample from a silver mine was used to conduct bench scale treatability tests. We designed and built a prototypic ISIS unit equipped with two 21 inch diameter screened cassettes each capable of holding approximately 12 oz of thiol-SAMMS™ sorbent material. The immersion depth of these cassettes were approximately 7 – 8 inches and were driven by a speed controlled 1/15 HP motor. Depending on the immersion depth and the rotation speed, we estimated the sorbent-contacted solution flow rates to be ~ 3 – 8 gpm.

We conducted this test Battelle ISIS demo test in a tethered mode because the current prototypic unit lacked, 1) a guidance system and, 2) a self-contained power source. The power for the ISIS unit during the test was drawn from an on-shore source. We conducted these test for about 3 days using about 4300 gallons of barren effluent solution at a silver mine site in Nevada. The barren effluent was contained in a 5000 gallon capacity Flex Tank (FT) and we used a second



Figure 1. A view of the FTs installed at the Coeur Rochester Mine Site.

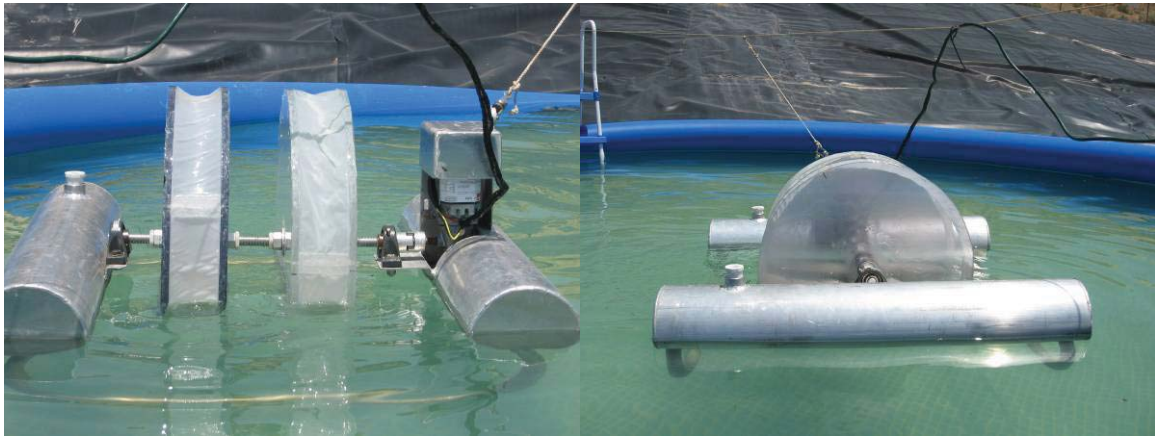


Figure 2. Battelle ISIS unit set up for the field test

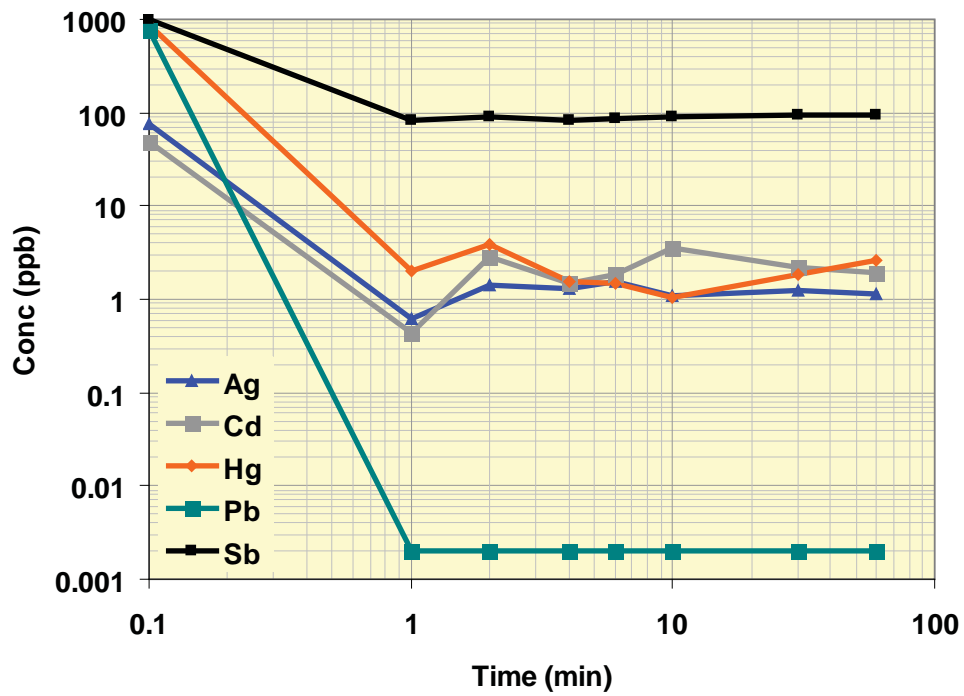


Figure 3. Kinetics of Adsorption for selected COC at Solution to Solid Ratio of 500 ml/g

FT containing ~3400 gallons of solution as a control and a third FT was used as reserve storage (Figure 1, 2). We allowed the thiol-SAMMS™ containing cassettes to soak overnight, and after completing all the safety checks, we initiated the test by powering up the cassette rotors. We collected aliquots of treated solution and the solution in the control FT and measured concentrations of mercury.

Results

The results of the bench-scale adsorption kinetics experiment indicated that bulk of the adsorption (90 – 100%) occurred in < 1 min of contact time (Figure 3). Overall, about 90 – 100% of the contaminants of concern (COC) were adsorbed by thiol-SAMMS™. At the end of tests, we found that the residual concentrations of all COC were 2 to 5 orders of magnitude less than the UTS effluent standards. For all RCRA metals (Ag, Cd, Hg and Pb) the residual concentrations even met or exceeded the drinking water standards (Table 1).

At the end of first day of operations, we observed that the Battelle ISIS unit had reduced the mercury concentration in the FT to ~550 ppb from an initial concentration of 1110 ± 30 ppb (Figure 4). After 48 hours of continuous operation, the mercury concentration had been reduced by almost 75% of the initial concentration. When we stopped after ~3 days, the residual concentration of mercury had dropped to ~180 ppb. This terminal residual concentration is close to

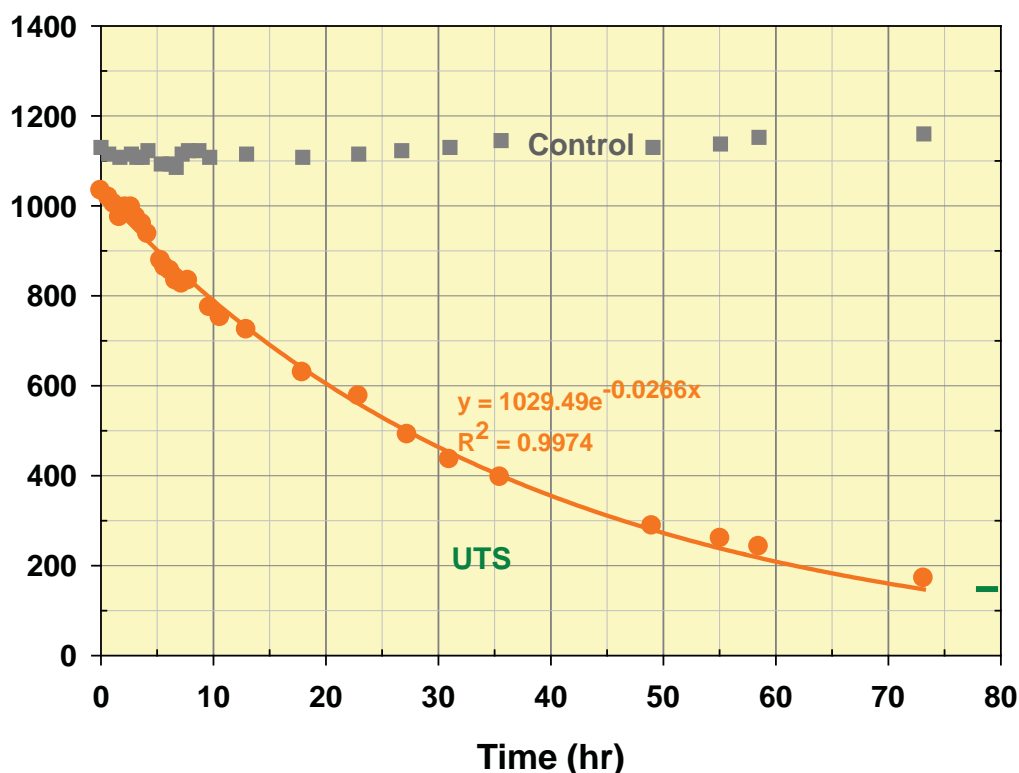


Figure 4. Mercury removal performance of Battelle ISIS unit

Table 1. Residual concentrations of COC observed in bench-scale kinetic Tests

COC	Initial Conc. (ppb)	Residual Conc. (ppb)	Reduction (%)	RCRA UTS* (ppb)	DWS** (ppb)
Hg	891	<0.05 - 2	>99.9 – 99.8	150	2
Ag	75	1 - 4	98.7 – 94.7	430	100
Cd	48	2 - 5	95.8 – 89.6	690	5
Pb	769	<0.002	>99.9	690	15
Sb	1005	90 - 120	91.0 – 88.1	1900	6

*EPA 40 CFR 268.48 Universal Treatment Standards (UTS)

**EPA 2006 Edition of the Drinking Water Standards (DWS) and Health Advisories, EPA 822-R-06-013, Office of Water, Environmental Protection Agency, Washington DC. August 2006.

the UTS of 150 ppb. The rate of reduction of mercury over the three day test period exhibited an exponential decay functional relationship with respect to time (Figure 4). Based on the functional relationship, it appeared that if we had continued the test for an additional time period of 7 hours, the residual mercury concentration would have approached ~120 ppb, well below the UTS concentration of 150 ppb.

The cumulative mercury loading on the SAMMS™ sorbent as a function of time confirmed that mercury was binding on to only one type of high energy binding sites, namely thiol sites that populates the SAMMS™ sorbent surfaces (data not included). Calculated cumulative mercury adsorption indicated that ~680 g of SAMMS™ sorbent had irreversibly bound a total mass of ~15.3 g of mercury from solution in three days out of ~18.1 g of total mass initially present in ~4300 gal of untreated solution. These adsorption data indicated that a limited mass of SAMMS™ sorbent contacting a large volume of barren solution (i.e. each gram of sorbent contacting ~6 gal of solution) was capable in 3 days of removing ~85% of the mercury from solution.

We calculated the cumulative mercury adsorption density to be ~22 mg/g of sorbent. This value confirmed the mercury loading capacity predicted for thiol-SAMMS™ from the isotherm data generated during the bench-scale tests (data not included). Considering that thiol-SAMMS™ sorbent has an ultimate mercury adsorption capacity of ~600 mg/g, the adsorption capacity achieved at the end of this test (~22 mg/g) indicated that the sorbent had considerable remaining reserve adsorption capacity that could be exploited fully in a flow-through treatment system. Based on these field test we believe that the Battelle ISIS technology with appropriate scale-up and added refinements such as, an onboard power source and a programmable GPS system can be very effective in removing in-situ dissolved mercury from mining impoundments. Such a self-contained treatment system, which can operate relatively unattended, can be deployed at minimal cost.

References

1. Feng, X., Fryxell, G. E., Wang, L. Q. Kim, A. Y. Liu. (1997). "Organic Monolayers on Ordered Mesoporous Supports", *Science*, 276, 923-926.
 2. Liu, J.; Feng, X., G. E. Fryxell, L. Q. Wang, A. Y. Kim and M. Gong (1998). "Hybrid Mesoporous Materials with Functionalized Monolayers". *Advanced Materials*, 10, 161-165.
 3. Fryxell, G. E., J. Liu, M. Gong, T. A. Hauser, Z. Nie, R. T. Hallen, M. Qian, and K. F. Ferris, (1999). "Design and Synthesis of Selective Mesoporous Anion Traps", *Chemistry of Materials*, 11, 2148-2154.
 5. Mattigod, S. V., R. Skaggs, and G. E. Fryxell (2003). "Removal of Heavy Metals from Contaminated Waters Using Novel Nanoporous Adsorbent Materials" in 9th Annual Industrial Wastes Technical and Regulatory Conference, Industrial Wastes Conference Water Environment Federation.
- Fryxell, G. E., Y. Lin, H. Wu, and K. M. Kemner, (2003). "Environmental Applications of Self-Assembled Monolayers on Mesoporous Supports (SAMMS)" in *Studies in Surface Science and Catalysis Vol. 141*, A. Sayari and M. Jaroniec Elsevier.
- Mattigod, S. V., G. E. Fryxell, K. Alford, T. Gilmore, K. E. Parker, J. Serne, M. Engelhard, (2005). "Functionalized TiO₂ Nanoparticles for Use for in Situ Anion Immobilization", *Environ. Sci. Technol*; 39(18); 7306-7310.
- Mattigod S. V., G. E. Fryxell, R. L. Skaggs, and P. J. Usinowicz (2004). "Nanoporous Sorbent Materials Developed for Arsenic Removal". *Industrial Wastewater*. 3, 11- 12.
- Mattigod, S.V., G. E. Fryxell, K. E. Parker (2007). "Anion binding in self-assembled monolayers in mesoporous supports (SAMMS)", *Inorganic Chemistry Communications*, 10 (6), 646-648.
- Fryxell, G.E, S. V. Mattigod, Y. Lin, H. Wu, S. Fiskum, K. E. Parker, F. Zheng, W. Yantasee, T. S. Zemanian, R.S., Addleman, J. Liu, K. Kemner, S. Kelly, X. Feng (2007). "Design and synthesis of self-assembled monolayers on mesoporous supports (SAMMS): The importance of ligand posture in functional nanomaterials" *Journal of Materials Chemistry*, 17 (28), 2863-2874.
- Mattigod, S. V., G. E. Fryxell, K. E. Parker (2007) "Functionalized Nanoporous Sorbents for Adsorption of Radioiodine from Groundwater and Waste glass Leachates" in *Environmental Applications of Nanomaterials*. G. E. Fryxell and B. Cao, Imperial College Press.
- Mattigod, S. V., G. E. Fryxell, K. E. Parker (2007). "A Thiol-functionalized Nanoporous Silica Sorbent for Removal of Mercury from Aqueous Waste Streams" in *Environmental Applications of Nanomaterials*. G. E. Fryxell and B. Cao, Imperial College Press.

Conference Questions and Answers

Question:

Can the SAMMS® be regenerated?

Answer:

The thiol-SAMMS® can be regenerated with hydrochloric acid up to 10-15 times.

Dechlorination of Polychlorinated Biphenyls by Pd/Mg Bimetallic Corrosion Nano-Cells

*Shirish Agarwal, Civil and Environmental Engineering,
University of Cincinnati, Cincinnati, Ohio, U.S.A.*

*Souhail R. Al-Abed, National Risk Management Research Laboratory,
U. S. Environment Protection Agency, Cincinnati, Ohio, U.S.A.*

*Dionysios D. Dionysiou, Civil and Environmental Engineering,
University of Cincinnati, Cincinnati, Ohio, U.S.A.*

Introduction

Polychlorinated biphenyls (PCBs), manufactured until mid-1970's for use as electrical insulators, were banned in 1979 due to their toxicity and persistence in the environment (1). Dechlorination of PCBs using bimetallic systems is a promising technology wherein enhanced corrosion of a reactive metal is combined with catalytic hydrogenation properties of a noble metal to drive the reduction of PCBs at the bimetallic interface (2). Pd/Fe bimetallic systems have been demonstrated to completely dechlorinate trichloroethylenes (3) and PCBs (4). Mg has an oxidation potential of 2.372 V that is significantly higher than 0.44 V of Fe (5), and thus a greater force to drive the hydrodehalogenation reaction (6). The high oxidation potential of Mg, coupled with its natural abundance, low cost and environmentally friendly nature has led to growing interest in Mg-based dechlorination systems. Hence, the primary objective of this study was to evaluate Mg as a substrate in Pd-doped bimetallic particles for dechlorinating PCB matrices.

Experimental

Synthesis: Calculated amounts of K_2PdCl_6 were added to ethanol (Fisher) and stirred for 1 h. Mg particles (-325#, Sigma) were then added to each of the flasks and the resulting slurry was stirred for 2 h wherein elemental Pd deposited onto Mg to form the bimetallic particles. The slurry was then vacuum filtered, the particles washed with acetone and stored anaerobically.

Characterization: The Pd content of bimetallic particles was determined by an ICP-AES (IRIS Intrepid, Thermo Electron Corporation, CA) after microwave-assisted digestion (EPA Method 3051). The size of Pd crystallites on the Mg particles was determined by X-ray diffraction (Phillips PW3040/00 X'Pert-MPD Diffractometer system) using Scherrer formula (7). A mechanical mixture of Pd and Mg was used as reference (8). The distribution of Pd-islands on the surface of Mg was determined by an ESEM with field emission gun (Phillips XL 30 ESEM-FEG).

Degradation Studies: Pd/Mg was weighed out in vials and 50 ml of a 4 ppm aqueous solution 2-chlorobiphenyl was added. Sampling was at 0.25, 0.5, 0.75, 1, 1.5, 2, 3 and 4h. The samples were extracted in 4 ml vials (Fisher) with 2 ml hexane and analyzed in GC (HP 6890)/MS (HP 5973).

Results and Discussion

Characterization: The XRD patterns obtained for Pd/Mg bimetallic particles (0.58% Pd), a mechanical mixture of Pd-Mg (reference) and elemental Mg are shown in Fig. 1. The broadening of the Pd peak in Pd/Mg particles as compared to the Pd-Mg reference mixture was used to calculate the size of Pd crystallites (8). The Pd crystallite size was consistently between 45-48 nm. SEM images of a bimetallic particle sample with 0.58% Pd taken by secondary and backscattered electron detectors (SE and BSE) are shown in Fig. 2a and 2b respectively. As seen in Fig. 2a, the Mg surface is rich in contours making identification of tiny Pd-islands difficult with an SE detector which provides a more detailed surface imagery. The Pd-islands were clearly identifiable as minute bright spots in the BSE image shown in Fig 2b. This is because elements with higher atomic number (Pd) appear significantly brighter than ones with a lower number in a BSE image (9). Also, from Fig 2b, it can be said that the Pd-islands have a small size distribution between 50-100 nm and are sparsely distributed on the Mg surface. Some agglomeration of Pd crystallites was noted at 1.62% Pd doping.

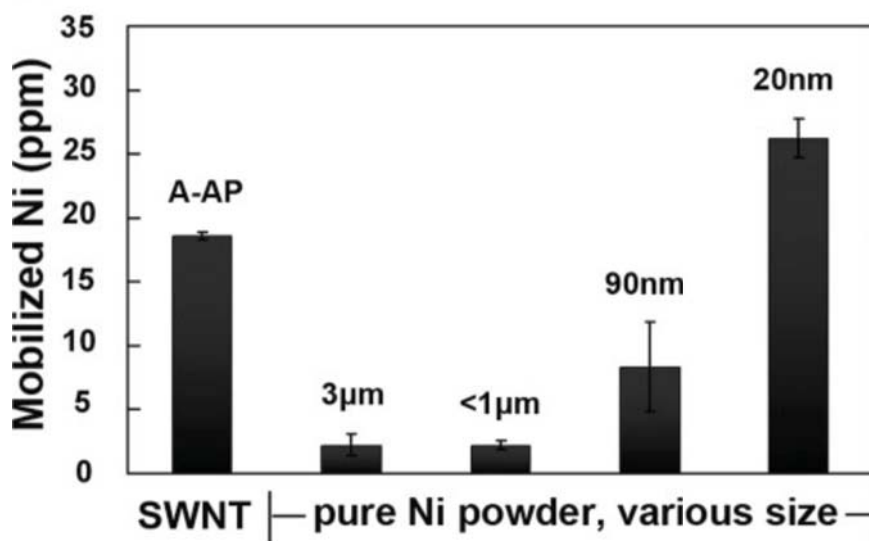


Figure 1. Nickel mobilization from carbon nanotubes and nickel particles (Liu et al., 2007).

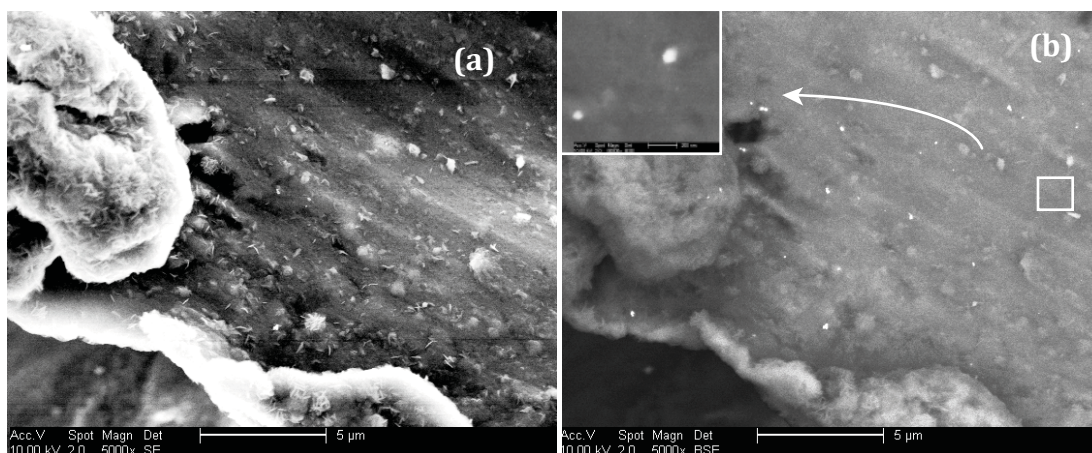


Figure 2. ESEM images of a Pd/Mg particle with 0.58% Pd taken by secondary (a) and backscattered (b) electron detectors. Inset shows two Pd-islands magnified at 80,000x.

Dechlorination studies

Effect of Bimetallic loading: Dechlorination of 2-CIBP was found to be rapid and complete with 0.5 g of bimetallic particles as shown in Fig. 3. The difference in dechlorination rates between systems with 0.05 and 0.2 g bimetallic particles, though not remarkable, was observed in all sets of constant Pd-doped systems, more so in terms of biphenyl generated. Systems with 1.62% Pd were an exception where rapid dechlorination kinetics, almost as fast as those in 0.5 g systems, were seen with 0.2 g of the bimetals (Fig. 3b).

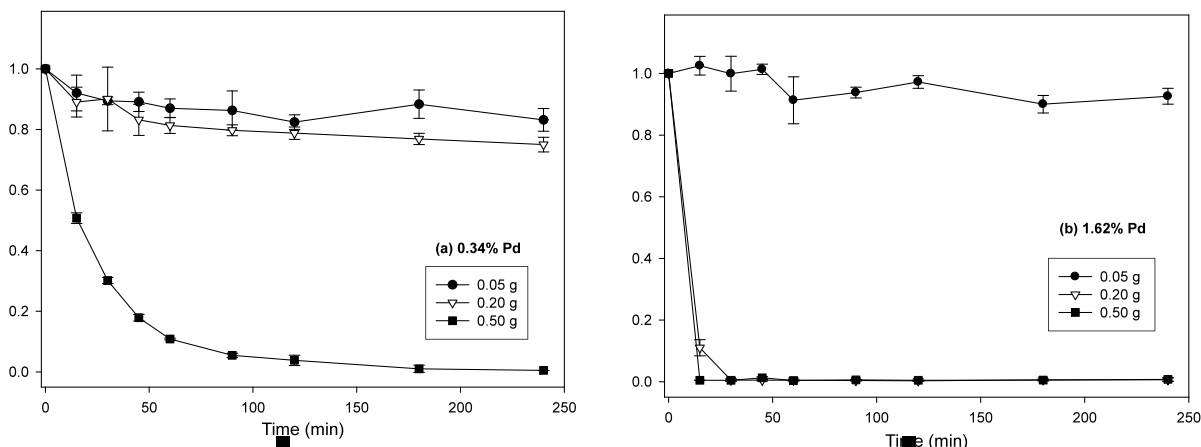


Figure 3. Effect of Pd/Mg loading on the kinetics of dechlorination of 2-CIBP at (a) 0.34% Pd and (b) 1.62% Pd.

Effect of Pd-doping levels: Vastly improved dechlorination kinetics with increased Pd-doping was seen in units with 0.5 g of bimetal loading (Fig 4). The pseudo first order constants plotted against their total Pd content showed a linear trend ($R^2 = 0.97$) indicating a direct correlation between the two. Increased doping at a given Pd/Mg loading and fairly constant Pd-island size means increased number of Pd-islands. The dechlorination reactions occur at the bimetallic interface (2). Hence, an increased number of Pd-islands imply increased dechlorination sites.

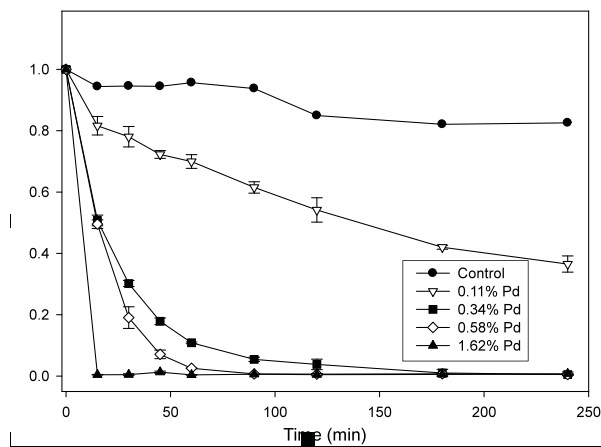
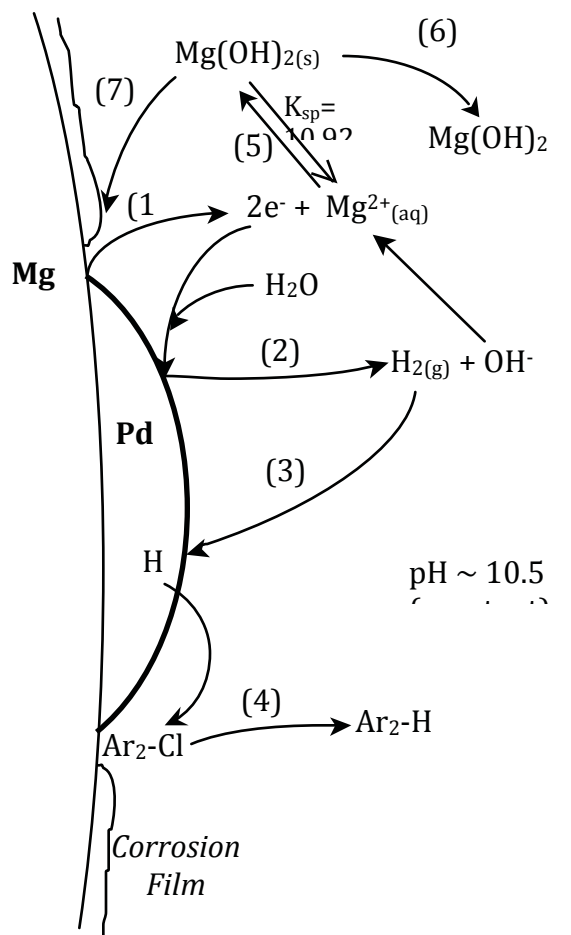


Figure 4. Effect of Pd-doping levels on the dechlorination kinetics of 2-CIBP with Pd/Mg loading constant at 0.5 g.

PCB dechlorination mechanism: The widely accepted dechlorination mechanism in Pd/Fe particles (2) is being modified by including the self-limiting corrosion behavior of Mg to propose a mechanism for dechlorination in Pd/Mg systems (Schematic 1)



Schematic 1. Proposed scheme for enhanced corrosion-based Pd/Mg bimetallic systems for dechlorination of PCBs.

Implications

Pd/Mg bimetals can be used in reactive barriers to treat highly chlorinated plumes in groundwater aquifers and submarine matrices where the redox environment often favors reduction. Pd/Mg barriers in sediment beds can deplete the dissolved organics adjacent to the contaminated sediments inducing their desorption into the aqueous phase thereby reducing their concentrations in the sediment. Pd will be contained in such barriers allowing recycling of Pd while ensuring that it is not free to enter the natural waters. Reductive dechlorination by Pd/Mg can also be a primary treatment step before the application of oxidative technologies which may falter with highly chlorinated organics (10).

Acknowledgements

This paper has not been subjected to internal policy review of the US Environmental Protection

Agency. Therefore, the research results presented herein do not, necessarily, reflect the views of the Agency or its policy. Mention of trade names or commercial products does not constitute endorsement or recommendation for use.

References

1. Ross, G. The public health implications of polychlorinated biphenyls (PCBs) in the environment. *Ecotoxicology and Environmental Safety* 2004, 59, 275-291.
2. Cheng, I.F.; Fernando, Q.; Korte, N. Electrochemical dechlorination of 4-chlorophenol to phenol. *Environmental Science and Technology* 1997, 31, 1074-1078.
3. Muftikian, R.; Fernando, Q.; Korte, N. A method for the rapid dechlorination of low molecular weight chlorinated hydrocarbons in water. *Water Research* 1995, 29, 2434-2439.
4. Grittini, C.; Malcomson, M.; Fernando, Q.; Korte, N. Rapid dechlorination of polychlorinated biphenyls on the surface of a Pd/Fe bimetallic system. *Environmental Science and Technology* 1995, 29, 2898-2900.
5. Vanysek, P. Electrochemical Series, In *CRC Handbook of Chemistry and Physics: 71st Edition*. 71st ed.; Lide, D.R., Ed.; Chemical Rubber Publishing Company: Boston, 1991; pp. 8-16-8-23.
6. Engelmann, M.D.; Doyle, J.G.; Cheng, I.F. The complete dechlorination of DDT by magnesium/palladium bimetallic particles. *Chemosphere* 2001, 43, 195-198.
7. Xu, X. and Song, C. Improving hydrogen storage/release properties of magnesium with nano-sized metal catalysts as measured by tapered element oscillating microbalance. *Applied Catalysis A: General* 2006, 300, 130-138.
8. Matyi, R.J.; Schwartz, L.H.; Butt, J.B. Particle size, particle size distribution, and related measurements of supported metal catalysts. *Catalysis reviews* 1987, 29, 41-99.
9. John J. Bozzola, Lonnie D. Russell *Electron Microscopy*. Jones and Bartlett Publishers International: London, England, 1992; pp. 205.
10. Liu, Y.; Schwartz, J.; Cavallaro, C.L. Catalytic dechlorination of polychlorinated biphenyls. *Environmental Science and Technology* 1995, 29, 836-840.

Save

Sand-Tank Test on Injectability of Nano-Size ZVI into Saturated Sand for Mending an Existing Permeable Reactive Barrier in the 100-D Area at the Hanford Site

Gilbert M. Zemansky, Adam Logar, Kenneth R. Manchester, Marek H. Zaluski, Michael Hogan, and Nick Jaynes, MSE Technology Applications, Butte, Montana, U.S.A.

Scott Petersen, Fluor Hanford, Washington, U.S.A.

Abstract

MSE conducted investigations for Fluor Hanford and DOE associated with a proposed injection of nano-size ZVI (nZVI) into the subsurface at the 100-D Area of DOE's Hanford Site in Washington State. The purpose of this work was to demonstrate the feasibility of using nZVI to repair portions of the ISRM barrier located in the 100-D Area that had been installed to intercept a hexavalent chromium plume moving towards the Columbia River. Laboratory investigations consisted of several phases. The final phase used a sand-filled tank with a central well to simulate an actual field injection in a Hanford well. nZVI was injected at a concentration of 9,030 mg/L total iron (1% solids) into a synthetic aquifer composed of medium and very coarse sand arranged in three layers. The injection took place at a flow rate of about 3 gpm for approximately 100 minutes. Measurements of fluid variables and fluid samples were taken during the injection. After the injection, sand from the tank was excavated and sampled. It was found that iron deposition occurred predominantly in the very coarse sand layer. The zone of highest deposition formed a ring around the injection well at a radial distance of about 1.5 foot from the center of the tank.

Introduction

An In Situ Redox Manipulation (ISRM) barrier was constructed at the U.S. Department of Energy's (DOE) Hanford Site by injection of sodium dithionite through 65 wells. This created an aquifer environment capable of reducing mobile hexavalent chromium to intercept it from entering the Columbia River. Localized signs of failure of this barrier were discovered within 18 months of treatment. The probable cause of premature barrier failure is believed to be heterogeneities in the aquifer from laterally discontinuous, high permeability units, having lower inherent reductive capacity due to lower natural iron content. To remedy this, it was recommended that the possibility of injecting ZVI be investigated (Fruchter, et al., 2000 and Oostrom, et al., 2005). MSE was commissioned to carry out a series of laboratory tests to explore this alternative. These indicated that RNIP-M2 offered the best potential mobility and reactivity for this application. RNIP-M2 is a nZVI formulation in a polymer carrier that facilitates transport in porous media. It was decided that an intermediate-scale tank test would be useful in evaluating the application of smaller-scale laboratory tests to the full-scale field situation before proceeding. This paper reports on the results of a laboratory sand-tank test conducted by MSE for DOE's Office of Environmental Management.

tom layer of medium size sand at the same radial distance (wells D1 and D2, respectively)

After the tank test apparatus had been constructed and filled with sand as described above, the tank was filled and flushed with fresh water. Water was injected through the central 6 inch well and drained from the four outlets. Next, slug tests were performed in all five wells prior to the injection. When the tank was ready for the injection test, nZVI was mixed in a separate tank with fresh water to achieve a 1% solids concentration ZVI fluid for injection (9,030 mg/L total iron). ZVI fluid was recirculated both by pump and through an ultra high-shear, rotor-stator combination disperger back to the mixing tank under a nitrogen gas atmosphere. These measures were intended to help minimize the tendency for agglomeration to increase particle size.

ZVI fluid from the mixing tank was injected into the central 6 inch well using a centrifugal pump. The injection was maintained at a rate of 3.1 gallons/minute (gpm) for 100 minutes. Peristaltic pumps and a multiparameter probe were used to monitor water quality in the four monitoring wells and tank effluent during the injection. As ZVI fluid sequentially impacted each well (in the order of S1, S2, D1, and D2), the well was sampled. Sampling continued at 15 minute intervals thereafter until completion of the injection.

When the injection was completed, all wells were again hydraulically tested. The tank was then drained. Sand was excavated and sampled at pre-selected depths on four perpendicular radials (including a radial through wells S1 and S2 and a radial through wells D1 and D2).

Results

Results from this sand-tank test fall with three categories of data: (1) analysis of pre- and post-injection hydraulic testing response data; (2) field measurements and laboratory analysis of monitoring well and tank effluent fluid samples taken during the injection; and (3) post-injection visual observations of excavated sand and laboratory analysis of post-injection sand samples. These results indicated the following:

Hydraulic testing – Pre-injection testing indicated that the hydraulic conductivity of the very coarse sand was about 20 times that of the medium sand. Post-injection testing indicated that for the two wells in very coarse sand, the hydraulic conductivity of the well closest to the injection well (S1) decreased by 21 percent while the decrease for the well farther away (S2) was 14 percent. For the two wells in medium sand, the hydraulic conductivity of the well closest to the injection well (D1) decreased by 16 percent while there was no change for the well farther away (D2).

Fluid samples – ZVI impact was rapidly observed in the two shallow wells screened in very coarse sand. Impact was seen for the well closest to the injection well (S1) within 10 minutes and for the well farthest away within 20 minutes (S2). Impact was seen in effluent from the tank shortly after that. For the wells screened in medium sand, impact was not seen for the well closest to the injection well (D1) until after 55 minutes and for the well farthest away 91 minutes (D2). The highest total iron concentration measured of 738 mg/L was for a sample from the well in very coarse sand closest to the injection well (S1). Samples from wells S2, D1, and all tank outlets were on the order of 55 mg/L. The sample from well D2 was less than half of that value.

Sand – Visual observations of sand indicated that dark discoloration occurred only in the very

coarse sand with a black ring between wells at a radial distance of about 1.5 feet from the center



Figure 2. Iron Deposition Near Bottom of Very Coarse Sand Layer

of the tank. The greatest extent of discoloration was seen near the bottom of the very coarse sand layer (see Figure 2). This was confirmed by sand sample analysis.

Conclusions

The following are conclusions based on results from this tank test:

Injected ZVI fluid flowed predominantly through the very coarse sand layer of the simulated aquifer. Little flow of injected ZVI fluid occurred in the medium sand layers.

Taking background sand iron content into account, maximum iron deposition was approximately 1,750 mg/Kg (0.175 %) near the bottom of the very coarse sand layer. Lower concentrations of iron were also deposited throughout the very coarse sand layer from the injection well to the tank wall. Little iron deposition occurred in the medium sand layers.

The procedures developed first for flow cell tests and then modified for this tank test formed a satisfactory basis to guide field scale injection of RNIP-M2 at the Hanford Site.

Acknowledgements

A major portion of this work was conducted through the DOE Environmental Management Con-

solidated Business Center at the Western Environmental Technology Office under DOE Contract Number DE-AC09-96EW96405.

References

Fruchter, et al. (2000). "Creation of a subsurface permeable treatment zone for aqueous chromate contamination using in situ redox manipulation." *Ground Water Monitoring & Remediation*, Spring, pages 66-77.

Oostrom, et al. (2005). "Experimental study of micron-size zero-valent iron emplacement in permeable porous media using polymer enhanced fluids. Report PNNL-15573, Pacific Northwest National Laboratory, Richland, WA.

Save

Geochemical Laboratory Testing of Nano-Size ZVI for Mending an Existing Permeable Reactive Barrier in the 100-D Area at the Hanford Site

*Gary Wyss, Adam Logar, Martin Foote, Nick Jaynes, Marek H. Zaluski,
and Michael Hogan, MSE Technology Applications, Butte, Montana, U.S.A.*

Scott PetersEn, Fluor Hanford, Washington, U.S.A.

Abstract

MSE Technology Applications Inc. has conducted investigations associated with injection of nano-size zero-valent iron (nZVI) into the subsurface at the 100-D Area at the U.S. Department of Energy (DOE) Hanford Site, Washington State. The purpose of this work was to demonstrate the feasibility of using nZVI to repair portions of the In situ Redox Manipulation (ISRM) barrier located in the 100-D Area of the Hanford Site that was installed to intercept a hexavalent chromium (Cr^{6+}) plume moving towards the Columbia River. The investigation included geochemical column tests to evaluate the potential for nZVI-impregnated soil to reduce Cr^{6+} .

Geochemical column tests were performed to simulate geochemical conditions found in the highly permeable zones within the Ringold formation at Hanford. Two nZVI materials were investigated in the geochemical column tests, RNIP-M2, manufactured by Toda Kogyo Corporation Japan and Polymetallix, manufactured by Crane-Polyflon. Approximately 40 (37 to 48) pore volumes of surrogate groundwater containing 0.55 mg/L Cr^{6+} were flushed through columns packed with nZVI impregnated Ringold E soil. The geochemical column effluents were collected and analyzed for physical and chemical parameters at six sampling events throughout the three-week test. RNIP-M2 (RNIP) consistently showed greater reduction of Cr^{6+} and oxidation-reduction potential (ORP), and increase pH, than the Polymetallix.

This work was conducted through the support of Fluor Hanford, a subcontractor to the DOE, under Contract Number 30994.

Introduction

We have conducted investigations associated with the injection of xZVI into the subsurface at the 100-D Area at the U.S. Department of Energy (DOE) Hanford Site in Washington State. The purpose of this work was to demonstrate the feasibility of using nZVI as a source of electrons to repair portions of the ISRM barrier. The ISRM barrier was installed at that site to intercept a Cr^{6+} plume moving towards the Columbia River. The ISRM barrier was installed from 1999 to 2002 (DOE, 2006) by injecting sodium dithionite to the Ringold Formation aquifer and creating persistent reducing conditions by converting native Fe^{3+} to Fe^{2+} . Although laboratory and field tests indicated that barrier would effectively treat Cr^{6+} for nearly 20 years, a few of the barrier wells exhibited signs of breakthrough after less than two years.

The work reported here was performed to support testing an alternative technology to mend the ISRM barrier, by injecting nZVI into the Ringold aquifer through existing injection wells.

The purpose of the geochemical column test was to evaluate which of the nZVI's (Table 1) were most likely to sustain chemical reactivity when injected into the subsurface by assessing the reduction of Cr⁶⁺, and changes in ORP, pH, and other chemical constituents between the effluent and the influent surrogate groundwater.

ZVI	Particle Size Range	Dispersant	Shipped form of material	Coating
RNIP – M2	D ₅₀ – 70 nanometers	Olefin maleic copolymer	Water-based slurry: 80% water, 17% solids, and 3% polymeric additive	Magnetite coating surrounding alpha-iron core
Polymetallix	100 to 200 nanometers	Vendor recommendation: 5 to 10% by weight sodium hexametaphosphate	Water-based slurry: 51% water, 54% solids, 5% sodium hexametaphosphate	None

Table 1. Geochemical Test – nZVI Properties

Materials and Methods

The experiments used vertical columns packed with nZVI materials and Ringold sediment. A column flow rate of 1 ml/min was used to replicate the regional groundwater flow rate in the high permeable zones of the 100D Area. Each column measured approximately 55 centimeters in length and 7.6 centimeters in diameter and was placed vertically during testing. Three concentrations of each ZVI material were used in the columns. Those concentrations by weight were as follows: high (1.5%); medium (0.15%); and low (0.015%). The surrogate groundwater chemical composition was formulated to mimic the composition of the groundwater from the Hanford 100-D Area.

Approximately 40 (37 to 48) pore volumes of surrogate groundwater were passed through each column during the test and effluent samples from the geochemical columns were taken at six intervals throughout the study. The column effluent pH, ORP, specific conductance (SC), dissolved oxygen (DO), temperature and the head differentials across the column were measured during each sampling event. Effluent samples were collected for laboratory analysis for the constituents: nitrogen as ammonia, nitrate, and nitrite; alkalinity; sulfate; iron speciation; and Cr⁶⁺.

Results

The primary objective of the testing was to determine which of the two nZVI materials could sustain removal/reduction of Cr⁶⁺ for the longest time period. At 1.5% nZVI, both materials were able to remove the Cr⁶⁺ from the surrogate groundwater to levels below detection throughout the entire test duration. The 0.15% columns showed a distinct difference in Cr⁶⁺ reduction from the surrogate groundwater (Figure 1). The RNIP at 0.15% was able to remove the Cr⁶⁺ from the surrogate groundwater nearly completely throughout the entire duration of the test, while Polymetallix was not able to remove the Cr⁶⁺ from the surrogate groundwater to below detection limits at any point during the test. By the end of the test, the 0.15% Polymetallix column removed approximately 20 to 25% of the Cr⁶⁺. The 0.015% RNIP columns removed approximately 75% of the Cr⁶⁺ from the surrogate groundwater during the initial stages of the test and then decreased to approximately 15% during the latter stages of the test. The 0.015% Polymetallix columns were not able to remove any appreciable amount of Cr⁶⁺ at any point during the test (Figure 2).

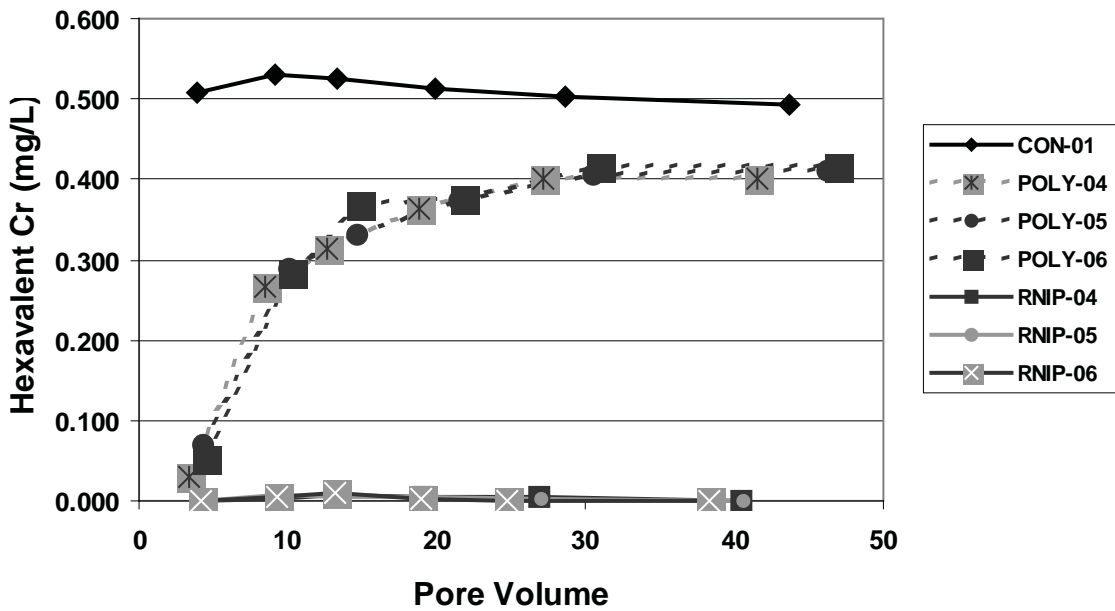


Figure 1. Geochemical Test - Chromium Reduction by 0.15% Concentration of nZVI

Effluent ORP and DO were monitored to quantify reducing conditions. These parameters were used as indicators of reducing conditions, which appears to be the primary removal mechanism of Cr^{6+} by nZVI materials. As shown in Figure 3, both nZVI materials were able to reduce the ORP at 1.5% during the initial stages of the test. However, between 10 and 15 pore volumes the

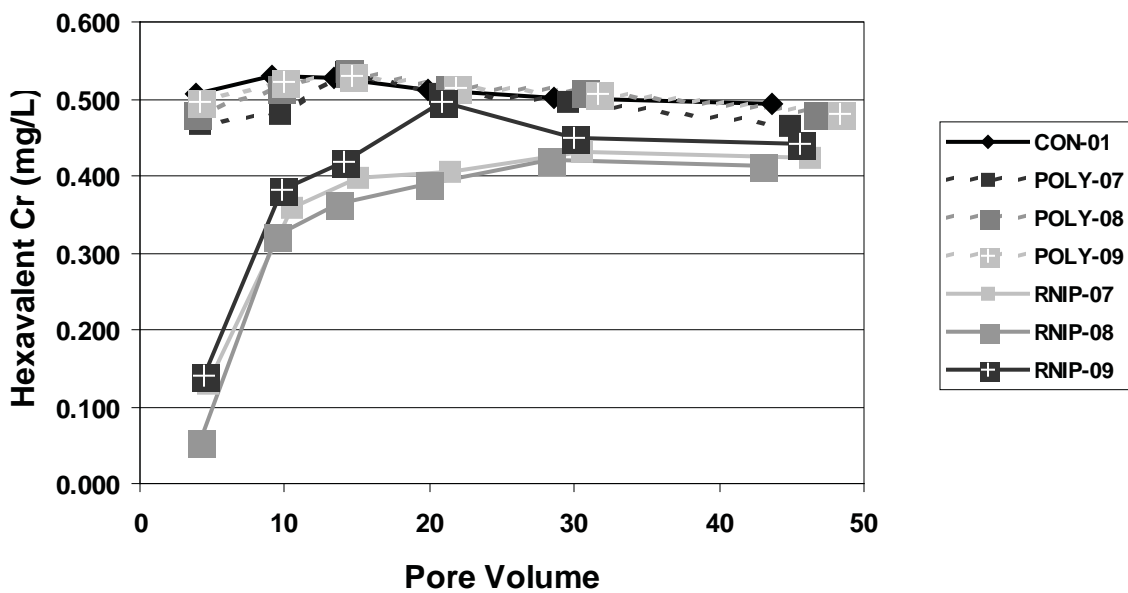


Figure 2. Geochemical Test - Chromium Reduction by 0.015% Concentration of nZVI

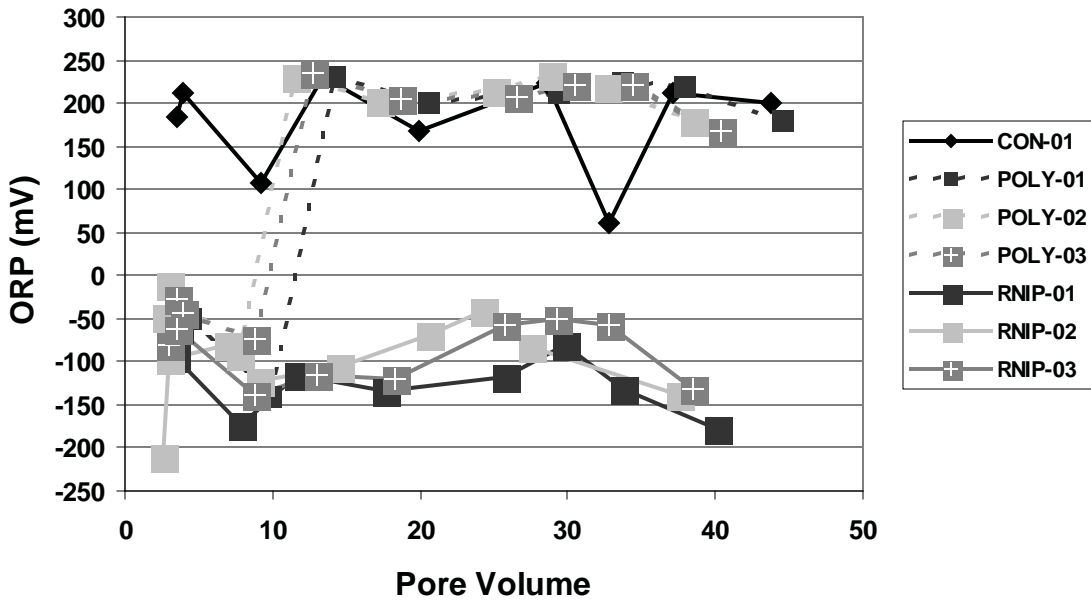


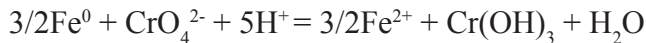
Figure 3. Geochemical Test – ORP in 1.5% Concentration of nZVI

Polymetallix columns began to lose their ability to reduce the ORP while the effluent from the 1.5% RNIP columns continued to be strongly reducing throughout the remainder of the test.

The 0.15% nZVI columns showed a distinct difference in their ability to lower the ORP of the column effluent. The RNIP columns were able to moderately reduce the ORP in the effluent while the Polymetallix was not able to show a significant effect on the ORP of the column effluent. Neither of the two nZVI materials at 0.015% was able to significantly lower the ORP.

The DO in the 1.5% RNIP columns was initially reduced, but rose to values similar to the control column between 5 and 10 pore volumes.

Another objective of this testing was to evaluate the ability of nZVI impregnated Ringold soil to increase the pH of the groundwater. An increase in the pH of the column effluent relative to the control-column effluent demonstrated the reactivity of the nZVI materials. Increases in the pH of the effluent are due to the effects of the oxidation/reduction couple between iron and chromium as shown in the following reaction:



The 1.5% RNIP columns significantly raised the effluent pH. Initially, the pH was near 10 and remained above pH 9 throughout the test (Figure 4). The pH of the 0.15% RNIP columns was greater than the control column throughout the test by approximately 0.5 to 1.0 pH units. None of the Polymetallix columns exhibited pH values significantly different from the control column. These results indicated that RNIP was more reactive than the Polymetallix.

Physical examination on four of the columns was conducted subsequent to the geochemical testing. The columns were cut open along the long axis of each column for examination. Two RNIP and two Polymetallix columns, one 1.5% and one 0.15% from each nZVI were examined.

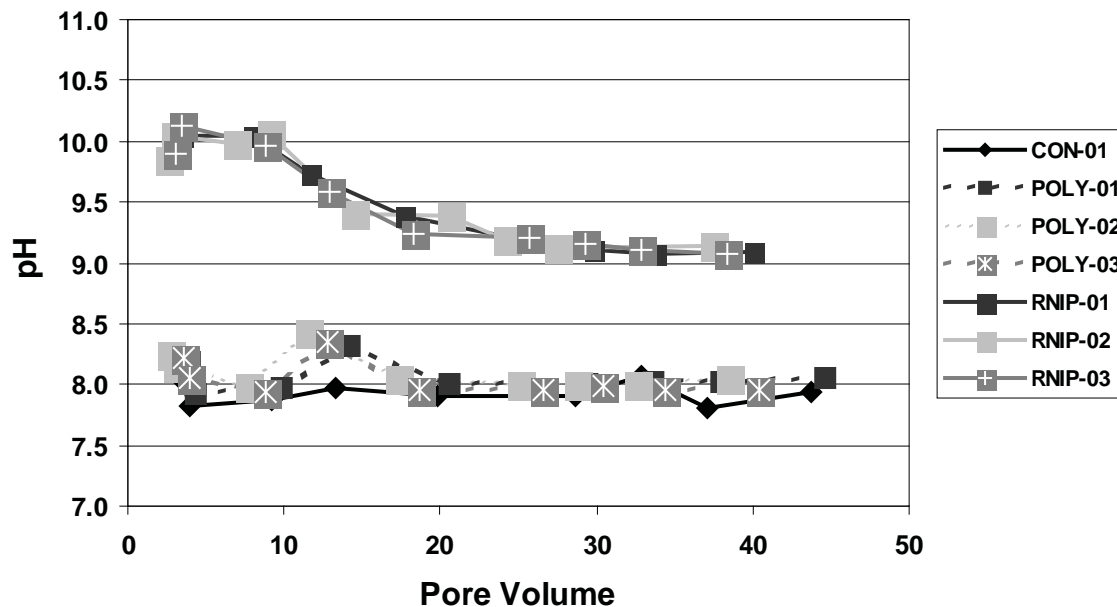


Figure 4. Geochemical Test – pH effect in 1.5% Concentration of nZVI

The 1.5% RNIP column appeared to be unoxidized, with only a very thin band (approximately ¼ inch) of oxidized material present at the influent screen. The 0.15% RNIP and the 1.5% Polymetallix column were similar with approximately 25% of the column appearing to be oxidized. The 0.15% Polymetallix column was nearly completely visibly oxidized.

Conclusions

RNIP appeared to have a greater ability to sustain the reduction of Cr^{6+} for a longer period than Polymetallix. RNIP removed Cr^{6+} more effectively than Polymetallix. RNIP lowered the ORP longer than the Polymetallix columns. Additionally, RNIP was more reactive than Polymetallix as displayed in its ability to increase the effluent pH, and sustain it. Physical examination revealed that the RNIP columns showed less oxidized material than Polymetallix. The ability of RNIP-M2 to remove hexavalent chromium, reduce ORP, and increase pH make it more suitable candidate for sustaining removal/reduction of hexavalent chromium in the subsurface at the 100-D Area at Hanford.

Acknowledgements

The authors appreciate the insight of and helpful discussions with Drs. P. Tratnyek, G. Lowry, C. Palmer, and A. Jazdanian during execution of the investigations.

References

DOE (2006). “The Second CERCLA Five-Year Review Report for the Hanford Site.” DOE/RL-2006-20, Revision 1.

Save

Screening of Available ZVI Products for Mending an Existing Permeable Reactive Barrier in the 100-D Area at the Hanford Site

Nick Jaynes, Adam Logar, Martin Foote, Gary F. Wyss, Marek H. Zaluski, and Michael Hogan, MSE Technology Applications, Butte, Montana, U.S.A.

Scott Petersen, Fluor Hanford, Washington, U.S.A.

Abstract

MSE Technology Applications, Inc. (MSE) has conducted investigations associated with the injection of nano and micron-size zero-valent iron (ZVI) into the subsurface at the 100-D Area at the U.S. Department of Energy (DOE) Hanford Site in Washington State. The purpose of this work was to demonstrate the feasibility of using nZVI to repair portions of the In Situ Redox Manipulation (ISRM) barrier located in the 100-D Area of the Hanford Site that was installed to intercept a hexavalent chromium plume moving towards the Columbia River. As a result of an extensive literature research and consultation of internal and external resources, we developed a database in September of 2007 that contained 30 ZVI candidate materials for potential use at the Hanford 100-D Area. Using a comprehensive screening process we were able to effectively evaluate and compare the various materials on their ability to create a reducing environment and reduce hexavalent chromium. The screening process included tests ranging from simple tabletop batch experiments to highly controlled horizontal flow cell injection and vertical geochemical columns. As a results of this testing, we identified RNIP-M2, a product of Toda Kogyo Corporation of Japan, as most suitable for mending the ISRM barrier. This work was conducted through the support of Fluor Hanford under Contract Number 30994.

Introduction

We have conducted investigations associated with the injection of nano-sized zero-valent iron (nZVI) into the subsurface at the 100-D Area at the U. S. Department of Energy Hanford Site in Washington State. The purpose of this work was to demonstrate the feasibility of using nZVI as a source of electrons to repair portions of the ISRM barrier. The ISRM barrier was installed at that site to intercept a Cr⁶⁺ plume moving towards the Columbia River. The ISRM barrier was installed from 1999 to 2002 (DOE, 2006) by injecting sodium dithionite to the Rongold Formation aquifer and creating persistent reducing conditions by converting native Fe³⁺ to Fe²⁺. Although laboratory and field tests indicated that the barrier would effectively treat Cr⁶⁺ for nearly 20 years, a few of the barrier wells exhibited signs of breakthrough after less than two years.

A Technical Assistance Team (TAT) recommended that an alternative technology, injection of micron-size zero-valent iron (MZVI), be tested and possibly deployed to mend the barrier, and to eliminate the need of periodically re-injecting the ISRM wells with sodium dithionite (Fluor Hanford, 2004). Following the recommendations from the TAT, we investigated Micropowder™ S-3700 material (MP) and later other ZVI materials as candidates for injection into the ISRM barrier.

We performed extensive literature research, consulted both internal and external resources, performed on-line searches and developed a database in September 2007 that contained 30 separate ZVI candidate materials for potential deployment at the Hanford 100-D Area. Upon examination using a number of selection criteria (including their reactivity, injectability and other related characteristics), the top six ranked materials in the database and MP (due to its previous history with the project) were tested in the laboratory under a set of three screening tests to further evaluate the injectability and reactivity of these materials.

The results of the screening tests left only two materials that were deemed as suitable for further geochemical and injectability testing. Of these two remaining materials, RNIP-M2, a product of Toda Kogyo Corporation of Japan, was selected for further large-scale tank testing and a field-injection demonstration, which was performed at the Hanford 100-D Area in August 2008. The methods and results of the additional geochemical and injectability testing, large-scale tank injection, field-injection testing, and numerical modeling are not discussed in this paper.

Methodology and Results

The initial work scope of laboratory geochemical and injection testing, using MP, was designed to answer the primary question of whether MZVI and its polymer carrier fluid would cause nitrates in the groundwater to be reduced to ammonia, and whether or not carbonates would be formed, which may adversely impact the aquifer properties. The testing also addressed the mobility of the MP and its effectiveness at reducing Cr^{6+} to Cr^{3+} once it is emplaced and flushed with Cr^{6+} contaminated surrogate groundwater. We conducted this initial geochemical and injection testing using columns packed with 100-D Area sediments from the Ringold formation. The columns were then injected with the fluid containing MP and its additives (polymer and dispersant) in water followed by injection of a surrogate groundwater with approximately 450 parts per billion (ppb) Cr^{6+} and matching the groundwater chemistry of the 100-D Area.

The results of this initial testing indicated that the MZVI distribution in the columns was less than desired, that a portion of the nitrates in the surrogate groundwater might be reduced to ammonia and that reduction of Cr^{6+} to Cr^{3+} was less than expected. These results lead us to conclude that using this MP slurry had not adequately addressed the project goals and concerns.

We then conducted several batch tests in which specific geochemical reactions were observed over a period of approximately 66 hours using various mixtures of MP, polymer, surfactant and surrogate groundwater and a mixture of “sponge” iron powder and surrogate groundwater. The results of the batch test indicate that MP did not adequately reduce the Cr^{6+} and that it may be further inhibited by the addition of polymer. The mixtures tested and their results of this test are presented in Table 1.

In response to the findings from the initial work scope, and as requested by FH, we developed a database in September 2007 that contained 30 separate ZVI candidate materials for potential use at the Hanford 100-D Area. A listing of these materials and their manufacturers are shown in Table 2. We also developed a scoring system based on a number of selection criteria, which we felt best described the material's injectability and Cr^{6+} reduction capacity. Based on this scoring system, we chose to test the top six ranked materials in the database (EZVI, Polyflon Particles, NanoFe I, NanoFe II, Zloy, and RNIP-M2) under a set of 3 screening tests to further evaluate

Batch Test Description	Total Cr (ppb)	Cr⁺⁶ (ppb)	% Cr⁺⁶ Reduced
Surrogate Groundwater	303	245	NA
MZVI	153	131	46.5%
MZVI+Aerosol	128	121	50.6%
MZVI+Aerosol+Polymer	223	163	33.5%
Sponge Iron Powder	11	0	100%

Table 1. Total Cr and Cr+6 Analytical Results.

Table 2. ZVI Materials and Manufacturers

ZVI Material Name	Manufacturer
Cellulose stabilized NZVI	Auburn University
CIP-EQ	BASF
CIP-EW	BASF
CIP-HQ	BASF
CIP-HS	BASF
Connelly CC-1200	Connelly GPM Inc.
EZVI	Toxicological and Environmental Associates Inc.
EHC-M TM	Adventus Americas Inc.
H-200	Hepure Technologies Inc.
HC-5	Hepure Technologies Inc.
HC-15	Hepure Technologies Inc.
H2OMet-56 TM	Quebec Metal Powders Ltd.
H2OMet-414 TM	Quebec Metal Powders Ltd.
H2OMet-XT TM	Quebec Metal Powders Ltd.
Iron Metal	CERAC
LD-80	North American Hoganas Inc.
Metamateria A	Metamateria Partners
Metamateria B	Metamateria Partners
Metamateria C	Metamateria Partners
Micropowder S-3700 TM	International Specialty Products
NanoFe TM	Lehigh Nanotech – dist. By PARS Environmental
NanoFe TM Slurry I	Lehigh Nanotech
NanoFe TM Slurry II	Lehigh Nanotech
NF-325	North American Hoganas Inc.
Peerless TM Iron Powder	Peerless Metal Powders and Abrasives
Polyflon Particles	Crane Polymetallix – dist. by Nanitech LLC
R-12	North American Hoganas Inc.
RNIP-10DS	Toda Corporation
RNIP-M2	Toda Corporation
Zloy TM	OnMaterials LLC.

the injectability and reactivity of these materials. MP material was also tested for comparison purposes due to its previous history with the project.

Controlled batch screening tests were performed on the top six ranked materials in the database. The experiments consisted of a 4-hour batch test performed on a mixture of the ZVI material, clean silica sand and surrogate groundwater as a way of evaluating the materials' ability to create a reducing environment and reduce hexavalent chromium. Measurements of specific conductivity, pH, ORP, temperature and dissolved chromium were taken upon completion of the testing. All six materials were successful at reducing the dissolved chromium in the batch test and they were advanced for further testing.

A set of injection screening tests were developed in which the six materials were evaluated on their ability to distribute iron throughout the horizontally placed flow cells as well as their effect on the hydraulic conductivity. Each material was injected through a horizontal flow cell packed with a surrogate blend of silica sand. Samples of the flow cell effluent, solid core samples, and visual observation were used to evaluate the mobility of each ZVI material. The results of the injection tests are presented in Figure 1 and Figure 2. Two of the materials tested are not present in these figures due to their inability to effectively distribute throughout the flow cells during testing.

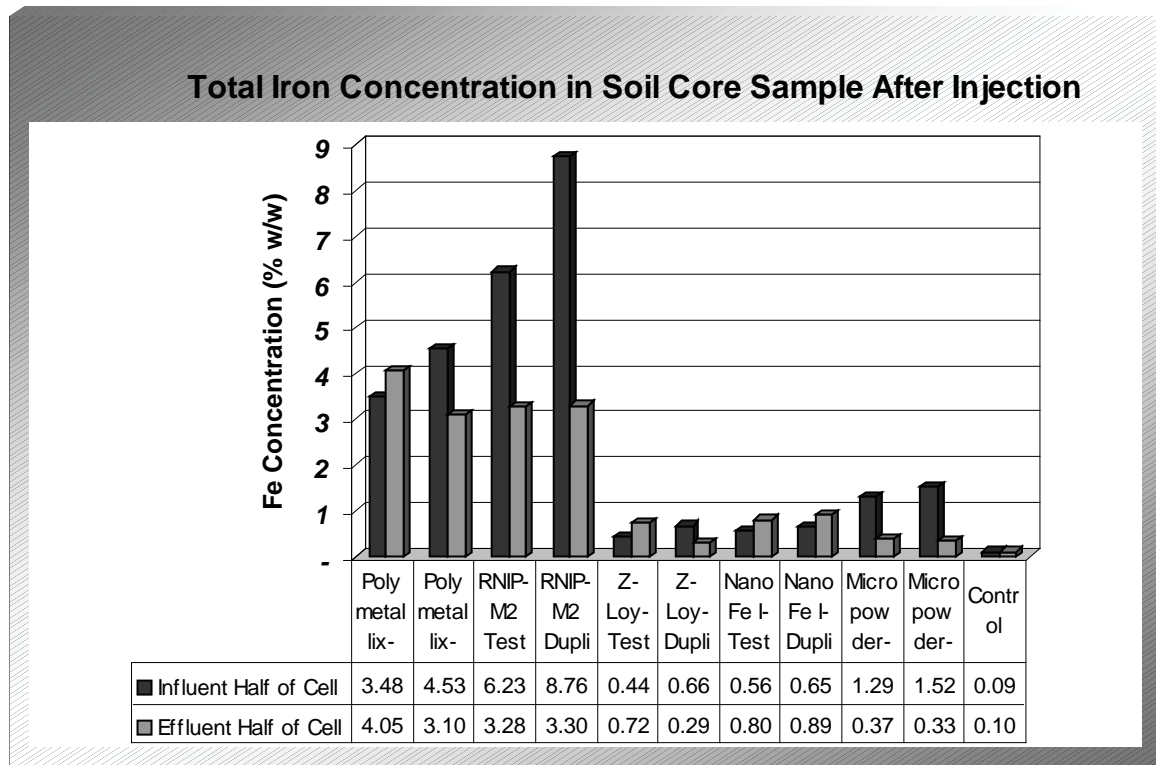


Figure 1. Iron Emplacement from Core Samples After Injection.

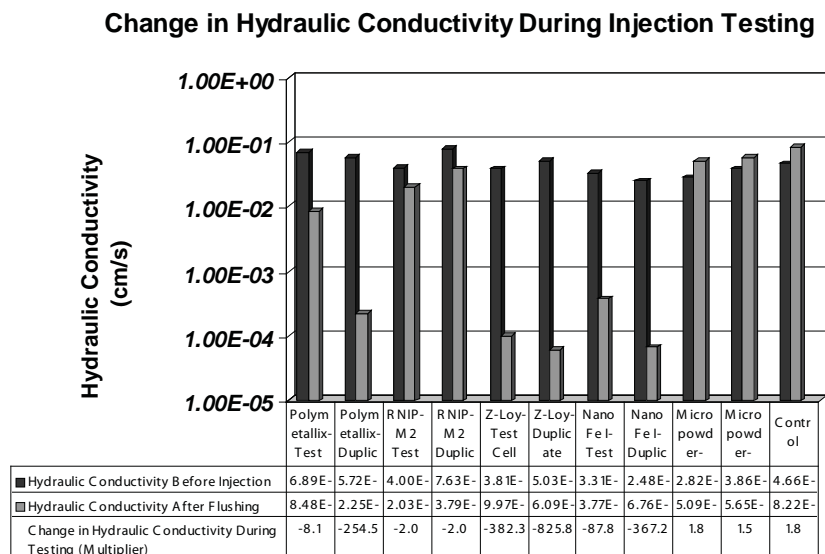


Figure 2. Effect on Hydraulic Conductivity After Injection.

Based on the injection screening tests, we selected two ZVI materials, Polymetallix and RNIP-M2, for further geochemical column testing. Micropowder S-3700 was also selected for further testing for comparison purposes. Surrogate groundwater containing 572 ppb Cr⁺⁶ was injected through vertical columns containing 1.5% and 0.075% ZVI for approximately 20 pore volumes. The materials were evaluated on their ability to reduce Cr⁺⁶ without producing any unwanted by-products such as ammonia. The Cr⁺⁶ results from the completion of the test are shown in Figure 3 where ZVI concentrations of 1.5% and 0.075% are referred to as high and low, respectively.

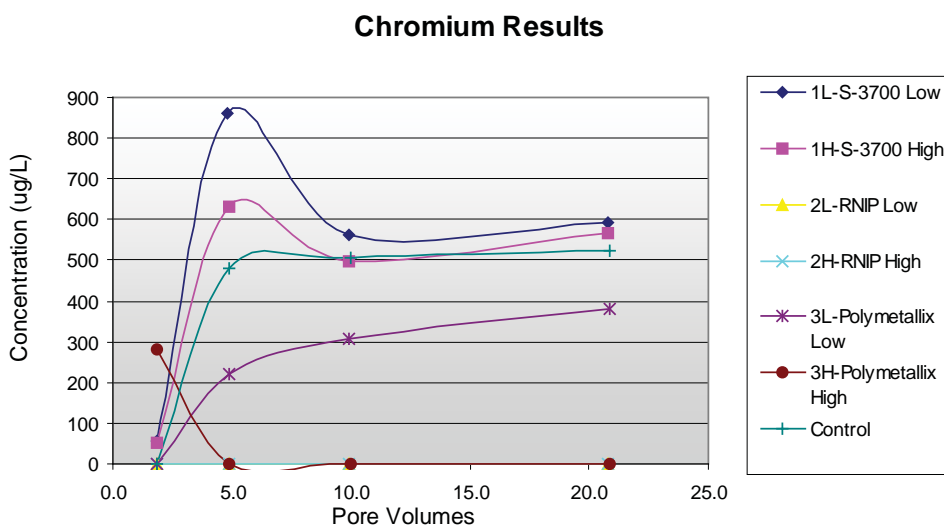


Figure 3. Chromium Reduction After 20 Pore Volumes.

Because RNIP reduced Cr⁺⁶ concentration to a level non-detectable the lines representing this reduction are not visible in the figure. Based on both the injection and geochemical screening tests, we concluded that the MP was ineffective at significantly reducing chromium concentrations.

Conclusions

As a result of the screening tests discussed in this paper, we recommended further geochemical column, injection flow cell, and large-scale tank testing of only Polymetallix and RNIP-M2 to further evaluate these two materials under a larger scale and using larger volumes of materials. As a result of the further testing, we have concluded that RNIP-M2 is the best candidate and have performed a field-scale injection of RNIP-M2 at the 100-D Area of the Hanford Site using RNIP-M2.

Acknowledgements

The authors appreciate the insight of and helpful discussions with Drs. P. Tratnyek, W.X. Zhang, G. Lowry, C. Palmer, and A. Jazdanian during execution of the investigations.

References

- DOE (2006). "The Second CERCLA Five-Year Review Report for the Hanford Site." DOE/RL-2006-20, Revision 1.
- Fluor Hanford (2004). Evaluation of Amendments for Mending the ISRM Barrier. WMP-28124, Rev. 0, Fluor Hanford, Richland, Washington.

Chapter 2 – Introduction

Using Nanomaterials in Air & Water Pollution Control

Charles G. Maurice

United States Environmental Protection Agency

This chapter covers the two keynote papers and the platform and poster sessions addressing applications of nanotechnology to enhance air and water pollution control. One keynote paper is by Dr. Glen Fryxell and associates and addresses the use of nanoparticles embedded in pores of ceramic substrates to remove metal contaminants from water. The other is by Dr. Marie-Isabelle Baraton who covers the use of nanotechnology-enhanced sensors to more effectively monitor carbon monoxide (CO), nitrous oxide (NO), nitrogen dioxide (NO₂), and ozone (O₃) for better control of these air pollutants. Papers from the platform and poster sessions cover a wide array of nanotechnology applications used to enhance air and water pollution control. However, a theme of exploiting the potential for nanoscale particles to have enhanced sorbent or catalytic properties, weaves its way through many of these papers.

Nanosorbents are demonstrated to hold great promise for capturing mercury fumes following compact fluorescent lamp (CFL) breakage. Cerium dioxide (CeO₂), commonly used to control air pollution from mobile sources and fuel cells, is unstable and thus has a short functional period. A titanium dioxide (TiO₂) – CeO₂ nanocomposite is shown to potentially solve this problem by exhibiting a more stable nature while preserving the catalytic properties of CeO₂. Lastly among the air pollution control directed papers, there is a thoughtful piece on using decision analysis and real option analysis (ROA) to evaluate potential for, and implications of, using nanotechnology to ameliorate the greenhouse gas (GHG) emissions which drive global climate change issues.

Nanomembranes can be used to obtain drinking water by effectively filtering otherwise non-potable brackish groundwater. Nanoscale crystalline zeolites are shown to be effective adsorbents in polluted water treatment and can be used as environmental catalysts. Nanoscale zero-valent iron (NZVI) is shown to effectively treat semiconductor and optoelectronics industry wastewater and nanoscale photocatalysts are shown to be effective in treating water contaminated with 4-chlorophenol, a common wastewater constituent of the pulp and paper, pharmaceutical, and dye industries. Finally, enzyme-magnetic nanoparticle conjugates are demonstrated to improve biocatalytic efficacy for contaminated water bioremediation. Efficacy is shown to be improved both by enzyme stabilization resulting in longer productive activity and by enabling better control of enzyme spatial distribution in the water being treated.

The papers contained in this chapter convincingly demonstrate that nanotechnology has a large role to play in the future of pollution control, whether in air or water.

Save

Water Pollution Control Using Functional Nanomaterials

Glen E. Fryxell, Richard Skaggs, Shas V. Mattigod, Dawn Wellman, Kent Parker, Wassana Yantasee, R. Shane Addleman, Xiaohong S. Li, and Yongsoon Shin, Pacific Northwest Laboratory, U.S. Department of Energy, U.S.A.

Water is emerging as a global issue. Pure, clean drinking water is arguably the most important factor in determining quality of life in human society. Biological and chemical contamination are the two primary concerns for drinking water contamination. Biological contamination can be effectively treated with by a number of existing technologies (e.g. chlorination, ozone, UV, etc.), but chemical contamination is a more challenging hurdle, particularly heavy metals. Toxic metallic contamination (e.g. Hg, Pb, Cd, etc.) can be partially addressed by using ceramic oxide filters/sorbents (e.g. gamma alumina), but these are non-specific (meaning that they sorb all metal ions), saturating valuable sorbent capacity with common ions like Ca, Mg and Zn (which are in fact essential nutrients, and certainly don't need to be removed). In addition, metal ion sorption to a ceramic oxide surface is generally an equilibrium process, so even though these metals may be retained by the filter matrix, they can easily desorb to be released right back into the drinking water supply by these materials. Metal ions can also be removed via flocculation/precipitation, but these methods are best suited to contaminants at high concentrations, while the toxic metals problem is usually at much lower concentrations, where flocculation/precipitation is generally less effective.

The presence of heavy metals in aqueous systems jeopardizes the health and well-being of the global community. For example, in Bangladesh most of the drinking water wells are naturally contaminated with small amounts of arsenic due to the native geochemistry of the area. Similar problems are faced in the United States with arsenic in the water supplies of many parts of the western US. With stringent new arsenic guidelines being enforced by the US-EPA, arsenic in drinking water is an issue that will command increasing attention.

Mercury emissions in many parts of the world are of significant environmental concern. Current estimates suggest that China is the world's largest producer of Hg emissions. A recent comprehensive study of Chinese mercury emissions revealed over 500 tons of total Hg were released into the environment in 1999 and almost 700 tons in 2003, with the vast majority coming from coal combustion and metal smelting. Because of the mobility of Hg in nature, these emissions are truly a global issue, and have an impact on the water quality of the entire planet.

Other metals are also of concern to water quality (like lead, cadmium, copper, etc.), as are various radionuclides (like cesium, uranium, etc.). The bottom line is that an efficient, chemically selective method of capturing these deleterious metal ions from natural waters is a priority goal.

In the course of the last decade, there has been an explosion in the amount of research performed in the area of nanostructured materials. Of central importance in this arena is the multitude of reports dealing with the surfactant templated synthesis of mesoporous ceramic materials. Porosity in the "meso-" range (i.e. between about 2 nm and 200 nm) provides a huge amount of surface

area in a very small volume. Surface area is a key consideration when designing and building a sorbent material since all sorption events take place at a surface. Another advantage provided by these mesoporous ceramics is the rigid nature of the ceramic backbone alleviates the problems associated with solvent swelling and particle attrition encountered with typical polymer-based ion exchange resins.

This presentation will discuss the functionalization of these mesoporous materials with functionalized organosilanes that are tailored to bind heavy metals to remove them from contaminated waters. For example, Hg is a “soft” Lewis acid, therefore we targeted the installation of “soft” Lewis bases, in this case alkyl thiols, to take advantage of sulfur’s legendary affinity for mercury. Preparation of thiol terminated self-assembled monolayers in mesoporous supports (SAMMS®) is readily accomplished in an environmentally friendly (“green”) fashion, and creates a powerful new class of mercury sorbent. These functional nanoporous materials are now commercially available from Steward Environmental Solutions (of Chattanooga, TN). Laboratory tests have shown that Hg is captured quickly and efficiently from a variety of media, including groundwater, contaminated oils, and even contaminated chemical warfare agents. Once bound, the Hg is held fast and does not leach off. Other classes of SAMMS have been tailored to bind other targets, like arsenate, chromate, uranium, and cesium.

Engineering considerations are a major concern when deploying any water purification technology in the field to treat process streams at industrially relevant scales. Examples will be discussed in which these nanomaterials have been engineered into process streams and have been successfully used to treat large quantities of water, achieving very low discharge limits (e.g. single digit parts per trillion Hg levels).

The synthetic tools used to make these functional nanomaterials can also be used to enhance the sensitivity and selectivity of analytical methodology. Since any environmental remediation effort depends heavily on fast, accurate analytical data, such performance enhancement is clearly beneficial. Recent results will be presented demonstrating how these functional nanomaterials can be used to enhance electrochemical and spectroscopic detection of heavy metal contamination.

Lastly, new classes of functional nanomaterials are on the horizon. Recent results obtained with sulfur-functionalized mesoporous carbon (S-FMC) will be presented, demonstrating that it is capable of efficiently capturing Hg from contaminated water. S-FMC has outstanding chemical and thermal stability and has been shown to be able to capture Hg at pH’s ranging from 1 to 13, as well as being able to capture Hg from the vapor phase at elevated temperatures.

Nanoparticle-based Gas Sensors for an Intelligent Air Quality Monitoring Network

Marie-Isabelle Baraton, CNRS & University of Limoges, Limoges, France

Concept

There is a growing concern worldwide about the consequences of urban air pollution on public health. In the European Union for example, every country has been instructed to establish a network of air quality monitoring (AQM) stations in its main cities and to inform citizens about the air quality. These accurate but bulky stations are based on complex equipment, mainly relying on electro-optical methods. However, their prohibitive cost prevents the development of dense networks in most cities. Moreover, the lengthy air sampling and data processing do not allow “real time” dissemination of the information to the public.

The final objective of our European projects (funded by the European Commission) was to propose alternative air quality monitoring microsystems based on cost-effective semiconductor chemical gas sensors. Due to the tiny size of semiconductor sensors, it can be envisioned to assemble the different sensors in small sensing units, thus transforming the bulky expensive AQM stations into cost-effective portable devices. In a second step, these portable gas sensing units associated with global positioning systems (GPS) will communicate with a central computer via a wireless network based on the GSM protocol. These microstations, installed on mobile carriers such as city buses, would constitute a dynamic network covering the city and complementing the existing AQM stations. It appears that this second step of the project designed by the Consortium as early as the beginning of 1999, has now come down to the modification of existing GSM/GPS systems for our specific application.

The case is totally different for gas sensors. Indeed, commercial semiconductor sensors still do not meet the detection threshold criteria set by the official organizations in charge of environment protection (1-3). As a consequence, our proposed dynamic network will be relevant only if semiconductor chemical sensors can be successfully and reliably improved. The performance of these sensors has to be enhanced especially in terms of higher sensitivity to gaseous pollutants and lower cross-sensitivity to humidity. Therefore, our fundamental objective in these European projects was the improvement of the semiconductor gas sensor characteristics by using nanosized semiconducting particles for CO, NO, NO₂ and ozone detection.

Approach to Sensor Improvement

The most popular semiconductor chemical gas sensors are solid-state devices composed of sintered metal oxides (mainly tin oxide, SnO₂) (4). All these resistive gas sensors detect gases through variations of the electrical conductivity when reducing or oxidizing gases are adsorbed on the semiconductor surface. Due to their low cost, the resistive sensors are very popular for in-

door air quality control. But, they are not suitable for outdoor air quality monitoring due to their cross-sensitivity to humidity and their high detection thresholds (5).

In resistive sensors, the grain or crystallite size is the predominant factor affecting the sensing properties. For most conventional materials, the particle size is much larger than the depth of the space-charge layer and the electrical conduction is controlled by the grain boundaries. But, in the case of nanoparticles, the particle size is comparable to the space-charge depth and the space-charge layer may occupy the whole particle, thus leading to drastic resistance increase (6). Indeed, in the first stages of our projects, our Consortium proved that the use of nanosized semiconductor particles in the fabrication of chemical gas sensors via thick film technology greatly enhances the sensor sensitivity (7, 8).

However, additional improvements of our prototypes were still needed. It became clear that the control of the surface chemistry of the nanosized particles plays a significant role in the reproducibility of the sensor characteristics. Besides, the optimization of the screen-printing process for the sensor fabrication appeared to be a necessary step to take full advantage of the nanometer size of the particles.

Results

The semiconducting nanoparticles were synthesized by laser evaporation of commercially available micron-sized particles (9). A major advantage of this synthesis method is the absence of contamination by non-dissociated precursors and of surface contaminant. In order to perfectly control the reproducibility of the crystalline phase, of the particle size, and of the degree of agglomeration, X-ray diffraction (XRD) and transmission electron microscopy (TEM) analyses were systematically performed on all produced batches.

The control of the chemical composition and of the surface chemistry of the nanoparticles was ensured by Fourier transform infrared (FTIR) spectroscopy. This characterization method was proved to be an extremely relevant technique to obtain a thorough understanding of the surface phenomena at the origin of the gas detection mechanism (10-12). It has been realized that this fundamental approach was a critical step to refine the sensor optimization by tailoring the surface chemical composition and reactivity of the nanoparticles during and eventually after their synthesis (13). In particular, the FTIR technique was used to monitor the functionalization the tin oxide nanoparticles surface by grafting hexamethyldisilazane (HMDS). The surface modification was intended to reduce the cross-sensitivity to humidity which is an important drawback of the semiconductor sensors. The results of the HMDS grafting on both the surface reactivity and the electronic properties of tin oxide nanoparticles have been described elsewhere (14).

After the fabrication of the first prototypes, it rapidly appeared that the standard screen-printing method to fabricate thick-film gas sensors had to be modified for accommodating nanoparticles. Indeed, when using nanoparticles, cracks and grain growth were observed in the sensitive layer. At first, a homogeneous dispersion of the nanoparticles in the solvent was achieved by determining the appropriate concentration and by applying ultrasonication before printing. Then, the sintering temperature which had a strong influence on the grain growth and therefore on the sensor sensitivity, was set below a critical value depending on the metal oxide (e.g. 450°C for tin oxide). At that point, our sensor prototypes were tested and evaluated against commercially available

sensors. Although the performance of our sensors was comparable to commercial semiconductor and electrochemical sensors, the detection thresholds were still too high to meet the criteria for outdoor air quality monitoring defined by official organizations.

The suppression of agglomerates remained the major issue to overcome in order to take full advantage of the nanometer size of the semiconducting particles. To this end, we developed a low-cost layer-by-layer deposition method via a wet route because industrial considerations preclude the manipulation of nanoparticles one by one. The major advantage of this deposition method is that the nanoparticles preferably pile up in a regular 3D network because they have essentially the same size.

Table 1 summarizes our achievements in terms of sensor sensitivity. For comparison, the typical performance of commercial electrochemical and semiconductor sensors are given along with the detection thresholds we targeted to meet the EU directives for outdoor air quality monitor-

Table 1

Polluting gases	CO	NO ₂	NO	O ₃
Ambient Air Quality Standards (EU / EEA)	9 ppm (10 mg/m ³) 8 hour average	105 ppb (200 µg/m ³) 1 hour average 22 ppb (40 µg/m ³) Annual	800 ppb ½ hour average	60 ppb (120 µg/m ³) 8 hour average
Ambient Air Quality Standards (USA / EPA)	9 ppm (10 mg/m ³) 8 hour average	53 ppb (100 µg/m ³) Annual		75 ppb (150 µg/m ³) 8 hour average
Target for the detection threshold	3 ppm	50 ppb	100 ppb	20 ppb
Commercial sensors: Electrochemical Semiconductor (typical data)	1 ppm 5 ppm	100 ppb	500 ppb	50 ppb
Our sensors	3 ppm	15 ppb	100 ppb	15 ppb

ing. The obvious conclusion is that our sensors can compete with commercial devices. But more important, our sensors can fully meet the required targets for outdoor air quality monitoring whereas commercial electrochemical and semiconductor sensors cannot.

Outlook

Our Consortium showed that nanoparticles-based semiconductor sensors exhibit higher sensitivities to air pollutants, lower detection thresholds, lower operating temperatures. The device optimization is not a straightforward procedure and requires controlled surface chemistry of nanoparticles, homogeneous dispersion of nanoparticles, deposition of homogeneous layers, a low level

of dopant if any and mild firing conditions. Although our sensors are chemically and electrically stable, the long-term stability over extended periods of time (several months) has still to be checked. Cross-sensitivity to humidity and response time have been addressed independently of the sensing layer optimization.

The sensing element represents the most challenging component in our concept of mobile communicating AQM microstations. Indeed, even though the booming development of telecommunication networks and the integration of GSM and GPS technologies in commercially available devices have allowed researchers and engineers in the field of wireless communications to extend these communication technologies to sensor networks, no such mobile sensor network has yet been commercially implemented in any city. Only network prototypes have been tested or are being tested in some limited places. Yet these network prototypes are based on commercially available gas sensors whose either performance are far below the requirements for outdoor air quality monitoring or costs are well above market acceptance.

We have now proved that our low-cost semiconductor chemical gas sensors can meet the requirements in terms of detection thresholds for polluting gases in air. Our concept can now proceed further with the continuous improvement of the sensors and with the complete development of the AQM microstations which could be implemented easily, rapidly and in a sufficient number in any city of any country at low cost.

References

1. European Environment Agency, <http://www.eea.europa.eu/>
2. European Commission's Environment Directorate-General, <http://ec.europa.eu/environment/>, <http://ec.europa.eu/environment/air/quality/standards.htm>
3. Environment Protection Agency, <http://www.epa.gov/air/criteria.html>
4. Figaro Engineering Inc., <http://www.figarosensor.com/>
5. R.S. Morrison (1994). "Chemical Sensors." in Semiconductor Sensors, S.M. Sze, New York (USA): John Wiley & Sons, 383-413.
6. Y. Shimizu and M. Egashira (1999). "Basic Aspects and Challenges of Semiconductor Gas Sensors." MRS Bulletin 24 (6), 18-24.
7. G. Williams and G.S.V. Coles (1998). "Gas Sensing Properties of Nanocrystalline Metal Oxide Powders Produced by a Laser Evaporation Technique." Journal of Materials Chemistry 8 (7), 1657-1664.
8. M.-I. Baraton and L. Merhari (2001). "Influence of the Particle Size on the Surface Reactivity and Gas Sensing Properties of SnO₂ Nanopowders." Materials Transactions 42 (8), 1616-1622.
9. W. Riehemann (1998). "Synthesis of Nanoscaled Powders by Laser-Evaporation of Materials." in MRS Symposium Proceedings Vol. 501 "Surface-Controlled Nanoscale Materials for High-Added-Value Applications.", K. E. Gonsalves, M.-I. Baraton, R. Singh, H. Hofmann, J. X. Chen, and J. A. Akkara, Warrendale, PA (USA): MRS Publisher, 3-13.

10. M.-I. Baraton (1999). "FT-IR Surface Spectrometries of Nanosized Particles." in Handbook of Nanostructured Materials and Nanotechnology, H.S. Nalwa, San Diego, CA (USA): Academic Press, 89-153.
11. M.-I. Baraton and L. Merhari (2001). "Determination of the Gas Sensing Potentiality of Nanosized Powders by FTIR Spectrometry." Scripta Materialia, 44, 1643-1648.
12. M.-I. Baraton and L. Merhari (2005). "Investigation of the Gas Detection Mechanism in Semiconductor Chemical Sensors by FTIR Spectroscopy." Synthesis and Reactivity in Inorganic, Metal-Organic and Nano-Metal Chemistry, 3, 733-742.
13. M.-I. Baraton and L. Merhari (1998). "Surface Properties Control of Semiconducting Metal Oxides Nanoparticles." NanoStructured Materials, 10 (5), 699-713.
14. M.-I. Baraton (2003). "Surface Chemistry and Functionalization of Semiconducting Nanosized Particles." in NATO Science Series "Synthesis, Functional Properties and Applications of Nanostructures.", T. Tsakalagos, I.A. Ovid'ko, Dordrecht (The Netherlands): Kluwer Academic Publishers, 427-440.

Nanotechnology for Suppressing Mercury Release from Fluorescent Lamps

*Love Sarin, Natalie Johnson, Indrek Kulaots, Brian Lee, Steven Hamburg, Robert Hurt
Division of Engineering and Institute for Molecular and Nanoscale Innovation,
Brown University, Providence, Rhode Island, U.S.A.*

Abstract

This paper describes ongoing work at Brown University to characterize the release of mercury vapor from compact fluorescent lamps that break during shipping, handling, recycling, and disposal. Also described is the development of new, high-activity nanosorbents capable of capturing mercury vapor at room temperature, and their application for break site remediation, in disposal/recycle bags, and in multi-lamp shipping and collection boxes.

Introduction

Fluorescent lighting technologies are undergoing rapid market growth as part of a resurgent societal interest in energy efficiency. Much of the current and projected growth is in the domestic use of compact fluorescent lamps (CFLs), which offer consumers approximately 75% reduction in energy usage and ten-fold increase in lifetime relative to incandescent bulbs. CFLs, however, contain 3-5 mg of mercury, which is a well-known human toxicant that is of special concern for neural development in the fetus and in young children [Baughman, 2006]. The OSHA occupational exposure limit is 100 $\mu\text{g}/\text{m}^3$, while the Agency for Toxic Substances and Disease Registry recommends 0.2 $\mu\text{g}/\text{m}^3$ level for continual habitation by children, [Baughman, 2006] a level that can easily be exceeded by a single CFL break. The present work is motivated by two specific issues in the management of Hg from CFLs: (i) direct exposure of consumers or workers to Hg vapor from fractured lamps, and (ii) release of Hg to the environment at end of lamp life.

This paper describes the development of a nanomaterial-based technology for suppressing the release of mercury from broken CFLs. Experiments were first conducted to characterize the dynamic release of mercury vapor as a function of bulb type, age, substrate (carpet and hard surface) and flow environment. A wide range of nanomaterials and reference materials were then evaluated for mercury vapor capture under conditions relevant to these release profiles (time, temperature, mercury vapor concentration, and gas environment). Several nanomaterials were found to offer higher capacity than conventional sorbents and one nanomaterial (a particular formulation of nano-selenium) was found to have a 50-fold higher activity than any sorbent commercially available today.

Finally, the most promising sorbent materials were used to fabricate prototypes of a CFL spill kit, a new retail packaging concept, and a new disposal concept that avoid the release of mercury vapor at various stages of the lamp lifecycle. The prototypes were tested for in situ capture under scenarios relevant to domestic breakage and disposal. The outlook for widespread implementation of this new nanotechnology will be discussed.

Methods

To characterize the release of Hg vapor under ambient conditions, bulbs were catastrophically fractured (either within a flexible Teflon enclosure of 2 L volume, on a carpet, or in a prototype recycle bag or box) and the Hg vapor transported away by a metered flow of nitrogen (1 LPM). A portion of the Hg-contaminated flow was passed to a gold amalgamation atomic fluorescent vapor-phase mercury analyzer (PSA model 10.525), and the concentration-time profiles were measured and integrated to obtain total mercury release [Manchester et al., 2008].

A variety of nanosorbents and reference materials were synthesized or acquired. Details of the synthesis and characterization can be found in Johnson et al (2008).

Results and Discussion

Figure 1 shows time-resolved mercury release data from two CFL models. The release is initially rapid producing vapor concentrations in the effluent from 200-800 $\mu\text{g}/\text{m}^3$ during the first hour, which decay on a time scale of hours but continues at significant rate for at least four days. Over 4 days (extended data not shown), the 13 W bulb released 1.34 mg or 30% of the total Hg. In general, Hg^0 evaporation is known to be slow under ambient conditions, and our data suggest that much of the original mercury remains in the bulb debris after 96 h and will continue to evaporate slowly.

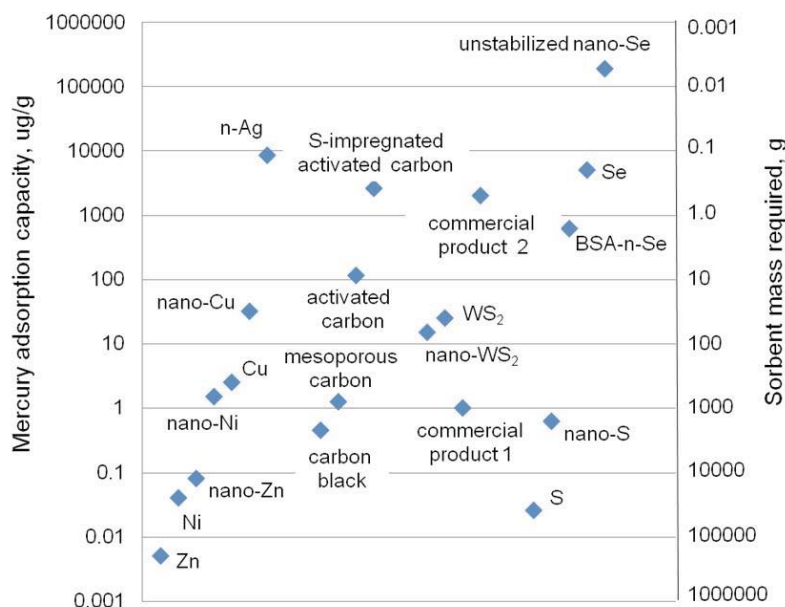


Figure 1.

Figure 2 shows all of the sorbents tested and their Hg capacities under our standard conditions (60 $\mu\text{g}/\text{m}^3$ inlet stream). The capacity of the sorbents varies widely depending on particle size and chemistry. Nanosynthesis offers capacity increases in most cases relative to the conventional micro-scale powder formulation of the same materials. For application to CLFs, the right-hand axis gives the amount of sorbent required to capture 1 mg of Hg vapor, typical of CFL release. Surprisingly, some common sorbents such as powdered S or Zn require enormous amounts of

material (>10 kg) to treat the vapor released from a single CFL and most of the sorbents require amounts that are not attractive for incorporation into consumer packaging (>10 g). A small number of sorbents (nano-Ag, S-impregnated activated carbon, and two selenium forms) have capacities that should allow <1 g of sorbent to be used. The most effective sorbent is uncoated nano-Se, which can capture the contents of a CFL with amounts less than 10 mg.

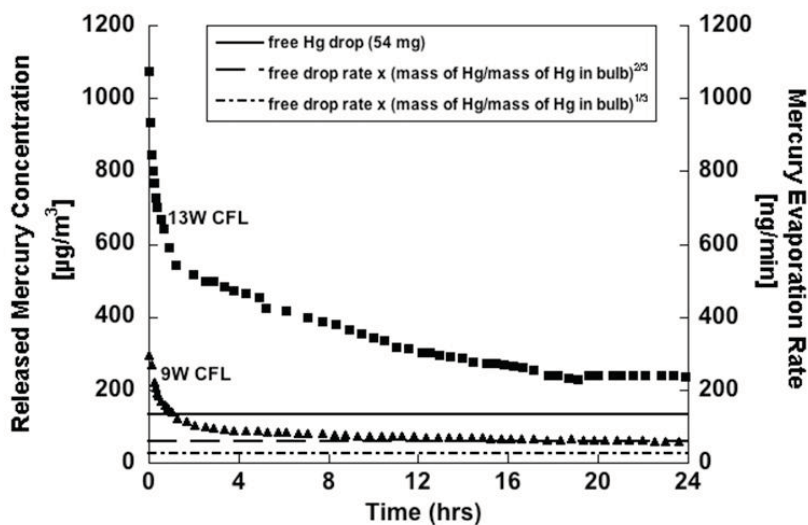


Figure 2.

Ongoing work has concentrated on the use of the most promising sorbents in the development of engineering solutions for break sites, and containers for shipping, recycling, and disposal. Figure 3 shows the preferred formulation for nano-selenium, which is a porous cloth loaded with nSe by capillary infiltration and drying. This form distributes the nanoparticles evenly, imbeds them within the cloth fiber network, and allows incorporation of the nSe into reactive barriers that hinder mercury escape during the process of reactive stabilization.

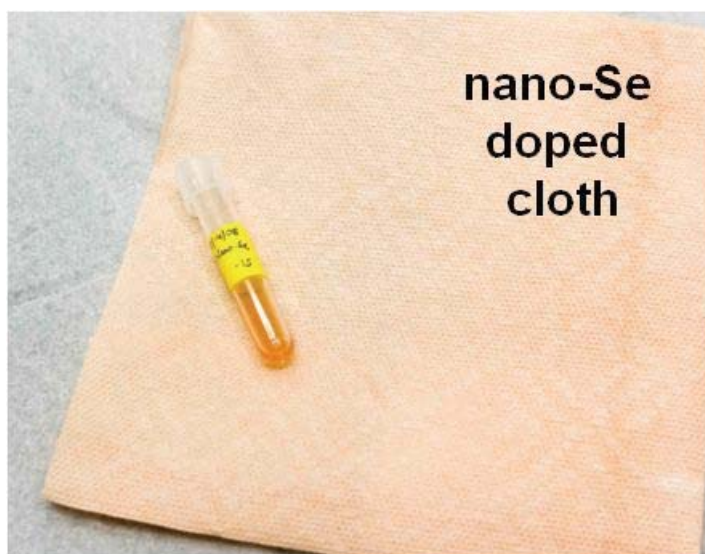


Figure 3.

Figure 4 shows the reactive barrier concept and its application for break site remediation on carpets. The concept of the 3 ply system is to have a barrier layer that slows the escape of Hg vapor allowing time for the active (sorbent-doped) middle layer to stabilize the Hg through formation of a non-volatile product. The protective layer exists to prevent direct contact or damage to the active layer.

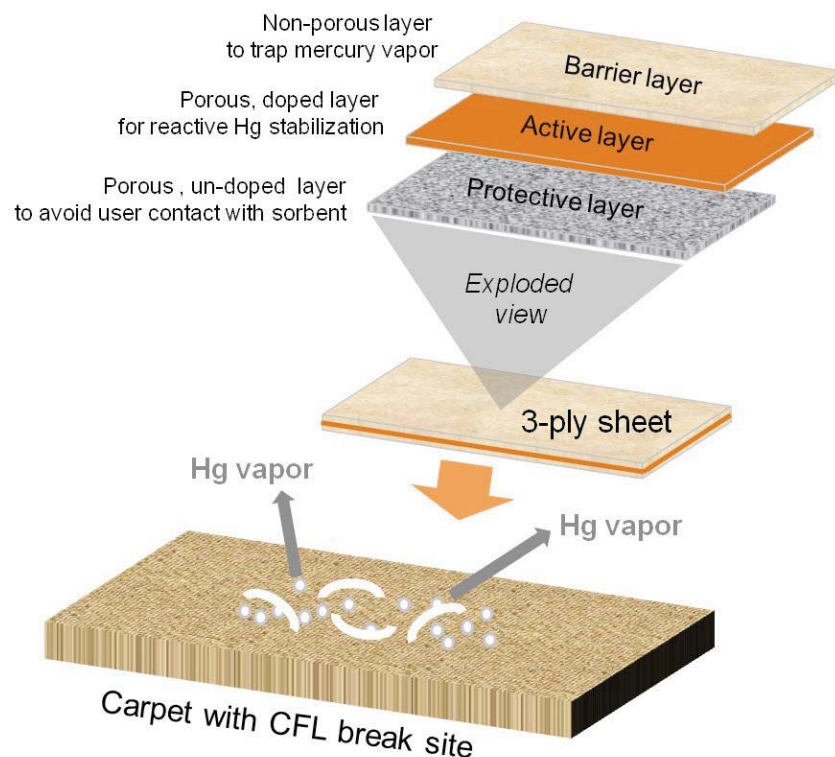


Figure 4.

To test the nano-selenium reactive barrier, commercial bulbs were broken on carpets and the bulb base and larger fragments were removed by hand. The smaller shards and any spilled powder were left, and a sampling probe was placed 1 inch above the break epicenter and the Hg vapor concentration measured using a 0.2 l/min air flow and analysis by the atomic fluorescence technique described earlier. Measurements were taken with and without the reactive barrier present.

Figure 5 shows some example test data, in which bulbs were broken and the sites covered with a 3-ply barrier in which the active layer was a paper towel doped with 10 mg of uncoated (protein-free) nano-selenium. The barrier essentially eliminates the Hg release as measured 1-inch above the break epicenter. If the barrier is removed after 5 hours, a small but measurable release of mercury occurs, presumably due to trapped and adsorbed mercury vapor in the gas between the barrier and the carpet as well as mercury left in the bulb shards or phosphor. Maintaining the barrier in place for 24 or 48 hrs reduces this residual release to even lower values. We recommend that the reactive barrier be held in place as long as possible, but at least 48 hrs to prevent significant further release upon final cleanup.

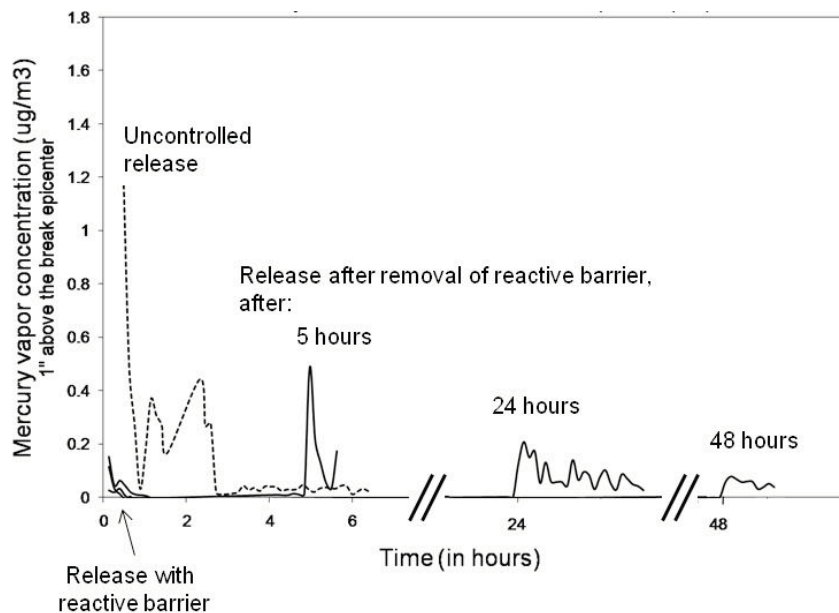


Figure 5.

Conclusions

Compact fluorescent lamps release easily measurable amounts of mercury vapor upon breakage in a dynamic process that takes place over hours and days. In many exposure scenarios the amounts of released mercury will be too small to constitute a significant health risks, but cases involving multiple bulb breaks and/or continued habitation by small children or pregnant women could benefit from a cost-effective technology for clean up or active suppression through adsorption. Chemical adsorption is a promising route, and one particular formulation of nano-selenium is extremely active for Hg vapor capture, thus allowing the use of very small amounts of sorbent incorporated into packaging or remediation products. A prototype of a reactive barrier for remediating CFL break sites has been developed and tested.

Work is underway at Brown to examine the landfill stability of new and spent sorbents, to develop and optimize bags and boxes for shipping and collection applications, material safety issues, the fundamental permeability of mercury through barrier materials, and the optimization and scale-up of several promising sorbents.

References

- Baughman, T. A. Elemental mercury spills. *Environ. Health Perspect.* 2006, 114 (2), 147–152.
- Johnson NC, Manchester S, Sarin L, Gao Y, Kulaots I, Hurt RH, “Release of Mercury vapor from Broken Compact Fluorescent Lamps and In Situ Capture by New Nanomaterial Sorbents,” submitted to *Environmental Science and Technology*, in press (2008).
- Manchester, S.; Wang, X.; Kulaots, I.; Gao, Y.; Hurt, R. High capacity mercury adsorption on freshly ozone-treated carbon surfaces. *Carbon* 2008, 4 (3), 518–524.

Conference Questions and Answers

Question:

Sulfur-impregnated activated carbon is readily available and cheap. Will nano-selenium be as inexpensive?

Answer:

The best commercially available sorbent we know of is sulfur-impregnated activated carbon, but it takes 70-100 times more of it to achieve the same effect as nano-selenium. Based on our cost estimates, we think the costs will be equivalent or cheaper, because the nano-selenium will be used in such small amounts. By the pound it might be expensive, but we will be using it in milligram amounts.

Question:

Is there not a maximum contaminant level (MCL) for selenium?

Answer:

Yes. Selenium is a very complex element; it is chemopreventive and essential to human health, but it can be toxic at higher concentrations. In this case, there are no free nanoparticles, because the selenium is bound up in the support. The selenides and selenous acid are toxic, but this application involves elemental selenium, which is not a toxic form. Plus, the amounts used are so small that they are close to the dietary supplement levels. We think the reactive cloth can be engineered to be a very safe product.

Question:

How do you recommend we remove broken compact fluorescent lamp (CFL) bulbs? You advised against the use of plastic bags. What kind of container is appropriate?

Answer:

Use a glass jar or a metal-lined bag, the kind used by waste recyclers. The most practical approach is just to place the bulb in the most readily available container to limit exposure to mercury vapor and take it outdoors as soon as possible, without opening the container again. Metal and glass will contain the mercury, but they do not stabilize it.

Question:

Can you comment on the nano-selenium particle size and surface area?

Answer:

It is made colloiddally and is 10-20 nm in size when first made. It will start to ripen, and the particles will grow and aggregate, especially the uncoated ones. Dynamic light scattering is used to characterize it. We make it fresh, capillary infiltrate it, and dry it. For an estimate of the surface area, we can provide only a nominal one from the density in that size. When we make enough of it, we can freeze-dry it and do a conventional surface area characterization.

Question:

What is the preferred disposal method for the reactive cloth?

Answer:

The reactive elements in the cloth stabilize the mercury as mercury selenide, so the cloth can be tossed in a garbage can.

Question:

Have you considered testing this technology in a high-pressure, high-temperature environment, such as a flue gas stream or a power plant stack?

Answer:

We began this project looking at mercury capture from coal combustion, but that was complicated by the presence of sulfur oxides, nitrous oxides, and chlorine in the gas stream, so we migrated to the chemistry of mercury in air at room temperature. It might be possible to use nano-selenium for flue gases, but we have not examined it closely. Selenium does have a vapor pressure, so at flue-gas temperatures, the selenium might become its own pollutant.

One Step Flame Synthesis of TiO₂/CeO₂ Nanocomposite with Controlled Properties for VOC Photooxidation

V. Tiwari, and V. Sethi, Centre for Environmental Science and Engineering,
Indian Institute of Technology Bombay, Mumbai, India

P. Biswas, Department of Energy, Environmental and Chemical Engineering
Washington University, St. Louis, Missouri, U.S.A.

Cerium oxide is being used in several industrial catalytic processes, as a key component in the formulation of catalysts for the control of some emissions from mobile sources (Boaro *et al.*, 2003; Kasper and Fornasiero, 2003) and also in fuel cells (Park *et al.*, 2000). Under alternating lean and rich fuel conditions, ceria stores and releases oxygen thereby enabling the oxidation of CO and volatile organics, and the reduction of NO_x (Kasper and Fornasiero, 2003; Bunleusin *et al.*, 1997). Mixed oxide catalyst has been found to be helpful in overcoming the poor thermal stability of CeO₂ by substitution of another metal or metal oxide into the ceria lattice (Reddy *et al.*, 2003). TiO₂ is well known for its photocatalytic activity because of its special properties, such as high dielectric constant, excellent optical transmittance, high refractive index, high chemical stability and suitable band gap.

There are several studies on the wet chemical synthesis of CeO₂-TiO₂ nanocomposite reported in the literature. Rynkowski *et al.* (2000) studied the redox properties of CeO₂-TiO₂ composites. Nakagawa *et al.* (2007) synthesized cubic-shaped CeO₂ nanoparticles with a length of 2.7–3.8 nm and also showed that catalyst activity enhances when the sample is calcinated at higher temperature. Periyat *et al.* (2007) synthesized CeO₂ doped TiO₂ powder via sol-gel route to enhance the high temperature stability of the anatase phase TiO₂. Compared to conventional wet chemical method flame synthesis offers good control on catalyst properties, less post-processing steps (*viz.*, filtration, drying or calcination) and produces less waste material. In the present study TiO₂/CeO₂ mixed oxide was synthesized using a flame reactor with controlled Ti/Ce ratio and quenching system (Jiang *et al.*, 2007). Surface area can be controlled by quenching the flame at various heights. Ti/Ce ratio is controlled by varying the ratio of precursor feed rates (TTIP: Cerium Nitrate).

Methodology

Pristine TiO₂, pristine CeO₂ and TiO₂/CeO₂ mixed nanocomposite were synthesized using Flame Aerosol Reactor (FLAR). The experimental setup consists of precursor feed systems, three port co-flow diffusion burner, quench/dilution system and particle collection system (Tiwari *et al.*, 2008). A bubbler has been used as feeding system to introduce titanium tetra-isopropoxide (TTIP, 97%, Aldrich) precursor in vapor form. The temperature of bubbler was kept constant at 90 °C. The cerium (III) acetate (99 %, Aldrich) dissolved in water was atomized using atomizer with nitrogen carrier gas at 35 psig. Precursor feed rate was controlled by controlling the carrier gas flow rate. Both the precursor was fed in the inner most port of the burner. Fuel methane

(CH₄) at 1~1.5 lpm flow rate and oxidant oxygen (O₂) at 5 lpm flow rate, were fed in the middle port and outer port of the burner respectively. All the flow rates were controlled by mass flow controllers (MKS Instruments). Nanoparticles were collected downstream by a glass fiber filter assisted by a vacuum pump. A quench ring has been fabricated and used around the flame at different height from the burner outlet by moving the quench ring up and down to control flame temperature and the size of TiO₂ particles. In flame synthesis of metal oxide particles, the residence time and temperature of the flame zone must be sufficient to transform the volatile precursors into oxide molecules and to reach the desired crystalline structure of particles formed by the collision/coalescence process. Further exposure to high temperature results in loss of valuable surface area by sintering, but this can be avoided using quench-cooling.

Results and Discussion

Particle size and crystallinity of pristine CeO₂, pristine TiO₂ and TiO₂/CeO₂ catalyst

Experimental conditions and key results of synthesis are shown in Table 1. Particle size of the synthesized catalysts was measured real time using SMPS. Geometric mean diameter of pristine TiO₂ and pristine CeO₂ was in range of 45~60 nm. For higher methane flow rate (1.5 lpm), TiO₂ particle size was 52.6 nm compared to 61.5 nm TiO₂ particle that synthesized at 1.0 lpm methane flow rate. At lower methane flow rate, sintering of particle occurs because of higher flame temperature, results in smaller particle size. Figure 1 shows the TEM micrographs, electron diffraction pattern and PSD of the synthesized TiO₂ and CeO₂ nanoparticles.

Table 1. Experimental conditions for synthesis of TiO₂/CeO₂ nanocomposite using Flame Aerosol Reactor (FLAR).

Sample No.	Powder	CH ₄ (lpm)	O ₂ (lpm)	CeO ₂ content	SMPS Diameter (nm)	Crystallinity
1	TiO ₂	1.5	5	0	52.6	Anatase
2	TiO ₂	1.0	5	0	61.5	Anatase+Rutile
3	TiO ₂ /CeO ₂	1.0	5	10%	-	Anatase+Rutile
4	TiO ₂ /CeO ₂	1.0	5	15%	-	Anatase+Rutile
5	CeO ₂	1.0	5	100%	46.5	Cubic fluorite

Figure 2 shows the XRD patterns of the catalysts synthesized (Table 4.2). Pristine CeO₂ sample showing diffraction prominent peaks at $2\theta = 28.5, 33.1, 47.5, 56.3$, which are characteristic of the cubic fluorite structured CeO₂. XRD pattern of pristine TiO₂ synthesized at different methane flow rate in burner, 1.5 lpm and 1.0 lpm shows that at higher methane flow rate pure anatase was obtained whereas at 1.0 lpm methane flow rate mixture of anatase and rutile was obtained. Anatase phase of TiO₂ is a metastable state which transforms to rutile phase at higher temperature. At higher methane flow rate the flame temperature drops because of lower oxygen to fuel ratio, and results in pure anatase phase TiO₂. In mixed oxide (TiO₂/CeO₂) nanocomposite both

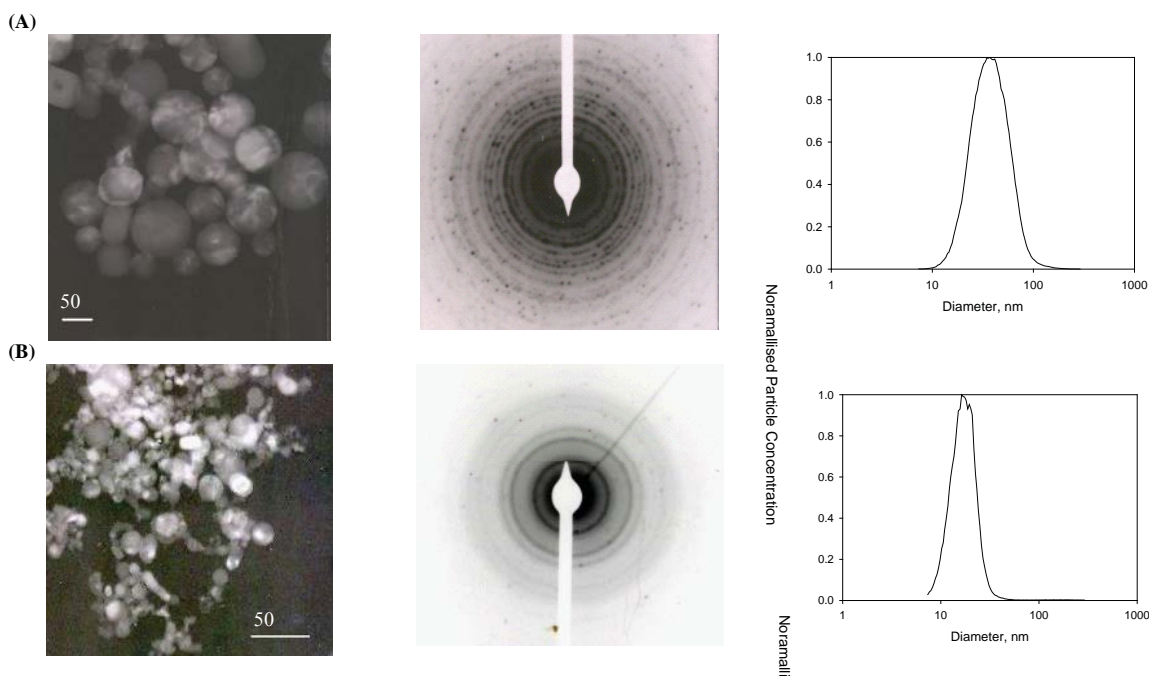


Figure 1. TEM micrographs, diffraction patterns and PSD of synthesized nanoparticles. (A) $\text{TiO}_2/\text{CeO}_2$, (B) Pristine CeO_2

mixture of anatase and rutile TiO_2 were present. The rutile content of the $\text{TiO}_2/\text{CeO}_2$ was less than pristine TiO_2 due to surface modification of the TiO_2 particles with CeO_2 nanoparticles which changes the temperature of transformation from anatase to rutile phase. In mixed $\text{TiO}_2/\text{CeO}_2$ nanocomposites characteristic peaks of Ceria (111, 200) were observed.

FTIR spectra of synthesized catalysts

Figure 3 shows the FTIR spectra of flame synthesized CeO_2 , TiO_2 and $\text{TiO}_2/\text{CeO}_2$ composite in the range of $400\text{-}4000\text{ cm}^{-1}$. IR spectrum of the pristine CeO_2 agrees with the reported data (Periyat et al., 2007). For $\text{TiO}_2/\text{CeO}_2$ nanocomposite two small vibrations at 3200 cm^{-1} can be observed which are missing in pristine TiO_2 but present in pristine TiO_2 spectra. These vibrations may be due to Ce-O bond stretching. The FTIR results needs to be further analyzed.

UV-vis Spectrum of pristine TiO_2 and $\text{TiO}_2/\text{CeO}_2$ nanocomposite

The UV Visible spectrum shown in Figure 4 was used to obtain the optical absorption properties of the pristine TiO_2 and $\text{TiO}_2/\text{CeO}_2$ nanocomposite. Periyat *et al.*, (2007) reported that with increase in cerium content, the absorption shifted to the longer wavelength side (red shift). Similar results were obtained for our samples. Absorption clearly increases from pristine titania to 10% $\text{CeO}_2/\text{TiO}_2$ and 15% $\text{CeO}_2/\text{TiO}_2$.

Future Work Plan

Further work includes synthesis of catalysts with different sizes and surface properties by quenching the reactions in the flame at different heights. Catalyst activity will be tested using a

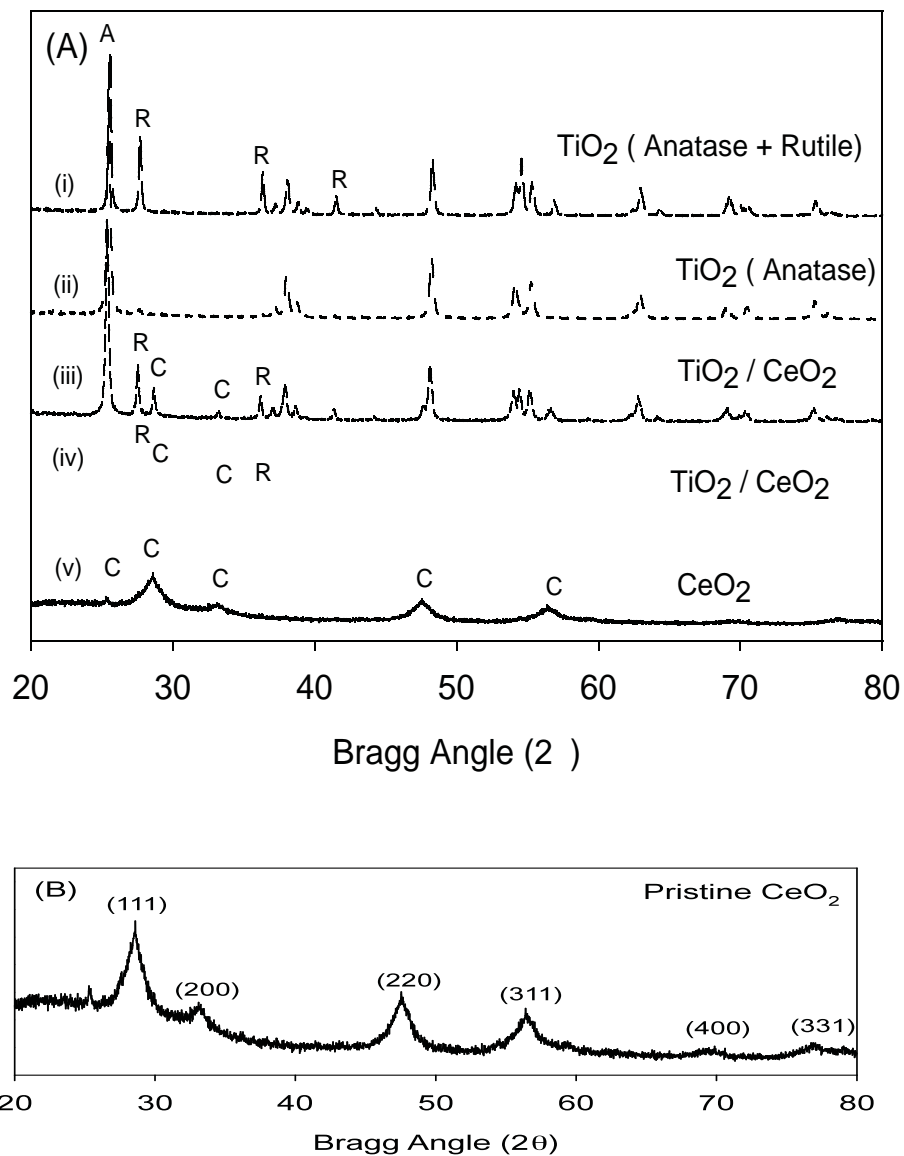


Figure 2. (A) XRD patterns of pristine TiO_2 , pristine CeO_2 and $\text{TiO}_2/\text{CeO}_2$ powder. Pristine TiO_2 synthesized at higher methane flow rate (i) pure anatase phase was obtained whereas at 1.0 lpm methane flow rate (ii) mixture of anatase and rutile was obtained. Crystal phase of CeO_2 (v) was cubic fluorite. In mixed oxide ($\text{TiO}_2/\text{CeO}_2$) (iii, iv) nanocomposite both mixture of anatase and rutile TiO_2 were present and characteristic peaks of Ceria (111, 200) were also observed. (B) Enlarged CeO_2 (v) XRD pattern with characteristic peak. A = Anatase, R = Rutile, C = Ceria (Cubic) and $\text{TiO}_2/\text{CeO}_2$ nanocomposite spectra which are missing in pristine TiO_2 but present in pristine TiO_2 spectra which may be due to Ce-O bond stretching.

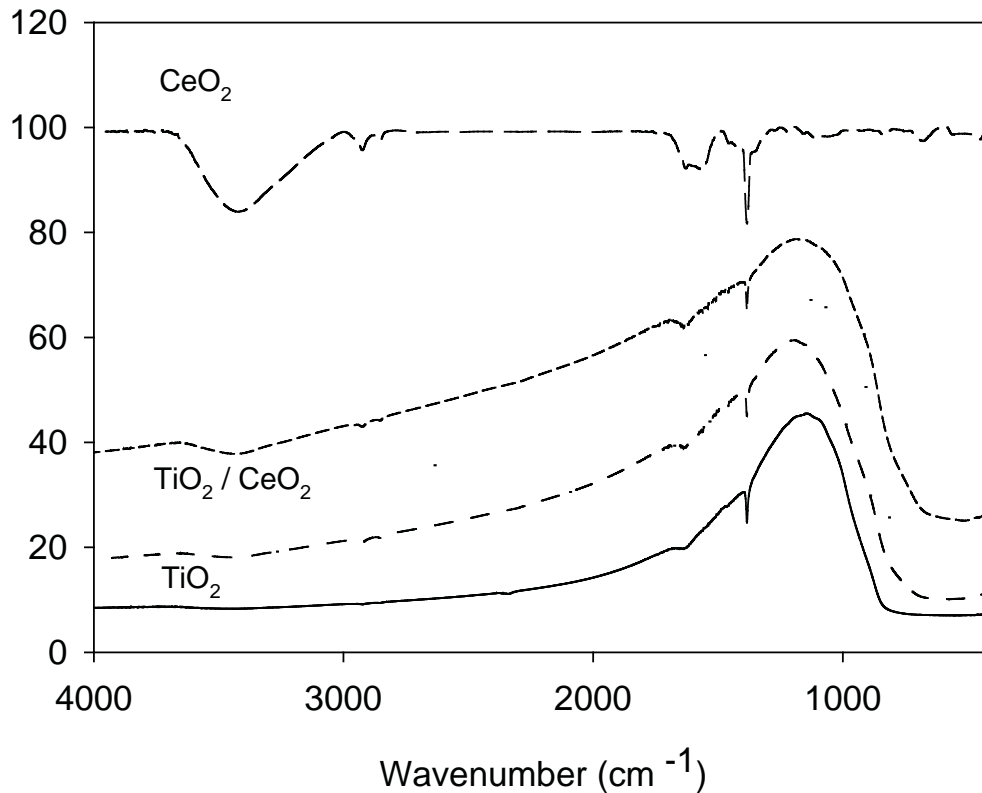


Figure 3. TIR spectra of pristine TiO_2 , pristine CeO_2 and $\text{TiO}_2/\text{CeO}_2$ powder in the range of 400-4000 cm^{-1} . Two small vibrations at 3200 cm^{-1} can be observed in pristine CeO_2 .

photocatalytic reactor for the gas phase photo-oxidation of a volatile organic compound (VOC). The influence of Ti:Ce ratio, temperature and surface area on the catalytic activity will be studied.

Acknowledgements

Financial support from Department of Science and Technology (DST), India, for the study is gratefully acknowledged.

References

- Boaro, M., Vicario, M., Leitenburg, C., Dolcetti, G., and Trovarelli, A., (2003), "The use of temperature-programmed and dynamic/transient methods in catalysis: characterization of ceria-based, model three-way catalysts", *Catalysis Today*, 77, 407–417
- Bunluesin, T., Gottea, R. J., and Grahamb, G.W., (1997), "CO oxidation for the characterization of reducibility in oxygen storage components of three-way automotive catalysts", *Applied Catalysis B: Environmental*, 14, 105-115
- Jiang, J., Chen, D.R., Biswas, P., (2007), "Synthesis of Nanoparticles in a Flame Aerosol Reac-

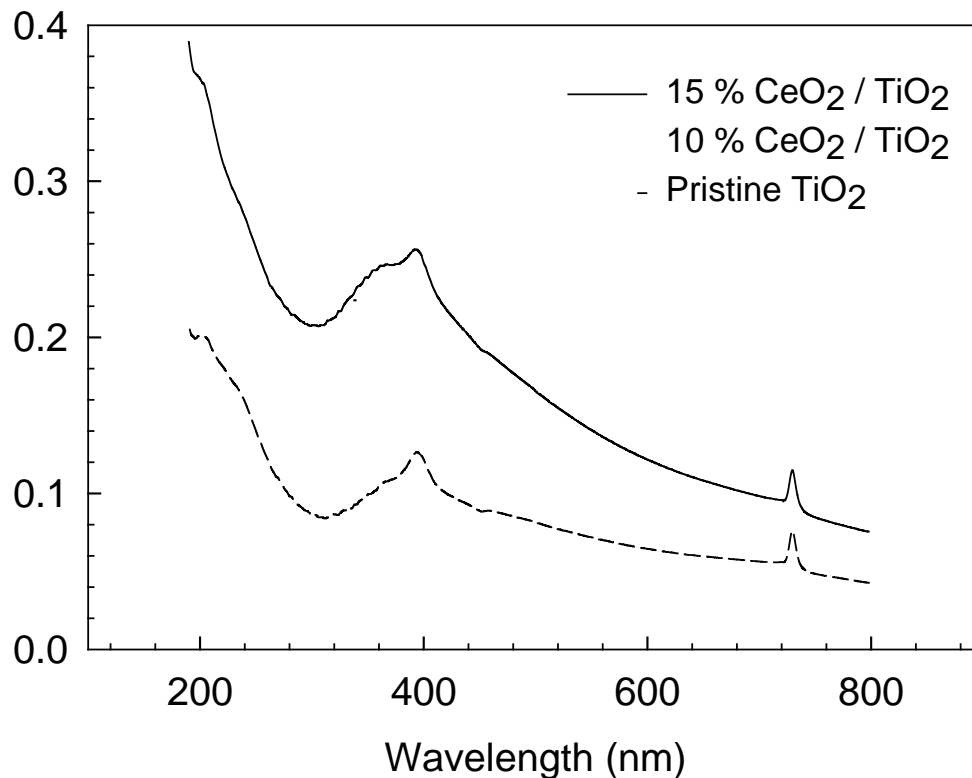


Figure 4. UV-vis spectrum of pristine TiO₂ and CeO₂/TiO₂ mixed oxide nanocomposite. The absorption of CeO₂ / TiO₂ nanocomposite is more compared to pristine TiO₂. When CeO₂ content increase from 10% to 15%, the absorption does not change much in UV range.

tor (FLAR) with Independent and Strict Control of Their Size, Crystal Phase and Morphology”, *Nanotechnology*, 18, 285-303

Kaspar, J., and Fornasiero, P., (2003), “Nanostructured materials for advanced automotive depollution catalysts”, *Journal of Solid State Chemistry*, 171, 19–29

Nakagawa, K., Murata, Y., Kishida, M., Adachi, M., Hiro, M. and Susa, K., (2007), “Formation and reaction activity of CeO₂ nanoparticles of cubic structure and various shaped CeO₂-TiO₂ composite nanostructures”, *Materials Chemistry and Physics*, 104, 30-39.

Park, S., Gorte, R. J. and Vohs, J. M., (2000), “Applications of heterogeneous catalysis in the direct oxidation of hydrocarbons in a solid-oxide fuel cell”, *Applied Catalysis a-General*, 200, 55-61.

Periyat, P., Baiju, K. V., Mukundan, P., Pillai, P. K. and Warriar, K. G. K., (2007), “Aqueous colloidal sol-gel route to synthesize nanosized ceria-doped titania having high surface area and increased anatase phase stability”, *Journal of Sol-Gel Science and Technology*, 43, 299-304.

Reddy, B. M., Khan, A., Yamada, Y., Kobayashi, T., Loridant, S. and Volta, J. C., (2003), “Struc-

tural characterization of CeO₂-TiO₂ and V₂O₅/CeO₂-TiO₂ catalysts by Raman and XPS techniques”, *Journal of Physical Chemistry B*, 107, 5162-5167.

Rynkowski J., Farbotko J., Touroude, R., and Hilaire, L., (2000), “Characterization of Ru/CeO₂-Al₂O₃ catalysts and their performance in CO₂ methanation”, *Applied Catalysis A: General*, 203, 335–348.

Tiwari V., Jiang J., Sethi V., and Biswas P., (2008), “One-step synthesis of noble metal titanium dioxide nanocomposites in a flame aerosol reactor”, *Applied Catalysis A: General*, 345(2), 241-246.

Environmental Applications of Nanocrystalline Zeolites

*Shebere Adam, Melissa Torres, Karna Barquist, and Sarah C. Larsen,
Department of Chemistry, University of Iowa, Iowa City, Iowa, U.S.A.*

Abstract

Nanocrystalline zeolites (with crystal sizes of less than 50 nm) are versatile, porous nanomaterials with potential applications as adsorbents for polluted water or as environmental catalysts.

(1) We have developed efficient, synthetic methods for the preparation of high quality, monodisperse, nanocrystalline (<50 nm) zeolites such as silicalite, ZSM-5, or faujasite.(2,3,4,5) The advantages of nanocrystalline zeolites include increased surface area, improved optical properties (transparency), improved diffusion/mass transfer properties and the ability to form hierarchical zeolite structures. The large external and internal surface areas lead to unique surface chemistry relative to more conventional microcrystalline zeolite materials.

In this study, the external surface of the zeolite, silicalite, was functionalized with organosilanes resulting in zeolite materials tailored for adsorption applications. The nanocrystalline zeolite external surface was functionalized with an organosilane, such as aminopropyltriethoxysilane (APTES) or aminopropyltrimethoxysilane (APDMMMS) forming an aminopropyl functionalized zeolite surface. Under acidic conditions, aqueous metals, such as chromium and copper, were effectively adsorbed onto the surface of the aminopropyl functionalized silicalite. Bifunctional nanocrystalline zeolites are also being evaluated as adsorbents for contaminated water. These bifunctional zeolites have magnetic iron species on the zeolite interior and an aminopropyl functional group on the external surface. In this case, metal ions in aqueous solution can be adsorbed on the bifunctional zeolite and the material can be recovered from solution using a magnet.

Introduction

Zeolites are aluminosilicates with pores of molecular dimensions that are widely used in applications, such as catalysis and water softening. The MFI zeolite structure consists of intersecting sinusoidal and straight channels with pore diameters of approximately 5.5Å. Zeolites ZSM-5 (aluminosilicate) and silicalite (purely siliceous form of ZSM-5) both have the MFI framework structure.

Nanocrystalline zeolites are zeolites with crystal sizes of less than 100 nm.(1,6) Nanocrystalline zeolites are porous nanomaterials with very large internal and external surface areas. We have previously developed efficient, synthetic methods for the preparation of high quality, monodisperse, nanocrystalline (<50 nm) zeolites, such as silicalite, ZSM-5, or faujasite. (2,3,4,5) The advantages of nanocrystalline zeolites include increased surface area, improved optical properties (transparency), improved diffusion/mass transfer properties and the ability to form hierarchical zeolite structures. The large external and internal surface areas lead to unique surface chemistry relative to conventional, microcrystalline zeolite materials. The external surface can be functionalized in order to tailor the properties of the nanocrystalline zeolite.(7,8) Ideally, the external

surface functionality will be coupled to the internal surface function to create a bifunctional zeolite material.

In this study, the external surface of the zeolite, silicalite, was functionalized with an organosilane. The nanocrystalline zeolite was functionalized with aminopropyltriethoxysilane (APTES) or aminopropyltrimethylmethoxysilane (APDMMS) forming an aminopropyl functionalized zeolite surface. The structures of APTES and APDMMS are shown in Figure 1. Under acidic conditions, aqueous metals, such as chromium and copper, can be effectively adsorbed onto the surface of aminopropyl functionalized silicalite. Silicalite samples with two different crystal sizes (60 and 600 nm) were functionalized to demonstrate the importance of crystal size. In another set of experiments, nanocrystalline silicalite with two different functional groups (APTES and APDMMS) was evaluated for copper adsorption.

Methods

Silicalite samples with crystal sizes of approximately 30, 60 and 600 nm were synthesized according to the method described previously(4,9). The external surface areas of the uncalcined silicalite-30 nm, silicalite-60 nm and silicalite-600 nm were 99, 53 and 5 m²/g, respectively. To functionalize the silicalite, 0.5 g of calcined silicalite was added to 60 mL toluene and ~0.5 mL APDMMS or APTES.(7,10) The reaction mixture was heated to 90°C for 4 h and then was centrifuged. The solids were washed with water and ethanol and dried overnight at 85°C. The resulting zeolite materials were characterized by x-ray diffraction, solid state NMR, BET adsorption isotherms, dynamic light scattering (DLS), zeta potential measurements, and thermal gravimetric analysis (TGA).

For the adsorption experiments, approximately 10 mg of zeolite sample was added to 10 mL of 60-100 ppm solution prepared from copper nitrate and controlled at pH 4 with HNO₃. The zeolite/metal solution was stirred for 2 hours at room temperature. After centrifugation, the solids were separated from the supernatant and both were analyzed for copper content using a Varian 720-ES Inductively Coupled Plasma/Optical Emission Spectrometer (ICP/OES) spectrometer.

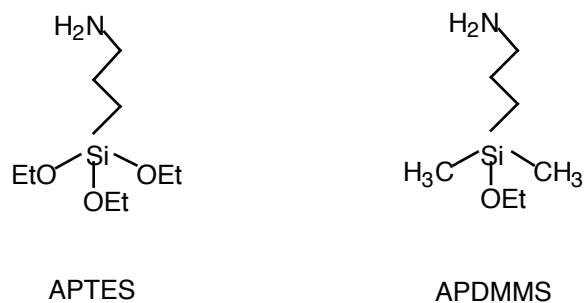


Figure 1. Structures of organosilanes, APTES and APDMMS.

The solids were dissolved in 3 mL HF, 1 mL HNO₃ and 15 mL H₃BO₄, diluted to 25 mL with deionized water and the resulting solutions were analyzed for copper concentration by ICP/OES. Calibrations were done before each set of measurements using three solutions of known concentration (25, 50 and 100 ppm) made from standards purchased from Inorganic Ventures. Three sample replicates were run for each sample and were averaged to provide the final copper solution concentrations.

Results and Discussion

Silicalite with two different crystal sizes (60 and 600 nm) was functionalized with APDMMS. The characterization and adsorption results are listed in Table 1. The external surface areas of silicalite-60 nm and silicalite-600 nm are 53 and 5 m²/g, respectively, which indicates that silicalite-60 nm has significantly more external surface available for functionalization. After functionalization with APDMMS, the specific surface area decreased from 391 to 219 m²/g for silicalite-60 nm and from 346 to 192 m²/g for silicalite-600 nm. This decrease in surface area has been observed previously and is attributed to a pore-blocking due to the external surface functionalization.^(8,10) The zeta potential at pH=7 increased from ~ -20 mV to 20 mV for silicalite-60 nm-APDMMS suggesting that the surface is functionalized with aminopropyl groups. A similar increase in zeta potential was observed for the functionalized 600 nm silicalite as listed in Table 1. The functionalization was quantified using TGA and it was found that silicalite-60 nm-APDMMS has 0.41 mmol APDMMS/g silicalite compared to 0.14 mmol APDMMS/g silicalite for silicalite-600 nm-APDMMS. The increase in loading of aminopropyl groups for silicalite-60 is attributed to the increased external surface area.

The adsorption of copper (Cu²⁺) from aqueous solution on APDMMS functionalized silicalite was measured using ICP/OES. It was found that silicalite-60-APDMMS adsorbed 0.34 mmol Cu²⁺/g zeolite compared to 0.17 mmol Cu²⁺/g zeolite for silicalite-600-APDMMS. Qualitatively, this result is expected since the silicalite-600 nm has a lower loading of APDMMS on the surface and the amino groups serve as binding sites for the copper. The Cu/N ratio for silicalite-600

Table 1. Physicochemical and Adsorptive Properties of Aminopropyl Functionalized Silicalite.

Sample	SSA (m ² /g) ^a	mmol aminopropyl/ g silicalite ^b	Zeta potential ^c (mV)	Copper adsorbed (mmol metal/g zeolite) ^d	Cu/N
Silicalite-60	391 (53)	--	-20	--	--
Silicalite-60-APDMMS	219	0.41	+20	0.34 ^d	0.8
Silicalite-600	346 (5)	--	-31	---	--
Silicalite-600-APDMMS	192	0.14	+29	0.17 ^d	1.2
Silicalite-30	444 (99)	--	-41	--	--
Silicalite-30-APTES	121	0.40	-3.4	0.96 ^e	2.4

^aSSA= specific surface area measured using the BET method- number in parenthesis is the SSA for the as-synthesized silicalite

^bDetermined from TGA

^c Solution pH=7

^dDetermined by ICP/OES from metal remaining in solution (~85 ppm starting solution, pH=4)

^eDetermined by ICP/OES from metal remaining in solution (~60 ppm starting solution, pH=4)

nm is 1.2 which is slightly higher than the Cu/N of 0.8 for silicalite-60 nm. These results suggest that the adsorbed copper is complexed to approximately one amine group in these samples.

Silicalite-30 was functionalized with APTES, which has different branching groups relative to APDMMS (Figure 1). Silicalite-30-APTES has a specific surface area of 121 m²/g and an APTES loading of 0.40 mmol APTES/g silicalite-30. The adsorption of copper from aqueous solution for silicalite-30-APTES was 0.96 mmol Cu²⁺/g zeolite which results in a Cu/N ratio of 2.4. The Cu/N ratio for the APTES functionalized sample is significantly higher than for the APDMMS functionalized sample. This suggests that the copper binding to the APTES functionalized silicalite may be different than for APDMMS-silicalite. Further studies are in progress to investigate this further and to measure detailed adsorption isotherms for each of these functionalized silicalite samples.

In future work, bifunctional nanocrystalline zeolites will be evaluated as adsorbents. These bifunctional zeolites have magnetic iron species in the zeolite interior surface and an aminopropyl functional group on the external surface. In this case, copper or chromate in aqueous solution is adsorbed on the bifunctional zeolite and the material is then recovered using a magnet.

Conclusions

In conclusion, aminopropyl functionalized silicalite is an effective adsorbent for aqueous copper and chromate (not discussed here). The effect of silicalite crystal size on functionalization and adsorption was investigated. The results confirm that nanocrystalline silicalite (60 nm) can be functionalized to a greater extent by APDMMS as measured by TGA and consequently can adsorb more copper from aqueous solution than the larger size APDMMS functionalized silicalite (600 nm). These results were compared to adsorption on an APTES functionalized nanocrystalline silicalite with similar functional group loading and the APTES functionalized silicalite adsorbed significantly more copper relative to the APDMMS functionalized silicalite. Future work will focus on understanding the copper adsorption on a molecular level and on developing a bifunctional nanocrystalline zeolite.

Acknowledgements

Dr. Weiguo Song is acknowledged for synthesis of silicalite-1 samples. This material is based on work supported by the Environmental Protection Agency through EPA grant no. R82960001, NSF (CHE-0639096) and PRF (44756-AC5).

References

1. Larsen, S. C. (2007). «Nanocrystalline zeolites and zeolite structures: Synthesis, characterization, and applications.» *Journal of Physical Chemistry C* 111(50), 18464-18474.
2. Song, W., V. H. Grassian, et al. (2005). «High yield method for nanocrystalline zeolite synthesis.» *Chem. Commun.*(23), 2951-2953.
3. Song, W., R. E. Justice, et al. (2004). «Synthesis, characterization, and adsorption properties of nanocrystalline ZSM-5.» *Langmuir* 20(19), 8301-8306.
4. Song, W., R. E. Justice, et al. (2004). «Size-dependent properties of nanocrystalline silicalite

- synthesized with systematically varied crystal sizes.» Langmuir 20(11), 4696-4702.
5. Song, W. G., G. H. Li, et al. (2005). «Development of improved materials for environmental applications: Nanocrystalline NaY zeolites.» Environ. Sci. Technol. 39(5), 1214-1220.
 6. Tosheva, L. and V. P. Valtchev (2005). «Nanozeolites: Synthesis, crystallization mechanism, and applications.» Chem. Mater. 17(10), 2494-2513.
 7. Zhan, B.-Z., M. A. White, et al. (2003). «Bonding of organic amino, vinyl, and acryl groups to nanometer-sized NaX zeolite crystal surfaces.» Langmuir 19, 4205-4210.
 8. Song, W., J. F. Woodworth, et al. (2005). «Microscopic and macroscopic characterization of organosilane-functionalized nanocrystalline NaZSM-5.» Langmuir 21(15), 7009-7014.
 9. Song, W., V. H. Grassian, et al. (2005). «High yield method for nanocrystalline zeolite synthesis.» Chemical Communications(23), 2951-2953.
 10. Barquist, K. and S. C. Larsen (2008). «Chromate Adsorption on Amine-Functionalized Nanocrystalline Silicalite-1 « Micropor. Mesopor. Mat. 116, 365-369.

Conference Questions and Answers

Question:

Are nanocrystalline zeolites known or thought to be bio-persistent?

Answer:

We think not, but I cannot answer definitively.

Question:

For mesoporous materials, it is possible to use brute force techniques, such as ball milling, to reduce the particle size? Have you tried that with zeolites?

Answer:

We believe it is easier and more effective to control the crystal size synthetically and have a smaller distribution of sizes.

Question:

What is the real benefit of using zeolites over mesoporous materials? Most of the organic contaminants cannot really get into the pores.

Answer:

The greatest benefit to be gained by using zeolites is being able to take advantage of the bi-path functional capability. Zeolites have some additional flexibility in terms of compositional variations, as in putting aluminum into the framework and looking at catalytic applications. In direct

adsorption, when the surface area and available surface sites are of primary importance, mesoporous silica will win; however, comparison of results reported in the literature for chromate adsorption on mesoporous silica materials with minopropyltriethoxysilane functionalization showed that although mesoporous silica was higher, our chromium-to-nitrogen ratio was higher. So there can be a benefit to a different mode of binding on the surface, depending on the application.

The Testing of a Nanomembrane Filtration Unit for the Production of Potable Water from a Brackish Groundwater Source

M. Hlophe, North-West University, , Mmabatho, South Africa

T. Hillie, Council for Scientific and Industrial Research, Pretoria, South Africa

Abstract

A brackish groundwater treatment study was carried out in North West Province of South Africa which is situated on a semiarid region. A nanomembrane technology unit was tested for the treatment of brackish groundwater at Batlhaping Primary School (BPS) in Madibogo village. This technology was chosen for two reasons: its low cost; ease of operation and maintenance. The major contaminants in the brackish groundwater at the school are nitrate, chloride, sulfate, calcium and magnesium ions. Three nanofiltration (NF) and three reverse osmosis (RO) nanomembranes were tested for the treatment of the brackish groundwater. The nanomembranes were initially characterized on a dead-end module reactor using the water permeability and retention coefficient methods. The three RO nanomembranes (BW30, S5 and GM) and NF90 (a nanofiltration nanomembrane) had high retention coefficients for all the determinands. Nanofiltration nanomembranes, Desal-DL and NF270, had poor rejection coefficients, particularly for NO_3^- and Cl^- . The rejection coefficient for NF90 was intermediate between that of RO and the other NF nanomembranes. The raw water was treated on a cross-flow module reactor pilot water treatment plant using the six nanomembranes at the study area. The raw water was permeated through the nanomembrane at a pressure of 16 bars. The results showed that the RO and NF90 nanomembranes could all be used for the treatment of the brackish groundwater since the water quality of their permeates complied with the South African National Standard (SANS-241) for drinking water. The NF90 nanomembrane was selected for the treatment of the brackish groundwater at BPS in Madibogo village.

Introduction

The Department of Water Affairs and Forestry (DWAf) in Mmabatho expressed concern over the anomalous concentration of nitrate ion in some naturally occurring water sources in North West Province of South Africa in the early nineteen nineties. A research project which was funded by the Water Research Commission (WRC) of South Africa was executed by the Department of Chemistry of North-West University to address this problem. Initially the project aimed to survey the extent of nitrogenous pollution in the province. The survey involved the collection of water samples and the quantitative determination of inorganic nitrogenous pollutants (ammonium, nitrate and nitrite ions) in these samples. The nitrogenous pollution problem was confirmed in some areas of the province^[1]. Nitrate ion can be reduced to the toxic nitrite ion which causes methaemoglobinemia (blue-baby syndrome) in infants from zero to six months^[2,3]. Nitrite ion also reacts with amino compounds to form nitrosoamines which cause various cancers^[4]. The highly nitratepolluted water sources were also found to be salty and probably contained other ions like calcium, magnesium, chloride and sulphate ions. Apart from this, high fluoride concentrations, which can cause skeletal and dental fluorosis, were detected^[5,6].

The pollutants are a health risk to consumers and therefore the water must be treated. That is, the pollutant concentrations of the determinands should be reduced to acceptable levels. A second research grant was secured from the WRC to investigate membrane technology for the removal of the pollutant concentrations of the determinands in order for the water to be compliant to the South African National Standard (SANS-241) for drinking water^[7]. The objectives of the study were to identify an appropriate membrane process for treatment of brackish (salty and hard) borehole water (groundwater), train local community members to operate and maintain the water treatment plant. Batlhaping Primary School (BPS) in Madibogo village at North West Province of South Africa was selected as the study area on the basis of the following criteria: high nitrate ion concentration; relatively high population density; groundwater sole source of water; security considerations for pilot water treatment plant.

Experimental

Analytical reagent grade chemicals were used for the preparation of the solutions for characterization of the nanomembranes: potassium chloride; sodium chloride; sodium fluoride; sodium sulphate; calcium chloride; magnesium sulphate. A dead-end module reactor was used for the characterization of the nanomembranes by the clean water permeability and salt retention methods. The cross-flow module reactor was used for the treatment of the brackish groundwater.

Membranes

Three nanofiltration (NF) membranes (Desal-DL, NF90 and NF270) and three reverse osmosis (BW30, S5 and GM) membranes were tested for the removal of pollutant concentrations of the determinands. These membranes are nanostructured as their pore sizes are less than 2 nanometers and are thus referred to as nanomembranes henceforth. The nanomembranes were supplied in flat-sheet and spiral-wound configurations. The flat-sheet nanomembranes were supplied by Filmtec (USA) and the spiral-wound ones by CHC (Pty) Ltd, a South African company based in Cape Town and is a subsidiary of Filmtec. The flat-sheet nanomembranes were used for characterization on the dead-end module reactor. The spiral-wound nanomembranes were used for water treatment on the cross-flow module reactor.

Dead-end module reactor

The dead-end module reactor is a bench-scale unit that is made of stainless steel and has a capacity of approximately a liter. A nanomembrane of 9.0 cm diameter is placed on a porous support which is located at the bottom of the unit. Nitrogen gas pressure is used to force raw water or feedwater through the nanomembrane. The permeate is collected in an appropriate container.

Cross-flow module reactor (pilot water treatment plant)

The cross-flow module reactor pilot water treatment plant consists of several sections. The feed section comprises a feed tank, feed pump and cartridge filters. The feed pump supplies water to the nanomembrane. The next section comprises the high-pressure pump, feed flow adjustment, NF/RO nanomembrane, back-pressure adjustment and the permeate. The high-pressure pump forces the feed water through the nanomembrane. The nanomembrane is housed in either a 2540 or 4040 inch pressure vessel. The resulting permeate is collected in a product tank and the brine or retentate in a brine tank. The pilot water treatment plant is equipped with a chemical in-

process (CIP) cleaning tank. A cleaning solution is permeated through the nanomembrane repeatedly for a predetermined period to clean a clogged or fouled nanomembrane. Sampling points are provided for the sampling of feed, permeate and brine samples.

Determination of chemical and physical water quality

The concentrations of anions (NO_3^- , Cl^- , F^- , SO_4^{2-}) in the water samples (feed, permeate and brine) were determined by means of an ion chromatograph (Dionex Instrumentation) and those of cations by an atomic absorption spectrophotometry (GBC 905 model). The physical determinands that were investigated were pH, electrical conductivity (EC) and total dissolved solids (TDS). The pH was measured with a CyberScan pH meter and the EC with an electrical conductivity meter.

Characterization of nanomembranes

The two methods that were used for the characterization of the nanomembranes were the clean water flux (A_w) and retention coefficient (R) methods. Clean water permeability was found by permeating deionized water through a dead-end module reactor that was fitted with a nanomembrane at 20 bars of nitrogen pressure. A stop watch was used for recording the permeation time. The data that was generated was then used to calculate A_w . A 20.00 ppm solution of a determinand solution (KNO_3 , NaCl , NaF , Na_2SO_4 , CaCl_2 and MgCl_2) was used for the determination of R. The solution was permeated through the nanomembrane that was fitted to the dead-end module reactor. The concentration of the determinand in the feed, permeate and brine were found in order to calculate R.

Quality of product water

The nanomembrane pilot water treatment plant was used for the treatment of the brackish groundwater at BPS in Madibogo village. The feed water was permeated through the nanomembrane at a pressure of 16 bars and the permeate or product water was collected in a product water storage tank. The South African National Standard (SANS-241) for drinking water (Class I) was used for assessing the quality of the brackish groundwater. Class I water^[8] is one that can be consumed indefinitely without causing any ill effects on the consumer. The SANS-241 for drinking water and the concentrations of the determinands in BPS brackish groundwater are given in Tables 1 and 2 for respectively chemical and physical water quality.

The water quality of the product water or permeate is given in Tables 3 and 4 for respectively chemical and physical water qualities. Two methods were used for the selection of the most appropriate nanomembrane for the treatment of the brackish groundwater: multivariate cluster analysis; a plot of the concentration of the determinand versus nanomembrane performance. The results that were obtained by subjecting the data to multivariate cluster analysis are given in Figure 1. The results that were obtained by plotting the concentration of the determinand versus nanomembrane performance are illustrated in Figure 2 which shows the retention of NO_3^- ion by the six nanomembranes.

The results of the multivariate cluster analysis indicate that the three RO nanomembranes (BW30, S5 and GM) and the NF90 nanomembrane have comparable performances. It means that any one of the four nanomembranes can be used for the treatment of the brackish groundwater

Table 1. Chemical water quality of the brackish groundwater at Batlhaping Primary School.

Determinand	SANS-241/ppm	Water quality of BPS brackish water/ppm
NO ₃ ⁻	<10	23.6
Cl ⁻	< 200	637
F ⁻	<1.0	4
SO ₄ ²⁻	< 400	110
Ca ²⁺	<150	176
Mg ²⁺	<70	102

Table 2. Physical water quality of the brackish groundwater at Batlhaping Primary School.

Determinand	SANS-241/ppm	Physical quality of BPS brackish water
pH	5.0 – 9.5	7.85
EC	<150 µS/cm	229
TDS	<1000 mg/l	91.9

Table 3. Chemical quality of nanomembrane permeate at BPS in Madibogo village.

Nanomembrane	NO ₃ ⁻ /ppm	Cl ⁻ /ppm	F ⁻ /ppm	SO ₄ ²⁺ /ppm	Ca ²⁺ /ppm	Mg ²⁺ /ppm
Desal-DL	15.1	393	0.774	10.0	104	56.5
NF270	11.7	246	0.436	6.71	64.6	28.0
NF90	3.19	45.0	0.221	5.39	9.84	5.37
BW30	1.93	10.5	0.108	10.0	2.81	0.500
S5	1.42	17.7	0.163	2.00	2.96	1.50
GM	0.833	15.7	0.239	4.11	4.91	1.69

Table 4. Physical quality of nanomembrane permeate at BPS in Madibogo village.

Nanomembrane	pH	EC/ µS cm ⁻¹	TDS/mg l ⁻¹
Desal-DL	8.18	181	72.6
NF270	7.27	113	45.3
NF90	6.81	25.5	10.7
BW30	6.78	7.22	3.03
S5	6.46	10.3	4.33
GM	6.88	6.33	2.66

as the respective water qualities of their permeates comply to the SANS-241 for drinking water. However, it also shows that the two NF nanomembranes, Desal-DL and NF270, are not suitable for the treatment of the brackish groundwater at BPS. The results in Table 3 confirm that nanomembranes Desal-DL and NF270 would not be effective for the treatment of the water. The concentrations of NO₃⁻ and Cl⁻ in their permeates are greater than the corresponding values of the SANS-241 for drinking water. The RO nanomembranes, owing to their denser network structure relative to the NF nanomembranes [9], had the highest retention coefficients for all determinands. Furthermore, the RO nanomembranes virtually removed all the Ca and Mg ions from the raw water, thus rendering it to be of less nutritional value for the normal development of the human body. The retention coefficient of NF90 was intermediate between that of the RO and NF nanomembranes.

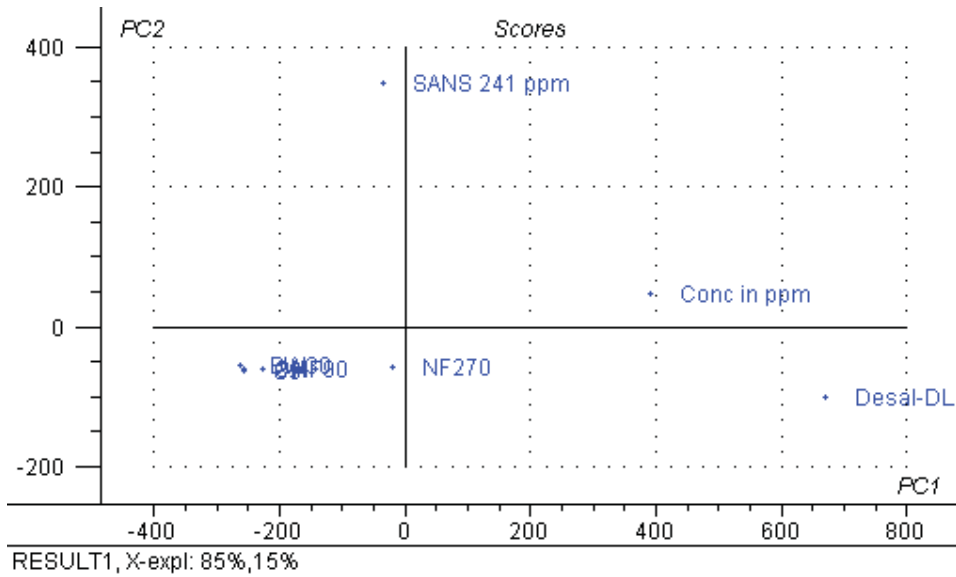


Figure 1. Multivariate cluster analysis for selection of appropriate nanomembrane for brackish groundwater treatment.

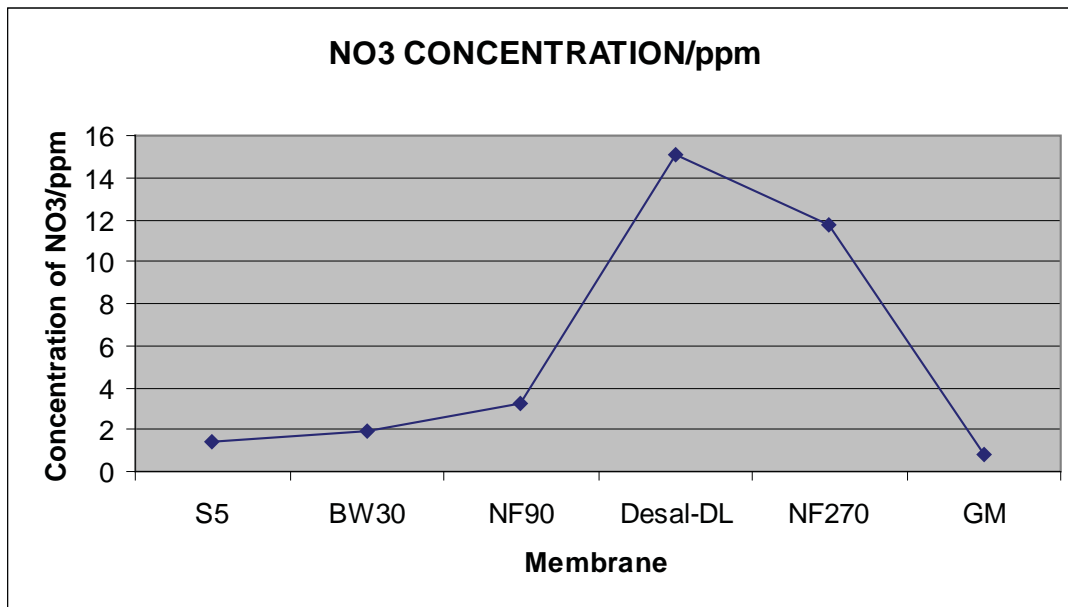


Figure 2. A plot of the concentration of NO₃⁻ versus nanomembrane performance.

Conclusions

The nanofiltration membranes, Desal-DL and NF270, are not suitable for the treatment of brackish groundwater. The RO nanomembranes are not appropriate for the removal of pollutant concentrations of the determinands. The optimal nanomembrane for the treatment of the brackish groundwater at BPS in Madibogo village is NF90.

References

1. Hlophe, M. (1999). Quantitative determination and removal of nitrogenous pollutants from water. Report to the Water Research Commission (WRC) of South Africa. Report no.: 99/1/K5/715.
2. Hill, M.J., Hawksworth, G. and Tattersall, G. (1973). Bacteria, nitrosamines and cancer of the stomach. *Br. J. Cancer*, 28, 562 – 567.
3. Fan, A.M., Willhite, C.C. and Book, S.A. (1987). Evaluation of the nitrate drinking water standard with reference to infant methaemoglobinemia and potential reproductive toxicity. *Regulatory Toxicol. Pharmacol.*, 7, 135 – 148.
4. Reche, F., Carrigos, M.C., Marin, M.L. and Jimenez, A. (2002). Determination of N-nitrosamines in latex by sequential fluid extraction and derivatization. *Journal of Chromatography A*, 976, 301 – 307.
5. Chibi, C. and Vinnicombe, D.A. (1999). WRC Workshop on fluorides and nitrates in rural water supplies.
6. Department of Water Affairs and Forestry, and Department of Health. (1996). A guide for the health related assessment of the quality of water supplies.
7. South African National Standard , SANS-241 (2005), for drinking water.
8. Quality of domestic water supplies. (2001). Volume 1: Assessment Guide. Water Research Commission No.: TT 101/98.
9. Mulder, M. (1998). *Basic Principles of Membrane Technology* (Second edition, pp. 299 – 301) Dordrecht, Kluwer Academic Publishers.

Conference Questions and Answers

Question:

Are all of the nitrate-affected wells community wells?

Answer:

Yes. In the affected rural areas, ground water is the sole supply of drinking water. There is no infrastructure in these remote rural areas, not even electricity. We considered a reverse osmosis system, which costs in the region of \$500-700, with filter replacement costing \$100-150 annually. The average lifespan of a nanomembrane is about five years, however, and that is affordable for most. Appropriate technologies for cleaning the ground water are still being sought; “appropriate” signifies technologies that do not operate on electricity and methods that preferably use local materials.

Treatment of Hi-tech Industrial Wastewaters Using Iron Nanoparticles

*Gordon C.C. Yang, and Chia-Heng Yen, Institute of Environmental Engineering,
National Sun Yat-Sen University, Kaohsiung, Taiwan*

Abstract

In this work laboratory-prepared nanoscale zero-valent iron (NZVI; also known as nanoiron) was used for the treatment of two wastewaters from the semiconductor industry and optoelectronics industry. These two industrial wastewaters were from the manufacturing processes of Cu-CMP (chemical mechanical polishing of the copper layer) and STN-LCD (super twisted nematic-liquid crystal display), respectively. A promising treatment result was obtained for each wastewater. Under ambient conditions the concentrations of COD (chemical oxygen demand) for both wastewaters were reduced to the levels lower than the local discharge standards for effluents. Experimental results also showed that nanoiron was capable of chemically reducing the contained nitrates in Cu-CMP wastewater and STN-LCD wastewater with treatment efficiencies of over 70% and 99%, respectively. Additionally, due to the mechanism of metal displacement, 99% of copper ions in Cu-CMP wastewater were removed as a result of nanoiron application.

Introduction

Environmental nanotechnology is a relatively new area of research in environmental science and engineering. In the past decade nanoscale zero-valent iron has proved its capability in treating many types of environmental pollutants including chlorinated hydrocarbons (Wang and Zhang, 1997; Lowry and Johnson, 2004; Quinn et al., 2005), nitrate (Choe et al., 2000; Yang and Lee, 2005), heavy metals (Ponder et al., 2000), azo dye (Shu et al., 2007), and other contaminants (Zhang, 2003; Joo et al., 2004).

Chemical mechanical polishing (CMP) of wafers has been considered as a high pollution process because it would generate a tremendous amount of wastewater containing nanoscale abrasive particles and many chemicals. In the past few years Cu-CMP process has gained its popularity in new wafer manufacturing. However, such a copper-containing CMP wastewater would not be allowed to discharge without treatment to the receiving water body due to its rather high copper content. Several studies on Cu-CMP wastewater treatment have been reported using various technologies such as chemical pretreatment plus microfiltration plus ion exchange (James et al., 2000); biosorption (Stanley and Ogden, 2003), chemical coagulation plus sedimentation (Sha et al., 2004), photochemical remediation (Li et al., 2005), electrocoagulation plus ion exchange (Yang, 2001), electrocoagulation plus sedimentation (Lai, 2006), simultaneous electrocoagulation/electrofiltration (EC/EF) (Yang and Tsai, 2006; Yang and Tsai, 2008).

Normally, manufacturing processes of liquid crystal display (LCD) in the optoelectronics industry consist of three major process groups: the array process, the cell process, and the module assembly process. In the first two process groups several kinds of acids, bases, and organic chemicals are used. As a result, many refractory organic compounds, sulfur-containing compounds, and nitrogenous compounds would be found in LCD wastewaters. Currently, LCD wastewaters

are mainly treated by biological processes. Ozone and/or reverse osmosis (RO) process coupled with a biological process were also reported for treating LCD wastewaters (Chen and Chen, 2004; Chen et al., 2005). The biological related processes, however, would result in an increased nitrate concentration in the system (Chen et al., 2003a; Chen et al., 2003b; Chen and Chen, 2004; Chen et al., 2005; Lin and Chang, 2006). Further removal of nitrate before discharge is thus needed.

Currently, in the literature no research has been reported using nanoiron against pollution in hi-tech industrial wastewaters. Therefore, the objective of this study was to evaluate the feasibility of using laboratory-prepared nanoscale zero-valent iron for the proper treatment of Cu-CMP wastewater and STN-LCD wastewater.

Materials and methods

In this work all chemicals used are reagent grade. The authors used a solution chemistry method for the preparation of nanoiron (Glavee et al., 1995). Target wastewaters tested were: (1) Cu-CMP wastewater obtained from a wafer fab in Taiwan and (2) STN-LCD wastewater obtained from a local LCD manufacturer as well.

The authors employed X-ray diffractometry and environmental scanning electron microscopy for characterization of nanoiron prepared. For water quality analysis the following equipment and methods were used: (1) TOC analyzer for determining the concentration of total organic carbon; (2) ion chromatography for the concentration analysis of NO_3^- and NO_2^- ; (3) colorimetry for determining the concentration of $\text{NH}_3\text{-N}$; (4) distillation unit for the determination of TKN; and (5) flame atomic absorption spectroscopy for the determination of copper ion concentration.

A dose of 2 g/L of nanoiron was added to 250 mL of Cu-CMP wastewater and STN-LCD wastewater, respectively with 200-rpm stirring in beakers to study the effects of initial pH of wastewater (i.e., intrinsic pH, pH=3, and pH=10) on treatment performance of nanoiron towards target wastewaters at different treatment time periods. The water quality used for evaluating the treatment performance included concentrations of chemical oxygen demand (COD), total Kjeldahl nitrogen (TKN), NO_3^- , and Cu^{2+} .

Results and discussion

Characterization of prepared particles

The XRD pattern confirmed that Fe^0 was the main species in the prepared particles. The micrograph of ESEM further showed that the prepared nanoiron was spherical with a diameter in the range of 50-60 nm, but in aggregate form.

Characterization of target wastewaters

The qualities of raw Cu-CMP wastewater and STN-LCD wastewater before treatment were given in Table 1. It was found that values of pH, TKN, and NO_3^- for Cu-CMP wastewater were lower than that of STN-LCD wastewater. However, the concentrations of $\text{NH}_3\text{-N}$ and TOC were opposite. It was also noticed that Cu-CMP wastewater had a high concentration of copper ions, 6.92 mg/L.

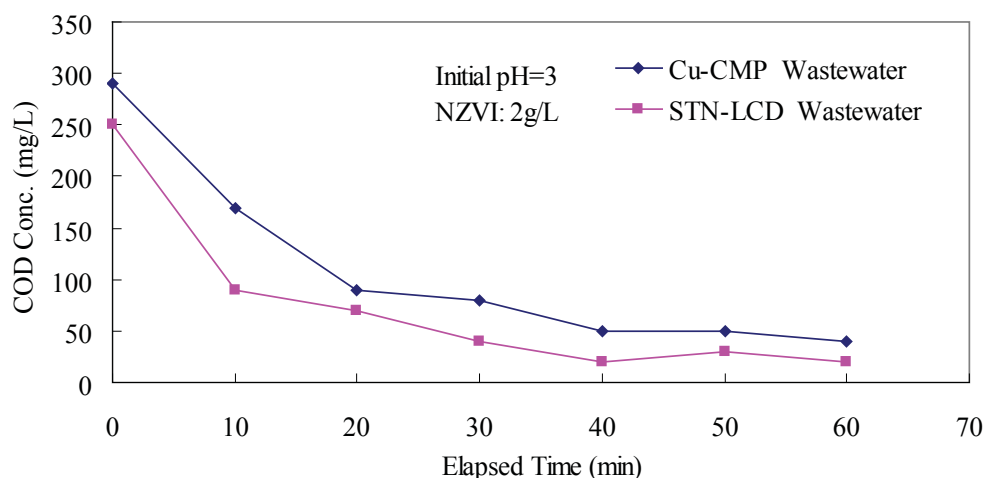


Figure 1. Variations of COD concentration in Cu-CMP wastewater and STN-LCD wastewater treated by nanoiron under initial pH of 3.

Treatment of Cu-CMP wastewater and STN-LCD wastewater by nanoiron

Experimental results showed that about 90% of COD in both Cu-CMP wastewater and STN-LCD wastewater could be properly removed to meet the local effluent discharge standards (i.e., COD < 100 mg/L) by NZVI with a dose of 2 g/L in 60 min under various pH conditions tested. Fig. 1 showed the test results for these target wastewaters under initial pH of 3.

The influence of pH on the variations of TKN and NH₃-N in Cu-CMP wastewater was found to be negligible in a general sense. Based on the test results, the TKN concentration has been reduced from ca. 41 mg/L to 27-28 mg/L (see Fig. 2) and the concentration of NH₃-N of 25-26 mg/L was determined after 60 min of reaction. In other words, a removal efficiency of ca. 85%

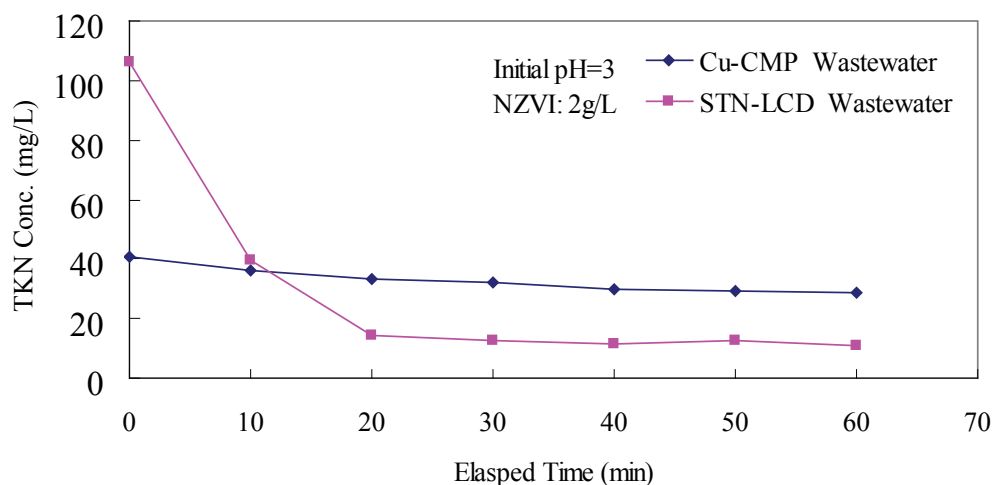


Figure 2. Variations of TKN concentration in Cu-CMP wastewater and STN-LCD wastewater treated by nanoiron under initial pH of 3.

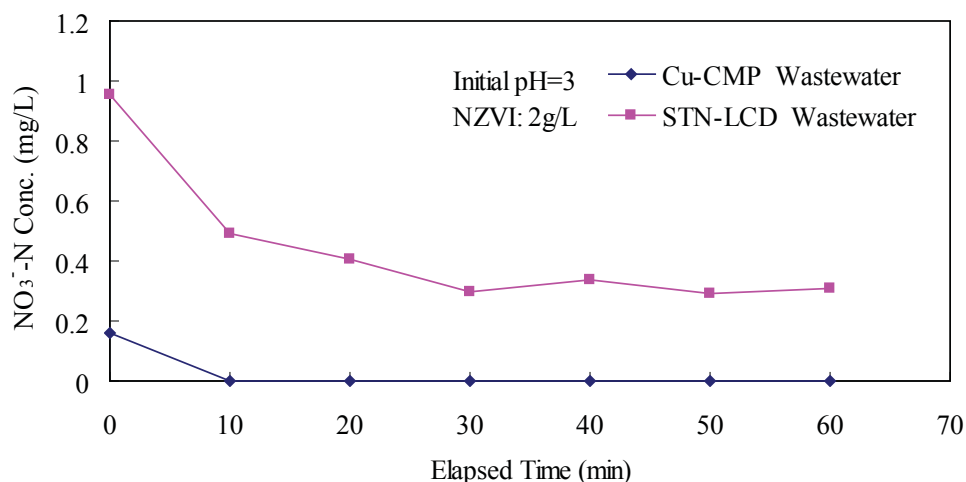


Figure 3. Variations of NO_3^- -N concentration in Cu-CMP wastewater and STN-LCD wastewater treated by nanoiron under initial pH of 3.

for organic nitrogen was obtained in Cu-CMP wastewater under the test conditions. In the case of STN-LCD wastewater, due to its low initial concentration of NH_3 -N (i.e., 0.2 mg/L), the variation of TKN concentration would reflect the variations of organic nitrogen. Fig. 2 showed that a TKN removal of ca. 85% was obtained after 20 min under initial pH of 3. In fact, the effect of the initial pH of the system in TKN removal for this wastewater is negligible.

Experimental results showed that over 99% of nitrate ions in Cu-CMP wastewater was rapidly reduced by nanoiron at pH 3, whereas only 68% reduction was obtained at pH 10. Similarly, a greater reduction rate of nitrate ions was found for STN-LCD wastewater at pH 3 than that of in the alkaline system. A removal efficiency of 70% could be obtained after 30 min of reaction. Fig. 3 showed the removal of NO_3^- -N for these two target wastewaters under initial pH of 3.

Experimental results showed that the Cu^{2+} concentration in Cu-CMP wastewater dropped rapidly in the first 10 min of reaction. After a reaction time of 20 min, the Cu^{2+} concentration has reduced to a level of < 0.1 mg/L. This is ascribed to the replacement of copper by iron during the treatment reaction. This speculation was verified by the patterns of ESEM-EDS (not given) showing the existence of the characteristic peak of copper element on the surface of post-treatment nanoiron.

To evaluate the feasibility of using nanoiron for the full-scale treatment of the target wastewaters in the future, both Cu-CMP wastewater and STN-LCD wastewater were treated without prior pH adjustment. Table 1 presented the test results for these concerned wastewaters. In the case of Cu-CMP wastewater, COD has been reduced to a level of 40 mg/L representing a removal efficiency of 86.2%. As for TKN, nitrate ions, and copper ions, the corresponding removal efficiencies were determined to be 33.3%, $> 99.0\%$, and $> 99.0\%$, respectively. In the case of STN-LCD wastewater, the removal efficiencies for COD, TKN, and nitrate ions were determined to be 88.0%, 88.3%, and 34.3%, respectively. It was noticed that Cu^{2+} in Cu-CMP wastewater was removed to a trace level. As indicated above, wastewater treated by biological processes would

Table 1. Water qualities of Cu-CMP wastewater and STN-LCD wastewater before and after treatment by nanoiron without prior pH adjustment.

Water quality	Wastewater treated by nanoiron*			
	Cu-CMP		STN-LCD	
	Before	After	Before	After
pH	6.9	8.4	8.2	8.9
Turbidity (NTU)	106.2	--	44.5	--
Conductivity ($\mu\text{S}/\text{cm}$)	463	--	437	--
SS (mg/L)	1.14	--	9.10	--
COD (mg/L)	290	40	250.0	30.0
TOC (mg/L)	110.4	32.2	9.87	0.78
TKN (mg/L)	40.8	27.2	106.4	12.5
NH ₃ -N (mg/L)	25.7	26.2	0.21	0.69
NO ₃ ⁻ (mg/L)	1.27	< 0.10	7.49	4.92
Cu ²⁺ (mg/L)	6.92	< 0.10	--	--

* nanoiron dose of 2 g/L; treatment time of 60 min.

substantially increase NH₃-N concentration. However, this is not a problem for the treatment using nanoiron. The particulates remained in post-treatment wastewaters could be further removed by the simultaneous EC/EF process indicated above.

Conclusions

Experimental results have revealed that nanoiron is a novel and effective material for the treatment of Cu-CMP wastewater and STN-LCD wastewater to meet the effluent discharge standards. Copper removal is ascribed to metal displacement by iron nanoparticles in the system.

References

- Chen, T.K., and J.N. Chen. (2004). "Combined membrane bioreactor (MBR) and reverse osmosis (RO) system for thin-film transistor-liquid crystal display TFT-LCD, industrial wastewater recycling." *Water Sci. Technol.* 50(2), 99-106.
- Chen, T.K., C.H. Ni, and J.N. Chen. (2003a). "Nitrification-denitrification of opto-electronic industrial wastewater by anoxic/aerobic process." *J. Environ. Sci. Health A38*(10), 2157-2167.
- Chen, T.K., C.H. Ni, Y.C. Chan, and M.C. Lu. (2005). "MBR/RO/ozone processes for TFT-LCD industrial wastewater treatment and recycling." *Water Sci. Technol.* 51(6-7), 411-419.
- Chen, T.K., J.N. Chen, C.H. Ni, G.T. Lin, and C.Y. Chang. (2003b). "Application of a membrane

- bioreactor system for opto-electronic industrial wastewater treatment –a pilot study.” *Water Sci. Technol.* 48(8), 195-202.
- Choe, S., Y.Y. Chang, K.Y. Hwang, and J. Khim. (2000). “Kinetics of reduction denitrification by nanoscale zero-valent iron.” *Chemosphere.* 41, 1307-1311.
- Glavee, G.N., K.J. Klabunde, C.M. Sorensen, and G.C. Hadlipanayis. (1995). “Chemistry of borohydride reduction of iron (II) and iron (□) ions in aqueous and nonaqueous media. formation of nanoscale Fe⁰, FeB, and Fe₂B powders.” *Inorg. Chem.* 34, 28-35.
- James, D., D. Campbell, J. Francis, T. Nguyen, and D. Brady. (2000). “A process for efficient treatment of Cu CMP wastewater.” *Semicond. Intern.*, 5/1/2000.
- Joo, S.H., A.J. Feitz, and T.D. Waite. (2004). “Oxidative degradation of the carbothioate herbicide, molinate, using nanoscale zero-valent iron.” *Environ. Sci. Technol.* 38, 2242-2247.
- Lai, C.L. (2006). “Electrocoagulation and settled process of chemical mechanical polishing wastewater from semiconductor fabrication.” Ph.D. Thesis, Dept. Chemical Eng., Yuan Ze University, Chung-Li, Taiwan.
- Li, Y., J. Keleher, and N. Gao. (2005). “Photo-chemical remediation of Cu-CMP waste.” U.S. Patent 6916428.
- Lin, S.H., and C.S. Chang. (2006). “Treatment of optoelectronic industrial wastewater containing various refractory organic compounds by ozonation and biological method.” *J. Chin. Inst. Chem. Eng.* 37(5), 527-533.
- Lowry, G.V., and K.M. Johnson. (2004). “Congener-specific dechlorination of dissolved PCBs by microscale and nanoscale zerovalent iron in a water or methanol solution.” *Environ. Sci. Technol.* 38, 5208-5216.
- Ponder, S.M., J.G. Darab, and T.E. Mallouk. (2000). “Remediation of Cr (VI) and Pb (II) aqueous solutions using supported, nanoscale zero-valent iron.” *Environ. Sci. Technol.* 34, 2564-2569.
- Quinn, J., C. Geiger, C. Lausen, K. Brooks, C. Coon, S. O’hara, T. Krug, D. Major, W.S. Yoon, A. Gavaskar, and T. Holdsworth. (2005). “Field demonstration of DNAPL dehalogenation using emulsified zero-valent iron.” *Environ. Sci. Technol.* 39, 1309-1318.
- Sha, M., H. Ting, A. Chen, and L.C. Yang. (2004). “System and process for CU-CMP wastewater treatment.” U.S. Patent 6818131.
- Stanley, L.C., and K.L. Ogden. (2003). “Biosorption of copper (II) from chemical mechanical planarization wastewaters.” *J. Environ. Manag.* 69(3), 289-297.
- Shu, H.Y., M.C. Chang, H.H. Yu, and W.H. Chen. (2007). “Reduction of an azo dye acid black 24 solution using synthesized nanoscale zerovalent iron particles.” *J. Colloid Interface. Sci.* 314, 89-97.
- Wang, C.B., and W.X. Zhang. (1997). “Synthesizing nanoscale iron particles for rapid and complete dechlorination of TCE and PCBs.” *Environ. Sci. Technol.* 31, 2154-2156.

Yang, C.R. (2001). "Treatment of chemical mechanical polishing wastewater from semiconductor fabrication for reuse." MS Thesis., Dept. Chemical Eng., Yuan Ze University, Chung-Li, Taiwan.

Yang, G.C.C., and H.L. Lee. (2005). "Chemical reduction of nitrate by nanosized iron: kinetics and pathways." *Water Res.* 39, 884-894.

Yang, G.C.C., and C.M. Tsai. (2006). "Performance evaluation of a simultaneous electrocoagulation and electrofiltration module for the treatment of Cu-CMP and oxide-CMP wastewaters." *J. Membr. Sci.* 286, 36-44.

Yang, G.C.C., and C.M. Tsai. (2008). "Preparation of carbon fibers/carbon/alumina tubular composite membranes and their applications in treating Cu-CMP wastewater by a novel electrochemical process." *J. Membr. Sci.* 321, 232-239.

Zhang, W.X. (2003). "Nanoscale iron particles for environmental remediation: An overview." *J. Nanopart. Res.* 5, 323-332.

Conference Questions and Answers

Question:

Is it cost effective to use nanoscale iron to remove nitrate from wastewater? If microscale iron works effectively at pennies on the dollar, why go to nano? Did you perform a cost analysis?

Answer:

No. We did not examine the cost dimension. At present, we are trying to ascertain whether they can be made to work reliably. We will consider the cost factors afterward.

Conjugates of Enzyme-Magnetic Nanoparticles for Water Remediation

*You Qiang, Department of Physics and Environmental Science Program,
University of Idaho, Moscow, Idaho, U.S.A.*

*Andrzej Paszczynski, Environmental Biotechnology Institute and Department of Microbiology
Molecular Biology and Biochemistry, University of Idaho, Moscow, Idaho, U.S.A.*

*Amit Sharma, Agnes Che and Ryan Souza, Department of Physics and Environmental Science
Program, University of Idaho, Moscow, Idaho, U.S.A.*

Abstract

Enzymes are proteins that are utilized as biocatalysts in bioremediation. A concern in environmental applications of enzymes is their short lifetime and poor stability. Enzymes lose their activity due to denaturation, which render their stability and a shorter lifetime. An effective way to increase the stability, longevity, and reusability of the enzymes is to attach them to the solid surface particularly to the surface of magnetic nanoparticles. If enzymes are attached to the magnetic iron nanoparticles, we can easily separate the enzymes from reactants or products by applying a magnetic field. With this aim, two different catabolic enzymes, trypsin and peroxidase, were attached to uniform core-shell magnetic nanoparticles (MNP's) produced in our laboratory. Our study indicates that the lifetime and activity of enzymes increases dramatically from a few hours to weeks and that enzyme-MNP conjugates are more stable, efficient, and economical. TEM images show that the enzyme-MNP conjugate forms nano-rings secondary structure in water that prevents the enzyme molecules from denature and self-digest. This results in an increased functional lifetime of the enzymes. Because of the high magnetization (larger than 150 emu/g) of our core-shell MNPs, enzyme-MNP conjugates can be suspended in magnetic field, making enzymes-MNP conjugate catalytically more efficient than enzyme immobilized to the "macro" surface.

Introduction

Enzymes have long been used in industry as catalysts for catabolic processes or for the specific chemical products. Nano-size, high surface area and low toxicity has made magnetic nanoparticles (MNPs) most promising element for various fields such as biomedical and environmental applications [1-8]. MNP-enzyme conjugates (MNP-Es) represent a specific class of bio-NP conjugates that are of great interest for biotechnological applications where high catalytic specificity, prolonged reaction time, and in some cases the ability to recycle an expensive biocatalyst is required. In addition, magnetic field susceptibility provides a mechanism for efficient recovery of the enzyme complex from reaction products, which is especially important in the pharmaceutical industry where enzyme contamination of the final product can cause detrimental side effects. Contaminations in water are major concerns of environment. Xenobiotic chemical degrading enzymes attached to MNPs hold potential for use in novel nano-remediation technologies that will allow precise delivery (using electromagnetic probes) of the MNP-E conjugate to the contami-

nant source in locations such as aquifers while enabling recovery and reuse of the MNP-Es. The fate of biomolecules in natural or human-controlled environments (e.g., sewage treatment plants, aquifers, or soils) could be traced by tagging the biomolecules with MNPs. Researchers are improving current technologies and developing new applications that utilize enzymes immobilized on nanoparticles. During reaction enzyme retain their property, thus they can be cost effective if we could reuse them [14]. Enzymes can be reused if we immobilize them by attaching them on a solid surface, this will make it easier to separate enzymes from the solution. Using MNP-Es, we can easily separate the enzymes from reactants or products by applying a magnetic field. Short lifetime of enzymes limits their applications [9]. Attempts have been made repeatedly to increase the stability of enzymes by encapsulating biomolecules in silica gels but repeatability and long term stability still remains a concern [16]. Lack of stability of enzymes during storage is also one of the issues with enzymes.

MNP-Es will have a major advantage over metal-only particles such as those described by Elliot [2] that react stoichiometrically with substrates in equimolar reactions rather than catalytically; zero-valent metals are quickly consumed by water passivation and/or contaminant reduction. In contrast, particle-bound enzymes, when stabilized to prevent protein degradation, can act as true catalysts, turning over many moles of substrate molecules before ultimate enzyme inactivation. Moreover, immobilization of bioactive molecules on the surface of MNPs is of great interest because the magnetic properties of these bioconjugates promise to greatly improve the active delivery, recovery, and control of biomolecules in environmental and other applications.

Rossi et al. [3] covalently conjugated the enzyme glucose oxidase to 20-nm Fe_3O_4 MNPs for glucose sensors. Covalent immobilization increased the stability of the enzyme. The same reaction was used to examine cholesterol oxidase (CHO) properties after binding to Fe_3O_4 . Stability and activity of CHO was enhanced after attachment to MNPs, improving the potential for use of this enzyme in various biological and clinical applications [5]. Ohobosheane et al. [6] demonstrated modification of silica-based NPs whose surfaces were linked to glutamate dehydrogenase and lactate dehydrogenase allowing them to function as biosensors and biomarkers. The immobilized enzyme molecules were shown to retain excellent enzymatic activity in respective reactions.

Here we reported a new method to cross-linking enzymes with bifunctional reagents which help in increasing the lifetime of enzyme. We have found an efficient way of binding enzymes to MNPs. Attaching enzymes to MNPs extends their lifetime from few hours to weeks.

Experiments

Monodispersive core-shell iron nanoparticles were produced using third generation cluster deposition apparatus in our laboratory [10-12]. The size of the nanoparticles was controlled by varying the growth distance, power, and helium and argon gas ratio. For these experiments, uniform 20 nm size MNPs were deposited on a plastic substrate. The nanoparticles were then removed and collected in the solution of pH 7. Magnetic moment of the iron/iron oxide core-shell NPs produced in our lab is ~ 140 emu/g [4]. Two catabolic enzymes were attached to the nanoparticles namely trypsin and horseradish peroxidase (HRP). To prevent denaturation and leaching nanoparticles were coated with 3-aminopropyl triethoxy silane, thus prolonging the stability of the magnetic nanoparticle. The first reaction shown in Fig. 1 is an example of silanization of MNP passivated with ferric-oxyhydroxy-polymer with 3-aminopropyltriethoxysilane. Commercially

available cross-linking agents were used to attach activated enzymes to nanoparticles. Four different coupling reagents: **SANH** (succinimidyl 4-hydrazinonicotinate acetone hydrazone); **C6-SANH** (C6-succinimidyl 4-hydrazinonicotinate acetone hydrazone); **SFB** (succinimidyl 4-formylbenzoate) and **C6-SFB** (C6-succinimidyl 4-formylbenzoate) were used. These reagents prevent homopolymerization of MNP's and enzymes, and provide variability in spacer-arm length from 5.8 to 14.4 Å. The enzymes were covalently linked with nanoparticles by reacting them separately with amino-silane or peptide coated nanoparticles. After the modifications the MNP's were purified of excess reagent. The hydrazine/hydrazide-modified MNP's were reacted with the aldehyde-modified molecule to yield the desired MNP-E conjugates (Fig. 1). Both reaction mixtures (enzyme + SANH and MNP's + SFB) were incubated for 3 hours with no shaking in buffer (pH=7.3). The concentration of SFB and SANH were in 10 molar excess of protein or MNP's.

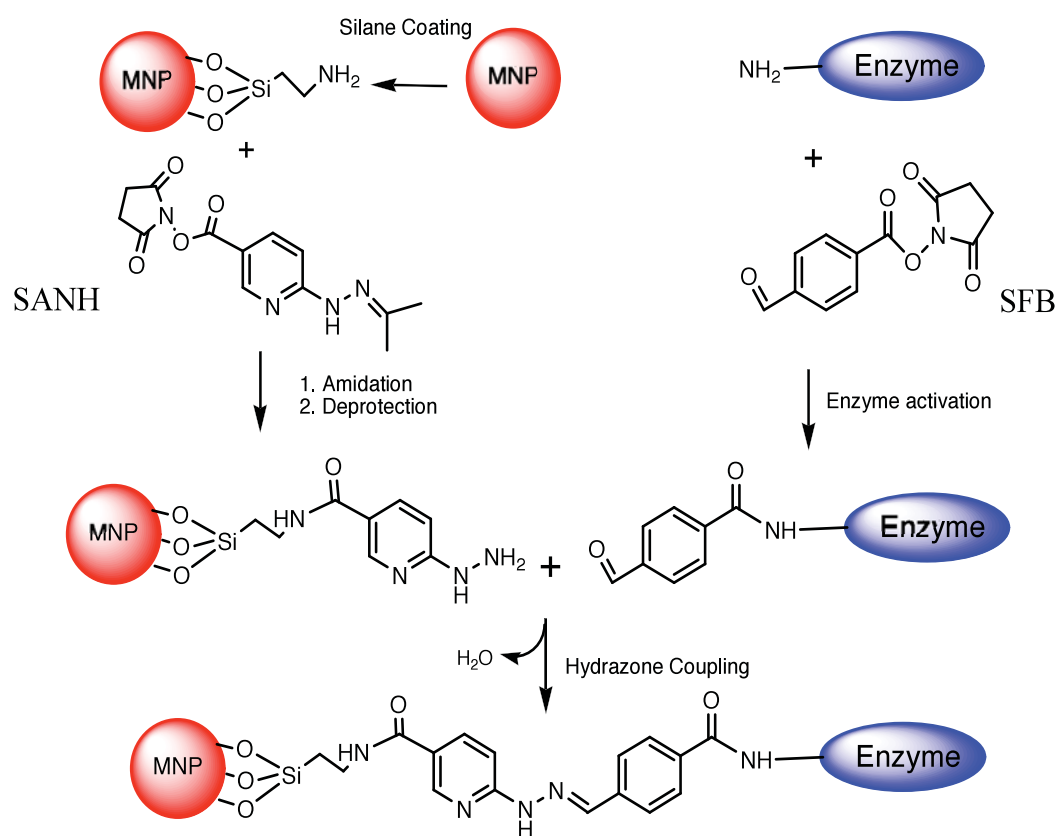


Figure 1. Reaction scheme used for producing MNP-Es using amino-silane-coated MNP's.

After activation the excess of the heterobifunctional coupling agent and the buffer replacement (to the conjugation buffer, pH=4.7) was performed in single chromatographic step using a Sephadex G25, PD10 column.

Results and Discussion

During coupling reaction activated MNP and enzyme solution were agitated using rocking shaker. The optimal molar ratio of enzyme to MNP was 10:1 and optimal pH was 4.7. We attached MNP's to trypsin, and found the stability of the trypsin is very good. Fig. 2A shows the relative activity of free trypsin and nanoparticle-trypsin conjugate. Clearly, free trypsin loses its activity after about 7 hours in comparison to the MNP-E conjugate which is active for more than twenty five hours. We also attached MNP to peroxidase and checked the activity of the peroxidase after every three hours. As seen in Fig. 2B peroxidase was active for more than seventy hours. Stability of enzymes was tested by incubating them for 5 weeks. Figure 3 shows the stability of enzyme with MNP. MNP's and enzymes were joined to each other by covalent bond using a heterobifunctional cross linkers. We used SANH and SFB as cross-linkers to attach MNP's and Enzymes. TEM images show that the enzyme-MNP conjugate forms nano-rings secondary structure in water that prevents the enzyme molecules from denature and self-digest. This results in an increased functional lifetime of the enzymes. We estimated the density of enzymes conjugated to the MNP's using protein concentration measurement techniques. Knowing available surface area, protein amount bonded, and enzyme dimensions, we were able to calculate the fraction of surface covered by a given enzyme; trypsin covered 20% of the available surface of MNP and peroxidase covered 25% of the available surface area of MNP. The productivity and cost efficiency of enzymes could be increased if we could reuse them. Iron nanoparticles being magnetic, we are able separate MNP-E conjugates after the reaction and immobilize enzymes making them

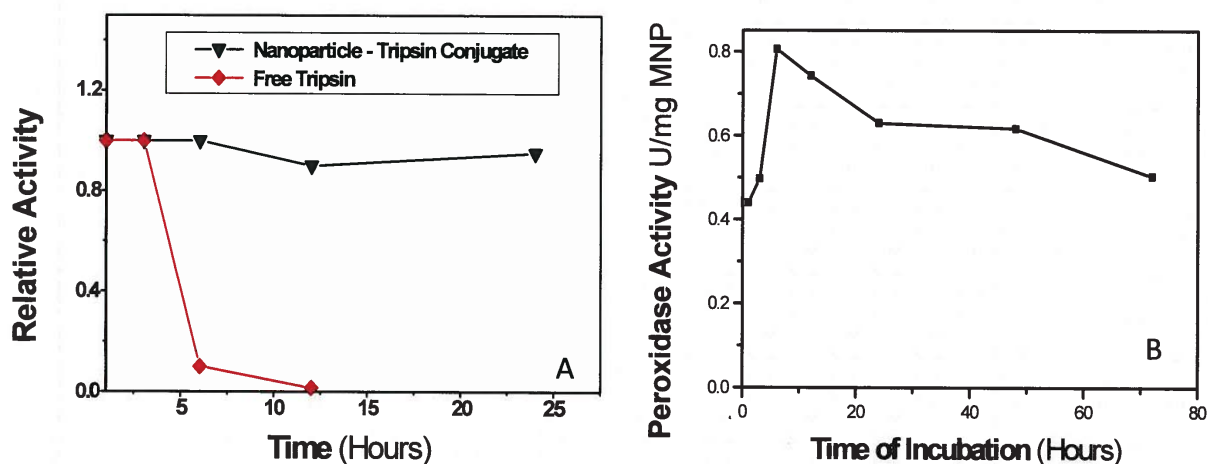


Figure 2. A) Stability of MNP-trypsin at pH=7 at 5 degree C and B) Optimization MNP-Peroxidase coupling reaction time (Conjugate Peroxidase - SANH/MNP's-SFB)

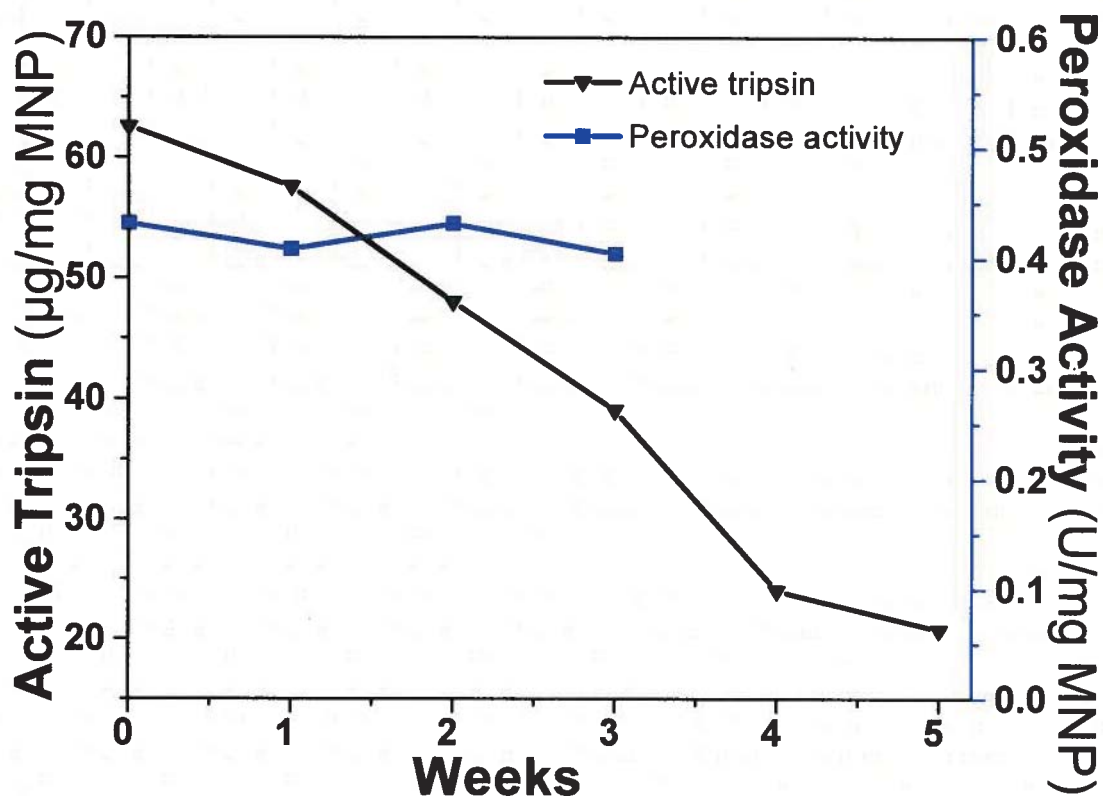


Figure 3. Stability of MNP-Es in weeks.

more productive. We did this by applying a very small magnetic field of < 100 gauss to MNP-E conjugates in vile. MNP-E conjugates were effectively separated in solution in about 30 seconds.

Acknowledgements

This work is supported by grants of DOE-BES (DE-FG02-06ER15777) and DOE-EPSCoR (DE-FG02-04ER46142).

References

- W. Andra, and H. Nowak. Magnetism in Medicine. 1998, Wiley-VCH, Berlin.
- D. W. Elliott and W. X. Zhang. "Field assessment of nanoscale bimetallic particles for groundwater treatment". *Environ. Sci. Technol.* 2001, 35:4922-4926.
- L. M. Rossi, A. D. Quach, and Z. Rosenzweig. Glucose oxidase-magnetite nanoparticle bioconjugate for glucose sensing. *Anal. Bioanal. Chem.* 2004, 380(4):606-613.
- G. K. Kouassi, J. Irudayaraj, and G. McCarty. Activity of glucose oxidase functionalized onto magnetic nanoparticles. *Biomagn. Res. Technol.* 2005, 200, 3(1):1-10.
- G. K. Kouassi, J. Irudayaraj, and G. McCarty. "Examination of cholesterol oxidase attachment to

magnetic nanoparticles". *J. Nanobiotechnology* 2005, 3(1):1-9.

M. Qhobosheane, S. Santra, P. Zhang, and W. Tan. 2001. Biochemically functionalized silica nanoparticles. *Analyst* 126:1274-1278.

Jungbae Kim, Yuehe Lin, Jay W. Grate "Single-Enzyme Nanoparticles on Nanostructured Matrices" 2003 Biological Sciences PN03083/1746

S. K., Ahuja G. M. Ferreira, and A. R. Moreira. 2004. Utilization of enzymes for environmental applications. *Crit. Rev. Biotechnol.* 24:125-154.

R.W.S. Weber, D.C. Ridderbusch and H. Anke: 2,4,6-Trinitrotoluene (TNT) tolerance and biotransformation potential of microfungi isolated from TNT-contaminated soil. *Mycological Research* **106**: 336-344, 2002

You Qiang, Jiji Antony, Amit Sharma, Sweta Pendyala, Joseph Nutting, Daniel Sikes and Daniel Meyer, "Novel Magnetic Core-Shell Nanoclusters for Biomedical Applications", *Journal of Nanoparticle Research*, 8, 489, (2006).

J. Antony, Y. Qiang, Donald R. Baer and C. M. Wang, "Synthesis and Characterization of Stable Iron-Iron Oxide Core-Shell Nanoclusters for Environmental Applications", *J. of Nanoscience and Nanotechnology*, 6, 568-572 (2006).

Y. Qiang, J. Antony, M. G. Marino, and S. Pendyala, "Synthesis of Core-Shell nanoclusters with High Magnetic Moment for Biomedical Applications", *IEEE Transactions on Magnetics*, 40(2004) 6, 3538-3540.

Kevin O' Grandy "Biomedical application of magnetic nanoparticle" *Journal of Physics D: Applied Physics: Editorial* 36,131 (2002)

Dongfang Cao, Pingli He, Naifei Hu " electrochemical biosensors utilizing electron transfer in heme proteins immobilized on Fe₃O₄ nanoparticles *Analyst*,2003,128,1268-1274

D. L. Graham, H. Ferreira J. Bernardo P. P. Freitas J. M. S. Cabral "Single magnetic micro sphere placement and detection on-chip using current line designs with integrated spin valve sensors: Biotechnological applications" *Journal of Applied Physics* volume 91, 10, 2002.

Jacques Livage, Thibaud Coradin and Cécile Roux "Encapsulation of biomolecules in silica gels" *J. Phys.: Condens. Matter* 13 (2001) R673-R691

Conference Questions and Answers

Comment:

Your slides showed that you can get a good suspension with iron particles.

Response:

You can get a good suspension if the particles are small enough. The mechanics, however, are still not clear.

Question:

What is the coating on your particles?

Answer:

For the conjugates you need a silica coating; otherwise you cannot make a cross link. The particle itself has an iron core and a shell of iron oxide.

Question:

With what types of nuclear compounds would this be most effective?

Answer:

Nuclear fuel waste.

Question:

What is the benefit from the enzyme?

Answer:

The enzyme is a catalyst to speed the reactions. It's very expensive, but if it lasts a long time, it can be collected and reused, which decreases costs.

Question:

The particles used by Toda and Zhang were not stable. Can you still form enzyme conjugates by taking fresh ones and functionalizing them?

Answer:

We tried Toda's method. It did not work, because the particles aggregated and became a few huge clusters. This provided less available surface area and a low level of surface activity relative to the surfaces of unaggregated particles.

Question:

Do you plan to use enzymes other than trypsin and peroxidase?

Answer:

We began with these two because they are very simple, but we plan to experiment with other enzymes in future work.

Exploring a Framework of Nanotechnology Research and Applications in Addressing Global Climate Change Issues

David J. LePoire, Argonne National Laboratory, Argonne, Illinois, U.S.A.

Abstract

Nobel Laureate Richard Smalley had suggested in the early part of this decade that nanotechnology be internationally researched and applied in solving the world's energy issue and thereby relieving many other related problems, such as the challenge of global climate change. While the scale and international collaboration towards this goal were not realized, many independent research activities are being pursued to address this air quality issue with the application and understanding of nanotechnologies. The recent U.S. science and technology strategic research plans concerning global climate change constitute a classification framework. Major components of this framework include aspects such as (1) system understanding, (2) mitigation efforts through non-energy sources, energy sources, efficient energy use, and direct CO₂ capture, (3) adaptation, (4) assessing potential impacts, and (5) evaluating policy responses. Various international reports and activities are placed in the context of this framework to identify progress, gaps and uncertainties in areas such as application of nanotechnology to understanding aerosols, better measures of the system dynamics, direct use in energy storage, transmission, efficiency, conversion, and how reduction of environmental emissions.

This project is an initial step in an effort to try to determine whether decision techniques such as a real options analysis approach might be suitable for this large public investment. On a smaller scale, commercial organizations have applied real options analysis to gain better understanding of research investments under large uncertainties. Options analysis includes accounting for future options such as deployment, abandonment, or continued research. As such it views research as an insurance policy against potential uncertain conditions such as the impacts of global climate change. Such an analysis could lead to better understanding and decision making concerning the public role of governments to speed learning curves, develop shared basic information, and correct environmental externalities.

Introduction

Nobel Laureate Richard Smalley had suggested in the early part of this decade that nanotechnology be internationally researched and applied in solving the world's energy issue and thereby relieving many other related problems, such as the challenge of global climate change. While the scale and international collaboration towards this goal were not realized, many independent research activities are being pursued to address this air quality issue with the application and understanding of nanotechnologies. The recent U.S. science and technology strategic research plans concerning global climate change constitute a classification framework. Major components of this framework include aspects such as (1) system understanding, (2) mitigation efforts through non-energy sources, energy sources, efficient energy use, and direct CO₂ capture, (3) adaptation, (4) assessing potential impacts, and (5) evaluating policy responses.

Nanotechnologies are expected to be useful in mitigation and energy generation and efficiency due to some of their unique properties of high surface area to volume, surfaces that might be more reactive for catalysis, strength to volume ratios of carbon nanotubes, ability to modify surface properties through coatings, ability to control material properties for electronics and heat transfer.

Methods

Various international reports and activities have been published regarding assessment of these technologies. For example the United Kingdom's Department for Environment, Food, and Rural Affairs published "Environmental Beneficial Nanotechnologies: Barriers and Opportunities" in May 2007. They identified a number of nanotechnologies in the energy efficiency and renewable category including: insulation, lighting, energy storage (batteries and Hydrogen), fuel additives, and solar photovoltaics placed in the context of this framework to identify progress, gaps and uncertainties in areas such as application of nanotechnology to understanding aerosols, better measures of the system dynamics, direct use in energy storage, transmission, efficiency, conversion, and how reduction of environmental emissions. They estimate that nanotechnology could soon reduce greenhouse gas emissions by about 2% but then expand to cut them by 20% in 2050.

They ranked the technologies were ranked based on criteria concerning 1) the benefits of the technology, 2) the impact of nanotechnology in the applications, 3) the distance to market, 4) the competition with alternative technologies, and the necessary 5) infrastructure change and 6) time required to implement. These last two are often related but the implementation rate is also dependent adoption time and the level of the decision, for example the substitution of residential incandescent lights to compact fluorescent lights is taking decades.

Results

Other energy generation projects that include an aspect of nanotechnologies include application of more efficient materials, coatings, and heat transfer for wind turbines, generators, and geothermal/heat pump systems. By improving material with good electrical conductivity but low heat conductivity thermoelectric devices might be developed with nanoparticles that may extract energy from waste heat or make more efficient cooling systems (Boston College and MIT). Cientifica estimated that the majority of the early greenhouse gas (GHG) savings will be through the use of lighter materials in the transportation sector such as General Motors nanocomposite thermoplastic olefin process. The technologies might also be applied to more efficiently transmit the energy over long distances with nanotechnology based superconductors. The potential for nanotechnologies in facilitating nuclear fusion energy is still unknown since the fundamental science and engineering are still being investigated.

Carbon sequestration is another parallel approach towards reducing greenhouse gases. The large reactive surface area of nanomaterials might allow more effective capture of the carbon dioxide after the burning of fossil fuels before emission. For example, Cornell and KAUST universities are investigating nanoparticles ionic materials for carbon sequestration. The particles with catalytic cores and attached amines assist in the capture, transport, and controlled disposal of the carbon dioxide.

The excess nitrogen applied to agricultural land contributes to the release of other green house

gases than carbon dioxide. The ability to control release of nutrients might allow nanoparticles to assist in the reduction of green house gases released during the application to agricultural areas.

The study of nanoparticles in the atmosphere may lead to a better understanding of the role of aerosols in the climate change process and also assist in the assessment of various geoengineering designs that might generate reflective particles in the atmosphere to increase the earth's albedo.

Adaptation strategies include changes in health, migration, and resource acquisition. Water and food resources are impacted by more efficient desalination membranes which use nanotechnology. Food products might also be modified to grow more effectively in stresses conditions like excess heat or draught conditions. Nanotechnology would is being applied in many ways to health care but might specifically applied to GCC in suntan lotions.

Results / Conclusions

New approaches to decision analysis under uncertainties, such as real options analysis (ROA), might provide a tool to evaluate various strategies. The uncertainties come from the uncertainty in nanoparticles regulations, GHG impacts and regulations, the economic uncertainties, and alternative competitive technologies. ROA has been applied to public research assessment in an effort to try to determine whether decision techniques such as a real options analysis approach might be suitable for this large public investment. On a smaller scale, commercial organizations have applied real options analysis to gain better understanding of research investments under large uncertainties. Options analysis includes accounting for future options such as deployment, abandonment, or continued research. As such it views research as an insurance policy against potential uncertain conditions such as the impacts of global climate change. Such an analysis could lead to better understanding and decision making concerning the public role of governments to speed learning curves, develop shared basic information, and correct environmental externalities.

References

U.K. Department for Environment, Food, and Rural Affairs, "Environmental Beneficial Nanotechnologies: Barriers and Opportunities" in May 2007 Available at <http://www.defra.gov.uk/environment/nanotech/policy/pdf/envbeneficial-report.pdf>

Smalley, Richard, "*Our Energy Challenge*," Columbia University Nanoscale Science and Engineering Center Presentation, September 23, 2003, available at <http://smalley.rice.edu/>

Ausubel, Jesse H., "Will the rest of the world live like America" *Technology in Society* 26 (2004)343- 360 available at http://phe.rockefeller.edu/PDF_FILES/LiveLikeAmerica.pdf

U.S. Climate Change Technology Program, Strategic Plan, September 2006, available at <http://www.climatechange.gov/stratplan/final/index.htm>

U.S. Climate Change Science Program Strategic Plan, July 2003, available at: <http://www.climatechange.gov/Library/stratplan2003/final/default.htm>

Siddiqui, “Real Options Valuation of US Federal Renewable Energy Research, Development, Demonstration, and Deployment”, <http://www.osti.gov/energycitations/servlets/purl/860783-3a2DPb/860783.PDF>

Photocatalytic Degradation of 4-chlorophenol Using New Visible Light Responsive $\text{ZrTiO}_4/\text{Bi}_2\text{O}_3$ Nano-Size Photocatalysts

B. Neppolian, Evrim Celik, and H. Choi, Department of Environmental Science and Engineering, Gwangju Institute of Science and Technology. Buk-Gu, Gwangju, South Korea

Abstract

$\text{ZrTiO}_4/\text{Bi}_2\text{O}_3$ visible light photocatalysts were synthesized by the ultrasonic assisted hydrothermal method. The absorption of the catalysts towards visible region of light was increased with increasing calcination temperature until 450 °C and then decreased. Around 7 nm size particles were formed during this combined method of preparation. ZrO_2 present in $\text{ZrTiO}_4/\text{Bi}_2\text{O}_3$ could be able to control the size of the particles. The photocatalytic activity was measured with 4-chlorophenol (4-CP), among the different calcined catalysts, 450 °C calcined catalysts exhibited profound effect on the degradation of 4-CP than the other calcined catalysts, including P-25 degussa catalysts. This new visible light photocatalysts can work efficiently under the visible region of light and proved to be one of the best photocatalysts for the commercial application studies.

Introduction

Chlorophenols are highly toxic, and hazardous compounds, normally present in soil, water and wastewater as persistent pollutants because of its non-biodegradable nature. Chlorophenols are widely used as herbicides, pesticides, and wood preservatives which are the main sources of chlorophenols. Among the different chlorophenols, 4-chlorophenol (4-CP) is commonly found in the wastewater of pulp and paper, pharmaceutical and dyestuff industries (1).

Many physicochemical methods have been employed for the safe removal or degradation of chlorophenols. However, each method has its own limitations. Heterogeneous photocatalysis has been considered to be one of best methods under the Advanced Oxidation Technologies (AOTs) for the efficient treatment of water, wastewater as well as air pollution. The main advantage of the heterogeneous AOTs is the complete degradation (oxidation) of organics into CO_2 and water along with mineral acids within a short period of time without leaving any other solid wastes (2).

Utilizing naturally available solar energy is a main focus in the near future, not only for facing the future energy demand but also for the complete degradation of pollutants using visible light responsive photocatalysts (2). In this regard, we have synthesized new $\text{ZrTiO}_4/\text{Bi}_2\text{O}_3$ nano-size photocatalysts which could be able to work under the visible light irradiation more effectively than the other commercially available catalysts.

Methods

$\text{ZrTiO}_4/\text{Bi}_2\text{O}_3$ nanoparticles were synthesized by ultrasonic assisted hydrothermal method in which bismuth nitrate hydrate, titanium tetra isopropoxide (TTIP) and a Zirconium (IV) isopropoxide isopropanol complex were used as precursors for Bi_2O_3 , TiO_2 and ZrO_2 , respec-

tively. The $\text{ZrTiO}_4/\text{Bi}_2\text{O}_3$ photocatalysts were characterized by X-ray diffraction studies (XRD), X-ray photo-electron spectroscopy (XPS), Diffuse reflectance spectroscopy (DRS), photoluminescence (PL) and TEM instruments. The photocatalytic activity was compared by the reaction rates for the oxidative degradation of 4-chlorophenol (4-CP). The photocatalyst (300 mg) was suspended in a quartz cell with an aqueous solution of 4-CP (1.25×10^{-4} M, 200 mL).

Results and discussion

$\text{ZrTiO}_4/\text{Bi}_2\text{O}_3$ nano-size photocatalysts were synthesized by ultrasonic assisted hydrothermal method. The prepared $\text{ZrTiO}_4/\text{Bi}_2\text{O}_3$ catalysts were calcined from 400 to 600 °C for 3 hrs and characterized by XRD, DRS, TEM, PL, BET and XPS instruments. These characterization studies were carried out to understand the nature of the catalysts for the photocatalytic degradation of organic pollutants.

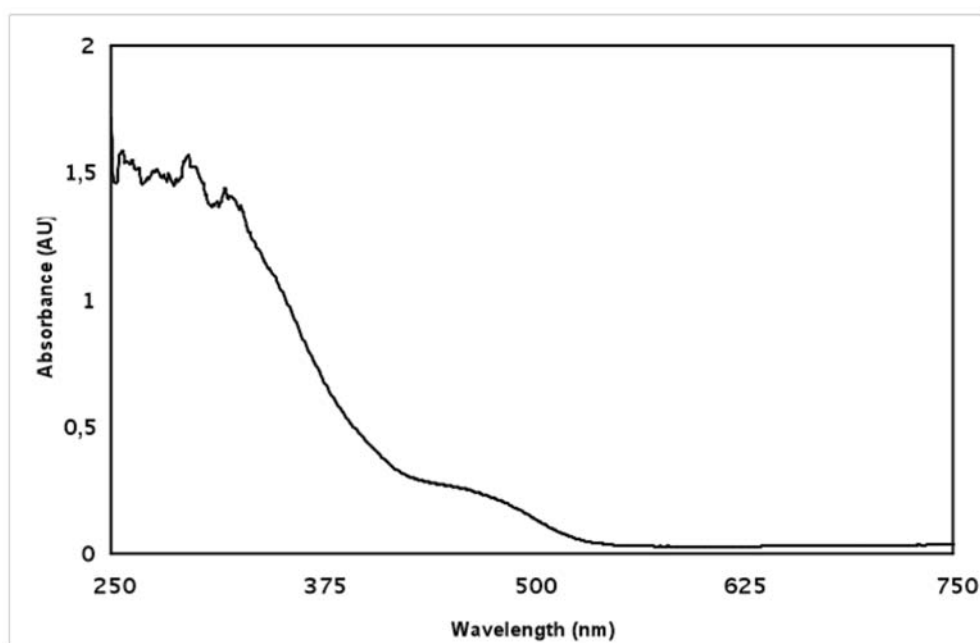


Figure 1. UV-Vis adsorbance spectra of $\text{ZrTiO}_4/\text{Bi}_2\text{O}_3$ calcined at 500 °C.

Figure 1 shows the absorbance spectra of $\text{ZrTiO}_4/\text{Bi}_2\text{O}_3$ mixed oxide photocatalysts calcined at 500 °C measured by diffuse reflectance spectroscopy, as a representative spectrum among other different calcined catalysts. It can be seen from the Figure 1 that there is a shift of absorption towards longer region of light (red shift) which is similar to the chemical doping of metals on TiO_2 photocatalysts (3). The absorption region of the mixed oxide photocatalysts was extended to the visible region, the maximum peak at visible region absorption was occurred at 450 nm and it extended until 561 nm. So that the Bi_2O_3 can effectively absorb (harvest) visible light and transfer the photo-formed electrons to the conduction band of TiO_2 . This combined mixed oxide photocatalysts could effectively prevent the electron-hole recombination of Bi_2O_3 (which is one of the main drawbacks of photocatalysts) and work significantly well than the bare photocatalysts (TiO_2 , Bi_2O_3 and ZrO_2).

The calculated band gap was 2.88 eV for $\text{ZrTiO}_4/\text{Bi}_2\text{O}_3$ at 450 °C calcined catalysts. XPS results evidenced that all the three metals (Ti, Bi and Zr) were exhibited in their oxides states. This result emphasized that there was no strong chemical interaction among the metals, and they just existed as their oxide forms.

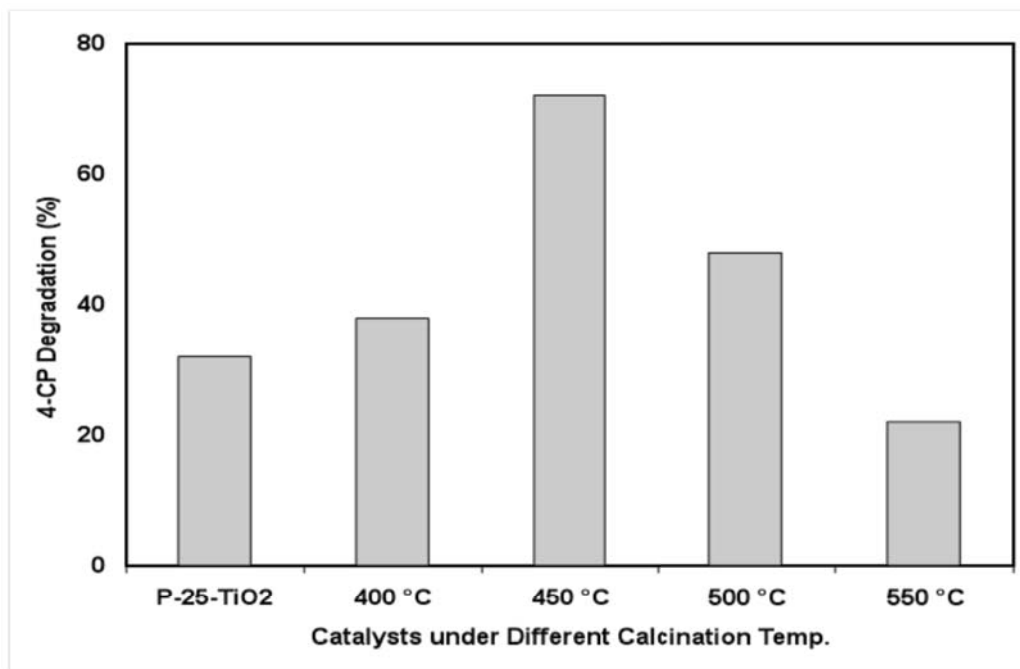


Figure 2. Photocatalytic Degradation of 4-CP under Visible Light Irradiation (3 hr).

Among the different calcined catalysts, 450 °C catalysts showed profound effect on the degradation of 4-chlorophenol in comparison to the other catalysts. The Figure 2 clearly shows the efficiency of the $\text{ZrTiO}_4/\text{Bi}_2\text{O}_3$ catalysts for the degradation 4-CP. High efficiency of 450 °C calcined $\text{ZrTiO}_4/\text{Bi}_2\text{O}_3$ photocatalysts is due to the nano-particle size (~ 7 nm), high crystallinity, high surface area of the catalysts as well as a strong absorption towards visible region of light than the other calcined catalysts. All these factors were responsible for the higher degradation of 450 °C calcined catalysts than others. Around 72 % degradation of 4-chlorophenol was achieved within 3 hrs irradiation, whereas, other catalysts including commercially available photocatalysts such as, P-25 showed less degradation. This new nanosize visible light responsive second generation $\text{ZrTiO}_4/\text{Bi}_2\text{O}_3$ photocatalyst may be an alternate and efficient catalyst for the degradation of organic compounds by utilizing visible light irradiation.

Conclusions

$\text{ZrTiO}_4/\text{Bi}_2\text{O}_3$ photocatalysts prepared by ultrasonic assisted hydrothermal method is proved to be an efficient visible light responsive photocatalysts for the effective degradation of organic pollutants within a very short period of time. Even though, the catalysts prepared by hydrothermal method, further calcination process at high temperatures only could induce well crystallization processes and bring the catalysts for catalytic application studies, which was proved by XRD patterns and other characterization studies. In addition to absorption of light towards visible region of light, particle size, surface area and morphology played significant roles for the complete

degradation of organic pollutants such as 4-CP.

References

- 1) Neppolian, B., Jung, H., and H. Choi. (2007). "Photocatalytic Degradation of 4-Chlorophenol Using TiO_2 and Pt- TiO_2 Prepared by Sol-Gel Method." *J. Adv. Oxidn. Techs.* 10, 369–374.
- 2) Anpo, M., (2004). "Preparation, characterization, and reactivities of highly functional titanium oxide-based photocatalysts able to operate under UV-visible light irradiation: Approaches in realizing high efficiency in the use of visible light." *Bull. Chem. Soc. Jpn.* 77, 1427–1442 and other references cited therein.
- 3) Yamashita, H., Harada, M., Misaka, J., Takeuchi, M., Neppolian, B., and M. Anpo. (2003). "Photocatalytic degradation of organic compounds diluted in water using visible light-responsive metal ion - implanted TiO_2 catalysts: Fe ion - implanted TiO_2 ." *Catal. Today* 84 (3–4), 191–196.

Chapter 3 – Introduction

Nanotechnology-Enabled Sensors & Monitoring

Heather Henry, National Institute for Environmental Health Sciences

The unique properties of nature found at the nanoscale present a tremendous opportunity for developing new signal, receptor, and transmission technologies, all giving rise to a new field of devices known as nanotechnology-enabled sensors. Nanotechnology can improve the performance of existing macrosensors or serve as a platform for extremely small sensing devices (nanosensors). Researchers from a variety of disciplines convened to share scientific and technical advances of environmental nanosensor development, to explore the overall net benefit of these approaches, and to identify challenges to come.

The session included a plenary by Dermot Diamond, followed by six presentations in the breakout session by Li Han, Ryan Westafer, Am Jang, Ian Kennedy, Hatice Sengul, and Ashok Vaseashta. The session concluded with a panel discussion on the future directions of nanosensors, which included all speakers as well as Glen Fryxell and Marie-Isabelle Baraton, both plenary speakers from other sessions.

The breadth of research presented provided an example of the many types of applications for which nanotechnology-based sensors are being developed: national security (ricin detection), pollution detection (air and water, ozone, particulate matter), exposure detection (e.g. farm worker exposure to pesticides), and other uses such as for assessing site characteristics such as oxidative reductive potential (useful to assess success of groundwater bioremediation applications), DNA detection (to verify presence of MTBE degrading bacteria in contaminated aquifers, and to screen for genetic diseases in humans).

There are many advantages to utilizing nanotechnology-based sensors as opposed to devices that rely on micro-scale technologies or phenomena. Portability is perhaps the most widely identifiable benefit to nanosensing devices; however, analyte specificity is a critical sensing quality that may be best achieved by functionalization of a specific group or chemical and allows for detection of compounds at zeptomolar concentrations. Other practical advantages, such as requiring minimum sample volume to conduct a reading, complement high throughput analyses and allow for rapid processing of samples.

Researchers also highlighted a variety of design features that are critical to nanosensor utility and are currently under development:

- Wireless – enabling internet monitoring
- Battery-less – allowing widespread placement of sensors
- Interchangeable detectors – allowing one device (hardware) to be used for multiple applications
- Multiplexing – enabling a single transmitted signal to convey multiple parameter readings

In addition to the features mentioned above, some sensors are being designed to be part of network to send signals to centralized networks or to authenticate readings from other devices, such as satellites.

Frequently, new sensor capabilities are being created solely as a proof of concept. These so-called “Chip in a Lab” devices are relegated to the laboratory because there is no real world application. Though there is merit to this discovery process, the suggestion was made that it would be better to work backwards from device application, optimizing the design from the beginning. For example, devices intended for widespread environmental use should be designed to be battery-less. Without these considerations, transfer of technologies to venture capitalists will be limited and the advancement of the technology may be hindered.

Common technical challenges for environmental applications of nanosensors included maintaining device shelf life, integrity in environmental matrices, and calibration; however, these issues are not necessarily unique to nanosensors.

The future direction of nanosensors was discussed, receiving input from representatives of academic researchers, industry, and government. Scientifically, advances in materials sciences are needed to develop the most efficient power-scavenging technologies for battery-less sensors, critical to large-scale use of nanosensors. There was an awareness of the importance of making devices sustainable – both in terms of economic as well as environmental sustainability (e.g. utilizing non-toxic components for certain applications, considering end-of-life disposal issues, etc.). Furthermore, it was recognized that there is tremendous potential to optimize sensors on all these matters using Life Cycle Analysis (LCA) software such as SimaPro and EcoInvent; however, there are few such studies on nanosensors to date. Researchers also expressed an interest in conducting toxicity studies in parallel with technology development to test the safety of nanosensors for certain applications; however, this was identified as a research funding need. It was also mentioned that risks of exposure to nanoparticles resulting from nanosensing devices is likely to be limited due to particle aggregation.

Current, Emerging and Future Technologies for Sensing the Environment

*Dermot Diamond, CLARITY, The Centre for Sensor Network Technologies,
National Centre for Sensor Research, School of Chemical Sciences,
Dublin City University, Dublin, Ireland*

Abstract

This paper reviews current technologies that are used for environmental monitoring, and presents emerging technologies that will dramatically improve our ability to obtain spatially distributed, real-time data about key indicators of environmental quality at specific locations. Futuristic approaches to environmental monitoring that employ fundamental breakthroughs in materials science to revolutionise the way we monitor our environment will also be considered. In particular, approaches employing biomimetic and ‘adaptive’/‘stimuli-responsive’ materials will be highlighted, as these could play an important role in the realization of small, low power, low cost, autonomous sensing and communications platforms that could form the building blocks of the much vaunted environmental ‘sensor web’.

Introduction

Around the world, the ability to monitor environmental status is now a priority for many countries. The prioritisation of environmental monitoring has been driven by a number of factors including climate change, recognition of the importance of the environment for sustainable economics, linking of environmental monitoring with threat detection and the implementation of an array of European Union environmental directives by Member States. The ability to accurately determine ‘environmental status’ is the prerequisite for quantifying environmental change, or for detecting pollution events in their early stages. Without this ability, it is impossible to implement policies aimed at improving the status of our environment, and the potential to waste enormous resources by Governments through ineffective or misguided policies is very real. There also is a need to define what we mean by environmental status, and whether this status is ‘good’ or ‘bad’, or whether the status is changing. For example, key indicators must be identified and tracked, both spatially and temporally, and status windows defined to enable ‘within specification’ or ‘out of specification’ conditions to be detected. When implemented at ‘internet-scale’ globally, this gives rise to the concept of the ‘environmental nervous system’ – a system that constantly monitors the status of our environment and can respond rapidly to sensed events through complex feedback loops to specialists, communities, individuals, control actuators etc.

This concept is clearly massive in scale, and its implementation requires many sensing modalities to be harnessed collectively in order to access the required analytical information. The term ‘internet-scale’ is appropriate as, in a way, what needs to be delivered is a sensor web, that is intimately woven into the existing internet, continuously gathering, filtering and interpreting sensed information relevant to the environment, detecting unusual patterns, classifying events, locating geographical locations and dynamics of these events, and ideally, predicting events and organising appropriate action in advance of any major environmental damage.

Now, the scale of this vision is truly enormous, and its realisation is still well beyond the current state-of-the-art. Perhaps the best-developed means of doing global scale sensing of environmental parameters is through satellite imaging. In recent years, the employment of specific spectroscopic probes for key target gases in the atmosphere has augmented the familiar weather information related to pressure fluctuations, temperature, cloud cover and rainfall activity. The coupling of widely distributed geographical coverage with specific molecular information enables the distribution of chemical targets to be monitored and variations mapped as a function of location and time. These fluctuations can be linked further to specific activities (e.g. to identify the source(s)) and to weather conditions (e.g. to understand the dynamics). Figure 1 shows the geographical distribution of averaged NO₂ levels over Ireland and part of Britain measured by the SCIAMACHY instrument on the Envisat satellite during April 2008. SCIAMACHY is an imaging spectrometer whose primary mission objective is to perform global measurements of trace gases in the troposphere and in the stratosphere [1]. During these measurements, the atmospheric column directly under the satellite is observed, with each scan covering an area on the ground of up to 960 km across the satellite track with a maximum resolution of 26 km x 15 km. The data, presented to the user as GIS coordinates with an accompanying NO₂ concentration value (in molecules per cm²), is imported into a 3-d visualisation program which is used to generate a colour contour plot and the resulting image mapped onto the appropriate region.

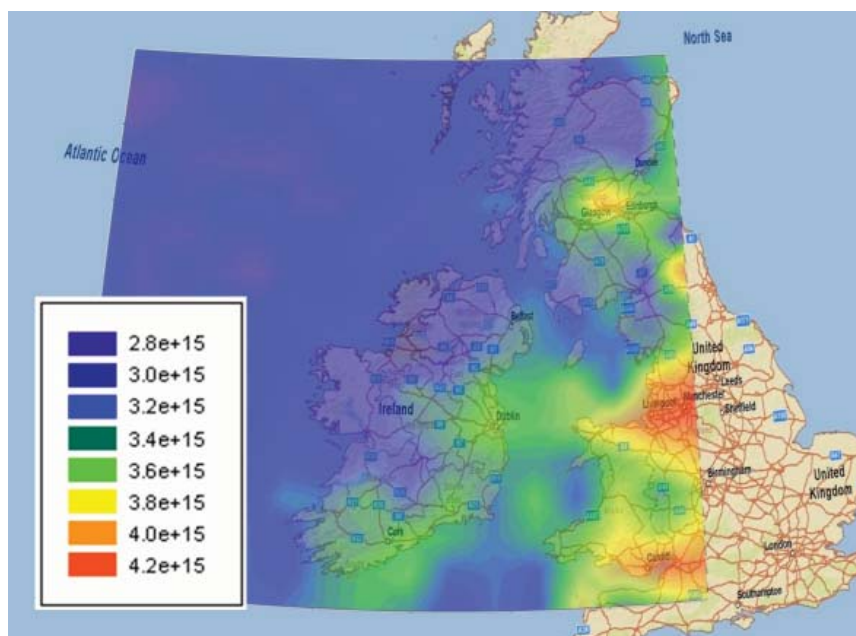


Figure 1. Average atmospheric levels of NO₂ over Ireland/UK during April 2008 measured by the SCIAMACHY instrument on the Envisat satellite. In this example the atmospheric volume directly under the satellite is observed. Each scan covers an area on the ground of up to 960 km across track with a maximum resolution of 26 km x 15 km. The NO₂ concentration scale unit is in molecules per cm². The concentration distribution image is generated by importing the European Space Agency data into Sigmaplot and generating a semi-transparent colour contour plot, which is then superimposed on the area map.

From Figure 1 it can be concluded that elevated levels of NO₂ are associated with heavily industrialised areas in the UK around South Wales and the Midlands, and Glasgow in Scotland. In

contrast, levels in Ireland are in general much lower, although there is evidence of higher levels around Dublin and on the east and south coasts. Similar approaches have been used to track SO₂ plumes originating from Mount Etna (Sicily) moving across Italy to Greece and Turkey, following a series of eruptions in May 2008 [2]. Satellite imaging can also be used to track the general quality of large water bodies. For example, Figure 2 shows the distribution of algal blooms off the west coast of Ireland in 2006 [3].

Clearly satellite-based imaging techniques can provide very useful information that can enable certain aspects of air and water quality to be monitored dynamically over large geographical areas. The ideal situation would be to augment the satellite-based information with data obtained from widely distributed surface deployed sensors, as through the latter we can obtain very specific and precise information about air and water chemistry/biology at particular locations. Hence, chemo/biosensors provide very complementary information to that obtained via satellite measurements. What is needed, therefore, are chemo/biosensors deployed in massive numbers at multiple locations, i.e. internet-scale environmental sensor web [4]. It follows, therefore, that massive scale-up in terms of the numbers of deployed sensors must happen, and these must be capable of integrating into existing communications infrastructure. However, massive scale-up implies that the cost base of the basic sensor/communications building blocks (sometimes referred to as sensor motes/nodes [5]) must be very low, and indefinitely self-sustaining [6].

Current Approaches and Emerging Technologies

From the above discussion, the ideal scenario for the realisation of a functioning environmental nervous system based on collaborative information harvesting from satellites and from extensive ground-based sensor network deployments. The problem is that the chemo/bio-sensor networks do not exist. The reason is simple but very difficult to overcome. The cost of ownership in terms of initial capital outlay and ongoing running costs is far too high. This, in turn, arises from the relatively complex mode of operation of these devices, compared to their better behaved and lower cost physical sensor cousins (thermistors, piezo-vibration sensors, light intensity detectors, etc.). Generally speaking, chemo/bio-sensors employ some kind of molecular recognition event (enzyme-substrate, ligand-ion), which is coupled with a transduction mechanism to generate (ideally) a molecule-specific signal that can be detected. Typically, these molecular recognition agents are immobilised on a surface or within a membrane that is housed in some type of sensor head or probe that is exposed to the sample. The sensor's task when immersed in the sample environment is to provide information about the chemical or biological composition of the sample through these tailored molecular binding events. The problem is that the sensor surface must therefore be 'active' in that these binding events must occur, and the sensitive molecular binding sites must be intimately exposed to the sample, which more often than not contains many components that can interfere or passivate this active surface. Therefore, it is not surprising that in order to function properly, chemo/biosensors need regular calibration and cleaning/servicing, which drives up the cost and complexity of these devices, and making large-scale deployments prohibitively expensive and difficult. For example, chemical analysers cost in the region of €5K-€50K, depending on the types of measurements being made [7].

It is understandable, therefore, that most chemical and biological water quality measurements

still involve taking samples manually which are analysed subsequently at centralised laboratory facilities using very sophisticated bench-top analytical instruments. One way to tackle this issue of how to maintain acceptable analytical performance with field-deployable systems is to employ microfluidic manifolds through which manual operations like sampling, sample processing, analytical measurement, and calibration can be integrated. These manifolds, when further integrated with electronics, fluid handling, and wireless communications, provide a route towards high performance, field deployable analytical instruments with a more acceptable cost base (€500-€5,000). For example, Figure 2 shows an instrument we have developed for the field deployment of nutrients such as phosphate in natural waters. The analyser is based on colorimetric methods that employ a reagent that reacts selectively with a target species (in this case, the yellow method for phosphate detection), with the resulting colour being detected using a low cost, low power LED-photodiode system [8,9,10]. The analyser performs 2-point calibrations (0 mg/l and 10 mg/l phosphate) at user-defined intervals, and can be left in-situ for several months unattended. Power is provided by an integrated lead-acid battery which can be augmented by a solar panel if required.

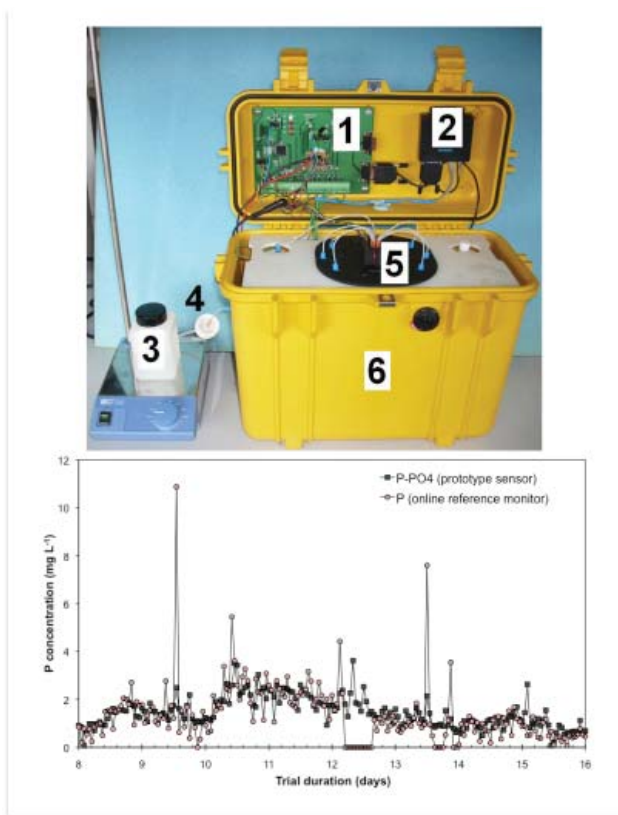


Figure 2. Top - the phosphate analyser during a typical laboratory trial. (1) Control board and data storage (2) GSM modem for transmitting data (3) Sample container (4) Sample filter (5) Microfluidic chip / detector assembly (6) Ruggedised container with storage space for reagent, calibration solutions, waste and power supply (12 V lead-acid battery). This is typical of the current form factor of analytical instruments designed for remote autonomous deployment in environmental monitoring situations.

Figure 2. Bottom - typical results generated during part of a 44-day trial at a waste-water plant. The prototype system data (squares) in general are in excellent correlation with the commercial reference system (circles), and the phosphate levels are typically below 4 mg mL⁻¹. High levels recorded with the reference system at ca. 9.6 days and 13.5 days are correlated with the presence of solid waste in the samples, which is filtered out by the prototype system but not by the commercial system. The baseline signals at ca. 12.2-12.6 days and around 13.6-14.0 days coincided with the reference system being down for servicing.

The data shown are a subset of results generated during a 44-day trial during June-August 2008 at a wastewater treatment plant (days 8-16 shown). Some features are immediately apparent; for example, the data is generally in excellent agreement with the plant's existing on-line monitoring reference system (Aztec P100, Capital Controls, UK), showing that the prototype analyser is capable of generating accurate analytical data. The analyser is completely autonomous, and in this particular trial, measured the phosphate level on an hourly basis, transmitting the data using SMS text messaging every 5-hours. There are occasional issues with bubbles that cause spikes in the prototype system detector output, but these can be easily filtered out from real analytical data using appropriate software algorithms. Also, spikes appear in the reference system due to solids that are digested within the instrument and add to the phosphate concentration, whereas these are physically filtered out in the prototype analyser.

Futuristic Approaches – The Role of Nanomaterials

Using similar approaches we have also built and field trialled autonomous systems for analysing greenhouse gas emissions from landfill sites (using IR sensors for CH₄ and CO₂) and for monitoring dust in air based on a portable XRF detector and in-house developed dust sampling unit (to detect a range of toxic metals). However, these platforms, while useful advances on available technology, are still too expensive and conventional to bring to 'internet scale' in terms of deployments. The price performance index still needs to be driven down by orders of magnitude, and this will require truly innovative thinking and fundamental breakthroughs that can only emerge from basic materials science. One approach we have been focusing on for the past few years is the development of materials that can switch between radically different sets of characteristics. This 'switchable' behaviour can extend across differences in colour, polarity, porosity, permeability, physical dimensions (expand, contract), chemical activity (active, inactive), and so on. Switching can be triggered using light, electrochemical potential, or local chemistry (e.g. pH). The motivation underlying this research effort is the realisation that next generation analytical platforms and sensors need to be much more sophisticated than existing devices, and this sophistication will emerge through control of materials behaviour at the molecular level. Two material types we have been focusing on are conducting polymers and photo-responsive 'spiropyrans'-type compounds.

With the conducting polymers, we have focused to a large extent on producing building blocks of next generation fluidic platforms that incorporate soft polymer actuators as the active basis for pumps and valves that are biomimetic in nature, rather than the conventional engineered micro-components employed in most microfluidics research. In contrast to these conventional components, soft-polymer actuators are low power, and less prone to malfunction due to particu-

late ingress. Figure 3 shows two subunits we have developed, a switchable mesh-valve structure [11] and a biomimetic polymer pump [12,13]. Integration of structures like these into circulation systems could lead to new fluidic platforms that are reliable, low-cost, and fully compatible with small, compact design formats. The incorporation of simple circulatory systems in analytical instruments is an attractive approach to adopt, as it enables more flexibility in terms of sensing strategy. Conventional chemo/bio-sensors tend to employ sensitive surfaces or membranes that have specific molecular receptors immobilised in such a way that they interact with the sample and generate a signal. Unfortunately, these surfaces, being active in nature (as they must interact with the sample at the molecular level), begin to change immediately on exposure to the real world. For example, the binding sites may become occupied or rendered inactive by fouling or strong interactions with sample components other than the species of interest. This gives rise to drift and loss of response sensitivity, and regular calibration is therefore a primary requirement if the sensor data is to be reliable.

In remote locations, this in turn means that the instrument must include all reagents and standards required to maintain the sensor within calibration. Pumps and valves drive up the price and power demand and limit scalability. Hence biomimetic approaches to fluid handling could simultaneously keep cost and complexity down, while still enabling the instruments to be calibrated. Furthermore, if chemo/bio-sensors are employed to generate the signal, they can be housed within the microfluidic platform rather than being exposed to the real world, which can help extend lifetime. Alternatively, reagent based approaches can be employed, as in the case of the phosphate instrument mentioned above, which opens up methods and approaches that are not possible using probe-type devices that are directly exposed to the sample.

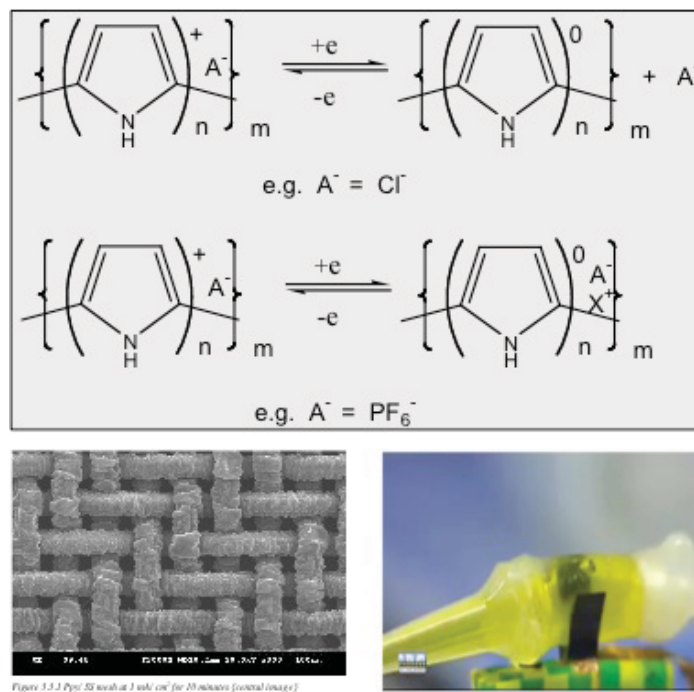


Figure 3. Top – polypyrrole can be reversibly switched between oxidised (positive) and reduced (neutral) forms by addition/removal of electrons. To maintain charge neutrality, ions move into/out of the polymer. This dramatic change in the local electrostatic environment is accompanied

by movement of associated water of hydration in/out of the polymer. Overall this results in swelling/contraction of polymer.

Middle (left) – Polypyrrole deposited on a stainless steel mesh substrate with a pore size ca. 20 μm , with the pore size dependent on the underlying mesh dimensions and the amount of polymer deposited. Switching the polymer through its redox cycle makes the average pore size expand and contract, which in turn enables the flow rate through the mesh to be controlled. Control of the nanostructure of the polymer (e.g. through modification of the monomer structure and polymerisation process) coupled with control of micro-scale structure (e.g. through the substrate configuration) is vital for tuning the behaviour of the bulk material.

Middle (right) – a biomimetic pump based on polymer actuator ‘benders’. These are constructed by laminating two polymer strips with an intermediate insulating, flexible porous layer and configuring the two polymer strips to actuate in opposite manner (one expands when the other contracts) to produce a bending effect. In this case, the effect is used to drive liquid from a chamber. Cycling through the polymer redox states results in a pumping effect reminiscent of a heart. Improvements in the efficiency of such structures requires a fundamental knowledge of the molecular basis of the mechanisms underpinning the macro-scale device.

While microfluidics and ‘lab-on-a-chip’ systems are a very attractive route to realising some degree of scale-up for distributed environmental monitoring, they still suffer from some inherent limitations. For example, reagents and standards will eventually be consumed or degraded, and devices will have to be replaced or serviced, even though scaling down the fluidic system results in dramatic reductions in the volume of reagents required for extended periods of operation [14,15].

A radically different approach to the use of highly calibrated sensors is to deploy large numbers of very simple sensors without calibration and to use the response patterns generated to cross-validate decisions. Figure 4 shows fabrication details and responses obtained with a very low cost gas sensor based on LEDs. The chemical response function is obtained by coating the LEDs with a film incorporating a chemo-responsive dye (in this case bromophenol blue immobilised in ethyl cellulose). The sensor and associated electronics have been integrated with a low-cost wireless communications circuit to produce a gas sensor node costing ca. €10. Despite its simplicity, this device has surprisingly good response characteristics, with the LOD for acetic acid in the mid-ppb range, excellent dynamic response (seconds) and reproducibility. We have used clusters of these simple sensors to detect not only that an acid plume has been released, but also to identify the likely source, and estimate the dynamics of plume movement [16].

However, these sensors employ relatively well-known and simple sensing approaches based on chemo-responsive dyes that have been known for decades. More recently, we have begun to work with dyes that can be switched between an inactive (non-binding) form and an active (binding) form using light [17,18]. For example, spiroopyran derivatives can be reversibly switched between the spiro (SP) form which is chemically inactive, and an active merocyanine (MC) form which is chemically active, using UV and white/green light, respectively (see Figure 5). Furthermore, the system is inherently indicating, as MC is strongly coloured (purple) while SP is colourless. The MC form is also strongly charged (zwitterionic) while the SP form is

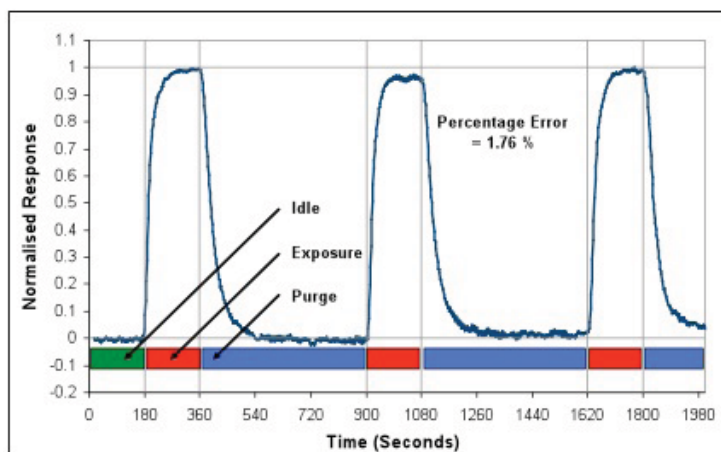
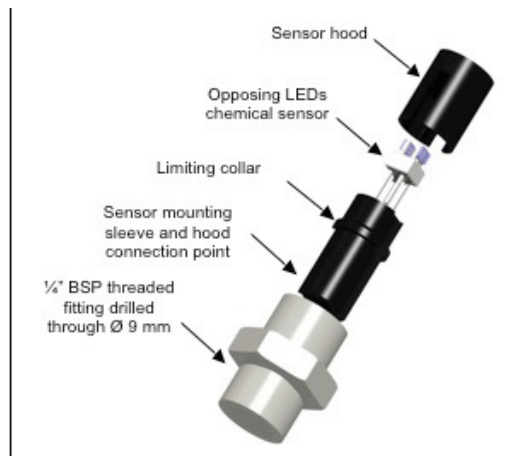


Figure 4. Top: Fabrication details for low-cost gas sensor based on LEDs coated with a film incorporating a chemo-responsive dye. Exposure to an acidic plume causes the dye colour to change which modulates the light flux between the LED emitter and a reverse-biased LED detector. The light flux is monitored by the time taken to photo-discharge a set voltage on the reverse biased LED. A critical challenge with such devices is the need to produce batches with more-or-less identical response characteristics (to reduce the need to calibrate). This in turn requires ****

Bottom: Response of the coated LED chemical sensor node to three consecutive exposures of 1 mg/l acetic acid vapour. Note the very rapid response and recovery, and excellent sensitivity and reproducibility.

uncharged. The MC form has been shown to bind certain metal ions and interact with amino acids [19], with the binding also indicated by new absorbance bands in the visible region. The binding can also be reversed using light, with white or green light causing the guest species to be expelled and the inactive SP form to be regenerated.

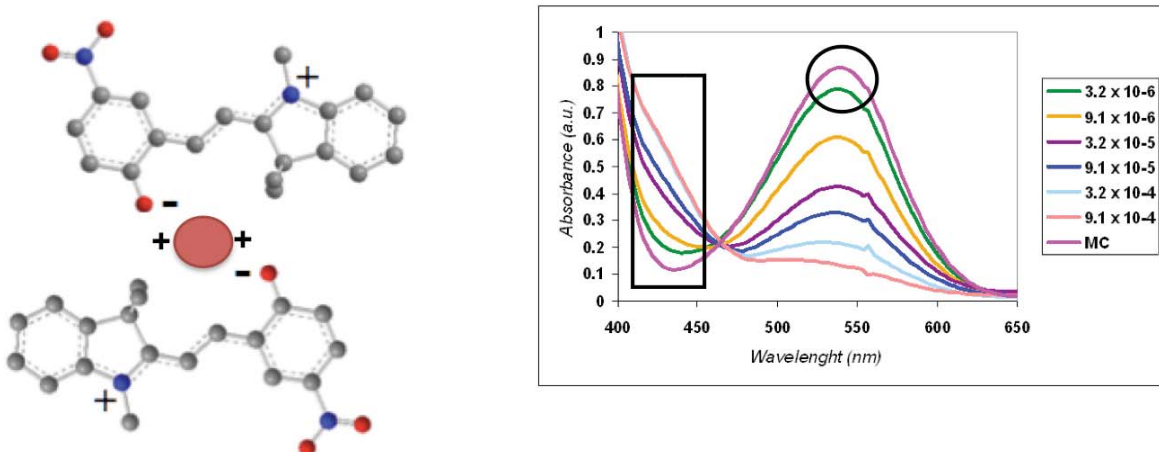


Figure 5. Left: Merocyanine forms a 2:1 sandwich-like complex with certain metal ions like Cu^{2+} and Co^{2+} , but the spiropyran form is inactive and does not interact with the metal ions.

Right: Spectral changes accompanying Cu^{2+} binding by merocyanine. The strong MC absorbance (λ_{max} ca. 540 nm) reduces in intensity and a new band associated with the complex simultaneously appears in the region 400-440 nm, with an isosbestic point at ca. 460 nm. Tuning of this behaviour requires careful optimisation of the surface nanostructure, and in particular, the tether length of the binding sites from the surface.

For sensor researchers, systems like SP-MC offer intriguing possibilities for the development of relatively simple sensing devices that nonetheless could possess sophisticated characteristics. For example, the sensing surface could be held in a passive form until a measurement is required. An external stimulus (UV light in this case) is used to generate the active form, which interacts with the sample, generating the signal in the process. Upon completion of the measurement, an external stimulus is used to expel the bound molecules from the surface, and regenerate the passive form (white or green light in this case). As each state has a different absorbance spectrum in the visible region, it can also report its status to the external world (i.e. whether it is in the active-free, active-bound, or passive states). We have shown that drift can be easily distinguished from a genuine response by monitoring the film's colour using clusters of LEDs, enabling a degree of self-diagnostics to be built into the measurements [20].

Conclusions

It is likely that in the near future, combinations of relatively simple sensors like these with more sophisticated calibrated devices will be deployed to provide a much more information-rich environmental monitoring capability than is currently available. This, coupled with satellite measurements, will enable our environment to be monitored dynamically on a global scale. However, if the visions of 'internet-scale sensing' and the 'environmental nervous system' are to be truly realised, it will require a well-coordinated, multidisciplinary global research effort that encourages linkages between established teams through multi-national programmes sponsored by agencies.

It also must integrate much more effectively research in fundamental materials science, analytical/sensor science, environmental science, instrumentation engineering, and satellite imaging, and bring together academic, governmental and industry research teams in a combined effort to drive the science and technology of distributed environmental monitoring forward. The pieces are already in place – now it is time to bring them together, and, as we know from thermodynamics, this will require effort and energy if it is to happen!

Acknowledgements

The author would like to acknowledge funding from Science Foundation Ireland under the CLARITY CSET initiative, and from the Irish Marine Institute and Irish Environmental Protection Agency, through the Smartcoast and other project awards. We also acknowledge support from Enterprise Ireland for the development of the nutrient analyser platform and phosphate sensor. I also wish to acknowledge the assistance of group members Stephen Beirne, John Cleary, Alexandar Radu and Jer Hayes in the preparation of this manuscript.

References

1. For more background on SCIAMACHY and its capabilities, see the European Space Agency website <http://envisat.esa.int/instruments/sciamachy/> (last visited August 2008).
2. See www.dlr.de/en/desktopdefault.aspx/tabid-1/86_read-12536/ for data generated by the atmospheric sensor GOME-2 (Global Ozone Monitoring Experiment) on the EUMETSAT satellite, MetOp-A, last visited August 2008.
3. See <http://geology.com/nasa/marine-phytoplankton.shtml>, last visited August 2008.
4. Internet Scale Sensing, Dermot Diamond, *Analytical Chemistry*, 76 (2004) 278A-286A.
5. Michael P. Hamilton, Eric A. Graham, Philip W. Rundel, Michael F. Allen, William Kaiser, Mark H. Hansen, Deborah L. Estrin. “New Approaches in Embedded Networked Sensing for Terrestrial Ecological Observatories,” *Environmental Engineering Science*, 24, No. 2, pps. 192-204, March 2007.
6. Integration of Analytical Measurements and Wireless Communications – Current Issues and Future Strategies, Dermot Diamond, King Tong Lau, Sarah Brady and John Cleary, *Talanta* 75 (2008) 606-612.
7. Wireless Sensor Networks and Chemo/Bio-Sensing, Dermot Diamond, Shirley Coyle, Silvia Scarmagnani and Jer Hayes, *Chemical Reviews*, 108 Issue: 2 (2008) 652-679.
8. Autonomous microfluidic system for phosphate detection, Christina M. McGraw, Shannon E. Stitzel, John Cleary, Conor Slater and Dermot Diamond, *Talanta* 71 (2007) 1180–1185.
9. Determination of phosphate using a highly sensitive paired emitter–detector diode photometric flow detector, Martina O’Toole, King Tong Lau, Roderick Shepherd, Conor Slater and Dermot Diamond, *Analytica Chimica Acta* 597 (2007) 290–294
10. An Autonomous Microfluidic Sensor for Phosphate: On-Site Analysis of Treated Wastewater, John Cleary, Conor Slater, Christine McGraw and Dermot Diamond, *IEEE Sensors Journal*, 8

(2008) 508-515.

11. Polypyrrole Based Switchable Filter System, Yanzhe Wu, Lorraine Nolan, Shirley Coyle, King Tong Lau, Gordon G. Wallace and Dermot Diamond, proceedings of the 29th Annual International Conference of the IEEE Engineering in Medicine and Biology Society, Lyon, France, 22-26 August 2007, pp 4090-4091.
12. Biomimetic, low power pumps based on soft actuators, Sonia Ramirez-Garcia and Dermot Diamond, *Sensors and Actuators A* 135 (2007) 229–235.
13. Internet-scale Sensing: Are Biomimetic Approaches the Answer? Sonia Ramirez-Garcia and Dermot Diamond, *Journal of Intelligent Material Systems and Structures*, 18 (2) (2007) 159-164.
14. Progress in the Realisation of an Autonomous Environmental Monitoring Device for Ammonia, Margaret Sequeira, Antoine Daridon, Jan Lichtenberg, Sabeth Verpoorte, N F de Rooij and Dermot Diamond, *Trends Anal. Chem.*, 21 (2002), 816-827.
15. Analysis of River Water Samples Utilising a Prototype Industrial Sensing System for Phosphorus based on Micro-system Technology, Michaela Bowden, Margaret Sequiera, Jens Peter Krog, Peter Gravesen and Dermot Diamond, *J. Environ. Monit.*, 4 (2002) 1–6.
16. Monitoring Chemical Plumes in an Environmental Chamber with a Wireless Chemical Sensor Network, Rod Shepherd, Stephen Beirne, King Tong Lau, Brian Corcoran and Dermot Diamond, *Sensors and Actuators B*, 121 (2007) 142-149.
17. LED Switching of Spiropyran-doped Polymer Films, Shannon Stitzel, Robert Byrne and Dermot Diamond, *J. Mater. Science*, 41 (2006) 5841–5844.
18. Photo-Regenerable Surface with Potential for Optical Sensing, Robert J. Byrne, Shannon E. Stitzel and Dermot Diamond, *J. Mater. Chem.* 16 (2006) 1332-1337.
19. Chemo/Bio-Sensor Networks, Robert J Byrne and Dermot Diamond, *Nature Mater.*, 5 (2006) 422-424.
20. Photonic Modulation of Surface Properties: A Novel Concept in Chemical Sensing, Aleksandar Radu, Silvia Scarmagnani, Robert Byrne, Conor Slater, King Tong Lau and Dermot Diamond, *J. Phys.D; Appl. Phys.*, 40 (2007) 7238-7244.

Nanofiber Sensor Platform for Environmental Pollutant Monitoring and Detection

Li Han, Kim Guzan, Anthony Andraday and David Ensor; RTI International, Research Triangle Park, North Carolina, U.S.A.

Abstract

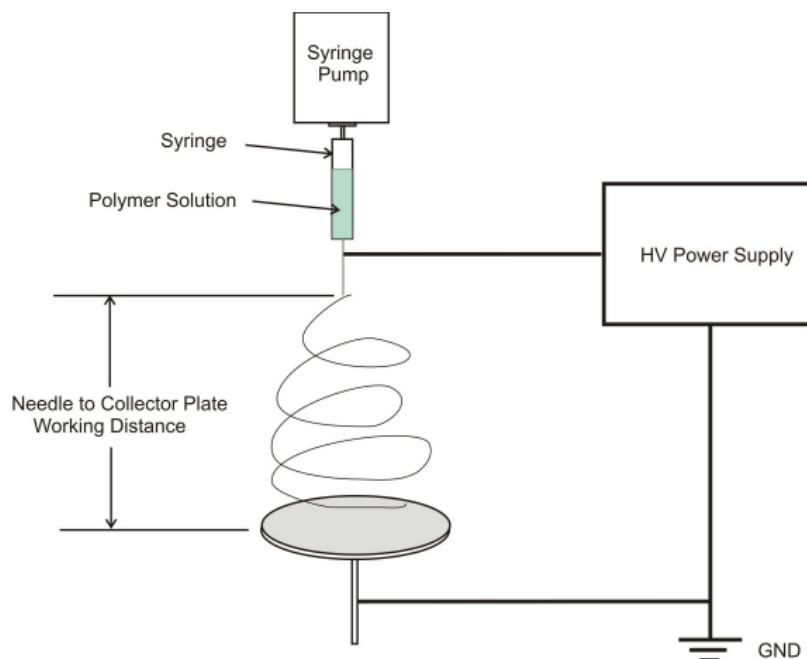
Electrospun polymer nanofiber materials have attracted tremendous interest in sensor applications as their effective sensing surface area dramatically increases with decreasing fiber diameter. The highly tunable polymer composite chemistry and surface functionality of the nanofiber material provides a platform for exploring different applications, such as filtration media, sound isolation materials, and as components within sensors. This paper presents for the first time, a Nanofiber Sensor Platform composed of electrospun polymer/carbon composite nanofibers combined with printed electrodes to form an integrated sensor system for detecting various chemical vapors, including volatile organic compounds and oxidative gases. In this platform, composite polymer nanofibers form the chemoresistor sensing material since the conductivity of these composite sensing materials varies with chemical vapor exposure, including volatile organic compounds (VOCs) and oxidative gases. The novel custom printed metal electrode can be directly deposited onto the surface of the electrospun fiber mat to enhance the contact between the electrode and the fiber mat. The sensor performance exhibits very stable baselines with dramatically reduced noise levels compared to nanofibers deposited on conventional interdigitated electrodes. Furthermore, the sensor response to different vapors shows a linear relationship between conductivity change and vapor concentration in the range of ppb – ppm for some analytes, including methanol at 200 ppb, chloroform at 3.3 ppm and ozone at 250 ppb level.

Introduction

VOCs and ozone are prominent Hazardous Air Pollutants (HAPs) in the outdoor and indoor environment. Between 30 and 70 million workers in the US are routinely exposed to potentially unhealthy working conditions due to poor indoor air quality^[1]. Also, high ambient ozone levels affect 8.4 million adults and 3.1 million child asthmatics living in high-ozone regions of the United States. Diseases such as chronic bronchitis and emphysema are known to be related to ozone levels as well as high VOC levels. Therefore, the development of reliable VOC and ozone sensors that can be used in large field studies is a particular interest. Recently, nanostructure sensing material has emerged as an important candidate for high performance sensing materials. The high specific surface area of the material provide much larger analyte-sensing material interface than planar thin film sensing materials, which leads to improved sensitivity and selectivity. Despite the advantages of these sensing materials, the design of a high sensitivity, high selectivity, wearable and low cost disposable sensor system always remains a challenge. Here we report the recent advances in our lab on Nanofiber Sensor Platform (NSP) using electrospun composite polymer nanofibers (ECPN) as sensing material. Electrospinning is reported to generate nanofibers with well defined surface and bulk structure. The ease of the material fabrication

make it an ideal candidate for a number of different application for large scale production and they have been used in several commercial applications, including filtration, sound proof materials etc. In this study, we choose resistivity detection for our sensor study as the capture of the sensor response can be easily done with either a handheld multimeter or custom designed portable electronics. While the selection of conducting polymer with desired surface and bulk material functionality is rather limited in this study, we fabricate polymer composite sensing material with the incorporation of Single Walled Carbon Nanotubes (SWCNTs) to adjust the conductivity for the composite materials. There are four major advantages: 1) ECPN have much larger surface area than comparable thin film material, thus lead to enhanced sensor sensitivity and selectivity; 2) ECPN can be a platform technology by changing polymer and composite chemistry to suit specific sensing needs; 3) the ECPN sensing materials are highly flexible and gas permeable which enable it to be easily integrated into a portable platform, or even cloth; 4) ECPNs are made of inexpensive starting material (Polymer and conductive additive) and rather simple and highly reproducible nanofiber manufacturing process, the total cost of the sensor system can be very low, thus making it a potential throw away device. Such structural and design advantages make the nanofiber sensor very practical in environmental monitoring applications and allow real time monitoring of a large number of locations in large field studies.

Experimental Design and Materials



Scheme 1. Schematic illustration of the electrospinning apparatus.

Electrospinning

The electrospinning mixture solution of Polymer and SWCNTs was first prepared in organic solvent prior to electrospin. There are three major components for the electrospinning setup, including high voltage power supply, a spinneret (metal needle) and a grounded collector. As

shown in Scheme 1, the metal needle is connected to a high voltage power source that can supply 10 -30 KV. During the electrospinning process, the polymer solution is pumped into metal needle with controlled flow rate of 0.1 – 1.5ml/hr. When the charge accumulated on the polymer droplet at the end needle overcomes the surface tension of the polymer solution, a Taylor cone is formed and as the polymer solution is ejected from the needle and pulled toward the grounded collector plate, the volatile solvent in the polymer solution evaporates forming polymer fiber structure subsequently deposited onto grounded plate.

Sensor transducers

We use both commercial electrode (Microsensor Systems, Inc.) and custom design printed electrode in this study. Printed electrodes was deposited on the electrospun nanofiber structure surface using Dimatix material printer DMP-2831 and silver nanoparticle conductive ink DGP 400 from Advance Nano Products (South Korea) followed by 60°C curing for 5 hours before conductivity measurement.

Polymers

Poly(methyl methacrylate) (PMMA, Mw 540,000) was purchase from Scientific Polymer Products and used as received.

Single Walled Carbon Nanotubes

Single Walled Carbon Nanotubes (SWCNTs) were purchased from Carbolex with carbon purity above 90wt%.

Chemical vapors

VOCs used in this study include hexane, methanol, ethanol, butanol, all with 99.9% purity, purchased from Aldrich and used as received. The ozone was generated using Primary Standard UV Photometric O₃ Calibrator (Model 49C, Thermo Environmental Instruments Inc.) with EPA-certified calibration.

Results and Discussion

Sensing material properties

To optimize the design of ECPN materials, we studied the percolation threshold of both composite polymer thin-films and corresponding nanofiber materials. We found that the threshold for PMMA/SWCNTs composite thin films is between 2% and 5% CNTs weight percentage to PMMA, while the threshold for comparable electrospun nanofiber materials is 10%. We believe this phenomenon is due to the structure difference films and fibers. While there is only one SWCNTs and polymer interface that will contribute the conductivity of the overall material for thin films, there are two interfaces for polymer/CNTs composite nanofiber material: 1) the interface between polymer and carbon nanotubes inside nanofibers; 2) the interface between nanofibers. It is clear that the interface between nanofibers plays an important role of the overall conductivity of the material.

VOC detection

The composite polymer nanofiber sensing material has different selectivity to vapor molecules

based on the interaction between sensing material and functional groups of the vapor molecules. It was demonstrated that the ECPN sensor membrane is selective to methanol but not hexane because of the favorable H-bonding interaction between $-C=O$ group of the methacrylate polymer and $-OH$ group of the methanol, while for hexane, only hydrophobic interaction exists between long carbon chain of hexane and polymer backbone. Not only is the composite sensing materials selective to hydroxyl group, it also shows different sensitivity to alcohols with different carbon chain length. Our preliminary experiment indicated that the order sensitivity of the PMMA/SWCNTs to different alcohol is in the order of methanol>ethanol>2-propanol (Figure 1). This indicates that beside the H-bonding formation, the molecule size and polarity could have also played an important role in different sensitivity. The ECPN also showed low detection limits to different VOCs (Table 1). We have demonstrated that it can detect example common VOCs with concentration of at least one order of magnitude lower than ACGIH-suggested TLV values. For methanol, we obtained three order of magnitudes lower detection limit than TLV value.

Ozone detection

We also demonstrated the sensing capability of the ECPN to oxidative gas. As ozone is a strong

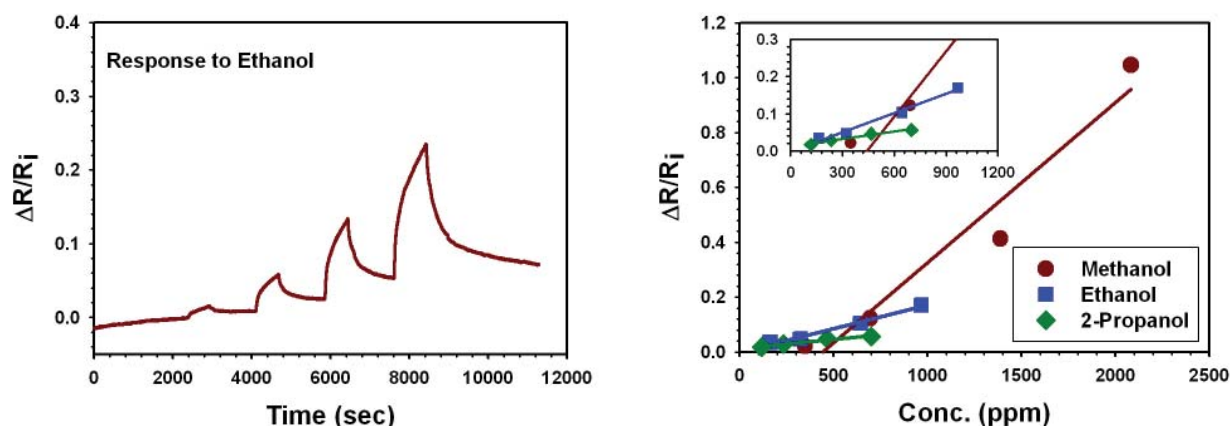


Figure 1. (Left) Typical sensor response profile to alcohol vapors, ethanol used as an example with vapor concentration of 161, 322, 644, 966 ppm; (Right) Sensitivity plot of relative resistance change vs vapor concentrations.(insert) magnified view of sensitivity plots for ethanol, 2-propanol and butanol. The sensitivities for different alcohols are: Methanol: 0.0006 ppm^{-1} ; Ethanol: 0.0002 ppm^{-1} ; 2-propanol: $0.000067 \text{ ppm}^{-1}$.

oxidizing agent, it can oxidize wide range of organic species. Ozone can react with unsaturated carbons and break the carbon-carbon double bond which can lead to material conductivity change. With this property in mind, we designed a nanofiber ozone sensing material based on conducting polymers, specifically polythiophene. Upon studying ozone with concentrations ranging from 250 ppb to 2ppm was studied (Figure 2), we observed a linear response for the polythiophene sensor to ozone at different concentration and a response to low ozone concentration at 250 ppb level.

Detection Range at Low Concentrations for Selected Common Volatile Organic Compounds		
	Nanofiber Sensor Detects	ACGIH TLV*
Methanol	0.188 ppm, <60 sec	200 ppm
Dichloromethane	6.4 ppm, <120 sec	50 ppm
Chloroform	3.3 ppm, <150 sec	10 ppm

* **ACGIH TLV** expressed as a time-weighted average of the concentration of a substance to which most workers can be exposed without suffering adverse effects.

Table 1. Comparison of the Detection Limit of the ECPN Sensing Membrane and ACGIH Threshold Limit Value of Different Common VOCs.

Enhanced sensitivity and reduced baseline noise level with printed electrodes

We developed an integrated ECPN sensor in RTI by directly printing electrodes on the sensor membrane, the conductive ink is sorbed into the membrane making excellent contact with sever-

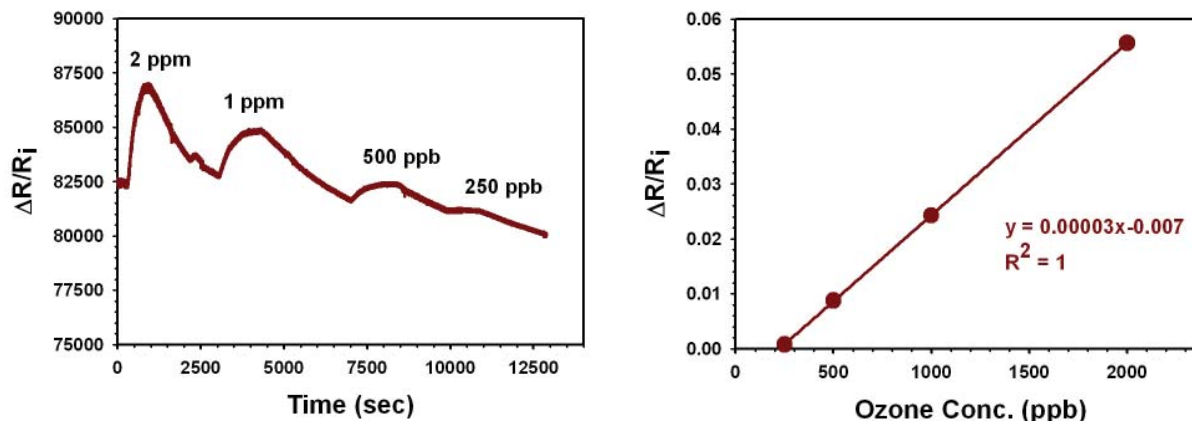


Figure 2. (Left) Response profile; and (Right) sensitivity plot of polythiophene sensing material to ozone.

al layers of nanofibers to yield a particularly effective sensor. There are two major advantages of such a design: 1) The flow-through configuration of the ECPN sensing membrane allows dramatically increased analyte-sensing material interaction by increasing the gas diffusion depth, thus enhancing sensing material sensitivity at a given concentration; and 2) The significantly improved contact between electrode and sensor membrane produced by printing techniques helps to dramatically reduce the sensor baseline noise level. One order magnitude higher response and dramatically reduced noise level was observed for ECPN sensor membrane with printed electrodes when compared to the nanofibers on a solid substrate with interdigitated electrodes (Figure 3).

Conclusions

We have demonstrated that ECPN can be used as chemical sensing materials for detection and monitoring environmental pollutants, including VOCs and ozone at low concentrations. The

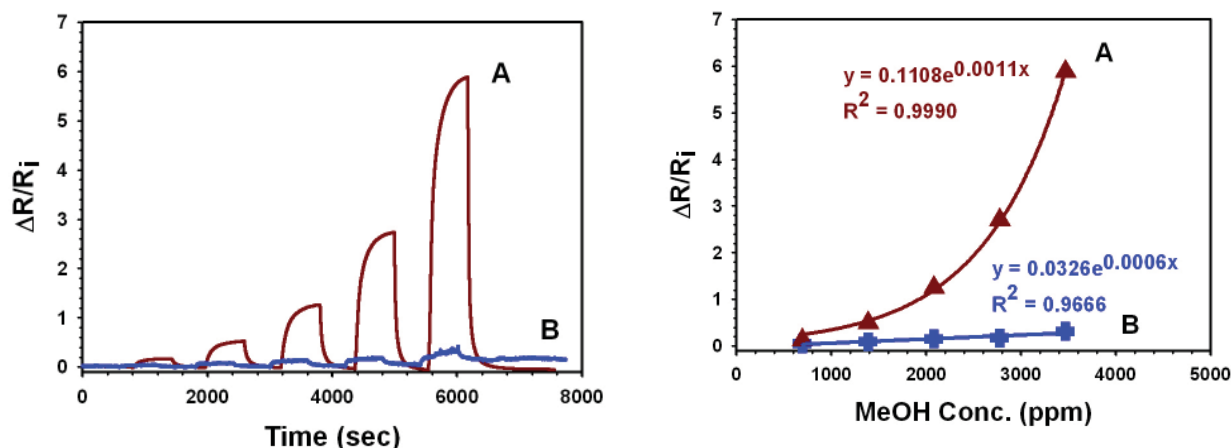


Figure 3. (Left) Comparison of the sensor response profile of ECPN sensing membrane with printed electrode (A) and on commercial IME electrodes (B) to Methanol vapors (concentration: 694, 1389, 2083, 2777, 3471 ppm). (Right) Comparison of the sensitivity plots of the two types of sensing material design.

structure advantages of the nanofiber material provide an excellent platform material with high tunability for specific gas detection needs. The ink-jet printing process to make electrical connections with fibers provides a simple way to fabricate integrated sensing materials and enhances the sensitivity and reduces response noise level. This combination of ECPN and printed electronic technique enabled the integrated sensor device, enhanced sensor measurement capability and low cost production of the sensor system. These findings have important implications to the design of low cost, flexible sensing material that can be integrated into portable platform for large scale field applications.

References

1. Kreiss, K. (1990). "The sick building syndrome: where is the epidemiologic basis" Am. J. Publ. Health. 80,1172–1173.
2. Han, L., D. R. Daniel, M. M. Maye, and C. J. Zhong (2001). "Core-Shell Nanostructured Nanoparticle Films as Chemically-Sensitive Interfaces" Anal. Chem. 73, 4441-4449.
3. Lei, H., W. G. Pitt. (2004). «Resistivity Measurements Of Carbon-Polymer Composites In Chemical Sensors: Impact Of Carbon Concentration And Geometry.» Sens. Act. B-Chem. 101(1-2), 122-132
4. Wang, F., H. W. Gu, and T. M. Swager. (2008). «Carbon Nanotube/Polythiophene Chemiresistive Sensors for Chemical Warfare Agents.» J. Am. Chem. Soc. 130(16), 5392-5393.
5. Becker, T., S. Muhlberger, C. Bosch-von Braunmuhl, G.Muller, T. Ziemann, and K. V. Hchtenberg (2000). "Air Pollution Monitoring Using Tin-Oxide-Based Microreactor Systems." Sens. Act. B-Chem. 69(1-2), 108-119.

Conference Questions and Answers

Question:

Has any of your work been done in the field?

Answer:

No. We are still working in the laboratory.

Question:

How is the vapor drawn through the sensing material?

Answer:

There is a fan in the box under the sensing material. When you turn the fan on, vapor is drawn through the sensing material, and the response appears on the display.

Question:

Are there separate boxes for different chemicals?

Answer:

We can change the inboard sensing system. For detection of specific analytes, the sensor can be changed as you would change a cartridge. These are interchangeable sensor elements.

Question:

You showed data for different processes; ethanol was one of the analytes. Is this a reversible chemistry, or is the effect cumulative?

Answer:

The chemical reaction is permanent; the material cannot return to its original form.

Question:

How do you overcome the effects of humidity and temperature?

Answer:

Although humidity is very important, we haven't done a detailed study yet. We do have some data on the physical reaction on the part of the sensor mechanism affected by the water.

Question:

What is the nanofiber made of?

Answer:

The nanofiber is made through a process called electron spinning. We have used pure polymer and different types of polymer composites, such as poly(methyl methacrylate) and polythio-

phene. We are experimenting with different types of polymers.

Ozone Sensors for Real-time Passive Wireless Application

Ryan S. Westafer, Georgia Institute of Technology, School of Electrical and Computer Engineering

Michael H. Bergin, Georgia Institute of Technology, School of Civil and Environmental Engineering

Dennis W. Hess, Georgia Institute of Technology, School of Chemical and Biomolecular Engineering

William D. Hunt, Georgia Institute of Technology, School of Electrical and Computer Engineering

Galit Levitin, Georgia Institute of Technology, School of Chemical and Biomolecular Engineering

*Desmond D. Stubbs, Oak Ridge Center for Advanced Studies
Peter J. Edmonson, Zen Sensing, LLC*

Abstract

There is an existing need to develop compact, robust, low-power, and inexpensive real-time sensors for air pollutants, such as ozone and particulate matter (PM), for personal exposure assessment [1]. For this reason we have developed radio frequency identification (RFID) surface acoustic wave (SAW) sensors. It has been shown that resonant acoustic mass sensors, such as the quartz crystal microbalance (QCM), can perform near real-time ozone detection [2]. Our approach [3] employs surface acoustic waves (SAWs) which offer several immediate advantages over QCMs: higher frequency and thus mass sensitivity, signal encoding capability, and passive (no battery) operation [4]. In this paper, we give our first results for gravimetric detection of ozone below 100 ppb. We further present the characteristics of ozone-sensitive polybutadiene (PB) films at nanoscale thicknesses which thereby enable the passive RFID ozone sensors.

Introduction

This manuscript focuses on recent developments in the proof-of-concept for a passive (batteryless) wireless ozone sensor. As a major component of urban smog, ozone is particularly troublesome because of its impact upon public health. Guidelines and regulations set forth by Occupational Safety & Health Administration (OSHA) specify a maximum allowed exposure of 100 parts per billion (ppb) over an 8 hour period. The authors found toxicity reported as low as 100 ppb over 2 hours [5]. In both industrial and residential environs, we see the need to monitor ozone exposure on a personal basis.

On March 12, 2008 the EPA revised the national air quality standards (NAAQS), reducing the

“8-hour primary ozone standard” to 75 ppb. Consequently we are developing radio frequency identification (RFID) sensor badges and a reader system to operate within this range.

While one conventional monitor employs an ultraviolet spectrophotometer [6], we use an ultra high frequency acoustic gravimetric approach. In this way we can:

- Achieve small size; enabling integration into a sensor badge.
- Reduce cost; offloading the electronics to the remote measurement unit(s).
- Eliminate batteries; the radio query powers the response.

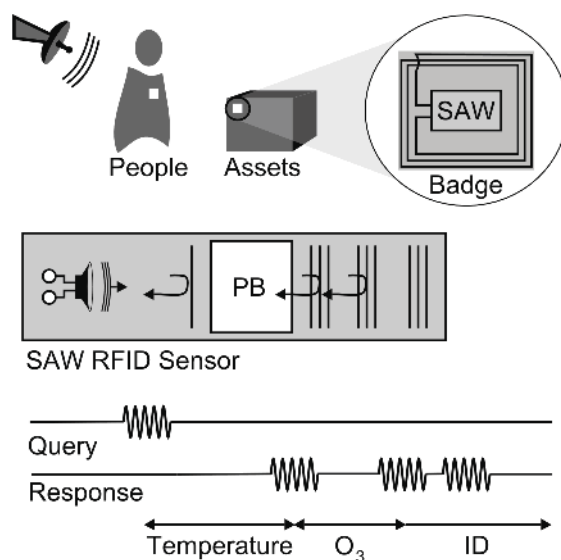


Figure 1. RFID system overview. “PB” represents a polybutadiene film sensitive to ozone.

To accomplish these objectives, the device must efficiently process the incoming electromagnetic energy, assess ozone reaction, measure temperature, and encode an identification response before reradiating a fraction of the energy received with the query signal. Figure 1 provides an overview of our system. The core of each badge is a surface acoustic wave (SAW) device which receives electrical energy from an antenna and transfers the energy to an acoustic wave on a piezoelectric substrate. By employing SAW technology, we gain convenient (and passive) signal processing capability without semiconductor electronics [7]. Furthermore, SAW devices serve as excellent sensors, and some RFID SAW sensors have been reported [8].

While our devices are mechanically robust and are 500 microns thick (compare to ~100 microns for QCMs), there is a drive toward nanometer dimensions. Communications requirements push toward high frequencies, and we have achieved this through electron beam lithography. Some of our devices operate with acoustic potentials just 324 nanometers wide. This enables operation in the GHz frequency range and yields: increased sensitivity, smaller antennas, and operation in the industrial, scientific, and machinery (ISM) band as high as 2.4 GHz.

Our present challenge is to perform chemical sensing in this framework. For device operation, the film often must be ~1% of the acoustic wavelength [9]. To this end, we developed a polyb-

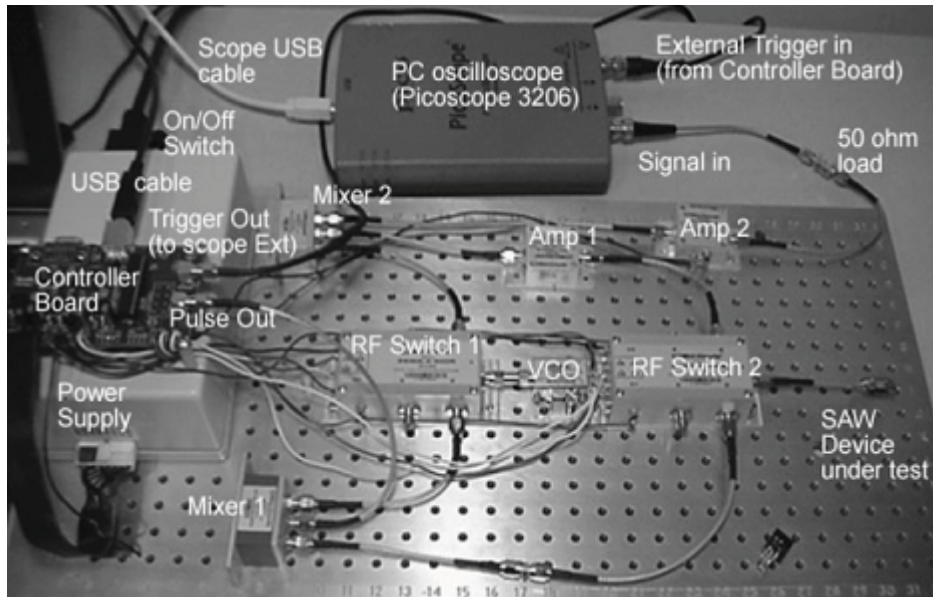


Figure 2. Prototype RFID system components.

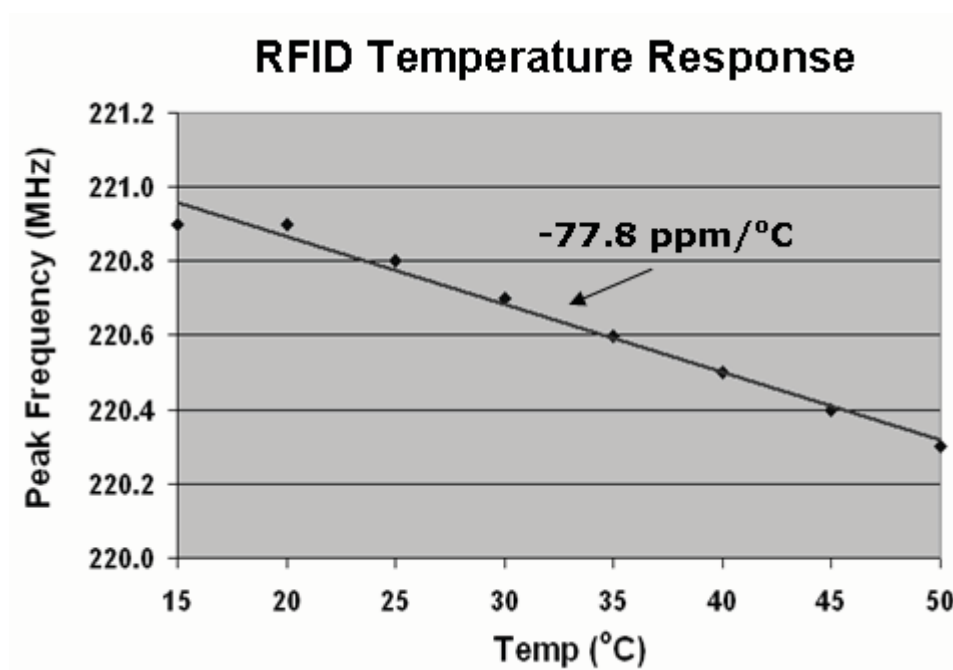


Figure 3. RFID device temperature response.

utadiene coating process which yields 200-300 nm films over the active device area.

Methods

We first tested the RFID sensor on a temperature controlled vacuum chuck. The device was wired to the transceiver electronics and time responses were captured on an oscilloscope and processed on a notebook computer, as in Figure 2. The response is shown in Figure 3.

For film characterization we used standard 10 MHz QCM crystals (ICM Mfg.). Polybutadiene (PB, 5000 mol. wt.) was dissolved in toluene to 5% wt. and spin-coated at 6000 rpm for 60 seconds. We measured 300 nm step heights using an Alpha-Step 500 surface profiler and ellipsometry.

Researchers have already demonstrated PB as selective for ozone [2, 10-11]. One study indicated less than 6% interference across many other salient gas constituents including: toluene, nitric oxide, and relative humidity. Water vapor and solvent absorption are important factors affecting acoustic properties of polymer films, so the relatively low interference makes this PB film a good choice. To further standardize the experiments, we flowed air through a particulate filter followed by a pump, desiccant dryer, and activated carbon filter. The air was then fed to a Thermo Electron Inc. O₃ Calibrator (Primary Standard). Its outlet was connected to a 600 mL aluminum-lined box which housed the sensor(s), and the air flow rate was 3.70 SLPM.

Results

In order to verify the response of the sensitive layer, we performed quartz crystal microbalance (QCM) trials. In the particular case of ozone detection, we show our results agree with those of Black, et al. [2]. We used the conventional Sauerbrey equation to determine the effective mass of the deposited film (over the active region) on the QCM. With $f_0=9970268$ Hz, $A_c=10$ mm², $\rho_q=2.648$ g/cm³, $\mu_q=2.947 \cdot 10^{11}$ g/cm-s, and $\Delta f=20.591$ kHz, the PB mass is computed to be 82

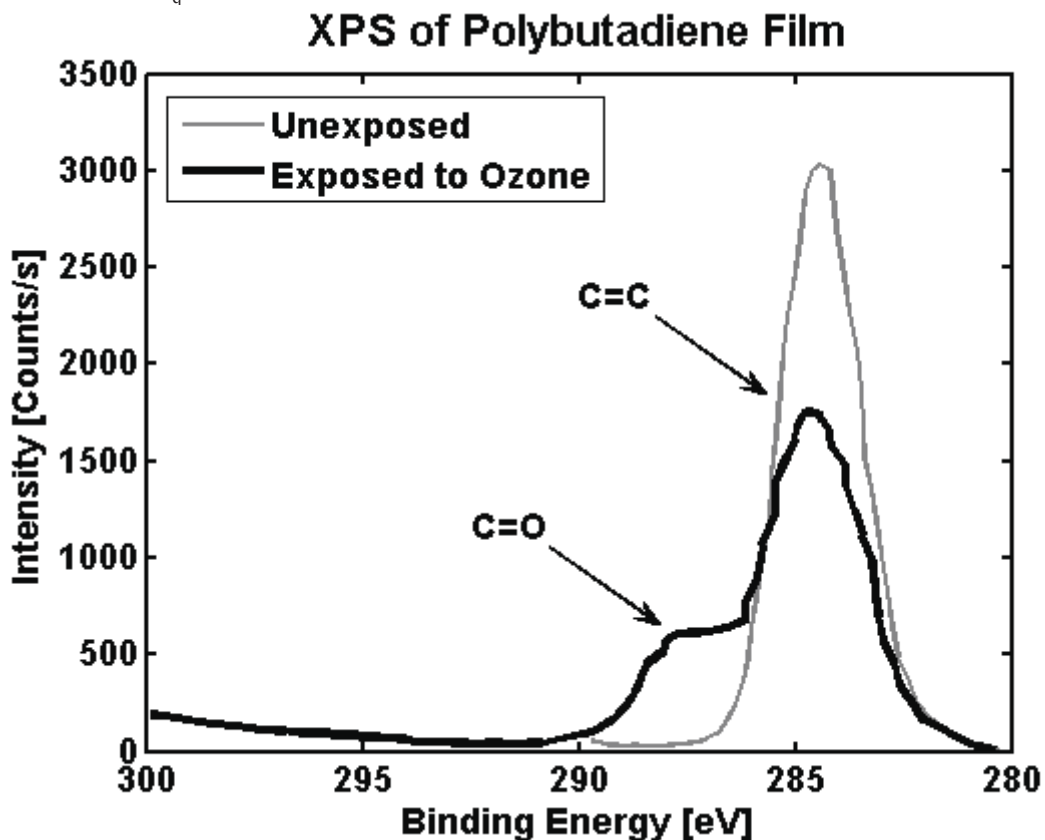


Figure 4. XPS before and after film exposure to ozone at 180 ppb for 3 hours.

μg . For an active area of 0.282 cm^2 and $\rho_{\text{PB}} \approx 1.3\text{ g/cm}^3$, the thickness is computed to be roughly 700 nm using polymer density of 1.3 g/cm^3 . This is justified because inspection revealed the QCM was coated on both sides.

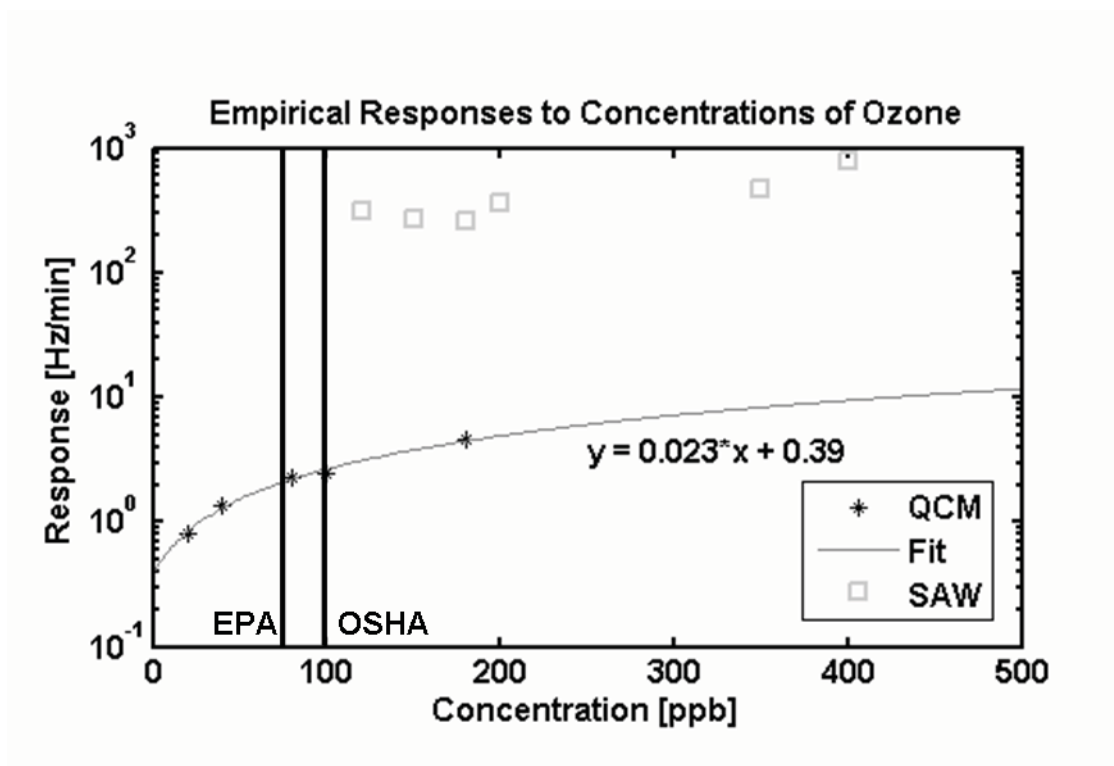


Figure 5. QCM and SAW sensor responses to ozone during 5 minute exposures.

We performed x-ray photoelectron spectroscopy (XPS) analysis on the top 10 nm of PB films exposed to 180 ppb for 3 hours. The results show both reduction of the carbon 1s peak and a new peak indicating formation of carbonyl groups when compared to the unexposed film. Refer to Figure 4. We believe this incorporation of oxygen increases the mass of the polymer.

In Figure 5 we provide the ozone response curve. The EPA 8-hour primary standard level is marked with a vertical line at 75 ppb, and the OSHA 2-hour exposure limit is indicated by the next vertical line at 100 ppb.

Discussion

In a wired laboratory setup, we demonstrated a significant and linear temperature sensitivity (-78 ppm) using the SAW RFID devices. In the field, we expect wireless interference and sub-second measurement intervals will yield resolution close to 0.1 degrees, which agrees with [11]. Although we have not investigated the response of the PB films to ozone at various temperatures, these films do tolerate solvent bake-out in air at 110 Celsius for several hours. We also anticipate concomitant temperature measurement will help the receiver correct for error correlated with temperature.

The QCM experiments demonstrated that the device frequency slope corresponds to ozone

concentration. While we used 5 minute intervals in this work, the swift response allows much shorter time periods, likely limited by the Allan variance. By comparison, the integration time on the primary standard ozone calibrator was thirty seconds.

While the ozone response was linear in the relevant range, the nonzero intercept indicates the linear fit diverges in the very low ppb range. Still our linear results were repeatable and even reproduced after storage of the sensors for two weeks at room ambient conditions. The latter case did show reduced sensitivity; a reduced response slope. This could be attributed to slow reaction of the film with ambient ozone or other chemicals in the laboratory air.

Though we always observed a downward and monotonic frequency decrease during ozone exposure, such response is not necessarily due to mass change. However, both XPS and FT-IR measurements confirm the incorporation of oxygen in the film. The cumulative dose applied to the polybutadiene sensor was at least 129 ppb-hours prior to saturation (assuming zero reaction in room air). This is five to ten times lower than quoted in Black, et. al. Our films are spin-cast to about 330 nanometers, whereas the quoted films were brushed on, likely to several microns in thickness. Assuming diffusion throughout the film, the earlier saturation we observe may be due to our nanoscale films. Other possibilities include degradation of the film at elevated temperatures encountered during preparation or different molecular weight PB.

The dependence of response saturation upon film thickness provides an opportunity. The saturation condition can be automatically identified, and therefore an array of varying thicknesses provides discrete checkpoints indicating sensor life.

Despite the given reasons to scale down devices, a large surface area is still desired to capture more analyte and maintain sensitivity. So, along one axis (the line of acoustic propagation) we have reduced device dimensions to the nanoscale for higher frequency operation: increasing both sensitivity and communication bandwidth. Meanwhile the width of the device may remain large by comparison: hundreds of microns or more.

Conclusions

We have fabricated surface acoustic wave RFID sensors suitable for low-cost, wireless, and personal environmental monitoring. Our multifunctional acoustic sensors are enabled by nanoscale fabrication techniques. We have prepared suitable polybutadiene films and tested them using conventional quartz crystal microbalances. The experimental results revealed the sensitivity, aging characteristics, and lifetime for nanoscale ozone sensitive films. Our ongoing work is improving the film deposition and curing process and will finally bring the complete sensor to fruition.

Acknowledgements

The authors thank several individuals for their assistance: John Perng for mask layout, Farasat Munir for experimental assistance, and George Yu for a creating a custom spin coating chuck.

References

1. NIH Grant, Solicitation. (2006). RFA-ES-06-011.
2. Black D.R., R.A. Harley, S.V. Hering, and M.R. Stolzenburg. (2000). "A New, Portable, Real-Time Ozone Monitor," *Environmental Science & Technology*, volume 34, number 14, pp. 3031-3040.
3. Stubbs, D. D., S. H. Lee, and W. D. Hunt. (2003). "Investigation of cocaine plumes using surface acoustic wave immunoassay sensors." *Anal Chem*, volume 75, pp. 6231-6235.
4. Edmonson, P. J. and Campbell, C. K. (2003). U.S. Patent No. 7,005,964. Washington, D.C.: U.S. Patent and Trademark Office.
5. *Toxicology Letters*. (Elsevier Science Pub. B.V., POB 211, 1000 AE Amsterdam, Netherlands) V.11-1977.
6. Thermo Electron Corporation. Model 49i Ozone Analyzer. UV photometric gas analyzer for ambient air monitoring.
7. Campbell, C. K. (1989). "Surface Acoustic Wave Devices and Their Signal Processing Applications." San Diego, CA: Academic Press, Inc.
8. Pohl, A., R. Steindl, and L. Reindl. (1999). "The 'Intelligent Tire' Utilizing Passive Saw Sensors - Measurement of Tire Friction." *IEEE Transactions on Instrumentation and Measurement*, volume 48, issue 6, pp. 1041-1046.
9. Ballantine, D.S., R.M. White, S.J. Martin, A.J. Ricco, E.T. Zellers, G.C. Frye, and H. Wohltjen (1997). "Acoustic Wave Sensors. Theory, Design, and Physico-Chemical Applications." p. 348. San Diego, CA: Academic Press, Inc.
10. Fog, H. M., and B. Rietz. (1985). "Piezoelectric Crystal Detector for the Monitoring of Ozone in Working Environments." *Analytical Chemistry*, volume 57, issue 13, pp. 2634-2638.
11. Hoummady, M., A. Campitelli, and W. Wlodarski. (1997). "Acoustic wave sensors: design, sensing mechanisms and applications," *Smart Materials and Structures*, (6), 647-657.
12. Scholl, G., C. Korden, E. Riha, C.C.W. Ruppel, U. Wolff, G. Riha, L. Reindl, and R. Weigel. (2003). SAW-based radio sensor systems for short-range applications." *Microwave Magazine*, IEEE, volume 4, issue 4, pp. 68-76.

Conference Questions and Answers

Question:

How do you account for the "skin effect"? I am referring to double-E.

Answer:

Our measurement is not electrical—it is mass, it is inertial. This depends upon the acoustic wavelength with which we measure. In many cases, the wavelength is around a micron, and we try to keep it there. The skin effect is not really relevant for the conductors, because the acoustic wave

is doing the sensing. Another angle on the skin effect is that the film could be activated only at the top layer; the rest is passivating and not reacting all the way through. The films are so thin that there could be a nano-porosity or subnano-porosity that allows it to diffuse. The response is very fast, almost like mass transfer.

Question:

If you change the chemistry of the surface, can you detect for different chemicals?

Answer:

Yes. One of the authors of this study, Desmond Stubbs, did that for detection of cocaine as well as for RDX, TNT, and other explosives. He was able to obtain excellent results in the laboratory using actual samples of rock for the explosives

Development of Disposable Microfabricated Chip Sensor Using Nano Bead Packing Method to Measure ORP

*Am Jang, Department of Civil and Environment Engineering,
University of Cincinnati, U.S.A.*

*Kang K. Lee, Se H. Lee, and Chong H. Ahn, Microsystems and BioMEMS Laboratory,
Department of Electrical and Computer Engineering, University of Cincinnati, U.S.A.*

*Paul L. Bishop Department of Civil and Environment Engineering,
University of Cincinnati, U.S.A.*

Introduction

The determination of oxidation–reduction potential (ORP or redox potential) in a variety of matrices, especially, in surface and ground water and during water treatment, is of great importance since solutions can be graded as oxidizing or reducing based on measurements of ORP value. Compared with pH, ORP values can not only monitor the system’s operational status, but also indicate the completion of nitrification/denitrification. In addition, ORP is a more precise measurement and has an advantage over the use of DO since DO measurements become unreliable at low DO levels (1). It is feasible to use ORP as one of the online-control parameters for biological wastewater treatment. There is an increasing demand for measurement of ORP in solutions, both in industry and in environmental research.

Although many studies have already pointed out that ORP can be used as an indication of biological treatment efficiency and water quality, little work of relevance has been done on monitoring soil or sediment with ORP measurements (2, 3, 4). The reasons are that traditional monitoring techniques are still based on the laboratory analysis of representative field-collected samples: they require considerable efforts, the sample ORP may change before analysis, and the results are often not available in due time to allow on-line updating of the process controller. Furthermore, unfortunately, most of these macro-electrodes are relatively large in size, on the order of 1-3 cm in diameter. They can be used to monitor bulk liquid concentrations when there is sufficient volume to wet the electrode contacts, but they are often inappropriate for measurements in small volumes of liquids or in soils. Due to these limitations, the continuous surveillance of hazardous areas is not possible. Remediation of Superfund and other hazardous waste sites, particularly those using bioremediation techniques, requires significant use of monitoring procedures. Rapid information feedback during waste site remediation for real time *on-site* monitoring capabilities is essential for the sustainable management of soils and sediments. Consequently, these reasons have prompted the need to develop sensitive, selective, portable and rapid methods to determine ORP in pore water.

The use of Micro Electro Mechanical Systems (MEMS) technology is most promising because of its ability to make possible mechanical parts at the micron size that can use very small volumes of liquid (a few μL). Moreover, by means of integrating the sensors with electronics, one can

fully automate the sample preparation and analysis. In this research, we adopted and optimized a self-assembly technique to fabricate a crystalline nano sphere column in a polymer lab chip. Our research goal is to develop miniaturized electrochemical sensors with planar microelectrodes using self assembly nano-beads packing technology. Such sensing system would be invaluable to remediation workers due to their numerous benefits, such as greatly reduced sensing cost, the portability of the entire sensing system, and its very easy use.

Materials and Methods

ORP measurements are based on the potential difference measured between a working electrode made of an inert material (platinum or gold) and an Ag/AgCl reference electrode. In this study, gold will be used not only as conductive layers for other microelectrodes but also as the working microelectrode for monitoring ORP potential.

Fabrication of Polymer Microfluidic Chips and Microelectrodes

A cyclic olefin copolymer (COC, Topas 5013, Ticona, Summit, NJ) plastic chip patterned with microfluidic channels was prepared by an injection molding technique using an electroplated nickel mold (6). As shown in Figure 1, the SU-8 2075 photoresist (Microchem Corp., MA, USA) were spin-coated on the 3-inch Ni disk to achieve a 100 μm thickness, followed by a pre-bake process. After the photoresist layer was exposed to a UV source, it was baked again for cross-linking. After developing, Ni electroplating was performed in a Ni plating bath, using a two-electrode system with a Ni anode and a Ni disk cathode with SU-8 patterns. Finally, a Ni mold with a 100 μm -thick plating microstructure was obtained after removal of the residual SU-8. The

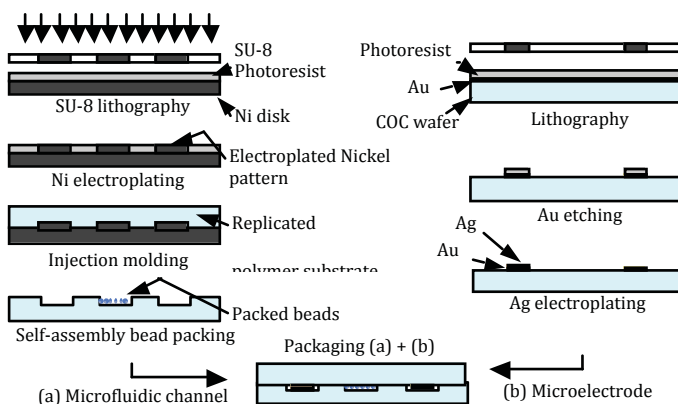


Figure 1. Schematic diagram of fabrication steps of a polymer lab chip with on-chip ion selective sensor using nano-bead packing.

microfluidic chip was then replicated from this mold over a COC substrate by injection molding process. The microelectrodes have been made by microfabrication technology illustrated in Figure 1. A gold (Au) layer of 100 nm was deposited on the 3-inch blank COC wafer using the e-beam metal evaporator. The Ag layer was deposited on the reference electrode using electroplating method on the Au seed layer.

Silica Nano Bead Packing

The patterned COC chip substrate was pretreated with O_2 plasma for 2 min to give hydrophilicity

to the microchannel surface (6). The aqueous colloidal silica solution (800nm, 0.1 wt %, Bang's Laboratories, Inc., Fisher, IN) was heated to 60 °C in a beaker with gentle stirring to prevent slow precipitation of the aggregated silica particles. Pretreated open microchannels showed enough high hydrophilicity to drive the water by capillary action to the ends of the channels along with silica colloidal particles suspended in it. Once the colloidal silica particles reached the end of the capillary channels, spontaneous three-dimensional packing of the silica beads started from the end of the microchannels due to the slow evaporation of water. The self assembly packing process continued toward the end of the empty microchannel at the bottom. The packed chip was washed very gently and cautiously with plenty of deionized water to remove extra silica particles at the dipped area and was dried completely at room temperature.

Bonding Process for Microchip Sensor

The patterned COC substrate was made of a resin having a high glass transition temperature ($T_g = 134$ °C). After packing with nano-size silica beads, the packed substrate was covered with a plain COC plate having low T_g (78 °C, Topas 8007, Ticona, Summit, NJ) and sealed using a homemade hot embossing machine (6). To avoid the destruction of the silica packing by the pressure applied during press-bonding, the temperature of the chip in the hot embossing machine was maintained at 85 °C for 20 min without pressing and the cover plate was allowed to soften. The softened cover plate was squeezed from the top with the weight of the hot plate of the embossing machine for 30 min in order to bond it to the packed substrate. Then it was cooled down to room temperature without removing the weight. Figure 2 shows the final microfabricated chip sensor using self assembly nano-bead packing method.

Calibration of ORP

Three calibration ORP solutions, including a commercial ORP calibration solution (Sensorex, USA), pH 4.0 and pH 7.0 buffer solutions of saturated quinhydrone (Sensorex, USA) was used. When coupled with an Ag/AgCl reference electrode, redox potentials for the pH 7 and pH 4 reference solutions, as recommended by the American Society for Testing and Materials (ASTM) (4), should be 92 and 268 mV, respectively, at 20°C; 86 and 263 mV, respectively, at 25°C. If the signal readings for the standard solutions showed them to be out of range (more than ± 10 mV from the known potential values), the ORP lab chips made in our laboratory were discarded.

Results and Discussion

To demonstrate ORP chip sensor, first, a COC plastic chip patterned with microfluidic channels was prepared by an injection molding technique using an electroplated nickel mold. This was followed by a dipping process for self-assembly bead packing column; a 50 μm width, 50 μm height, and 5 mm length microchannel was packed with 0.8 μm diameter silica beads. We expected to produce a micro-volume channel of 0.0125 mm³. Figure 3 shows images taken from video clips of the self-conditioning process recorded at a position 1mm from the center hole of the microchip as shown in Figure 2. The microchannel was completely filled with ORP standard solution by only the capillary force without air bubbles. It took 20 seconds to fill the packed column shown in the figure. The bead-packed microchannels were also working as a nano-filter without any purification or degassing steps for solutions. As shown in Table 1, the measured redox potentials of the ORP lab chip with respect to the Ag/AgCl reference electrode and 1 M

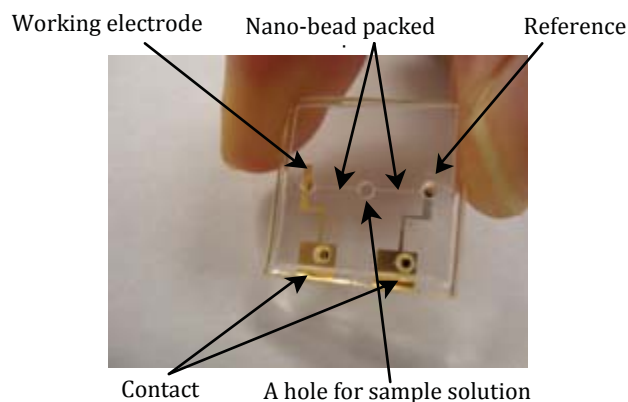


Figure 2. Microfabricated chip sensor using self assembly nano-beads packing method.

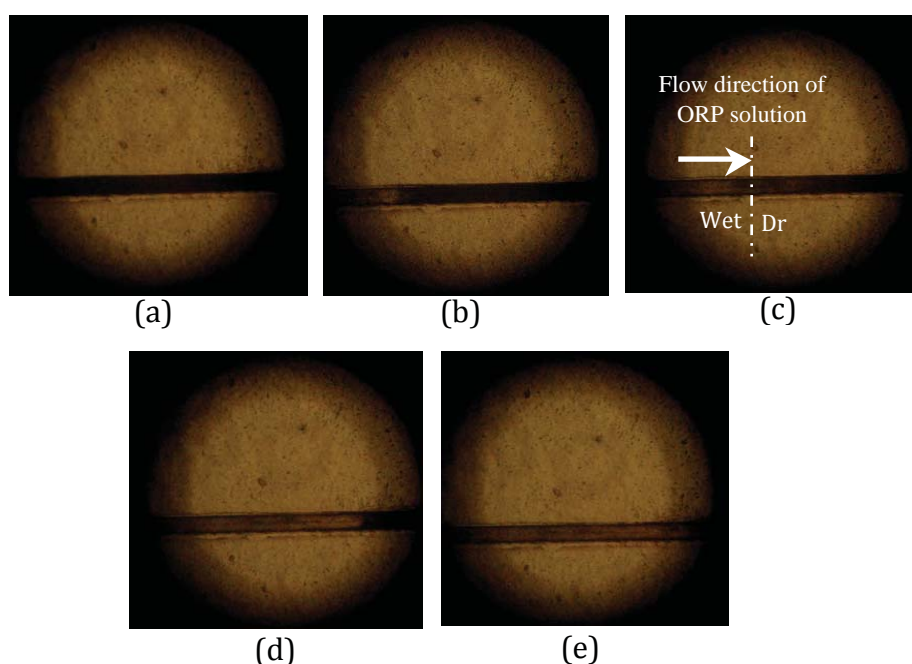


Figure 3. Images taken from video clips of self-conditioning process, where the ORP standard solution is filling the nano-bead packed column by capillary force; (a) $t = 0$, (b) $t = 3\text{s}$, (c) $t = 7\text{s}$, (d) $t = 11\text{s}$, (e) $t = 16\text{s}$.

KCl at 25 °C were 220.84 ± 1.49 mV for standard calibration solution, 261.54 ± 1.39 mV for pH 4 quinhydrone reference solution, and 82.69 ± 1.29 mV for pH 7 quinhydrone reference solution, respectively. The measured ORPs using the three kinds of redox potential solutions were typically slightly lower than those of the nominal redox potential. ASTM suggests that the measured redox potentials should be within 10 mV of the nominal redox potentials for a good redox electrode. Thus, all of the measurements should be deemed acceptable. The response time to stabilization of the ORP lab chip was fast according to the Table 1.

Table 1. Response time to stabilization and measured redox potential by the nano-bead packed microsensor with Ag/AgCl (1M KCl) reference electrode (number of measurement, n=10)

Redox standard or reference solution	Response time to stabilization (s)	Measured redox potential (mV)
ORP calibration solution	5.20 ± 0.63	220.84 ± 1.49
pH 4 quinhydrone reference solution	7.30 ± 0.82	261.54 ± 1.39
pH 7 quinhydrone reference solution	6.80 ± 0.63	82.69 ± 1.29

Acknowledgements

This research was supported by a grant from Plant Technology Advancement Program funded by Ministry of Construction & Transportation of Korean government.

References

- Lo, C. K.; Yu, C. W.; Tam, N. F. Y.; Traynor, S. Enhanced nutrient removal by oxidation-reduction potential (ORP) controlled aeration in a laboratory-scale extended aeration treatment system. *Water Research* **1994**, 28 (10), 2087-2094.
- Lissner, J.; Mendelssohn, I. A.; Anastasiou, C. J. A method for cultivating plants under controlled redox intensities in hydroponics. *Aquatic Botany* **2003**, 76(2), 93-108.
- Naidu R.; Sumner M. E.; Harter R. D. Sorption of heavy metals in strongly weathered soils: an overview. *Environ. Geochem. Hlth.* **1998**, 20, 5-9.
- Zhang, T. C.; Pang, H. Applications of microelectrode techniques to measure pH and oxidation–reduction potential in rhizosphere soil. *Environ. Sci. & Tech.* **1999**, 33(8), 1293-1299.
- Jang, A.; Lee, J. H.; Bhadri, P. R.; Kumar, S. A.; Timmons, W.; Beyette, F. R.; Papautsky, I.; Bishop, P. L. Miniaturized redox potential probe for in situ environmental monitoring. *Environmental Science & Technology* **2005**, 39(16), 6191-6197.
- Park, J.; Lee, D.; Kim, W.; Horiike, S.; Nishimoto, T.; Lee, S. H.; Ahn, C. H. Fully Packed Capillary Electrochromatographic Microchip with Self-Assembly Colloidal Silica Beads. *Analytical Chemistry* **2007**, 79(8), 3214-3219.

Conference Questions and Answers

Question:

You showed us a version packed with nanobeads. Can you pump against nanobeads that are tightly packed? That is getting into a high-pressure scenario. Do you have more than one design?

Answer:

If we have problems with the 800-nm size, we can try other sizes.

Comment:

The smaller you make the beads, the tighter they pack, and the stronger the back-pressure. As a result, you have to have a really powerful pump. This situation requires care not to pack them too densely. Some people are using silica structures with large pore sizes specifically to keep the pressure low. Bigger beads might work better, depending on what you are trying to do.

Response:

In order to find a proper vehicular membrane, we need to find the proper porosity. We are trying beads of alternative sizes.

Metal Oxide Nanoparticles: Applications for Biosensors and Toxicity Studies

*Ian M. Kennedy, Department of Mechanical and Aeronautical Engineering,
University of California Davis. Davis, California, U.S.A.*

Abstract

Lanthanide oxide nanoparticles have been developed by our group for application as platforms in sensitive bio-assays, including immunoassays and DNA assays. Immunosensors for pesticides and toxins have been deployed on nanoparticles that make use of multiple narrow bandwidth emissions for detection, along with magnetic separation in microchannels. Solution based assays for soil bacterial DNA have been demonstrated for application in bio-remediation of sites contaminated with MTBE. The potential health effects of metal oxide nanoparticles have been explored with in vitro studies that use human aortic endothelial cells and human lung epithelial cells. We have shown that the induction of inflammation depends on the composition of the metal oxide particles, probably as a result of differences in solubility.

Introduction

High sensitivity detection can be achieved with new, optically efficient luminescent labels for biomolecules. Continuing attention has been given over the years to the development of novel or improved fluorophores (Daniels et al. 1995). For example, the chelates of Europium, one of the lanthanide elements, have been used as fluorophores in immunoassays (Bathrellos et al. 1998, Mikola et al. 1995). Europium chelate has a broad UV absorption that can be excited by a flash-lamp. Its emission is shifted in wavelength by a substantial amount and, furthermore, its phosphorescence is long-lived with a lifetime in the micro to millisecond range. The long lifetime allows discrimination against background fluorescence temporally as well as spectrally.

Nanoparticles of simple lanthanide oxides can offer all the advantages of the lanthanide chelates without the complex synthesis and the somewhat uncertain composition, the latter issue leading to uncertainties in the conjugation chemistry. Due to their chemical inertness, and the fact that the lanthanide is sequestered in a crystal lattice, they are not susceptible to photo-bleaching or oxygen quenching. However, the key to their use is the development of a satisfactory functionalization method and the control of charges on the particle surfaces to minimize non-specific binding. Our synthesis method allows us to synthesize a range of lanthanide oxides that span the useful optical spectrum. We can include multi-wavelength labels for multiplexed assays with high throughput, using a number of the lanthanides (Eu - red, Tb - green and Dy - blue) doped into suitable host materials such as yttria or gadolinium oxide (Fig. 1).

We have gained a great deal of experience over the past few years in the use of these nanoscale materials for environmental and biomedical purposes. Multi-functional nanoparticles have been used in our assays for pesticides, for IgG, for bio-terror agents such as ricin in food, and for DNA and SNPs that are indicative of hereditary diseases. As a complement to the applications that we report, our studies of the ability of these materials to elicit inflammatory responses in human

cells in vitro reveal a range of toxic potential that depends on the particle composition.

Methods

Several groups have reported successful synthesis and characterization of particles that possess both fluorescent and magnetic properties (Hatanaka et al. 2003, Levy et al. 2002, Lu et al. 2004, Lu et al. 2002, Mulvaney et al. 2004, Sahoo et al. 2005, Wang et al. 2004). In most of the cases, the synthesis of particles with magnetic and fluorescent properties is complicated and expensive. Recently, we reported the synthesis of magnetic/luminescent core/shell particles using spray pyrolysis (Dosev et al. 2007). The general scheme of the aerosol synthesis method is shown in Fig. 1. Soluble precursors are delivered via syringe pumps to a nebulizer. The resultant spray is pyrolyzed in a high temperature hydrogen-oxygen-nitrogen flame. The particles that are formed are collected thermophoretically on a cooled surface.

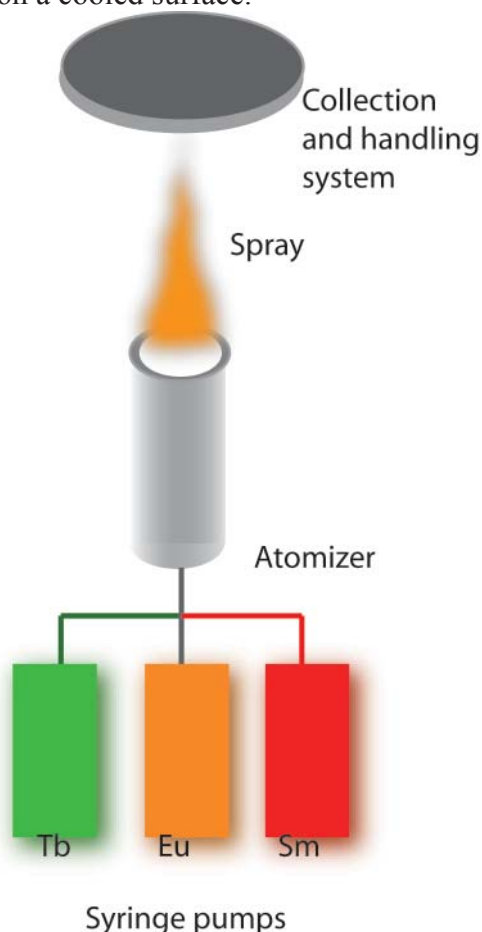


Figure 1. Spray pyrolysis of oxide nanoparticles that are doped with multiple lanthanide elements. The particles may also contain a magnetic iron oxide core.

The core-shell nanoparticles used for DNA detection were also synthesized by the spray pyrolysis process (Dosev et al. 2006, Dosev, Nichkova, Dumas, Gee, Hammock, Liu and Kennedy 2007). Magnetic cores (Fe_3O_4) synthesized via a co-precipitation method (Ma et al. 2005) were dispersed in a precursor solution of 20 % $\text{Eu}(\text{NO}_3)_3$ and 80 % $\text{Gd}(\text{NO}_3)_3$ in methanol and the

solution was then sprayed through a hydrogen flame. Consequently, Eu:Gd₂O₃ formed the luminescent layer on the surface of the magnetic core. Nanoparticles were functionalized by passive adsorption of NeutrAvidin (NA: Pierce, Rockford, IL) (Son et al. 2007).

Results and Discussion

The general format for immunoassay using our nanoparticles is illustrated in Fig. 2. Antibodies are passively adsorbed onto the particles, losing some activity due to non-optimal orientation but still providing enough binding sites to be effective. The secondary antibodies are labeled with fluorophores or other nanoparticles. In the case of our DNA assays, biotinylated probe oligos are attached to neutravidin on the surface of the particles. A signal DNA with fluorophore label is added after hybridization of the probe DNA to sample DNA.

Simple Eu:Y₂O₃ or Eu:Gd₂O₃ particles, without magnetic cores, have been used for environmental monitoring of pesticides and metabolites that are markers of exposure to environmental toxins (Cummins et al. 2006, Dosev et al. 2005, Koivunen et al. 2004, Nichkova et al. 2005, Nichkova et al. 2005). The composite particles have been successfully employed as carriers for multiplexed immunoassays in a solution and provided internal calibration for quantitative fluorescent measurements (Nichkova et al. 2007). In addition, we have demonstrated a similar approach for quantitative DNA hybridization with internal standard (Son et al. 2007). Introducing internal standards into analytical systems is essential in order to achieve good accuracy and reliability. Better precision in liquid arrays (Montes et al. 2006) and even in 2D gel electrophoresis (Wheelock et al. 2006) was achieved using an internal standard.

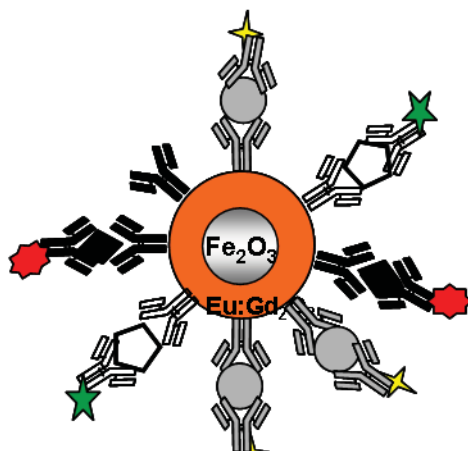


Figure 2. Format for a multiplexed sandwich immunoassay on a Eu:Gd₂O₃ nanoparticle with a magnetic Fe₂O₃ core. Analytes (circles, diamonds, pentagons) are captured by primary antibodies that are immobilized on the particles's surface. Secondary antibodies that bind to the analytes are labeled with fluorophores. The measurement of analyte concentration is derived from the ratio of the Eu signal and fluorophore signal. The Eu signal acts as an internal standard.

We have studied the potential for adverse health effects with our nanoparticles by adding them to cultures of human endothelial aortic cells (Gojova et al. 2006). Particles of Fe₂O₃, Y₂O₃ and ZnO were added to the cells with doses that were measured with ICPMS. We examined the induction of inflammatory responses by measuring markers such as ICAM, MCP and IL8. The iron oxide nanoparticles caused little change in gene expression or protein levels of these markers of

inflammation (see Fig. 3). Yttria, that we have used extensively as a host material for our lanthanide labels, induced a small change at the highest concentrations. Zinc oxide, however, caused a dramatic inflammatory response. The particles were endocytosed by the cells in all three cases and were sequestered by intracellular vesicles. In the case of ZnO, the vesicles (probably lysosomes) were very clearly enlarged by the presence of the Zn, suggesting an impact of the soluble, amphoteric ZnO on the pH and homeostatis of the cells.

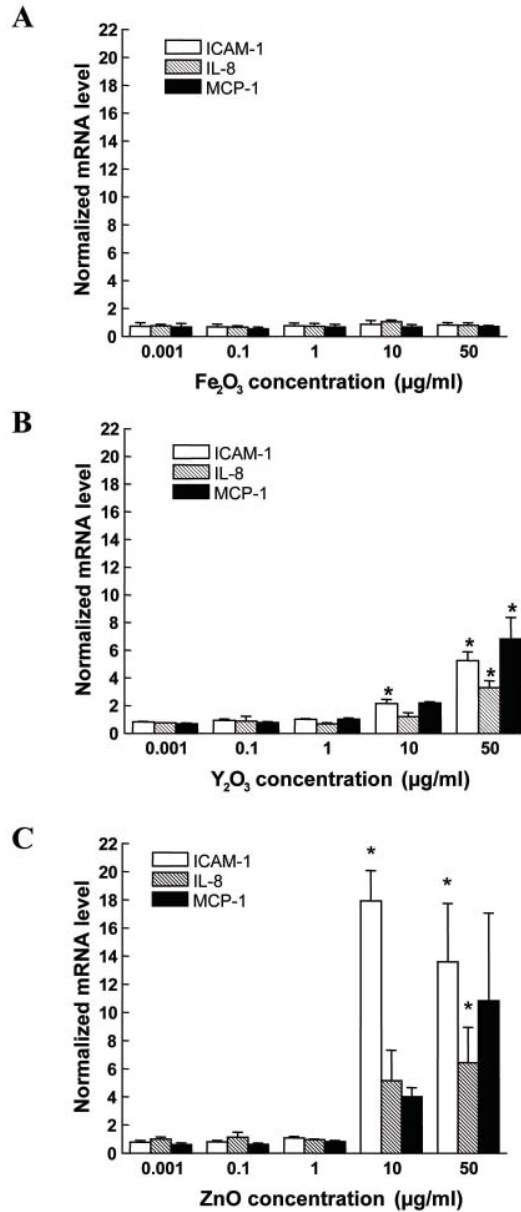


Figure 3. Gene expression of inflammatory markers affected by ZnO but not by Fe₂O₃ nanoparticles that were added to a culture of human endothelial aortic cells. From Gojova et al. (Gojova, Guo, Barakat and Kennedy 2006)

Conclusions

The aerosol synthesis of nanoparticles has been shown to be quite effective in yielding multi-functional materials that are applicable to biosensors and other biological systems. The lanthanide oxides are particularly attractive due to their unique optical properties which have been exploited in the development of sensors for pesticides, potential bio-terror agents such as ricin, and for the detection of bacterial DNA in soils and DNA in samples of blood. The application of these materials raises issues in regard to their safety. Tests of the potential for inflammatory responses in human aortic endothelial cells have shown that there is a range of toxic responses. Iron oxide, quite commonly used as a magnetic core in particles and as an anti-cancer therapy agent or an MRI contrast agent in biomedical applications, was found to be benign. Yttrium oxide, that we have employed frequently as a host material for doping with the lanthanides, showed only a very small potential for an inflammatory response. On the other hand, a semiconductor oxide material such as zinc oxide that is available in a wide range of morphologies and has a number of very useful potential properties for application in nanotechnology, was found to elicit a very strong inflammatory response. Screening of materials through in vitro testing is clearly a desirable first step before continuing with in vivo assays.

Acknowledgments

This publication was made possible by grant number 5 P42 ES004699 from the National Institute of Environmental Health Sciences (NIEHS), NIH and the contents are solely the responsibility of the authors and do not necessarily represent the official views of the NIEHS, NIH. The project was also supported by the National Research Initiative of the USDA Cooperative State Research, Education and Extension Service, grant number 2005-35603-16280. The work on particle-based biosensors and on the toxicity of metal oxide particles was the product of collaborations with many colleagues at UC Davis.

References

- Bathrellos L, Lianidou E, Ioannou P (1998) A highly sensitive enzyme-amplified lanthanide luminescence immunoassay for interleukin 6. *Clinical Chemistry* 44:1351 - 1353
- Cummins CM, Koivunen ME, Stephanian A, Gee SJ, Hammock BD, Kennedy IM (2006) Application of europium(III) chelate-dyed nanoparticle labels in a competitive atrazine fluoroimmunoassay on an ITO waveguide. *Biosensors & Bioelectronics* 21:1077-1085
- Daniels PB, Fletcher JE, Oneill PM, Stafford CG, Bacaresehamilton T, Robinson GA (1995) A Comparison of Three Fluorophores For Use in an Optical Biosensor For the Measurement of Prostate-Specific Antigen in Whole Blood. *Sensors and Actuators B-Chemical* 27:447-451
- Dosev D, Guo B, Kennedy IM (2006) Photoluminescence of Eu³⁺:Y₂O₃ as an indication of crystal structure and particle size in nanoparticles synthesized by flame spray pyrolysis. *J of Aerosol Science* 37:402-412
- Dosev D, Nichkova M, Dumas RK, Gee SJ, Hammock BD, Liu K, Kennedy IM (2007) Magnetic/luminescent core/shell particles synthesized by spray pyrolysis and their application in immunoassays with internal standard. *Nanotechnology* 18:055102

Dosev D, Nichkova M, Liu MZ, Guo B, Liu GY, Hammock BD, Kennedy IM (2005) Application of luminescent Eu : Gd₂O₃ nanoparticles to the visualization of protein micropatterns. *Journal of Biomedical Optics* 10 DOI 064006

Artn 064006

Gojova A, Guo B, Barakat A, Kennedy IM (2006) Induction of inflammation in vascular endothelial cells by combustion generated metal oxide nanoparticles. *Abstracts of Papers of the American Chemical Society* 231

Hatanaka S, Matsushita N, Abe M, Nishimura K, Hasegawa M, Handa H (2003) Direct immobilization of fluorescent dyes onto ferrite nanoparticles during their synthesis from aqueous solution. *Journal of Applied Physics* 93:7569-7570

Koivunen ME, Gee SJ, Kennedy IM, Hammock BD (2004) Nanoscale fluordimmunoassays with lanthanide oxide nanoparticles - 'Lab on a chip'. *Abstracts of Papers of the American Chemical Society* 227:U109-U109

Levy L, Sahoo Y, Kim KS, Bergey EJ, Prasad PN (2002) Nanochemistry: Synthesis and characterization of multifunctional nanoclinics for biological applications. *Chemistry of Materials* 14:3715-3721

Lu HC, Yi GS, Zhao SY, Chen DP, Guo LH, Cheng J (2004) Synthesis and characterization of multi-functional nanoparticles possessing magnetic, up-conversion fluorescence and bio-affinity properties. *Journal of Materials Chemistry* 14:1336-1341

Lu Y, Yin YD, Mayers BT, Xia YN (2002) Modifying the surface properties of superparamagnetic iron oxide nanoparticles through a sol-gel approach. *Nano Letters* 2:183-186

Ma ZY, Guan YP, Liu XQ, Liu HZ (2005) Synthesis of Magnetic Chelator for High-Capacity Immobilized Metal Affinity Adsorption of Protein by Cerium Initiated Graft Polymerization. *Langmuir* 21:6987-6994

Mikola H, Takalo H, Hemmila I (1995) Synthesis and properties of luminescent lanthanide chelate labels and labeled haptenic antigens for homogenous immunoassays. *Bioconjugate Chemistry* 6:235 - 241

Montes M, Jaensson EA, Rozco AF, Lewis DE, Corry DB (2006) A general method for bead-enhanced quantitation by flow cytometry. *Journal of Immunological Methods* 317:45-55

Mulvaney SP, Mattoussi HM, Whitman LJ (2004) Incorporating fluorescent dyes and quantum dots into magnetic microbeads for immunoassays. *BioTechniques* 36:602-609

Nichkova M, Dosev D, Gee SJ, Hammock BD, Kennedy IM (2005) Immunoassay microarrays based on microcontact printing of proteins and fluorescent Eu : Gd₂O₃ nanoparticles as novel labels. *Abstracts of Papers of the American Chemical Society* 229:U104-U104

Nichkova M, Dosev D, Gee SJ, Hammock BD, Kennedy IM (2005) Microarray immunoassay for phenoxybenzoic acid using polymer encapsulated Eu : Gd₂O₃ nanoparticles as fluorescent labels. *Analytical Chemistry* 77:6864-6873

Nichkova M, Dosev D, Gee SJ, Hammock BD, Kennedy IM (2007) Multiplexed immunoassays for proteins using magnetic luminescent nanoparticles for internal calibration. *Analytical Biochemistry* 369:34-40

Sahoo Y, Goodarzi A, Swihart MT, Ohulchanskyy TY, Kaur N, Furlani EP, Prasad PN (2005) Aqueous ferrofluid of magnetite nanoparticles: Fluorescence labeling and magnetophoretic control. *Journal of Physical Chemistry B* 109:3879-3885

Son A, Dosev D, Nichkova M, Ma Z, Kennedy IM, Scow KM, Hristova KR (2007) Quantitative DNA hybridization in solution using magnetic/luminescent core-shell nanoparticles. *Anal Biochem* 370:186-194

Son A, Dosev D, Nichkova M, Ma Z, Kennedy IM, Scow KM, Hristova KR (2007) Quantitative DNA hybridization in solution using magnetic/luminescent core-shell nanoparticles. *Analytical Biochemistry* 370:186-194

Wang DS, He JB, Rosenzweig N, Rosenzweig Z (2004) Superparamagnetic Fe₂O₃ Beads-CdSe/ZnS quantum dots core-shell nanocomposite particles for cell separation. *Nano Letters* 4:409-413

Wheelock AM, Morin D, Bartosiewicz M, Buckpitt AR (2006) Use of a fluorescent internal protein standard to achieve quantitative two-dimensional gel electrophoresis. *Proteomics* 6:1385-1398

Conference Questions and Answers

Question:

Do you see differences in pulmonary inflammatory response over the different lanthanides?

Answer:

We have not looked at the toxicity of europium or the other elements in the lanthanide series, except for cerium, which is a diesel fuel additive.

Question:

You showed a picture of zinc oxide in the vacuole. Do you know what the fate of the zinc oxide will be? Could it be precipitated?

Answer:

I think not. It would probably go into solution. There are many questions about this. Why would the cell react in this way? The cell might have tried to pump in protons to maintain the pH of the vessel, but that is outside my biological background. People also have shown that cells will accommodate these events over time, so we might see some accommodation of zinc exposure. With those kinds of doses in that situation, you see a significant loss of cell viability.

Comment:

The number of particles per cell looked to be quite large.

Response:

They are very large doses. When doing in vitro studies, you need a large dose to be able to see anything. But is it physiologically relevant? Probably not.

Question:

What kind of uniformity is achieved in the particles you make?

Answer:

A typical aerosol method produces a fully dispersed aerosol. The average size of a particle is 50 nm, with a range from 20 to 100 nm. That could be narrowed if we wanted to go to the trouble, but one of the great beauties of the lanthanides is that the lanthanide emission dispersion is insensitive to size. If you try to get too small, you end up with a loss of quantum efficiency due to the surface defect problem. A larger particle yields a better efficiency, but the size makes little difference. The important factor is the location of the line on the spectrum. As long as we have a consistent surface area per unit mass, the surface area per gram of material is constant.

Environmental Aspects of Applications of Quantum Dot-Based Nanosensors

*Hatice Şengül and Thomas L. Theis, Environmental,
Atmospheric, Earth and Marine Sciences Research Programme
TUBITAK (The Scientific and Technological Research Council of Turkey), and
Institute for Environmental Science and Policy, University of Illinois at Chicago, Chicago,
Illinois, U.S.A.*

Abstract

It is not yet clear if emerging technologies of the 21st century will bring us closer to sustainability as most have multi-faceted environmental aspects. Environmental tradeoffs of replacing current technologies with emerging ones must be identified prior to the widespread adoption of nano-based products. This paper reviews the environmental tradeoffs involved in the application of quantum dot-based nanosensors. On the positive side, quantum dot sensors are superior to current sensors due to their unique properties such as enhanced luminescence, band gap tunability, and the possibility of detection of multiple pollutants and pathogens simultaneously. These properties enable quantum dots to be applied as nanosensors for environmental analysis and monitoring (screening, diagnostic and monitoring). There are many alternative semiconductor materials for production of quantum dots, however, investigations have mostly concentrated on cadmium sulfide, cadmium selenide, or cadmium selenide/zinc sulfide quantum dots as candidate compound semiconductors for nanosensors, all of which are toxic and nonrenewable. This paper reviews some of the positive and negative impacts of quantum dot based nanosensors from an environmental perspective based on accounts of quantum dot based nanosensors in the literature as well as results of the life cycle inventory analysis of cadmium selenide quantum dots previously completed by our group.

Introduction

Knowledge and innovation will continue to play a major role in the advancement of nations and societies in the 21st century. As economies become more dependent on innovation and the role of emerging technologies in shaping nations increase, more resources are being allocated to follow new research trails, more capital flows to R&D and as a result, the transition time period between research and commercialization for new products is becoming shorter than ever. Shorter lifespans of products in the market means products become obsolete more quickly adding to the existing waste management issues. There is now a greater risk of impairment of ecological and public health due to emerging technologies if we fail to address their environmental impacts before, or at least while, investing in them. Hence, there is a growing need for investigation of environmental tradeoffs of replacing existing technologies with emerging ones to refrain the replacement of existing products with products that have significantly higher negative environmental impacts.

Sustainable development of emerging technologies is part of the Sustainable Consumption and Production (SCP) paradigm which is indispensable for the well-being and survival of humanity. SCP is one of the actions called for by the Johannesburg Plan of Implementation, agreed at the

World Summit on Sustainable Development in 2002 in Johannesburg, South Africa (United Nations 2009):

“All countries should promote sustainable consumption and production patterns, with the developed countries taking the lead and with all countries benefiting from the process, taking into account the Rio principles, including, inter alia, the principle of common but differentiated responsibilities as set out in principle 7 of the Rio Declaration on Environment and Development.”

Industries, government agencies, research institutions, NGOs, and all other interested parties should take part in ensuring sustainability of emerging technologies. The problem is little is known about the role of emerging technologies in sustainable development and their environmental impacts at the conception of products since concurrent engineering practices which would include implementation of “design for the environment” principles are still not widely practiced. Rapid assessment of environmental impacts of emerging technologies is key to address concerns, take actions swiftly, and aid in decision-making. The time constraint is an additional challenge for environmental engineers and scientists exploring environmental impacts of emerging technologies. But, by identifying environmental impacts early on, better manufacturing practices and materials may be selected resulting in huge environmental benefits over the long run.

This paper addresses some of the positive and negative impacts of quantum dot based nanosensors based on information from the literature and our life cycle analysis of cadmium selenide quantum dots completed previously (Sengul and Theis 2009a). Quantum dots are semiconductor nanocrystals that typically contain a semiconductor core and a capping agent. They are usually between 3-15 nanometers in diameter. Since the exciton bohr radius of a quantum dot is smaller than the size of the dot itself, quantum confinement is observed. As a result, with changes in composition (i.e. semiconductor core and capping agent), shape, temperature and pressure; optical and electronic properties of quantum dots can be changed which lead to diverse applications.

Quantum dot based nanosensors is one of the fourteen quantum-dot based technologies under investigation. Quantum dot based nanosensors are promising alternatives to conventional sensors for detection of pathogens, metal ions, hydrocarbons, and cyanide. Quantum-dot based nanosensors is one of the nano-based technologies that has positive environmental implications. On the other hand, semiconductors for quantum dots contain heavy metals and/or nonrenewable materials. In addition, the production of quantum dots is material and energy intensive. However, improvements in quantum dot production technology and transition to non-heavy metal compound semiconductors may enable nanosensors to be more competitive alternatives to conventional sensors.

Positive and negative environmental aspects of quantum-dot based nanosensors

Quantum dot-based nanosensors are optical sensors based on fluorescence measurements. When excited by an external stimulus, they emit light. They can respond to different analytes via changes in their emission (Jin et al. 2005)--either quenching or enhancement of the emission by the analyte. Different mechanisms for the changes in emission are investigated. In some cases, analytes may react with surface heteroatoms (S, Se, Te) to affect the optical properties of the material (Konishi and Hiratani 2006). In other cases, analyte may form complexes with the capping agent. Quantum-dot based nanosensors have superior properties than current sensors. Quantum dots have enhanced luminescence (narrow emission profile) and size tunable emission. Quantum

dots are resistant to photobleaching. In addition, simultaneous detection of more than one analyte (pollutants or pathogens) is possible with quantum dot based nanosensors (Riu et al. 2006). Environmental applications of quantum dot based nanosensors include:

- Pathogen detection,
- Metal ion detection,
- Hydrocarbon detection, and
- Cyanide detection.

Recent empirical studies report successful detection of a variety of pathogens. Examples of pathogen detection in the literature include the detection of *Cryptosporidium parvum* and *Giardia lamblia* quantum dot-antibody conjugates by Zhu et al. (2004), detection of *E. coli* using CdSe/ZnS quantum dots by Hahn et al. (2005), and detection of *E. coli* O157:H7 and *S. typhimurium* by Yang and Li (2006).

Examples of metal ion detection in the literature include the analysis of Cu(II) and Zn(II) ions in water samples by L-cysteine, and thioglycerol capped cadmium sulfide quantum dots by Chen and Rosenzweig (2002), copper ion (Cu(II) and Cu(I)) detection using an oligo (ethylene glycol) capped cadmium sulfide quantum dot nanosensor by Konishi and Hiratani (2006), and detection of Cu(II) and Ag(I) with a peptide-coated cadmium sulfide quantum dot nanosensor by Gattas-Asfura and Leblanc (2003). Chen and Rosenzweig (2002) observed quenching of the luminescence of quantum dots as a result of reduction of Cu(II) to Cu(I) by thioglycerol (i.e. the capping agent). In contrast, in the presence of zinc ions, they observed an enhancement of luminescence --two-fold increase in luminescence intensity-- which was attributed to the selectivity of quantum dots toward zinc ions due to the formation of a zinc-cysteine complex on the surface of quantum dots.

An example of detection of aromatic hydrocarbons was shown by Sirinakis et al. (2003) using CdSe/ZnS quantum dots. An example of cyanide detection was carried out by Jin et al. (2005) who observed quenching of luminescence with increase in cyanide concentration.

In this respect, the use of quantum dot nanosensors for environmental applications seems beneficial. This benefit, however, must be weighed against some of the negative impacts quantum dots have. There are more than 600 semiconductor materials available to researchers but quantum dots most commonly studied to date contain heavy metals and/or non-renewable materials, as can be seen in Figure 1. Cadmium and zinc containing quantum dots are more widely applied than all other quantum dots. In addition, as reported previously by our group (Sengul and Theis, 2009a), the production of quantum dots is both material and energy intensive, discovered via a cradle-to-gate life cycle analysis of cadmium selenide quantum dots using SimaPro (Pre 2008), Ecoinvent database (Ecoinvent Centre 2004), and various literature sources and patents. As can be seen in Figure 2, which shows Cumulative Energy Demand (CED) of some commonly used materials and nanoscale materials for which a cumulative energy demand data is available, the energy demand of quantum dots is the highest among all materials except carbon nanotubes.

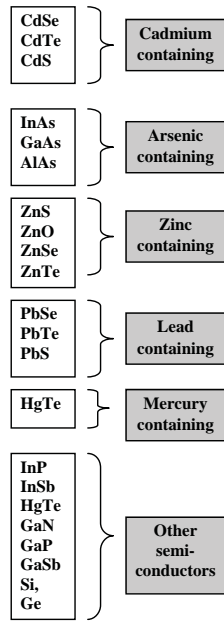


Figure 1. The list of candidate semiconductors for quantum dot-based applications.

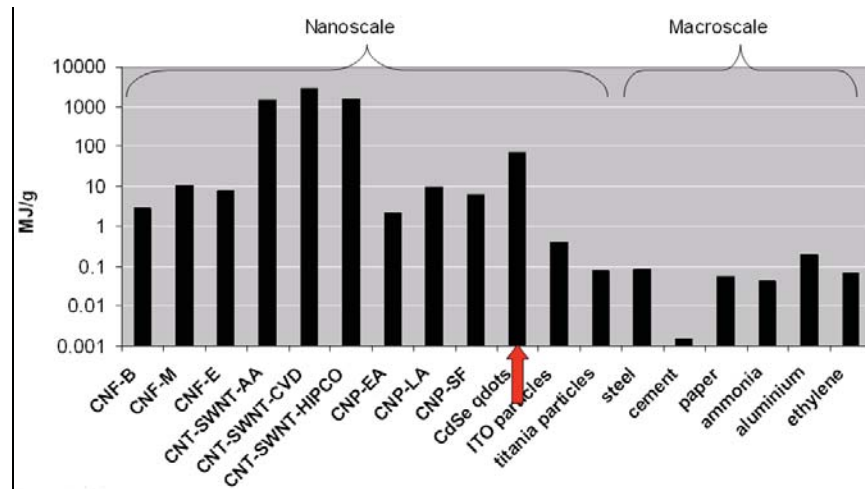


Figure 2. Cumulative Energy Demand (CED) comparison of materials.

Note: 1. Abbreviations: CNF: Carbon Nanofiber (-B: benzene as feedstock, -M: methane as feedstock, -E: ethylene as feedstock), CNT-SWNT: Carbon Nanotube-Single Wall Nanotube (-AA: Arc ablation, -CVD: Chemical Vapor Deposition, HIPCO: High-Pressure Carbon Monoxide (HiPCO) process). CNP: Carbon Nanoparticles (-EA: Electric Arc, -LA: Laser ablation, -SF: Solar Furnace). Data sources: CNF: Khanna et al. (2008), CNT: Isaacs et al. (2006), titania nanoparticles: Grubb and Bakshi (2008), CNP: Kushnir and Sanden (2008), CdSe qdots: Sengul and Theis (2009a), others: Ecoinvent (2007).

The major sources of energy consumption of quantum dots are due to solvent use associated with isolation and size selective precipitation, and the disposal of hazardous waste. Figure 3 shows

the contribution of materials and processes to the CED for CdSe quantum dot synthesis. Most of the energy demand comes from methanol and 1-butanol) with lesser amounts from TOP (TriOctylPhosphine) and TOPO (TrioctylPhosphine Oxide) and dimethyl cadmium.

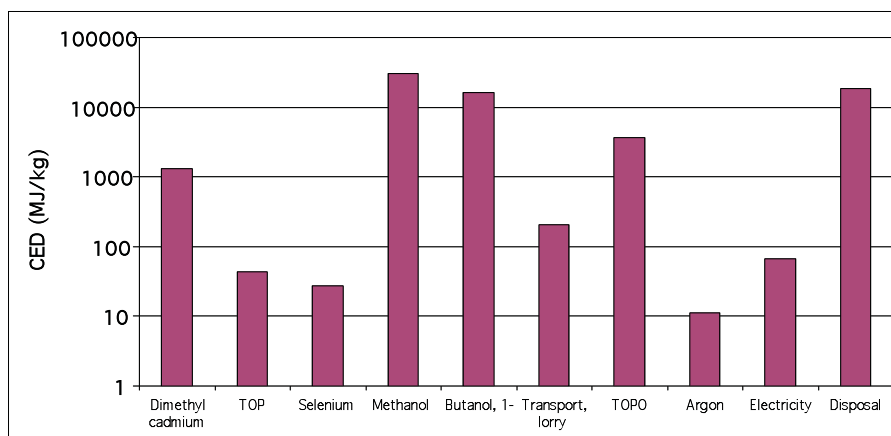


Figure 3. Contribution of materials and processes to the cumulative energy demand for sol-gel synthesis of CdSe quantum dots (TOP: trioctylphosphine, TOPO: trioctylphosphine oxide).

Interestingly, few existing research studies on the development of “greener” synthesis pathways for quantum dots has so far focused on replacing the most toxic solvents and dimethyl cadmium as a precursor material, rather than reducing the total amount of solvents used or instituting solvent recovery processes. We investigated the effects of alternative solvent systems and solvent recovery by distillation and reuse on the energy demand using pyridine/hexane and chloroform/methanol solvent systems as alternatives. Lower grade petroleum fractions (“petroleum ethers”) can also be substituted for hexane/1-butanol. In both systems the solvents can largely (95%) be recovered by distillation, resulting in a proportional decrease in hazardous waste (Murphy 2008). Distillation energy requirements of solvents were retrieved from Capello et al. (2007) who compiled energy requirements for various common solvents. Such substitution can result in as much as 55% reduction in CED of quantum dot production.

The multi-faceted nature of quantum dot nanosensors also exists in other quantum dot-based technologies. According to our recent results (Sengul and Theis 2009b), the market diffusion of quantum dot LEDs (Light Emitting Diodes) may result in energy, mercury consumption and emission savings while requiring cadmium and energy consumption. But, the mercury consumption savings with replacement of fluorescent and High Intensity Discharge (HID) lamps are much higher than cadmium consumption requirements if cadmium selenide quantum dot LEDs are to be adopted in the next decade in the United States. Similarly, for quantum dot PV modules, their environmental impacts (cumulative energy demand, global warming potential, SO_x and NO_x emissions, and heavy metal emissions) were found to be less than other types of PV modules, except heavy metal emissions. QDPV modules have a better environmental performance than carbon-based energy sources but they have longer energy pay back times than wind and hydro-power (Sengul and Theis 2009c). In the case of quantum dot-based sensors, a comparative analysis with competing technologies must be carried out to determine net loss or gain.

Conclusion

For sustainable technology development, there is a growing need for transition from sequential engineering practices to concurrent engineering practices in which case design for sustainability principles can be incorporated in all phases of development of a product or product line. However, until then, interdisciplinary research capabilities must be enhanced to shed light on the role of emerging technologies in sustainable development. We also need a life cycle approach which takes a systems approach and enable evaluation of impacts quantitatively. In this paper, we reviewed the environmental tradeoffs involved in the adoption of quantum dot nanosensors for environmental applications. Further research is needed to determine the net environmental gain or loss of use of quantum dot-based sensors. For comparative assessments with competing technologies (i.e. current applicable and available sensors), environmental impacts of current sensors must also be investigated.

References

- Capello, C.; Hellweg, S.; Badertscher, B., Betschart, H., Hungerbuhler, K. (2007) "Part 1: The ecosolvent tool - Environmental assessment of waste-solvent treatment options" *J. Ind. Ecol.* 11(4): 26-38.
- Chen, Y.F. and Z. Rosenzweig (2002). "Luminescent CdS quantum dots as selective ion probes" *Anal. Chem.* 74(19): 5132-5138.
- Ecoinvent Centre (2004). *ecoinvent data v2.0.*, Swiss Centre for Life Cycle Inventories, Dübendorf, Switzerland 2004.
- Gattas-Asfura, K.A.; Leblanc, R.M. (2003). "Peptide-coated CdS quantum dots for the optical detection of copper(II) and silver(I)" *Chem. Comm.* 21: 2684-2685.
- Grubb G.F. and B.R. Bakshi (2008). "Energetic and environmental evaluation of titanium dioxide nanoparticles" *P. IEEE Electron. Environ. Conf.* San Francisco. CA, U.S.
- Hahn, M.A.; Tabb, J.S.; Krauss, T.D. (2005). "Detection of single bacterial pathogens with semiconductor quantum dots" *Anal. Chem.* 77(15): 4861-4869.
- Isaacs, J.A., Tanwani A., Healy, M. L. "Environmental Assessment of SWNT Production" *P. IEEE Electron. Environ. Conf.* San Francisco. CA, U.S.
- Jin, WJ; Fernandez-Arguelles, MT; Costa-Fernandez, JM, Pereiro R, Sanz-Medel A. (2005) "Photoactivated luminescent CdSe quantum dots as sensitive cyanide probes in aqueous solutions" *Chem. Comm.* 7: 883-885.
- Khanna, V.; Bakshi, B.R.; Lee, L.J. (2008). "Carbon nanofiber production: Life cycle energy consumption and environmental impact" *J Indus. Ecol.* 12(3): 394-410.
- Konishi, K. and T. Hiratani (2006). "Turn-on and selective luminescence sensing of copper ions by a water-soluble Cd₁₀S₁₆ molecular cluster" *Angew. Chem. Int. Ed.* 45(31): 5191-5194.
- Kushnir, D. and B.A. Sanden (2008). "Energy requirements of carbon nanoparticle production" *J. Ind. Ecol.* 12(3): 360-375.

- Murphy C., University of Pennsylvania. Department of Chemistry. e-mail communication. 2008
- PRé Consultants, (2008). SimaPro, Life Cycle Assessment software package. Version 7.1.4 Amersfoort, The Netherlands.
- Riu, J; Maroto, A; Rius, F.X. (2006). "Nanosensors in environmental analysis" *Talanta* 69(2): 288-301.
- Sengul, H., Theis, T.L. (2009a). "Life cycle inventory of semiconductor CdSe quantum dots for environmental applications" In *Nanotechnology Applications for Clean Water* by Savage et al. Norwich: William Andrew Inc.
- Sengul, H., Theis, T.L. (2009b). "Quantum Dot-based Technologies for the Future: A Quantitative Assessment of Quantum Dot Consumption and Associated Environmental Impacts through Adoption of Quantum Dot LEDs in the United States in the Next Decade, 2009-2018" (to be submitted to *Journal of Industrial Ecology*)
- Sengul, H., Theis, T.L. (2009c) Environmental impacts of nanophotovoltaics: A life cycle analysis of QDPV modules. *Journal of Cleaner Production* (submitted for publication)
- Sengul H. (2009). "Life cycle analysis of quantum dot semiconductor materials". Ph.D. Thesis. 2009.
- Sirinakis, G., Zhao, Z.; Sevryugina, Y.; Petrukhina, M.; Carpenter, Michael A.; Tayi, A. (2003) "Tailored nanomaterials: Highly selective & sensitive chemical sensors for hydrocarbon analysis" Abstracts, 31st Northeast Regional Meeting of the American Chemical Society, Saratoga Springs, NY, United States, June 15-18
- United Nations (March, 2009). Department of Economic and Social Affairs Division for Sustainable Development. "Johannesburg Plan of Implementation" http://www.un.org/esa/sustdev/documents/WSSD_POI_PD/English/POIChapter3.htm
- Yang, LJ; Li, YB (2006). "Simultaneous detection of Escherichia coli O157 : H7 and Salmonella Typhimurium using quantum dots as fluorescence labels" *Analyst* 131(3): 394-401.
- Zhu, L; Ang, S; Liu, WT (2004). "Quantum dots as a novel immunofluorescent detection system for Cryptosporidium parvum and Giardia lamblia" *Appl. Environ. Microbiol.* 70(1): 597-598.

Conference Questions and Answers

Question:

Have you evaluated the potential for occupational exposure?

Answer:

No. Our analysis has not included toxicity at all.

Question:

How were the numbers calculated for energy consumption?

Answer:

Energy consumption was calculated per mass, per kilogram of material.

Question:

Would you conclude that production of quantum dots requires more energy and creates more waste, so that their waste-to-product ratio is higher?

Answer:

Yes. I think that is true.

Question:

Your group obviously is using quantum dots for applications. Do you see any potential for environmental conflicts?

Answer:

We are trying to understand the tradeoffs, or balance, by assessing the connection between nanotechnology and sustainability. Will it move us closer to sustainable living, or away from it?

Panel Discussion

Nanosensors – Where Are We Going?

Facilitators:

Heather Henry, National Institute of Environmental Health Sciences

Warren Layne, U.S. EPA

Panelists:

Dermot Diamond, Glen E. Fryxell, Li Han, Am Jang,

Ian M. Kennedy, Hatice Şengül, Ashok Vaseashta, Ryan S. Westafer

Warren Layne: What do you think about the future of nanosensing, and how would you improve on the devices being used for sensing now?

Glen Fryxell: It is important to use “nano-enabled” terminology, because our topic is not just small sensors. Nanosensors can be important sensing devices on their own, but nanotechnology also can improve the performance of existing macrosensors. For example, existing large devices for measurement and monitoring can be made hand-portable.

Ashok Vaseashta: Specificity is an important aspect of sensing that still needs to be addressed. A sensor may be able to detect half a dozen analytes yet still lack appropriate specificity, which is particularly important for biological sensing. The necessary level of specificity can be accomplished only with nano-enabled technology. Using specific functionalization, you can create a specific group that looks for a specific type of chemical composition.

Warren Layne: I believe the sensors being developed in Dr. Fryxell’s lab have different functionalities and can be used to detect many different analytes, with a particular emphasis on metals in the environment. Papers have been published that contain information about carbon nanotube-potentiated microdetectors that can detect chlorocarbons down to a few molecules. So far, that work seems to be in a preliminary stage confined to laboratories. Do any of you have additional information concerning that kind of research?

Dermot Diamond: A lot of work at the nanoscale is done just to show you can do it. People talk about a “lab on a chip.” There is a reverse side to that, however, referred to as the “chip in a lab.” This is a chip surrounded by huge pieces of sensitive equipment to pick up the tiny signal emitted by the chip. At any major conference we can see examples of fantastic work in materials science that is fundamental, but not practical.

Ian Kennedy: It is not always necessary to get down to single-molecule detection. For example, a paper from an Army research office discussed ricin detection at zeptomolar concentrations. This is certainly magnitudes lower than any detectable health effect. We know of EPA’s interest in highly sensitive sensor networks for atmospheric gases, but there are other avenues and interests, such as the biological exposure work supported by the National Institute of Environmental Health Sciences (NIEHS). Our work at the University of California at Davis is focused less on exquisite detection sensitivity than in being able to determine a whole class of pesticides. We need high throughput to handle large numbers of samples, and it may be necessary to trade off some sensitivity and specificity to achieve that.

Glen Fryxell: To follow up on that idea, information must be delivered quickly in instances of worker exposure to hazardous chemicals, such as aromatic hydrocarbons. The ability to detect a single molecule is not relevant when rapid delivery of data about a class of chemicals is needed to deal with a hazard and prevent excessive exposure in the workplace.

Ryan Westafer: Grants have been awarded for taking actual olfactory cells sustained on growth medium to use in detection. But that is not ready for the field!

Steve Takach (Gas Technology Institute): Is anyone able to address the issue of manufacturability at large scale, eventual cost, and when this will come to fruition? Also, when are we likely to get to the point where we might be able to incorporate these sensors into a material substrate, as in building them into the fabric of bridges for early detection of failure points, rather than applying them externally?

Li Han: When we talk about the industrialization of sensor material development, it depends on the type of material. Several companies are making electro-spinning equipment that can manufacture hundreds of meters of material per hour, as much as 45 meters per minute. But how to optimize the components of the composite sensing material has yet to be determined.

Dermot Diamond: There are several key blocks preventing fundamental advances. While many papers about sensor networks appear in the literature, most papers report on theoretical work or modeling what the systems will do. There are no reports of real deployments of notable scale. Also, almost all the devices in the literature rely on batteries. Why do they need a separate power supply? Why is there not a targeted initiative to integrate the latest materials in power-scavenging technology with those for the sensor communication mode to produce a platform that is autonomous in terms of power? The use of batteries is a limiting factor and requires appropriate waste disposal. We need to move beyond that. Fundamental advances in materials science are needed to develop power-scavenging technologies that can be integrated into autonomous sensor systems, and then systems that include vibration detectors, temperature sensors, light detectors, and acoustic sensors can be developed for incorporation into buildings, bridges, and roads. Even sensors capable only of very simple surrogate measurements could communicate that their measurements have departed from the standard range, which would alert someone to the need for a physical inspection and analysis of the sensor data.

Ryan Westafer: Nanoparticles are very difficult to move around and place exactly where you want them. Manufacturing something like quantum dots in quantity is likely to require a lot of man-hours and a great deal of energy.

Warren Layne: Has anyone seen any recent information on using arrays to magnify signals?

Dermot Diamond: A type of sensor array called the “artificial nose” was popular, became unfashionable, and now is resurfacing. Theoretical papers on the capacities of sensor arrays have been appearing in the literature since the 1980s, but there is considerable room for skepticism. Chemical sensors drift as they age, and their characteristics continue to change. How can you model them mathematically when they are constantly changing? Arrays are even worse, because the sensors are drifting at different rates and in different directions as they lose sensitivity and

selectivity. It is important to uncouple the hype from the reality.

Ashok Vaseashta: With regard to the future of sensor development, it is important for sensors to be able to detect an unexpected chemical or biological agent in a mixed, complex environment for general health and safety monitoring and for averting threats. We need to focus on developing sensors with high specificity toward known agents to pinpoint environmental health and safety problems.

Mark Bruce (TestAmerica): As a potential sensor user, I would like to find a Web site that summarizes all or most of the different chemical sensors and provides information on their performance characteristics. Is a Web site available for that? A European Web site, EVISA (European Virtual Institute for Speciation Analysis, www.speciation.net/), describes much of the metal speciation work going on in the world. If a similar site for chemical sensors does not exist now, it would be very useful to see one developed for the potential market.

Marie-Isabella Baraton (University of Limoges): It would be difficult to develop a Web site for sensors due to the fragmentation of research efforts and diversity of industry needs. Depending on the applications required by industry, sensor properties differ depending on whether they were developed with a focus on selectivity, sensitivity, or low cost. Some outstanding research is being done in areas of no interest to industry, because it is too expensive.

Dermot Diamond: Although it is not what Mr. Bruce asked for, the journal *Analytical Chemistry* publishes a biennial fundamental review of research that covers many areas, including chemical sensors. The review can provide a good idea of what has happened over the last two years in the research community.

Warren Layne: Where is your nano-enabled research going, Dr. Kennedy? Are human health and the environment factored into your plan? Would you put money into toxicity studies?

Ian Kennedy: We are trying to put our work into practice with a start-up company, so we are moving into applications. Making something practical is the next problem. We would like to put money into toxicity studies, but it is difficult to work toxicity testing into the budget in a start-up company, and it would be hard to find a sponsor who would pay for it. It probably will have to be done in a different context through NIEHS or EPA, because small companies are not likely to be able to afford it.

Warren Layne: Could you partner with an agency to do it?

Ian Kennedy: If we had a grant. Or the agency could add an addendum to Small Business Innovation Research grants to address the toxicity study issue.

Warren Layne: It is a burden, but the developers and manufacturers should be concerned whether the public is exposed or not.

Ian Kennedy: Is it really an issue? It seems unlikely that the public will be exposed to huge amounts of nanoparticles. Most nanoparticles will aggregate themselves, be bound up in soils or minerals, or be scavenged by other surfaces in the environment. They may preserve their surface area, but they are not likely to be presented to cells or organisms as distinct nanoparticles. The toxicity may be serious, but the potential for exposure may be quite small.

Glen Fryxell: That seems to have been borne out in earlier discussions today about the difficulties encountered in environmental testing. The particles tend to adhere, which makes them less mobile in the environment and, therefore, less of a risk.

Heather Henry: Does Europe's REACH (Registration, Evaluation, and Authorization of Chemicals) affect the research and development of nano-enabled sensors?

Dermot Diamond: Not in my area of research.

Marie-Isabelle Baraton: It is not affecting sensor research. For the sectors that are affected, a project submitted to the European Commission must include a risk assessment and a life-cycle analysis.

Warren Layne: At present, nanotechnology research is not putting massive amounts of nanoparticles into the environment. If the manufacturing of nanomaterials becomes a \$2.4 trillion industry in five to 10 years, as has been projected, will we reach a critical mass of nanoparticles in the environment that will produce unanticipated effects? That is the present concern of agencies like EPA, NIEHS, and the National Science Foundation. If nanotechnology is at the cutting edge of technology, where is it taking us?

Li Han: When use of nanomaterials becomes widespread, there also should be a great increase in nanoparticle wastes that require recycling or disposal. This prospect must be of concern to EPA.

Warren Layne: Yes. We have many concerns. For example, what happens to nanoparticles in an incinerator? That has not been studied.

Li Han: Some nanomaterials like cadmium/selenium will retain their toxicity, and if widely produced, they are likely to find their way into the soil.

Ian Kennedy: Incineration is not effective for cadmium; it would go up the stack, probably as nanoparticles of an oxide. Perhaps it could be captured at the stack, but it would seem safer to bury it.

Warren Layne: Nanomaterials, however, are going into tennis rackets and clothing and shoes that might be incinerated. When cars are recycled, some of the material separation processes involve high heat. How will the nanomaterials be affected by these processes when they are used extensively in cars? Examples like these are important topics for consideration in the future.

Chapter 4 – Introduction

Analysis & Characterization of Nanomaterials

Warren L. Layne, United States Environmental Protection Agency

The following chapter presents papers on the analysis and characterization of nanomaterials. No platform sessions were specifically devoted to this very important topic, so the results were presented during the poster session. Multiple techniques particularly useful for analysis and characterization of a number of nanomaterial preparations are described.

Detection and characterization of several elements present in nano dots are discussed in one of the papers. Currently, nano dots are incorporated into sensing devices for in vitro sensing of environmental contaminants and for in vivo measuring of chemical changes in cells. Cadmium selenide (Cd-Se) or zinc sulfide (Zn-S) containing quantum dots and silver nanoparticles (which have are being used as a bactericide) were fractionated with flow field-flow fractionation (FI FFF). The quantum dots and silver nanoparticles were then measured by real time, single particle mode inductively coupled plasma-mass spectrometry (ICP-MS). It should be noted that the paper involved the international collaboration of researchers from the Colorado School of Mines in the United States and the Gwangju Institute of Science and Technology in The Republic of Korea.

The other two papers are from the laboratory of Jamie Lead in the United Kingdom and address measurement of nanomaterial interaction with environmentally relevant materials. One paper investigates interaction of multi-walled carbon nanotubes with three surfactants to determine if the known stabilization of the nanotubes in water by soil humic substances (HS) is due to the surfactant nature of HS. The other paper uses transmission electron microscopy techniques to investigate uptake by the gram negative bacterium *Pseudomonas fluorescen*. Uptake of iron oxide nanoparticles is compared with uptake of dissolved iron in the presence of HS.

The instruments used for analysis and characterization of the nanoparticles and quantum dots are state of the art. These include: photon correlation spectroscopy, flow field–flow fractionation, and dynamic light scattering instruments for particle size analysis. Real time, single particle mode ICP-MS is able to detect and size elemental silver nanocrystals in parts per trillion concentrations. Near edge x-ray absorption spectroscopy is used to characterize the chemical nature of Aldrich humic acid (HA) and water-extractable Catlin soil HS containing aqueous media. These aqueous solutions mimic water both found in the natural environment and into which nanomaterials could be released.

In most cases, dedicated computer software programs are required to analyze the data produced from these instruments. The results are the product of international cooperation between industry and academia. In each laboratory, great care was taken to ensure reproducibility of identical engineered nanomaterials. The proof of this uniform engineering of environmentally relevant nanomaterial preparations required exhaustive observation and characterization of the physical and chemical properties of all preparations.

Detection and Characterization of Inorganic Nanoparticles Using Inductively Coupled Plasma-Mass Spectrometry in Hyphenated and Real Time Single Particle Modes

Emily K. Lesher, Colorado School of Mines, Golden, Colorado, U.S.A.

Sungyun Lee, Gwangju Institute of Science and Technology, Gwangju City, Korea

James F. Ranville, Colorado School of Mines, Golden, Colorado, U.S.A.

Abstract

With the growth of the nanotechnology industry, methods to characterize nanomaterials in environmental samples, where significant dilution and complex matrices are likely, are needed. Inductively coupled plasma-mass spectrometry (ICP-MS), when used hyphenated and real time single particle (RTSP) mode is a powerful detector for inorganic nanoparticles. We have used hyphenated ICP-MS, where particles are first separated by hydrodynamic diameter using flow field flow fractionation (FI FFF), to measure the size distribution, metal concentrations, and purity of quantum dots. We have used RTSP ICP-MS to detect the presence of silver nanoparticles at environmentally relevant concentrations.

Background

Inductively coupled plasma-mass spectrometry (ICP-MS) has been commercially available for over two decades and has been used extensively in biology, medicine, geology, and environmental science. Elements in the sample are ionized in the plasma, and those ions are focused through a lens, separated by a quadrupole, and counted by the mass spectrometer, producing an intensity reading. Intensity is converted to concentration by comparing readings to a multipoint calibration curve.

Data analysis software (Elan v. 3.2.1., Perkin Elmer) allows for transient signal acquisition, or the collection of many intensity readings taken back-to-back, as a function of time. We use transient signal acquisition in two modes to characterize nanoparticles: hyphenated mode, where samples are first size fractionated, and real time single particle (RTSP) mode, where the time increments of the transient signal are small enough to capture the composition of a single nanoparticle.

Hyphenated mode

In hyphenated mode, particles are first separated by hydrodynamic diameter using FI FFF. ICP-MS can then measure metal concentrations as the particles elute. FI FFF separation is similar to chromatographic techniques, but relies on a fluid cross-flow for separation instead of interactions between analytes and a stationary phase. A carrier fluid loads the particles in a 20 μ l sample onto the channel where a recirculating flow perpendicular to the channel flow pushes them against a 1 kDa membrane. This creates a concentration gradient, and the particles then tend to diffuse away

from the membrane, against the cross-flow. The diffusion coefficient is a function of particle size. These competing forces (the force of the cross-flow, which can be adjusted by altering the flow rate, and the diffusion of the particles) result in the particles attaining an equilibrium positioning within the thickness of the channel, with the smallest particles the farthest, on average, from the membrane. Flow within the channel is laminar, thus the particles that are farthest from the membrane are subject to greater velocities than those closer. This results in fractionation; smaller particles have greater diffusion coefficients and thus elute out first. FFF theory can link elution time to hydrodynamic diameter. A full explanation can be found in Schimpf et al. (2000).

Online elemental detection is a powerful add-on capability to FI FFF. The result is the ability to measure size-based elemental composition of particles, metal adsorption to nanoparticles and colloids, and metal complexation with natural organic matter. For this work, we used FI FFF-ICP-MS with a relatively long dwell time to capture the metal concentrations as the quantum dots eluted out of the FI FFF.

RTSP mode

In RTSP mode, ICP-MS detects the presence of some nanoparticles at environmentally relevant concentrations, and also has potential for use in sizing. RTSP mass spectrometry has been used in the past to monitor aerosols (Noble and Prather 2000) and larger lab synthesized colloids (De-geldre and colleagues 2004, 2006a, 2006b). We have used the RTSP method to detect and size elemental silver nanoparticles at environmentally relevant concentrations (parts per trillion).

In RTSP mode, a solution containing a dissolved metal will give a stable intensity versus time signal at a level proportional to the concentration of the metal. In contrast, a suspension containing just metal-bearing particles would only give an intensity greater than background when a particle is ablated in the plasma and the pulse of ions hits the detector. Thus, the signal should be steady at the baseline except when a particle goes through and creates a spike, or a single reading that is above the background. The concentration of particles is then proportional to the number of spikes observed during a run.

RTSP mode relies on a very short dwell time. The dwell time is the interval of time during which the mass spec is counting ions at a certain mass to charge ratio. While normal analyses for total concentration might use a dwell time of 200 ms and average three replicates, here we used a dwell time of only 10 ms. The detection limit of the method depends on the type of nanoparticle. For a single nanoparticle to be detected, the mass of metal divided by the volume of plasma analyzed during the dwell time must be greater than the detection limit of the instrument.

Methods and Materials

We have characterized polyethylene glycol (PEG) coated CdSe/ZnS core/shell quantum dots (type 2-MP, maple red-orange color, Lot# AWN 1312N, Evident Technologies, Troy, NY, US) using ICP-MS hyphenated with flow field-flow fractionation (FI FFF). We employed a FI FFF, model F-1000, made by FFFractionation, now called Post Nova (UT, USA). It was equipped with 1 kDa regenerated cellulose membrane (Post Nova, UT, USA), a 20 ul stainless steel injection loop (Rheodyne WA, USA), and was powered by two Acuflo Series II HPLC pumps. A solution of 0.01% FL-70 (Fisher Scientific, NJ, USA) and 0.1 mM sodium azide was used for

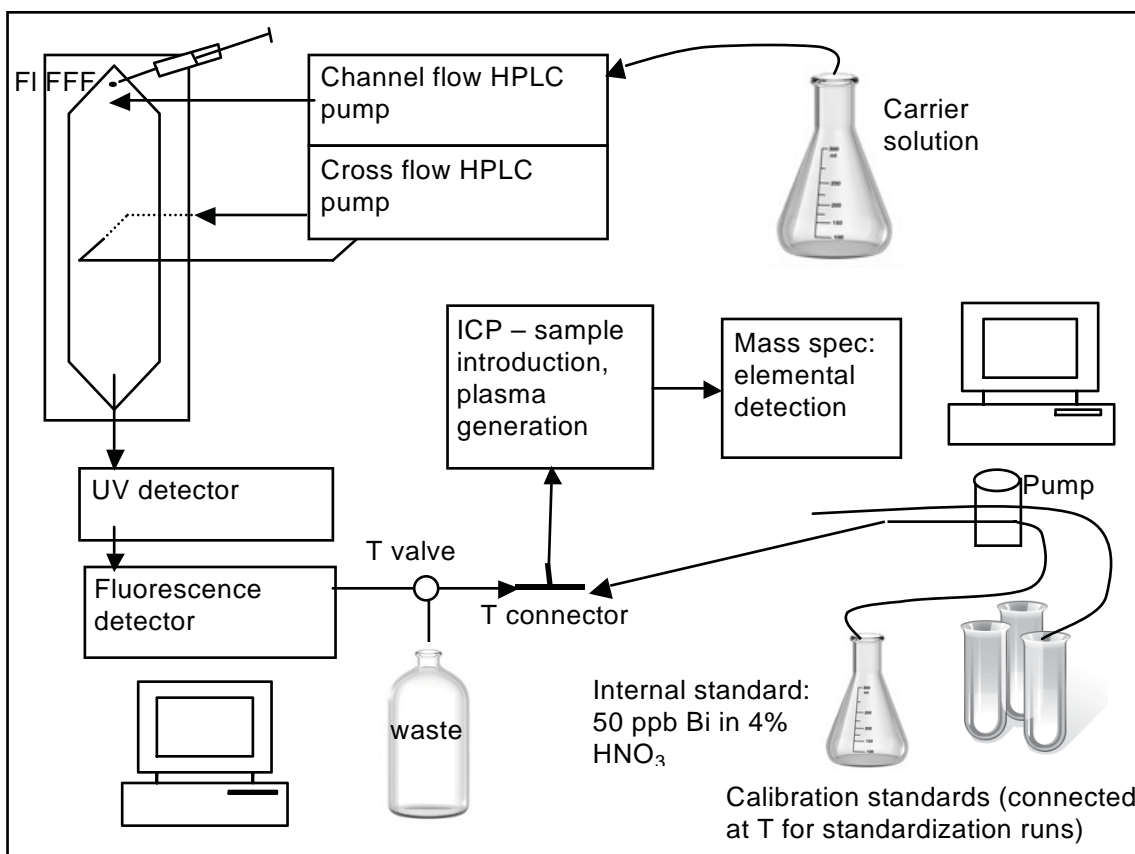


Figure 1. Schematic of FI FFF-ICP-MS hyphenation.

carrier solution. The ICP-MS (Elan 6100, Perkin Elmer, MA, USA) was operated in transient signal mode with a dwell time of 100 ms per element. Zn, Se, and Cd were monitored as analytes, along with Bi and Sc as internal standards. Figure 1, is a schematic of all system components.

For RTSP mode, a dilute silver nanoparticle suspension pumped directly to the ICP-MS while Ag was monitored. Twenty thousand readings were taken at a dwell time of 10 ms, which (accounting for dead time) takes approximately 260 seconds. The silver nanoparticles are marketed to ordinary consumers as a dietary supplement, and were purchased at a local natural food store in a 10 ppm aqueous suspension. The presence of nanoparticulate Ag was confirmed by scanning electron microscopy. The nanoparticles appeared cubic and polydisperse ranging from approximately 10 to 200 nm in diameter.

Results and Discussion

FI FFF-ICP-MS analysis of quantum dots

Analysis of the fluorescent response captured during FI FFF-ICP-MS characterization of the quantum dots gave a diameter of approximately 49.7 nm (Evident listed the dots as 44 nm). As

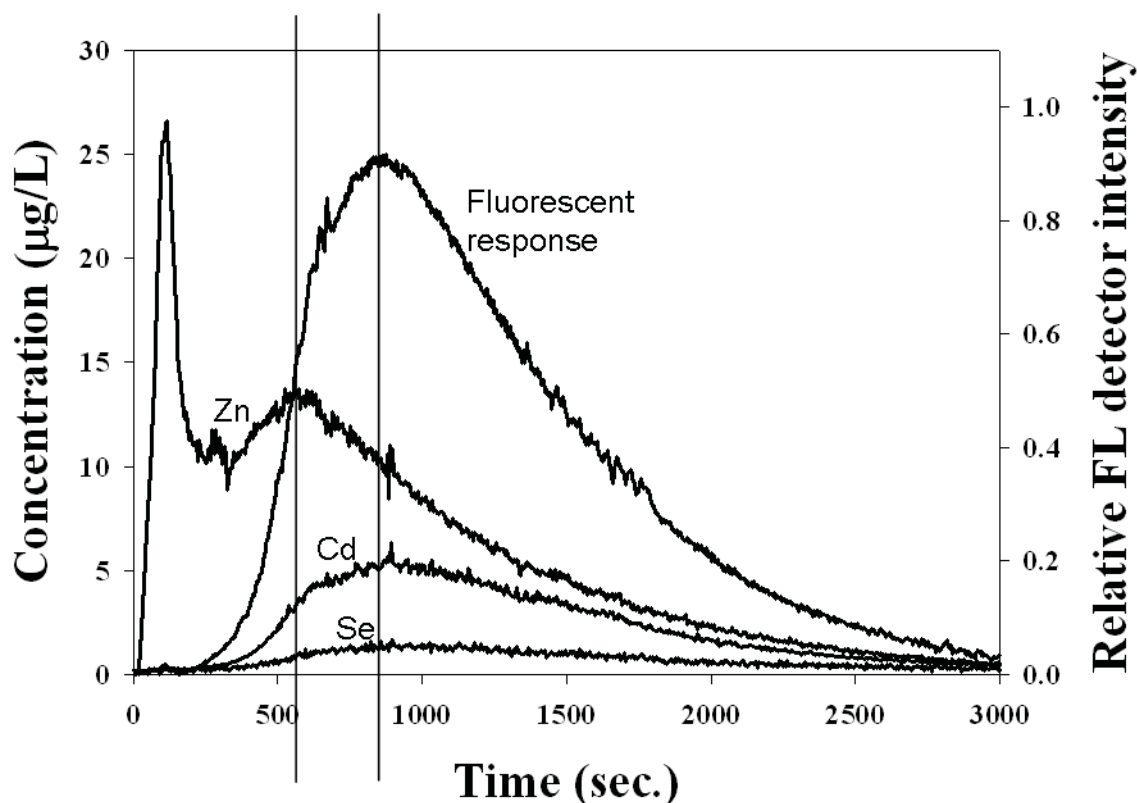


Figure 2. FI FFF-ICP-MS fractogram of PEG coated CdSe/ZnS quantum dots: Vertical lines show ~3.00 second lag between Zn peak elution time, and the fluorescence, Se, and Cd peaks. In the void peak (0 to 200 seconds) there is very small fluorescence, Se, and Cd signals, while there is large amount of Zn detected. This suggests the presence of a nanoparticulate Zn-containing impurity.

shown in figure 2, the Cd and Se signals peaked with the fluorescent curve, which is logical because it is the semiconducting CdSe core produces the dots' fluorescence. Unexpectedly, the Zn signal peaked earlier, and while the void peak of the fractogram (essentially materials that were not properly equilibrated or fractionated) contains no Cd or Se, and does not fluoresce, it has a large Zn content. The presence of a nanoparticulate Zn containing impurity in this particular lot of quantum dots explains these observations. The impurity is likely just a few nm in hydrodynamic diameter. The ICP-MS detection limit for sulfur is high, so it was not measured, leaving unresolved the possibility that the impurity could be ZnS core material.

RTSP ICP-MS analysis of "colloidal silver."

We analyzed milli-Q water dilutions of the silver nanoparticle suspension (10 to 1000 ppt Ag) and equivalent acidified solutions of dissolved silver (diluted from an Ag ICP standard) using RTSP ICP-MS. As was hypothesized, the Ag solutions, regardless of the concentration, produced intensity vs. time graphs containing a stable signal, with few spikes, where a spike is defined as an intensity greater than the mean intensity of the middle 99% of readings plus 6 standard deviations of the middle 99% of intensity readings. The average intensity was proportional

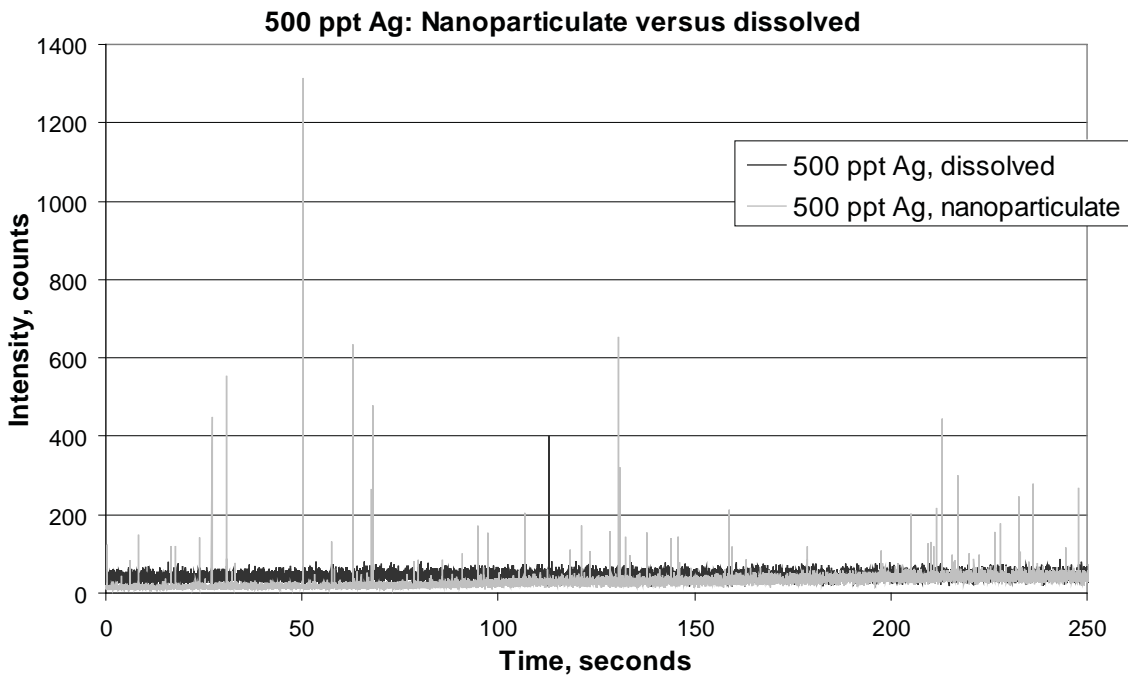


Figure 3. Intensity vs. time for dissolved and nanoparticulate samples, 500 ppt Ag: the signal for the dissolved sample is at a relatively constant background intensity, with one visible spike. The nanoparticulate sample is at a lower background intensity, and has many spikes that are well above that level.

to the concentration of silver. With the nanoparticulate silver suspensions, numerous spikes were observed. A graph of intensity versus time for dissolved and nanoparticulate Ag samples, both with 500 ppt Ag, can be found in figure 3.

The relationship between the number of spikes and concentration of Ag for dissolved and nanoparticulate samples is illustrated in figure 4. There is no increasing relationship for the dissolved samples, while there is an increasing relationship for the nanoparticles, although further testing should be done to grow the dataset and flush out the relationship. Figure 4 can be thought of as a calibration curve for water dilutions of the nanoparticle product, where concentration of nanoparticles can be determined based on the number of spikes measured. Since the dilution factors were between 10^4 and 10^6 we hypothesize that with further development the method could be used to detect silver nanoparticles in environmental samples.

With a calibration curve based on dissolved standards, the intensity of a spike can be used to estimate the size of the nanoparticle. Analysis of nanoparticle size (calculations and assumption not shown here) gave an average diameter of 31 nm, which is within the range (albeit the low end) indicated by SEM imaging of the particles.

Conclusion

The part-per-trillion detection limit for ICP-MS measurement of many metals makes it well-suited for analysis at the nano-scale. Using ICP-MS in non-traditional ways can move it beyond

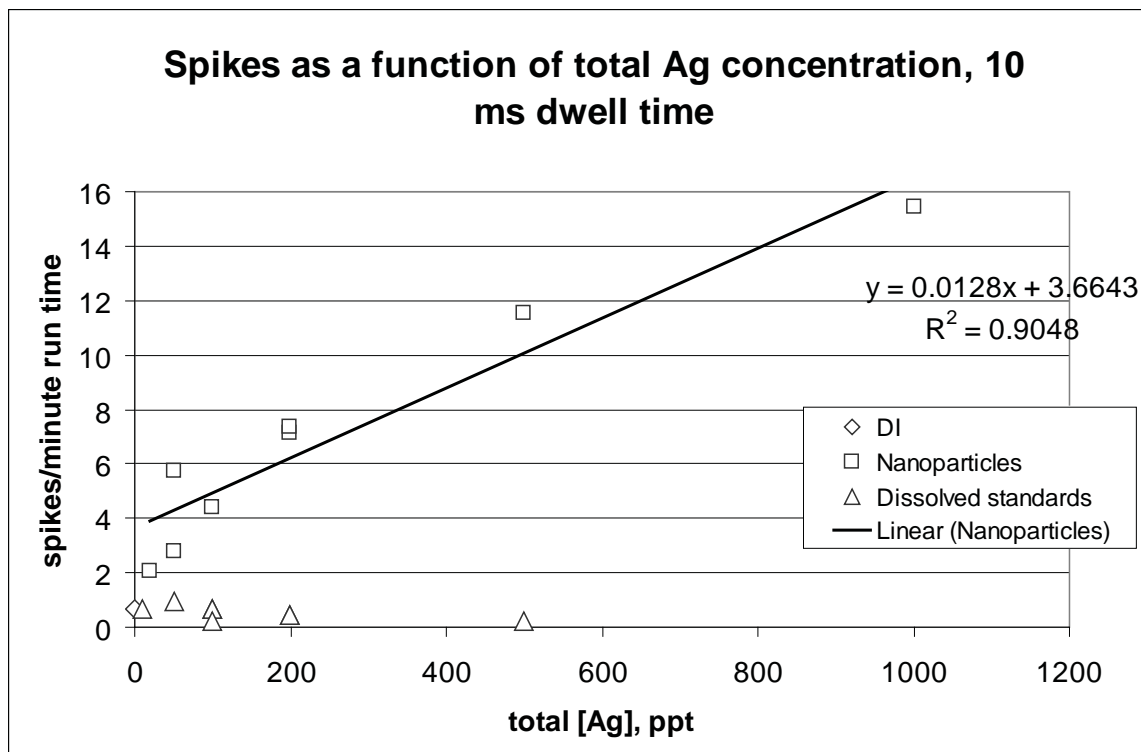


Figure 4. Relationship between number of spikes and total Ag concentration, a “calibration curve” for nanoparticle detection: an increasing relationship is observed from the nanoparticle samples. This is not seen with increasing silver content in dissolved standards.

measuring total metal concentrations, and can allow for the assessment of the presence of inorganic nanoparticles, their size, concentration, and composition.

References

- Degueldre, C., and P.Y. Favarger. (2004). “Thorium colloid analysis by single particle inductively coupled plasma-mass spectrometry.” *Talanta* 62 (5), 1051-1054.
- Degueldre, C., Favarger, P., Rosse, R., and S. Wold. (2006a). “Uranium colloid analysis by single particle inductively coupled plasma-mass spectrometry.” *Talanta* 68 (3), 623-628
- Degueldre, C., Favarger, P., and S. Wold. (2006b). “Gold colloid analysis by inductively coupled plasma-mass spectrometry in a single particle mode.” *Analytica Chimica Acta*, 555 (2), 263-268
- Noble, C. A., and K.A. Prather. (2000). “Real-time single particle mass spectrometry: A historical review of a quarter century of the chemical analysis of aerosols.” *Mass Spectrometry Reviews* 19 (4), 248-274
- Schimpf, M.E., Caldwell, K., and J.C. Giddings. (2000). *Field-Flow Fractionation Handbook*. New York, Wiley-Interscience.

Surfactive Stabilization of Multi-Walled Carbon Nanotube Dispersions with Dissolved Humic Substances

*Mark. A. Chappell, Environmental Laboratory, Engineering Research & Development Center,
US Army Corps of Engineers, Vicksburg, Mississippi, U.S.A.*

*Aaron J. George, Katerina M. Dontsova, and Beth E. Porter,
SpecPro, Inc., Huntsville, Alabama, U.S.A.*

*Cynthia L. Price, Environmental Laboratory, Engineering Research & Development Center,
US Army Corps of Engineers, Vicksburg, Mississippi, U.S.A.*

*Pingheng Zhou, and Eizi Morikawa, J. Bennett Johnston Sr. CAMD Louisiana State University,
Baton Rouge, Louisiana, U.S.A.*

*Alan J. Kennedy, and Jeffery A. Steevens, Environmental Laboratory, Engineering Research &
Development Center, US Army Corps of Engineers, Vicksburg, Mississippi, U.S.A.*

Abstract

Soil humic substances (HS) stabilize carbon nanotube (CNT) dispersions, a mechanism we hypothesized arose from the surfactive nature of HS. Experiments dispersing multi-walled CNT in solutions of dissolved Aldrich humic acid (HA) or water-extractable Catlin soil HS demonstrated enhanced stability at 150 and 300 mg L⁻¹ added Aldrich HA and Catlin HS, respectively, corresponding with decreased CNT mean particle diameter (MPD) and polydispersivity (PD) of 250 nm and 0.3 for Aldrich HA and 450 nm and 0.35 for Catlin HS. Analogous trends in MPD and PD were observed with addition of the surfactants Brij 35, Triton X-405, and SDS, corresponding to surfactant sorption behavior. NEXAFS characterization showed that Aldrich HA contained highly surfactive domains while Catlin soil possessed a mostly carbohydrate-based structure. This work demonstrates that the chemical structure of humic materials in natural waters is directly linked to their surfactive ability to disperse CNT released into the environment.

Introduction

Research over the past decade has elucidated much about the functionality of CNT and the many chemical derivatives possible, greatly expanding the potential uses of these materials. One potential use involves the environmental application of CNT for removing contaminants. Research was recently conducted in using CNT as a selective sorbent for organic/biological contaminants in water streams, such as carcinogenic cyanobacterial microcystins (Yan et al., 2006), a variety of nitro- and chloro-substituted aromatics (Thomas, 1994), and methanol (Burghaus et al., 2007). CNTs also effectively adsorb dissolved heavy metals and actinides, including Cd(II), Cu(II), Ni(II), Pb(II), Zn(II), and Am(III) (Chen and Wang, 2006; Rao et al., 2007; Wang et al., 2005). However, little is actually known regarding how CNT will interact with soil-water systems once

released into the environment. The poor water solubility of CNTs (unless chemically derivitized) makes it difficult to disperse these materials in aqueous solution. Yet, CNT was successfully dispersed by the addition of ionic surfactants such as SDS, NaDDBS, and Dowfax (Vaisman et al., 2006, and references therein). Hyung et al (2007) found that natural organic matter served to stabilize CNT aqueous suspensions, yet there is no agreement on the mechanisms by which this behavior occurs. Thus, it is difficult to predict whether some forms of naturally occurring, biopolymeric substances may promote dispersion, while other may not. For example, polysaccharides do not apparently promote CNT dispersion (Lead, 2008).

The purpose of this work was to demonstrate the mechanism by which humic materials stabilize CNT dispersions in aqueous solution. Discerning this mechanism will facilitate a better understanding of how HS promote CNT dispersion, as well as provide a means for making qualitative assessments regarding the type of dissolved HS in the environment.

Materials and Methods

Aliquots of dissolved humic stock solutions were added to 50-mL test tubes containing 100 mg L⁻¹ CNT suspension in 5 mM NaNO₃ solutions. In separate experiments, dissolved HS solutions were replaced with varying concentrations of the surfactants Brij 35, Triton X, or SDS. The tubes were capped and then shaken for 24 hours. Suspension settling was analyzed using a Varian Carey 50 UV-Vis-NIR spectrometer by reading the absorbance at 600 nm with time (Mathangwane et al., 2008). Suspension particle size was measured using a Brookhaven Instruments 90Plus/BI-MAS dynamic light scattering (DLS) spectrometer. Solution total organic carbon (TOC) was analyzed by a catalytic combustion technique.

Composition of carbon functional group was investigated by near-edge x-ray absorption spectroscopy (NEXAFS) at the carbon K edge. Measurements were carried out at the varied-line-space plane-grating-monochromator (VLSPGM) beamline at the J. Bennett Johnston Sr. Center for Advanced Microstructures and Devices (CAMD) synchrotron light facility, Louisiana State University. The photon energy scale was calibrated for the C 1s- π^* resonance peak using a polystyrene sample (Sigma-Aldrich) which was fixed at 285.4 eV. Sample spectrum were I_0 normalized using the total yield of clean gold mesh placed in the incident beam before sample. C-NEXAFS spectra was processed using the program Athena from the IFEFFIT software package (Newville, 2001). Linear combination fits of the C-NEXAFS spectra were compared to carbon reference standards also analyzed at VLSPGM beamline.

Results & Discussion

The settling behavior of CNT was studied in the presence of two different HS (Fig. 1). Settling data showed a rapid reduction in the solution optical density within the first 15 min. Afterwards, the suspension appeared to stabilize. Settling data showed that CNT suspensions demonstrated enhanced dispersion stability with Aldrich HA additions beginning at 150 mg L⁻¹ Aldrich HA, with approx. twice the concentration of dissolved humics required for the Catlin soil HS. Data from DLS measurements showed that CNT MPD readily dropped to 600 nm with the addition of 5 mg L⁻¹ Aldrich HA (Fig. 2). Further additions of Aldrich HA up to 150 mg L⁻¹ and Catlin HS up to 300 mg L⁻¹ resulted in a minimized MPD of approx. 250 and 420 nm, respectively. PD index also minimized to approx. 0.30 and 0.35 for the Aldrich HA and Catlin HS, respectively,

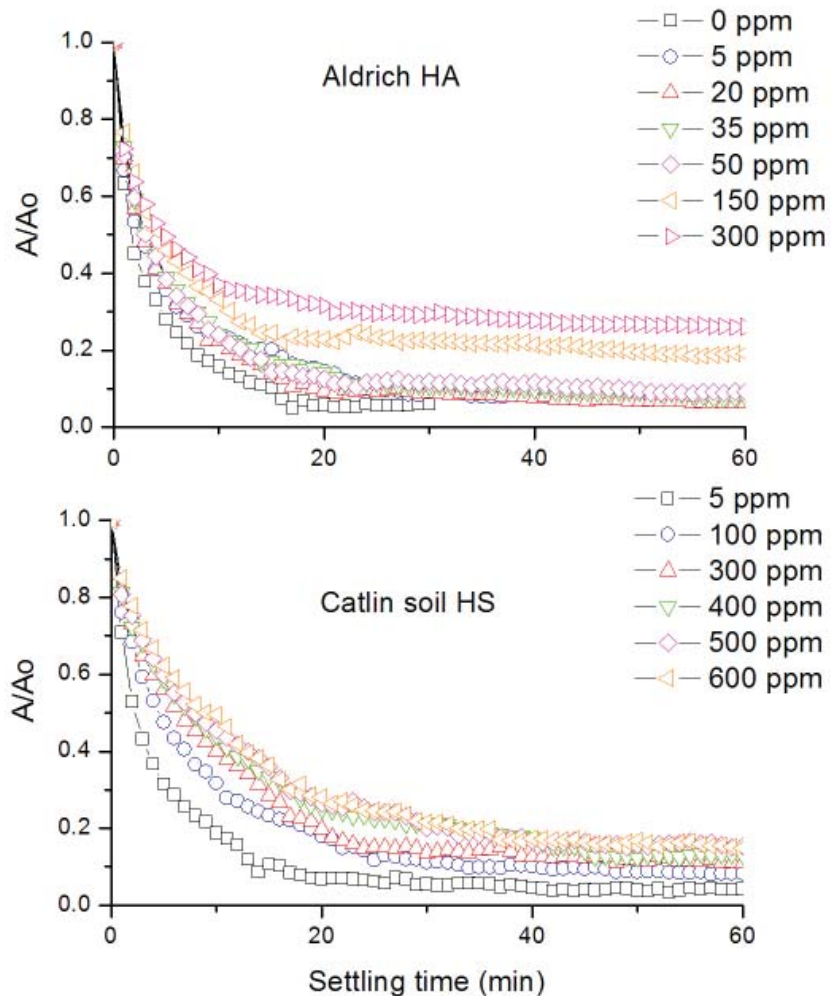


Figure 1. Settling data showing optical density (A/A_0 for $\lambda = 600$ nm) of a 100 mg L^{-1} CNT dispersion, suspended in 5 mM NaNO_3 background solution and varying initial concentrations of dissolved humic substances (obtained from Aldrich humic acid and a Caitlin soil) with time.

along with the MPD. Both trends correspond to enhanced dispersion stability and particle size homogeneity of CNT – a behavior particular to surfactive molecules.

To test this hypothesis, we conducted similar experiments investigating the effect of surfactants on CNT suspension particle size characteristics (Fig. 3). The data show that CNT MPD minimized to 210, 230, and 370 nm for SDS, Brij 35, and Triton X, respectively. Correspondingly, particle size PD minimized to 0.27, 0.26, and 0.32 for SDS, Brij 35, and Triton X, respectively. Note that CNT MPD and PD minimized in the presence of SDS and Brij 35 to values similar to the Aldrich HA system, indicating that the Aldrich HA exhibited strong surfactive ability. Fol-

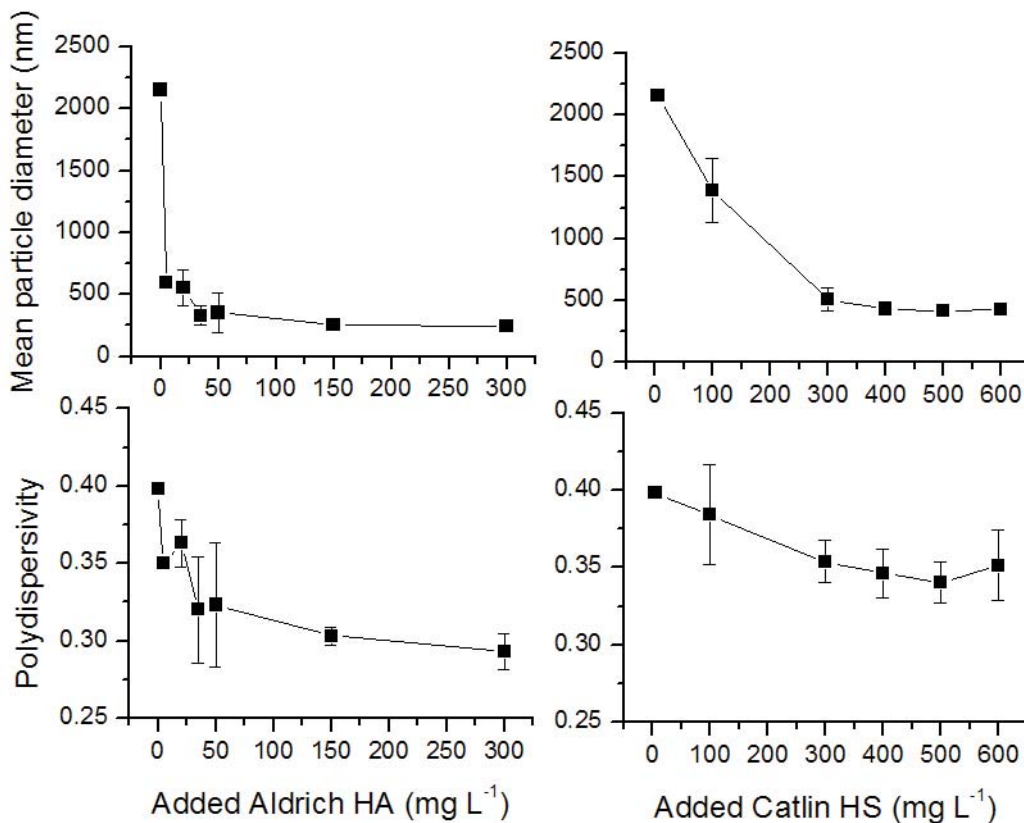


Figure 2. Effect of humic substances on the properties of CNT dispersions suspended in 5 mM NaNO₃ background solution. Mean particle diameter and polydispersity measurements were obtained by dynamic light scattering. Sorption of humic substances to CNT was calculated by difference. Connecting lines are to guide the eye.

lowing this reasoning, the surfactive ability of the Catlin soil HS (like the Triton X) was less capable of stabilizing CNT dispersions.

Minimization of MPD and PD values for CNT was compared to surfactant sorption isotherms (Fig. 3). All surfactants exhibited a high affinity of sorption for CNT, with individual differences in the sorption behavior. For Brij 35, minimization of CNT MPD and PD coincided with the surfactant saturation on the surface. This behavior is consistent with surfactant behavior in biphasic systems, where surfactant micelles tend to dissociate, and individual surfactant molecules adsorb to the surface, until the surface is saturated with surfactant (Chappell, 2004; Chappell et al., 2005). Surfactants tend to reach sorption maximum around its critical micelle concentration (Chappell et al., 2005, and references therein). Such a trend for the SDS and Triton X surfactants was more difficult to observe given the unexpected shapes of the sorption isotherms. However, for SDS, CNT MPD and PD does appear minimized with the first change in slope (perhaps an intermediate saturation point) of the biphasic sorption isotherm. Triton X sorption quickly maximized, then became negative, indicating reduction of Triton X surface coverage on CNT (sup-

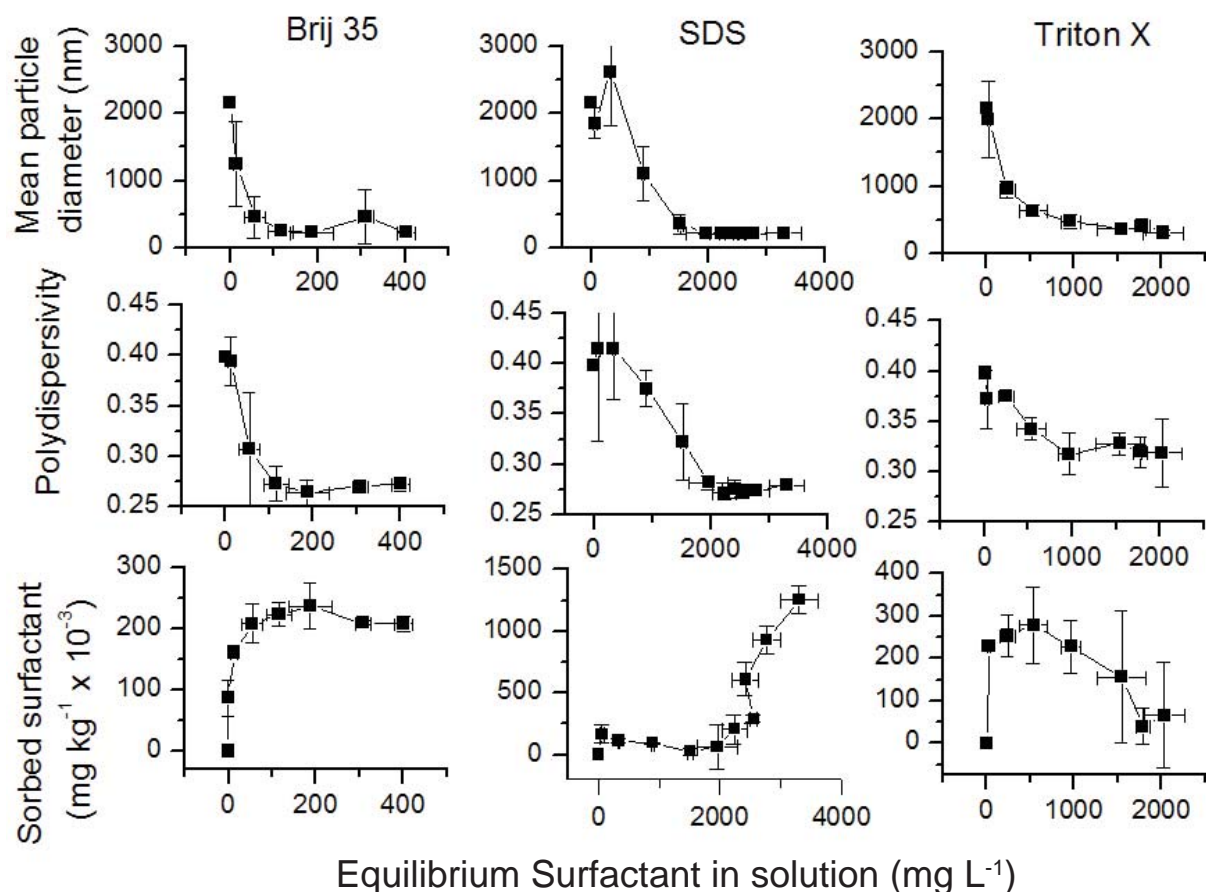


Figure 3. Effect of surfactants on the properties of CNT dispersions suspended in 5 mM NaNO₃ background solution. Mean particle diameter and polydispersity measurements were obtained by dynamic light scattering. Surfactant sorption on CNT was calculated by difference. Connecting lines are to guide the eye.

ported by both TOC and MS measurements), but the relatively large error associated with this data limits this interpretation.

Differences in surfactant sorption (and the resulting CNT MPD) are most likely attributed to differences in the surfactant's structure. For example, CNT exhibited a much higher sorption affinity for nonionic surfactants than the anionically charged SDS. However, the combination of both bulkier hydrophilic and lipophilic moieties of Triton X may have contributed to the poorer surfactive ability relative to Brij 35. Although anionic, SDS showed similar ability of Brij 35 to minimize CNT MPD. This ability may have been related to the simplicity in structure of the surfactant's hydrophilic/lipophilic moieties as well.

We investigated the structure of the Aldrich HA and Catlin soil HS using C-edge NEXAFS (Figure 4) to assess how the above relationships may influence their surfactive ability. Linear combination analysis of the NEXAFS data (Table 1) revealed that the Aldrich HA possessed a structure that was highly aromatic: 63 % analogous to an alkaloid reserpine, 18 % analogous to a black carbon (diesel soot) material, and 19 % analogous to a polymeric polysaccharide (alginate)

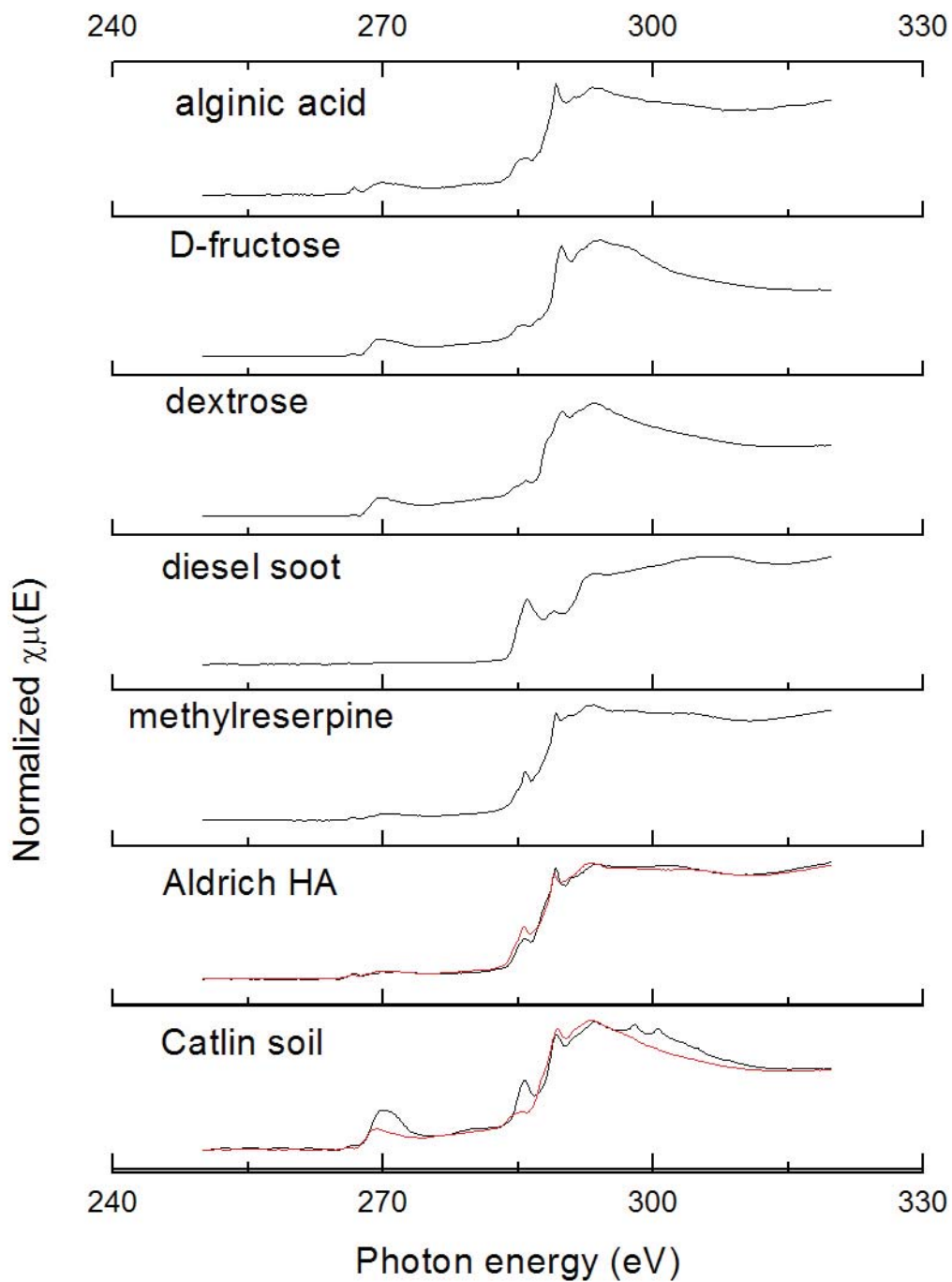


Figure 4. Carbon-edge NEXAFS for the Aldrich HA and Catlin soil HS compared to reference standards. Red lines demonstrate the linear combination fit of the spectra from standards to the Aldrich and Catlin samples. The peaks appearing at approx. 270 eV are due to 2nd order contribution from oxygen K edge absorption.

Table 1. Linear combination fits of the Aldrich HA and Catlin HS carbon-edge NEXAFS spectra.

sample	standard	weight	χ^2	R-factor
Aldrich HA	alginate acid	0.191	0.18776	0.001191
	diesel soot	0.179		
	methyl	0.629		
	reserpine			
Catlin soil HS	D-fructose	0.359	1.070372	0.017806
	glucose	0.641		

acid). The Catlin soil HS structure was dominated by simple sugars, consisting of glucose and D-fructose-type analogs. Clearly, the superior surfactive ability of the Aldrich HA was linked to the high aromaticity of the black carbon phase (representing the material lipophile), the high polarity of the polymeric polysaccharide phase (representing the hydrophile), and “mixed” alkaloid phase containing oxygen-rich aromatic groups. The saccharide polymer-rich Catlin soil HS exhibited a limited ability to stabilize CNT dispersion because the material lacked a significant hydrophilic domain necessary for surfactive activity.

Conclusion

In this work, the potential of humic substances to stabilize CNT dispersions was demonstrated. This behavior was attributed to the surfactive nature of humics and their ability to promote the smallest CNT particle sizes and homogeneities. As demonstrated with well-defined surfactants, this stabilization is maximized when CNT is saturated with a monolayer of surfactant, which corresponds to the sorption maximum of the sorption isotherm and closeness of the equilibrium surfactant concentration in solution to the CMC value. The superior surfactive ability of the Aldrich HA appeared to be linked to the mixture of strong hydrophilic and lipophilic domains, compared to the Catlin soil HS, which appeared to be overwhelmingly hydrophilic. We conclude from this work that the most natural humic materials should exhibit at least some ability to stabilize CNT dispersions in aqueous environments.

References

- Bohmer, M.R., L.K. Koopal, R. Janssen, E.M. Lee, R.K. Thomas, and A.R. Rennie. 1992. Adsorption of nonionic surfactants on hydrophilic surfaces. An experimental and theoretical study on association in the adsorbed layer. *Langmuir* 8:2228-2239.
- Burghaus, U., D. Bye, K. Cosert, J. Goering, A. Guerard, E. Kadossov, E. Lee, Y. Nadoyama, N. Richter, E. Schaefer, J. Smith, D. Ulness, and B. Wymore. 2007. Methanol adsorption in carbon nanotubes. *Chem. Phys. Lett.* 442:344-347.
- Chappell, M.A. 2004. Confounding factors and tertiary-phase control by a surfactive agent on the sorption of atrazine. Ph.D. dissertation, Iowa State University, Ames.
- Chappell, M.A., D.A. Laird, M.L. Thompson, and V.P. Evangelou. 2005. Co-Sorption of atrazine and a lauryl polyoxyethylene oxide nonionic surfactant on smectite. *J. Agric. Food Chem.* 53:10127-10133.

- Chen, C., and X. Wang. 2006. Adsorption of Ni(II) from aqueous solutions using oxidized multi-wall carbon nanotubes. *Ind. Eng. Chem. Res.* 45:9144-9149.
- Hyung, H., J.D. Fortner, J.B. Hugues, and J.-H. Kim. 2007. Natural organic matter stabilizes carbon nanotubes in the aqueous phase. *Environ. Sci. Technol.* 41:179-184.
- Lead, J. 2008. Interactions between natural aquatic colloids and manufactured nanoparticles: Effects on chemistry, transport, and ecotoxicology *Nanoparticles in the Environment: Implications and Applications*, Centro Stefano Franscini, Monte Verita, Ascona, Switzerland.
- Mathangwane, B.T., M.A. Chappell, J.R.V. Pils, L.S. Sonon, and V.P. Evangelou. 2008. Dispersion potential of selected Iowa lake sediments as influenced by dissolved and solid-phase constituents. *Clean* 36:201-208.
- Newville, M. 2001. IFEFFIT: Interactive EXAFS analysis and FEFF fitting. *J. Synchrotron Radiat* 8:322-324.
- Rao, G.P., C. Lu, and F. Su. 2007. Sorption of divalent metal ions from aqueous solution by carbon nanotubes: A review. *Separation Purification Technol.* In Press.
- Thomas, R.N. 1994. Effects of contaminants and charge transfer on the molar absorptivities of fullerene solutions. *Anal. Chim. Acta* 289:57-67.
- Vaisman, L., H.D. Wagner, and G. Marom. 2006. The role of surfactants in dispersion of carbon nanotubes. *Adv. Colloid Interface Sci.* 128-130:37-46.
- Wang, X., C. Chen, W. Hu, A. Ding, D. Xu, and X. Zhou. 2005. Sorption of $^{243}\text{Am}(\text{III})$ to multi-wall carbon nanotubes. *Environ. Sci. Technol.* 39:2856-2860.
- Yan, H., A. Gong, H. He, J. Zhou, Y. Wei, and L. Lv. 2006. Adsorption of microcystins by carbon nanotubes. *Chemosphere* 62:142-148.

Interactions Between Engineered Iron Oxide Nanoparticles and Microorganisms

Maria Casado, and Jamie R. Lead, School of Geography, Earth and Environmental Sciences, University of Birmingham, Edgbaston, Birmingham, United Kingdom

Abstract

The development of materials and products at the nanoscale has become a major investment area on a global scale and there are many products already on the market which use materials in this size range. Applications in medicine, cosmetics and personal care products, materials science, energy production and storage and electronics are just a few examples where benefits to society, human health and the environment are predicted. The anticipated increase in nanoparticle production makes exposure of the environment to these materials more and more likely. The biological effects and environmental fate and behaviour of engineered nanoparticles are relatively unknown. Assessing the benefits and risks of nanomaterials requires a better understanding of their chemistry, mobility, bioavailability and ecotoxicity in the environment.

Iron is an essential growth factor for most bacteria while bioavailability of iron will depend on its physico-chemical form. Gram-negative bacteria *Pseudomonas fluorescens* have been exposed to well-characterised manufactured iron oxide nanoparticles at different pH values, iron concentrations and in presence and absence of humic substances. Parallel experiments were performed with dissolved iron and latex beads. Results showed after 24h higher iron uptake when this was dissolved than when the case of nanoparticles. Although iron oxide nanoparticles are less accessible than the dissolved iron, bacteria are still able to uptake a proportion of the nanoparticles. This knowledge will help understanding the bioavailability of nanoparticles and the role of microorganisms on the behavior, fate, and segregation of particles in contaminated environments.

Introduction

The use of engineered nanoparticles is rapidly increasing due to their applications in areas such as textiles, electronics, pharmaceuticals, cosmetics and environmental remediation, which will very likely lead to the release of such materials into the environment. It is necessary to understand their mobility, reactivity, ecotoxicity and persistence in the environment to assess the risks of their environmental exposure (Nowack and Bucheli, 2007). The unique properties of engineered nanoparticles, such as the high specific surface area and abundance of reactive sites on the surface are of essential importance for their aggregation behavior, and thus for their mobility in aquatic systems and for their interactions with organisms. It seems likely that nanoparticles will penetrate cells more readily than larger particles. Inside cells, engineered nanoparticles might directly provoke alterations of membranes and other cell structures as well as protective mechanisms. A number of studies suggest that nanoparticles cause disruption to bacterial membranes, possibly by production of reactive oxygen species (Neal, 2008), although we may expect iron based nanoparticles to be beneficial to growth. These toxic effects might be transferred through food webs, thus affecting communities and whole ecosystems. Free metal ions originat-

ing from the nanoparticles can not be discounted, and interactions of engineered nanoparticles with natural organic matter have to be considered as well, as those will alter the aggregation behaviour of engineered nanoparticles in surface water (Diegoli, *et al.*, 2008, Baalousha, *et al.*, 2008). Research on natural organic matter has focused primarily on humics and fulvic acids.

In this project, we study the interactions when bacteria are exposed to different physico-chemical forms of iron, concentration, pH and organic matter. This knowledge will help understanding the bioavailability of nanoparticles and the role of microorganisms on the behavior, fate, and segregation of particles in contaminated environments

Methods

Iron oxide nanoparticles were initially synthesized at pH 2 by forced hydrolysis of homogeneous FeCl₃ solutions under controlled conditions (Kendall and Kosseva, 2006) and characterised under the experimental conditions used with bacteria. The nanoparticle diameter distribution was measured by photon correlation spectroscopy (PCS) particle size analysis and by transmission electron microscopy (TEM) of the iron oxide nanoparticles in different conditions of pH and in presence and absence of Suwannee River humic acid were taken.

Gram-negative bacteria *Pseudomonas Fluorescens* were harvested in their mid-exponential phase and exposed to the previously well-characterized manufactured iron oxide nanoparticles at different pH values, iron concentrations and in the presence and absence of humic substances. In addition, parallel experiments were performed with dissolved iron and latex beads. Cell growth was monitored by taking optical densities measurements on UV-vis at different times of exposure up to 24 hours. After 24 hours, samples were filtered and ultrafiltered to then be analysed on AAS for iron concentrations. TEM images of samples of bacteria with the nanoparticles were also taken after 24 hours exposure.

Results and discussion

Results for iron oxide nanoparticles dispersion showed a peak around 20 nm in size as was expected from previous research (Kendall and Kosseva, 2006) and a second peak near 200 nm in size, suggesting there is adhesion and aggregation between the nanoparticles. TEM images showed that the nanoparticles were generally aggregated. In the presence of humic acid these were bigger and more compacted.

Optical densities results showed after 24h no effect between the control and the latex beads samples. There was a positive effect when exposed to iron being higher when this was dissolved than when the case of nanoparticles. Presence of humic acid affected with faster and higher cell growth. TEM images showed iron oxide nanoparticles surrounding the bacteria which suggest, along with cell growth results, that bacterial iron uptake is taking place.

Conclusions

Although iron oxide nanoparticles are less bioavailable than dissolved iron, bacteria are still able to uptake a proportion of the nanoparticles and this is not via uptake of the dissolved phase iron.

References

Nowack, B. and T. D. Bucheli. (2007). "Occurrence, behavior and effects of nanoparticles in the environment." *Environmental Pollution* 150 (1), 5-22.

Neal, A. L. (2008). "What can be inferred from bacterium-nanoparticle interactions about the potential consequences of environmental exposure to nanoparticles?" *Ecotoxicology* 17 (5), 362-371.

Diegoli, S., A. L. Manciulea, S. Begum, I. P. Jones, J. R. Lead and J. A. Preece. (2008). "Interaction between manufactured gold nanoparticles and naturally occurring organic macromolecules." *Sci Total Environ* 402 (1), 51-61.

Baalousha, M., A. Manciulea, S. Cumberland, K. Kendall and J. R. Lead (2008). "Aggregation and surface properties of iron oxide nanoparticles: Influence of pH and natural organic matter". IN (Ed.^(Eds.). ed.

Kendall, K. and M. R. Kosseva. (2006). "Nanoparticle aggregation influenced by magnetic fields." *Colloids and Surfaces a-Physicochemical and Engineering Aspects* 286 (1-3), 112-116.

Ultracentrifugation onto Supporting Grids as a TEM Specimen Preparation Method for Carbonaceous Nanoparticles

*Emilia Cieslak, and Jamie R. Lead, School of Geography,
Earth and Environmental Sciences, University of Birmingham,
Birmingham, United Kingdom*

Abstract

Ultracentrifugation has been successfully used as a way of examining native colloidal material in natural waters with transmission electron microscopy. This and other techniques (resin embedding, ultramicrotomy) allow images to be obtained of minimally perturbed natural aquatic colloids. Here we apply a similar approach to study carbonaceous nanoparticles in water samples. Single-walled and multi-walled carbon nanotubes as well as water stirred fullerenes (nC_{60} clusters) were used in the experiments. Additionally, these nanoparticles were examined in the presence of natural aquatic colloids (like Suwannee River Humic Acid) to better understand interactions between them, i.e. the fate and behaviour of the nanoparticles in natural waters. The presented preparatory methodology proved to be superior to traditional ‘drop drying’ due to reduced aggregation and optimal grid coverage.

Introduction

Transmission electron microscopy (TEM) is a powerful tool for morphological characterisation of micro- and nanoparticles. Its adaptation for natural water samples has been well established in water science [1]. Along with other electron microscopy techniques it is also widely used to examine engineered nanoparticles thanks to its remarkable resolution.

There are a few specimen preparation methods for water suspensions, the simplest of which is leaving a drop of the sample to dry on a supporting grid. We applied this method in our earlier work to study interactions between single-walled carbon nanotubes and natural aquatic colloids. However, there are more effective ways to prepare water samples to be analysed with TEM (ultracentrifugation, resin embedding, ultramicrotomy) [2].

Here, we show our first results on implementation of the ultracentrifugation method to water suspensions of engineered nanoparticles (carbon nanotubes and fullerenes) in the presence and absence of natural aquatic colloids in order to better understand interactions between them. This would advance the knowledge of fate and behaviour of man-made nanoparticles once they enter natural waters.

Methods

In our experiments we used water suspensions of carboxylic acid functionalised single-walled carbon nanotubes prepared by sonification and water-stirred fullerenes (C_{60}). The samples were centrifuged in Beckman L7-65 ultracentrifuge (rotor type SW40) for 1 h in 15° C with 30.000 RPM. We used 10 ml centrifuge tubes with flat bottoms onto which holey carbon films on cop-

per mesh were placed. TEM images were obtained on the FEI Tecnai F20 Field Emission microscope.

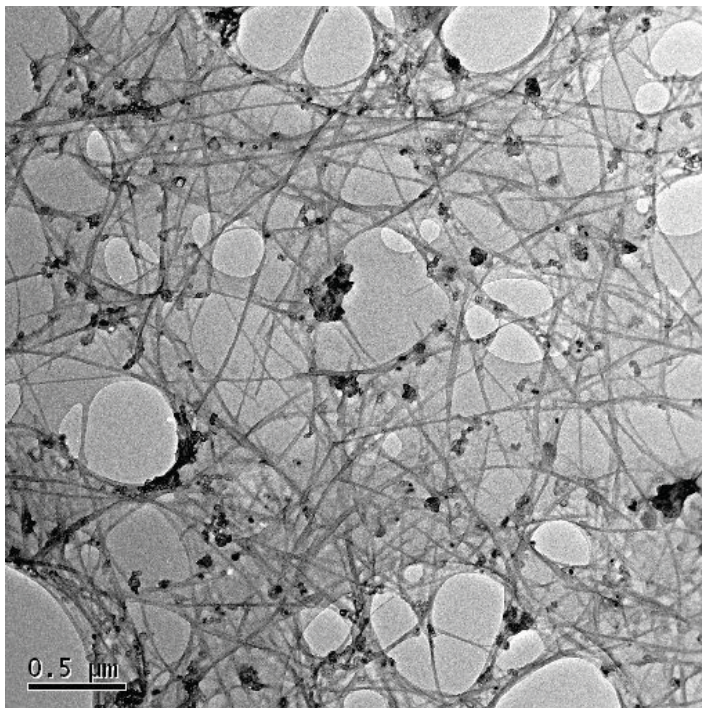


Figure 1. Single-walled carbon nanotubes in the presence of Suwannee River Humic Acid.

Results

Fig. 1 shows single-walled carbon nanotubes in the presence of Suwannee River Humic Acid (SRHA). Randomly entangled networks of nanotubes homogeneously coated with circular particles of humic acid can be seen. Fig. 2 shows an nC₆₀ aggregate.

Discussion

In our initial experiments the ultracentrifugation preparatory methodology proves superior to traditional drop drying due to substantially higher homogeneity and optimal grid coverage. The drop drying process intensifies natural aggregation of nanoparticles present in the sample and the coverage of the carbon film is highly random with big parts of the grid with no sample at all. Locating the studied nanoparticles on the grid tends to be a time consuming procedure. Homogeneous and optimal grid coverage easily obtainable with ultracentrifugation methods allows much easier and faster TEM analysis of the specimen. Secondly, the aggregation caused by drying is minimised thus the sample is less perturbed by the preparatory procedure.

Since this is an on-going work further analyses are to be conducted in the near future. This will include multi-walled carbon nanotubes as well as other natural aquatic colloids.

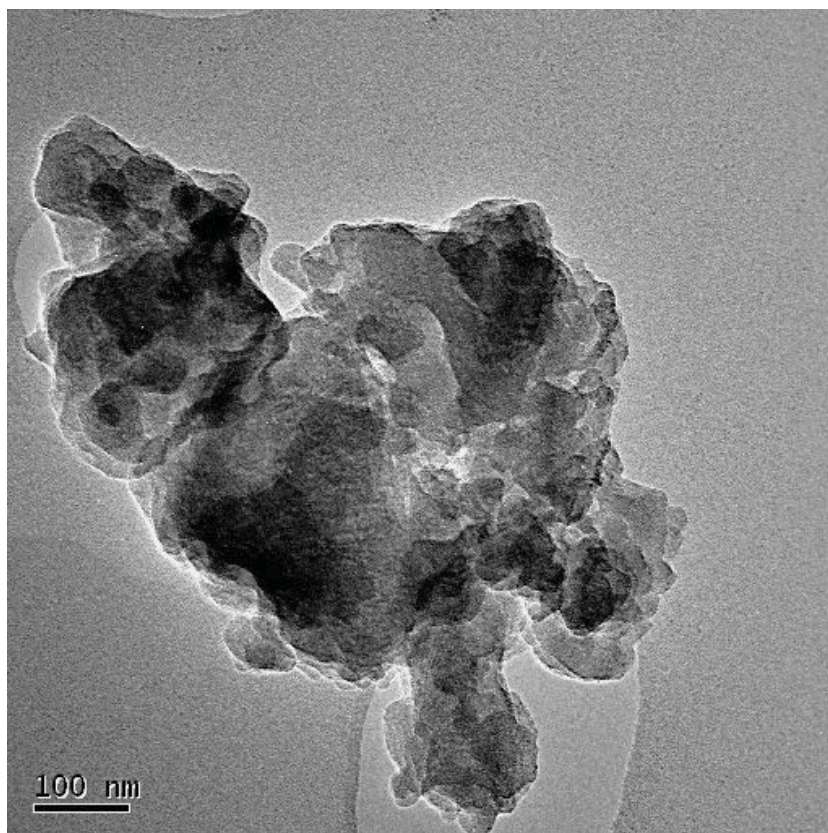


Figure 2. Fullerenes cluster.

References

1. Wilkinson, K. J., and J. R. Lead, editors (2007). Environmental Colloids and Particles. Behaviour, Separation and Characterisation (volume 10, pp.346-364) Chichester, John Wiley and Sons.
2. Lienemann, CP., A. Heissenberger, G. G. Leppard, D. Perret. (1998). "Optimal preparation of water samples for the examination of colloidal material by transmission electron microscopy." *Aquat. Microb. Ecol.* 14: 205-213.

Chapter 5

Report Back and Panel Discussion: Applications

Session Report Backs

Hazardous Substances Remediation

Reported by Deborah Elcock, U.S. DOE & Martha Otto, U.S. EPA

Participants heard from several engineering firms about field tests using nZVI and emulsified ZVI. Many of these tests were successful, and all contributed valuable information about maximizing contaminant reduction in situ. The tests looked at the effects on remediation of several variables such as surface modifications to the ZVI particles, delivery mechanisms, the geochemistry, geology, and hydrogeology of the site, and the size, shape and composition of the nZVI particles. The bottom line of the test results is that even a “silver bullet” technology will not meet cleanup goals if its design is based on inadequate site characterization.

Attendees heard about the following research topics:

- nZVI to oxidize arsenic;
- nZVI to reduce heavy metals;
- nanoscale titanium dioxide to oxidize arsenic;
- nZVI fixed on a functionalized film to dechlorinate perchloroethylene (PCE), TCE, and PCBs;
- field demonstrations of SAMMS® impregnated filters to remove mercury from heat-bleaching waste at a silver mine; and
- plans to use SAMMS® to remove mercury from contaminated water from off-shore drill rigs and from natural gas condensates.

There were presentations on field applications of nZVI and the development of other nanoscale particles for a variety of contaminants.

Participants heard about exciting research into the application of nZVI, much of which is moving from the laboratory to the field. nZVI is not just being used to treat chlorinated hydrocarbons, but nitrates, PCBs, PCP (pentachlorophenol), arsenic and chromium(VI) as well. Several ways to engineer nZVI to optimize design, synthesis, and performance were discussed including:

- Bimetallic nZVI was used with nickel and palladium to reduce nitrate.
- A hybrid technology that combines injection of palladium-iron slurry with electrokinetic remediation was used to remove and degrade TCE and nitrate in water.
- nZVI particles were encapsulated in porous silica spheres to reduce aggregation during trans-

port through sediment.

- Palladium-iron nanoparticles were immobilized on granular activated carbon to dechlorinate PCBs in sediment.
- nZVI was injected into the subsurface to repair a permeable reactive barrier that treats a chromium(VI) plume.
- The impact of adding trace metals to nZVI on the reactivity and aging behavior of the nanoparticles was examined.
- The effects of surface modifications of nZVI particles on the degradation of PCP were analyzed.
- The relative contribution of size and purity on determining the intrinsic reactivity of iron with carbon tetrachloride was examined.

In general, the research aimed to improve the removal efficiencies of remedial applications, but the studies also helped improve our understanding of environmental implications. For example, some techniques not only enhance degradation, but also lead to the production of degradation byproducts that are less toxic or less mobile than the original contaminant. Similarly, if copper is added to nZVI, the rate of degradation decreases; however, the amount of chloroform also decreases. The properties of nanoscale particles change with time exhibiting different phases in their life cycles, each with different implications for fate and transport.

As is often the case, the findings of these studies lead to new questions and research topics. For example, while a specific technique or engineered particle may work well in the laboratory, it may be much less effective in the field. Factors that may affect the field effectiveness include pH, humic properties, particle reactivity, contaminant concentration, contaminant mix, and contaminant depth. So although all these factors must be addressed, it is apparent from the presentations that there is significant potential for nZVI in various forms and combinations with other substances to contribute to cost effective remediation of soil and sediments.

Air & Water Pollution Control

Reported by Diana Eignor, U.S. EPA

These sessions covered a wide breadth of topics for uses of nanomaterials, ranging from fundamental research into the interaction of pollutants with different types of nanoparticles, to products nearly or now available in the marketplace, to actual field application.

All the basic research studies involved the removal of pollutants from water in areas that may eventually lead to commercial applications.

- Nanocrystalline zeolites are being studied as adsorbents for water contaminated with metals (e.g., chromate, copper) or as environmental catalysts.
- Iron nanoparticles are being evaluated for water treatment to meet effluent guidelines for industrial wastewater containing copper waste and material from LCD displays. The work includes an assessment of the effect of pH on the performance of iron nanoparticles.

- The performance of ceramic membranes containing titanium dioxide nanoparticles in aqueous solution chemistry interactions with natural organic matter is being studied in a hybrid ozonation-ultrafiltration water treatment system.
- Researchers are experimenting with conjugates of enzyme-magnetic nanoparticles for remediation of water and liquid wastes. Enzymes used as biocatalysts can be attached to the magnetic iron nanoparticles, and the resulting reactants or products can be easily separated from the enzymes by applying a magnetic field. This technology has potential for both environmental and medical applications

An invention for air pollution control with potential for commercialization in the near future is designed to address the release of mercury vapor from broken compact fluorescent lamp (CFL) bulbs. The device, a three-ply cloth impregnated with nano-selenium, is placed over the broken bulb, and the cloth absorbs the mercury over a period of several days. Because the cloth binds the mercury in a stable form, it can be disposed of in the trash. The material also might be used in CFL packaging to prevent mercury exposure when stored bulbs are broken.

Several commercially available products that contain nanomaterials were identified. Air filters incorporating nanocrystalline metal oxide aggregates have been developed for use in factory environments to mitigate toxic chemicals in the workplace. A toxic-chemical cleaner in the form of a dry powder composed of magnesium, titanium, and oxygen uses the tremendous surface area of nanoparticles to contain and neutralize a broad range of hazardous chemicals.

The presentations included a field study of the deployment of nanomembranes in a cross-flow module pilot water treatment plant to address brackish ground water heavily contaminated with nitrate in a remote village in South Africa. This study highlighted the need for low-cost devices that are simple to operate and perform reliably in the absence of an industrialized infrastructure.

Nanotechnology-Enabled Sensors & Monitoring

Reported by Heather Henry, U.S. NIEHS

Participants heard about many different types of sensing applications that can be accomplished through the incorporation of nanomaterials. In the area of security, the presenters described detection mechanisms for ricin, air and water pollution, ozone, air particulates, and exposure to hazardous chemicals in the workplace. For remediation applications, the speakers described a sensor for measurement of oxidative/reductive potential and another for DNA detection to verify the presence of MTBE-degrading bacteria in the field. Another application involved inexpensive high-volume throughput of samples for disease detection. Some of the sensors are standalone devices the size of a cell phone, while others comprise sensor networks that send signals to a monitoring center, some even routing information through satellite signals. One of the advantages of using nanomaterials is the potential for developing devices that are easily portable. Other desirable features that researchers have achieved or are working toward include wireless capability for expanding communication potential; power options that do not involve batteries, which will enable widespread placement; high throughput interchangeable detectors such that one device has the potential to measure multiple applications; and multiplexing such that one signal transmits multi-parameter readings.

Common challenges in the development of nano-enabled sensors include decreasing the cost to make and operate the sensor, maintaining sensor integrity in the environment, shelf life, calibration, sustainability, practicality, and determining the device's overall costs and benefits for society. Tremendous potential exists to do more work in sensor life-cycle analysis along the lines of the study presented by Hatice Sengül, "Life Cycle Impacts of Quantum-Dot based Nanosensors for Environmental Monitoring." Software, such as Sigma-Pro and EcoInvent, is available for developing a life-cycle analysis. Work also is needed to promote toxicity studies of nano-enabled devices that are released to the environment. An interesting idea along those lines was suggested during the panel discussion: agencies soliciting nanomaterials research through Small Business Innovation Research grants could include an addendum to address the toxicity study issue.

Panel Discussion

Moderator:

Warren Layne

Panelists:

*Heechul Choi, Marie-Isabelle Baraton, Diana Eignor,
Glen Fryxell, Heather Henry, Martha Otto, David Waite*

Warren Layne: Describe an important finding from your session and how you feel it has been affected by discussions amongst the international audience here.

Dermot Diamond: A key message to come from this meeting is the need to encourage material scientists to work with sensor and environmental scientists to align the research effort for sensors. In the future, we will develop network sensors to monitor the status of our environment (e.g., air and water quality). These sensors will be distributed on a wide scale as part of a network communications system and must be low-cost, reliable, and require little servicing. Due to the massive scale of such an effort, we need to reinvent how we do chemical sensing and biosensing. The network must serve as an "environmental nervous system" that responds quickly to events and perhaps predicts events before they happen. This is a huge challenge to the sensor community, but leads us to focus on important issues. The concept of nano-enabled sensors is the key to unlocking the dilemma we have regarding how to move to the next stage. To move to the next stage, we need to make sensors more efficient, effective, and sensitive, as well as less expensive. We must understand the processes that are happening in sensing devices at the molecular and nanoscale levels requiring coordination of several scientific disciplines.

Marie-Isabelle Baraton: I agree with Dermot regarding the need for fundamental science to understand how sensors work. Research on sensors has been fragmented. It is a very complex field involving many disciplines. We need to join forces on an international level to improve sensors. Air quality monitoring research must be funded by national and international organizations because it is not a commercially viable enough field to interest industry.

Heechul Choi: We have challenging opportunities for nanotechnology applications, especially in the area of water treatment. We mainly discussed the use of nZVI for groundwater and soil

remediation; however, we must overcome the secondary pollution caused by those nanoparticles unless we can immobilize or separate them from the water phase. Therefore, we must further develop the mobilized form of the devices in order to apply them more freely to the water phase. Furthermore, we need to look at other nanomaterials and mesoporous materials that have high potential for water treatment. We also need to look at modified membrane systems so we can apply reactive catalysts as nanomaterials or sorbents at the same time. In Korea, there are few research groups endeavoring in these emerging research areas. I hope that we can have more research in these areas so we can have a synergistic approach to developing high-tech processes with nanotechnology.

David Waite: The presentations on nanotechnology applications have been both encouraging and discouraging. They point out a big gap between science and application, which needs to be bridged quickly. We have exciting opportunities to apply new technologies, but we still see many applications failing. It is good to see these attempts, but we must try to apply nanotechnology more sensibly. Dr. Michael Borda (Golder Associates) gave an interesting summary of lessons learned from various field applications of nanoparticles that were successes and failures. I think these examples point to the need for better engineering. We need to couple science and knowledge of how nanoparticles work with the problems that occur in their application, including their complications in nature. We also need to consider the sustainability of the technologies. I am a strong proponent of the underlying science, but we must also do a better job of linking work on nanoparticles to mechanistic studies. Therefore, we need to call for more fundamental studies on how nanoparticles work.

Glen Fryxell: The two points that resonated with me from the presentations are: 1) the need to manufacture functional nanomaterials in a green manner; and 2) how to integrate nanomaterials into engineered forms so they are useful in the real world. It requires a massive scale-up effort to make the transition from the laboratory to field demonstrations to manufacturing of nanomaterials for application. Although there is good ongoing science at the bench-scale level, the “captains of industry” want to know if a technology will work on a large scale. To implement the technology on a large scale, we have to be able to make functional nanomaterials on a massive scale, which raises the issue of secondary pollution. We need to look at the engineered forms of how materials are deployed as well as the need to manufacture nanomaterials in a green manner while maintaining performance. To do this, the environmental nanomaterials community must align itself with the green chemistry community. Such an alignment will tell us interesting things about the supercritical fluids manipulation of nanomaterials as well as new solvent-less manufacturing methods being developed.

Diana Eignor: As part of USEPA’s Office of Water, I am interested in technologies for treating the influent and effluent of wastewater treatment plants as well as those with drinking water applications. That said, the Office of Water now considers nanomaterials to be contaminants of emerging concern. I do not want to have nanomaterials become legacy chemicals by moving ahead too quickly with their use. The work here is exciting and innovative, but at the same time, we need to know more about the environmental and human health implications of using nanomaterials. It is important to have this multidisciplinary approach in which we try to be “green” in the approaches we develop and also look at potential problems that may be encountered in the future. We need to look at doing human health studies, including studies of graduate students

working with nanomaterials who have probably been exposed.

Heather Henry: As part of the Superfund Basic Research Program, the funding arm of the National Institute of Environmental Health Sciences (NIEHS), I have heard many times that it is difficult to make these important international connections between researchers. NIEHS is looking into public/private partnerships as a way to move research in ways that might otherwise be restricted. If there is an example of a successful merging of international researchers, it would be helpful to have a starting point from a positive framework.

Deborah Elcock: In the remediation session, we heard about several remediation applications that have potential for cleaning up water, soil, sediment, and air. However, field conditions differ significantly from laboratory conditions. Because you cannot mimic all field conditions in the laboratory, it makes it important to consider the environmental implications and integrate them into the application as early as possible in its development. We have seen this problem in many other remediation approaches that did not consider environmental implications: contamination is removed from one medium and ends up in another. Although we have had sessions on both applications and implications of nanotechnology, there is a need to consider them together. Although I am not advocating a full life cycle analysis in the traditional sense, we must be aware of the possible changes in nanomaterials over time and how these changes may impact application.

Martha Otto: The Office of Superfund Remediation and Technology Innovation is interested in both applications and implications of nanotechnology. We are interested in: 1) sensors for detecting and monitoring traditional pollutants as well as nanomaterials in environmental media; 2) nanotechnology's potential for faster and cheaper cleanup of contaminated sites with the goal of reducing environmental exposures; 3) the proper disposal of wastes containing nanomaterials; 4) the effect nanomaterials have on treatment technologies, e.g., their effect on microbial populations used in wastewater treatment plants; and 5) working with industry and with our international partners to increase our ability to detect and measure nanomaterials as well as understand their fate and transport.

Question:

Can you comment on the potential use of sensor technologies for finding nanomaterials in complex environmental media and assessing their hazard and risk?

Fryxell:

I agree that it is a daunting challenge to find nanomaterials in the environment; it is a problem that will not be solved quickly or easily. Our work at Pacific Northwest Laboratory is mainly focused on chemical species in solution, but we are also looking at finding very small colloids (e.g., mercuric oxide colloids in crude oil). This work addresses your point regarding building in some type of host-guest chemistry designed at the macromolecular level that would allow for grabbing these clusters and selectively identifying them. For our materials to work, they rely entirely on diffusion. You are talking about fate and transport of nanoparticles in surface soil or ground water, which may be a more complicated scenario.

Diamond:

It is very difficult to come up with a panacea, because there are many different targets. Before devising an analytical method, you need to determine what nanomaterials you want to find and

where-in what matrix-you want to look. Also, the method will depend on whether you are trying to detect an artificial nanomaterial added to the environment or a naturally occurring one. One approach might be to label nanomaterials with a reporter group before deploying them, or to use an inherent unique property that allows the nanomaterial to be tracked.

Question:

Is it possible to develop the characteristics of the nanopores of a ceramic material to selectively collect a nanomaterial?

Fryxell:

We have successfully experimented with modifying pores to go after and bind iron oxide nanomaterials. Although these experiments were not done for remedial applications, we found that biofouling was a huge issue. The types of chemistries used to modify the pores to bind nanoparticles are very prone to fouling. Another labeling approach, which does not change the chemistry or introduce new hazards, is to vary the isotopic ratio of the iron used in nZVI to distinguish between synthetic iron and naturally occurring iron.

Question:

How do you handle your laboratory wastes?

Fryxell:

We use nanostructured materials in SAMMS®, but the actual particle sizes are tens of microns in size. Therefore, we do not use or produce any nanoparticles requiring disposal, just standard organic solvents.

Agnes Kane:

As part of our National Science Foundation grant, we worked closely with environmental health and safety experts at Brown University to determine how to handle wastes from laboratories testing the toxicity of nanomaterials. We decided to treat them like asbestos fibers. We use them under Class 2B hoods that are double HEPA-filtered and exhausted to the outside. We also use laboratory coats and gloves to avoid skin contact. All waste materials are collected in separate containers. The State of Rhode Island landfills the containers.

Question:

We heard about the impact of the aggregation of the nanoparticles on their surface area. With respect to remediating liquid that is in constant motion (e.g., ground water), is the internal surface area of the aggregate relevant? If the water can get in but not out due to the nanosized pores (similar to transport in clays), the effective surface area of the aggregate is more important, correct?

Fryxell:

The internal surface area is relevant in porous materials, because that is where the chemical functionality is. The comparison to transport in clay is not necessarily legitimate, because the structures in the porous materials are much larger than in clays. I attended a presentation on selectively functionalizing the outer surface of zeolites, leaving the inner surface area to other chemistry; it provided some interesting possibilities for taking zeolites in other directions. But the internal surface area in many porous materials makes up the vast majority of the available surface area, as well as being chemically available and useful. In our work we have been able to soak up over

half of the sorbent's weight in mercury and saturate it. We are able to use every active site inside the pores.

Response:

A flowing medium will go around the aggregate, rather than through the nano-size pores. Thus, I'm referring to "effective" surface area as that limited surface area in contact with fluid in motion.

Waite:

We heard several presentations about stabilizers used to coat particles and prevent aggregation. This is an important approach because diffusion into aggregates can be very slow. The application of adsorbed materials that increase surface charge and prevent aggregation will improve applications of nanomaterials.

Comment:

In response to the suggestion for isotopic labeling of nanoparticles, EPA SW-846 Method 6800 (Elemental and Speciated Isotope Dilution Mass Spectroscopy) addresses this type of monitoring, although it was not initially developed for nanoparticles. Two laboratories in the United States run the method for chromium speciation.

Question:

Is EPA or are the states developing policies and procedures for the disposal of solid nanowastes?

Otto:

EPA's current policy does not treat nanoparticles as unique. Under the Resource Conservation and Recovery Act (RCRA), all new substances must be evaluated as to their hazard, regardless of their size.

Comment:

Under EPA's pretreatment regulations, any wastewater discharge passing through a wastewater treatment plant can be regulated. Region 5 and the American Bar Association prepared a legal review stating that nanoparticles can be regulated separately. This review was prepared as a result of problems with wastewater containing nanosilver from washing machines.